EVAPOTRANSPIRATION IN A SUBARCTIC AGROECOSYSTEM: FIELD MEASUREMENTS, MODELING AND SUSTAINABILITY PERSPECTIVES

By

Watcharee Ruairuen

RECOMMENDED:

Dr. William Schnabel

Dr. Mingchu Zhang

Dr. Gilberto Javier Fochesatto
Advisory Committee Co-chair

Dr. Elena Bautista Sparrow
Advisory Committee Co-chair

Dr. Peter Fix
Chair, Dept. of Natural Resources Management

APPROVED:

Dr. Stephen Sparrow
Interim Dean, School of Natural Resources and Extension

Dr. John C. Eichelberger
Dean of the Graduate School

24 April 2015
Date

EVAPOTRANSPIRATION IN A SUBARCTIC AGROECOSYSTEM: FIELD MEASUREMENTS, MODELING AND SUSTAINABILITY PERSPECTIVES

A

DISSERTATION

Presented to the Faculty

of the University of Alaska Fairbanks

in Partial Fulfillment of the Requirements

for the Degree of

DOCTOR OF PHILOSOPHY

By

Watcharee Ruairuen, M.S.

Fairbanks, Alaska

May 2015

ABSTRACT

Northern latitudes are known to be the most vulnerable regions already witnessing the impacts of climate change. These impacts have not only affected a broad spectrum of ecological conditions but also physical and socio-economic functions and activities across the region. Uncertainties in climate change and its progression exposes agroecosystem development and sustainability to a great risk. Yet, not fully understood, climate feedbacks and influencing factors such as human population growth and consumption imposes economical and financial stress in the sustainability of agroecosystem activities. On the opposite direction, trends in this activity can drive regional modifications to climate to an extent that is still unknown and not yet forecasted. Over time, as the acreages of agricultural lands increase from conversion of natural lands such as boreal forests, unexpected changes in surface energetics and particularly overturning of evapotranspiration rates and changes in soil moisture regime may potentially accentuate regional climate change. These changes therefore are expected to introduce new challenges for Alaskan agriculturists because of increasing vulnerabilities and affecting conditions that shape resilience of agricultural systems and production.

This research focused on improving understanding of surface energetics in an agroecosystem of Interior Alaska. A synthesis study was conducted combining the analysis of intensive field experiments including direct measurements of micrometeorological, hydrological, meteorological variables and computational modelling during the summer growing season. The evaluation of evapotranspiration (ET) dynamical regime and surface energy processes showed that ET represented a large portion of surface energy balance with similar aspects to surface fluxing levels in Arctic tundra, and in contrast, with more abundant flux levels than in subarctic boreal forest. Surface heterogeneities due to soil moisture and temperature regime drive differences in energy balance closure as a function of spatial scales despite the mostly flat surfaces and stationary atmospheric surface layer flows in the experimental area. A fully coupled numerical simulation was performed to model fluxes at the land-atmosphere interface and compared to independent observations of surface energy.

A final assessment of experimental methodologies and numerical modeling is presented in preparation for integrative data fusion analysis and studies involving new satellite remote sensing capabilities, physical modeling and network field observations.

TABLE OF CONTENTS

SIGNATURE PAGE..... i

TITLE PAGE.....iii

ABSTRACT.....v

TABLE OF CONTENTS.....vii

LIST OF FIGURES.....xv

LIST OF TABLES.....xxiii

ACKNOWLEDGEMENTS.....xxvi

CHAPTER 1 Introduction.....1

1.1 General introduction.....1

1.2 Dissertation overview.....7

1.3 References.....11

CHAPTER 2 An overview of methodology, field experiments and data collection in a subarctic agroecosystem in Interior Alaska.....22

Abstract.....23

2.1 Introduction.....24

2.2 Site descriptions.....26

2.2.1 Location.....26

2.2.2 History.....27

2.2.3 Climate.....27

2.2.4 Soil.....28

2.2.5 Vegetation.....29

2.3 Field instrumentations and environmental measurements.....29

2.3.1 Calibration.....29

2.3.2 Meteorological data collection.....30

2.3.3 Eddy covariance installation.....31

2.3.4 Large aperture scintillometer installation.....32

2.3.5 Doppler acoustic sounder.....32

2.3.6 Lysimetry installation.....33

2.3.6.1 Lysimeter studies in summer 2012.....34

2.3.6.2 Lysimeter studies during summer 2013.....35

2.3.7 Determination of soil bulk density.....37

2.3.8 Soil texture.....38

2.3.9 Soil water characteristic analysis.....38

2.3.9.1 The soil water characteristic at field capacity.....38

2.3.9.2 The soil water characteristic at 1, 5 and 15 bars.....39

2.3.11 Soil thermal properties.....40

2.3.12 Other Data.....40

2.4 Methods to measure and estimate evapotranspiration.....41

2.4.1 Drainage lysimeters (Hydrological approach).....43

2.4.2 Evaporation pan.....44

2.4.3 Penman –Monteith equation.....45

2.4.4 Priestley-Taylor model.....49

2.4.5 Crop evapotranspiration: The FAO approach.....50

2.4.6 The energy balance and Bowen ratio method.....51

2.4.7 The eddy covariance.....54

2. 5 Meteorological and hydrological parameter measurements during the summer season.....55

2.5.1 Micrometeorological parameters.....55

2.5.2 Meteorological parameters.....56

2.5.3 Hydrological parameters.....57

2.5.3.1 The soil water characteristic curve.....57

2.5.3.2 Soil moisture, soil water potential and soil temperature in the lysimter plot.....58

2.5.3.3 Spatial variation of soil moisture and temperature under different surface cover.....58

2.6 Summary.....59

2.7 References.....76

CHAPTER 3 Evapotranspiration cycles in a high latitude agroecosystem: Potential warming role.....86

Abstract.....87

3.1 Introduction.....88

3.2 Materials and methods.....91

3.2.1 Experimental site.....91

3.2.2 Instrumentation.....93

3.2.2.1 Lysimeter setup.....93

3.2.2.2 Micrometeorological instrumentation.....94

3.2.2.3 Pan evaporation.....95

3.2.2.4 Surface energy balance.....95

3.2.2.5 Energy balance closure.....96

3.2.3 Estimation of evapotranspiration.....97

3.2.3.1 Penman-Monteith.....97

3.2.3.2 Priestley-Taylor coefficient.....99

3.2.3.3 Mass balance approach.....100

3.3 Results.....102

3.3.1 Meteorological and hydrological conditions.....102

3.3.2 Surface energy balance.....104

3.3.2.1 Energy closure at half-hour time-scale.....104

3.3.2.2 Energy balance and energy partitioning.....105

3.3.4 Evapotranspiration from water balance equation.....108

3.3.4.1 ET by mass balance from irrigated lysimeters versus ET by energy balance.....108

3.3.4.2 Penman-Monteith evapotranspiration (ET_{PM}) and pan evaporation (E_P).....110

3.4 Discussion.....111

3.5 Conclusions.....115

3.6 Acknowledgements.....117

3.7 References.....136

CHAPTER 4 Scale dependence of evapotranspiration estimates in a high latitude Alaskan agroecosystem.....154

Abstract.....155

4.1 Introduction.....156

4. 2 Field experiment and methodologies.....160

4.2.1 Study site and meteorological regime.....160

4.2.2. Experimental design.....161

4.3 Data processing and methods.....163

4.3.1 Eddy covariance.....163

4.3.2 Large aperture scintillometer.....164

4.4 ET Methods.....166

4.4.1 The energy balance.....166

4.4.2 Penman-Monteith (PM).....168

4.4.3 Priestley-Taylor (PT).....168

4.5 Results and discussion.....169

4.5.1 Comparison of the ground heat fluxes at the local and area-averaged scale.....170

4.5.2 Comparing the sensible heat fluxes from EC-based and LAS-based.....171

4.5.3 Retrieval of ET based on energy balance equation.....173

4.5.4 Energy balance closure at local and large scale using independent observations.....175

4.5.4.1 Determination the CF as function of sensible heat flux level.....178

4.5.4.2 Determination of CF as function of the Obukhov stability length (L).....179

4.5.4.3 Determination of CF as function of the kinematic conditions of the flow.....180

4.6 Conclusions.....180

4.7 Acknowledgements.....182

4.8 References.....193

CHAPTER 5 Simulating the coupled transport equations to compute evapotranspiration.....203

Abstract.....204

5.1 Introduction.....205

5.2 Materials and methods.....207

5.2.1 Field experiment.....207

5.2.2 Model implementation.....208

5.2.2.1 Model modules in Python.....208

5.2.2.2 The initial setting for model simulation.....209

5.3 Simulations scenarios.....210

5.3.1 Dry period.....210

5.3.2 Wet period.....211

5.4 Results and discussion.....211

5.4.1 Net radiation.....211

5.4.2 Latent heat.....212

5.4.3 Ground heat fluxes.....213

5.4.4 Sensible heat.....213

5.4.5 Soil moisture and soil temperature.....214

5.5 Conclusions.....215

5.6 Acknowledgements.....217

5.7 References.....230

CHAPTER 6 Summary and conclusion.....236

APPENDIX-A.....244

APPENDIX-B.....247

LIST OF FIGURES

Figure 1-1 Percent of landscape units with soils of agricultural potential for Alaska adapted from Stevenson et al. (2014).....10

Figure 2-1 Experimental site at the FEF during summer season. The location of the instrumentation is illustrated. The farm is more than 1 kilometer from East-West and about 600 m North - South. This figure was obtained from Google Earth on 9 September 2012.....62

Figure 2-2 Micrometeorological and Soil Moisture sensing. EC, LAS, soil potential data logger including picture of the installation process in the lysimeter plots, pan evaporation, with two treatments of the lysimeter study are shown.....63

Figure 2-3 Instrumentation of the lysimeter plot; (a) summer 2012 and (b) summer 2013. (T_{soil} = soil temperature sensor, SWP=soil water potential sensor, θ_{ly}=soil moisture sensor).....63

Figure 2-4 Micrometeorological conditions during the growing season; (a)- (h) represent the net radiation (at 3 m height), air temperature (at 1 and 3 m height), barometric air pressure, and static stability parameter for summer 2012 (left panel: a-d) and 2013 (right panel: e-h) respectively. Blank spaces in the graphs indicate missing data.....64

Figure 2-5 Soil Temperature and ground heat flux at EC tower location in summer 20 12 (left panel) and 2013 (right panel). (a) soil temperature at surface (red), at 15 cm (blue), and 30 cm (green) soil depths; (b) calculated ground heat flux (G) in 2012; (c) soil temperature at 5cm (red), 10 cm (black), 20 cm (blue), and 30 cm (green) soil depths; and (d) calculated ground heat flux (G) in summer 2013.....65

Figure 2-6 Meteorological condition during summer 2012 (left panel) and 2013 (right panel). (a)-(d) and (e)-(h) are one- minute records of air temperature, relative humidity, pressure, and

precipitation at 2 m height in summer 2012 and 2013 respectively. Blank spaces indicate missing or no data.....66

Figure 2-7 Histograms of wind speed and direction from June to September over the three summer growing seasons; (a) 2012 wind speed ranges from 0.4-12.5 ms^{-1}, prevailing wind direction is north-west, (b) 2013 wind speed ranges from 0.4-9.8 m s^{-1}, prevailing wind direction is north-west sector, and (c) 2014 wind speed ranges from 0.4-13 m s^{-1}, prevailing wind direction is west sector.....67

Figure 2-8 Refractive index structure parameter (C_n^2). (a) Summer 2012 and (b) summer 2013. Blank spaces in the graphs indicate missing data.....67

Figure 2-9 Class A pan evaporation data in summer 2013. Evaporation pan (Ep) in the study site versus the evaporation pan at NOAA meteorological station located at the Fairbanks Agricultural Experiment station (1000 m away) from the study site.....68

Figure 2-10 Doppler SODAR measured wind speed (a, e), wind direction (b, f), boundary development (c, g), and velocity (d, h) during July 29, 2013 and 5 August 2013 respectively...69

Figure 2-11 Soil moisture characteristic curve from the lysimeter soil sample; blue line represent the SMC curve for the nonlinear relationship fitting, the black dot is the moisture content at different air pressures, the red triangle is the moisture content measuring by 10HS sensor, and the green square is the gravimetric moisture content.....70

Figure 2-12 Sample data of soil moisture content and water potential within vegetated and unvegetated lysimeters in summer 2013; (a) soil moisture in vegetated lysimeter, (b) water potential in vegetated lysimeter, (c) soil moisture content in unvegetated lysimeter, and (d) water potential in unvegetated lysimeter. The arrows represent the precipitation and irrigation events.....71

Figure 2-13 Sample data of soil temperature and soil moisture under different fields in the farm during summer 2012; (a) –(c) soil temparature at barley field, brome grass, and fallow field, and (d) – (f) soil moisture (SMC) at barley, bromegrass, and fallow field, and (d) – (f) soil moisture (SMC) at barley, bromegrass, and fallow field respectively.....72

Figure 3-1 Fairbanks Experiment Farm (FEF) site at the UAF AFES. The location of the instrumentation is illustrated. The farm dimensions are: more than 1 kilometer on East to West and about 600 m North to South. EC tower (A), lysimeter plot (B), Meteorological station (C), LAS system (D).....118

Figure 3-2 Ensemble instrumentation during intensive observing periods. Panel (a) – (b) represent the lysimeter setup including drainage system and installation probes layout for summer 2012 and 2013.....119

Figure 3-3 Half hourly meteorological time series during growing seasons in 2012 and 2013 measured at the eddy-covariance tower. Panels: (a) net radiation R_{net} (W m^{-2}); (b) ground heat flux G (Wm^{-2}), (c) air temperature T_{air} (^{o}C); (c) relative humidity RH (%), (e) vapor pressure deficit VPD (kPa), and (f) precipitation (mm day^{-1}). The horizontal axis represents fractional Julian day in local Alaska Standard Time (AKST: UTC - 8 hrs).....120

Figure 3-4 Time-series of soil temperatures. Soil temperature at 15 cm depth at the experiment site 1 June to 17 September in 2012 (black trace) and 2013 (gray trace). The horizontal axis represents fractional Julian day in local AKST.....121

Figure 3-5 Frequency distribution of the wind speed and direction during summer. Panel (a) 2012 and (b) for 2013 at the experiment site during the period of study at 2 m height.....122

Figure 3-6 Scatterplot of energy balance closure. Horizontal axis is the available energy for fluxes (R_{net} - G) at the surface (W m^{-2}) and vertical axis of the sum of turbulent fluxes of sensible

(H) and latent heat (LE). Period of study (11 July to 31 August, summer 2013). Values were obtained after 30 minute average under stationary conditions (1540 of points). Correlation coefficient was 97 % with an offset of 10 W m^{-2}.....123

Figure 3-7 Diurnal cycle of Radiative and turbulent fluxes during clear sky conditions. Case of July 30 (Day of Year 211) at the experiment site. Horizontal axis in AKST time in (hrs.) and vertical axis is in W m^{-2}. R_{net}=net radiation, LE=latent heat flux, H= sensible heat flux, G= ground heat flux.....124

Figure 3-8 Monthly means estimates for the four components of the surface energy balance (R_{net}=net radiation, LE=latent heat flux, H= sensible heat flux, G= ground heat flux). The series covers from June to September of 2012 (panel-a) and 2013 (panel-b).....125

Figure 3-9 Monthly means estimates of energy partitioning. G, H and LE are referred to R_{net}. Panel-a represents 2012 and panel-b 2013 during the growing season. Statistical values to define the series are based on midday energy partitioning computed as a mean over 5 hours centered in solar noon.....126

Figure 3-10 Daily means of evapotranspiration. Measured by pan evaporation (E_P) and estimated based on Penman Monteith (ET_{PM}) from 10 July to 16 September 2013. Some data gaps were caused by power interruptions and instrument failure and repair.....127

Figure 4-1 Diagram of the field experimental site at the Fairbanks Experiment Farm (FEF), University of Alaska Fairbanks (UAF) Agricultural and Forestry Experiment Station (AFES) Fairbanks Alaska, USA. The experimental site display different surface cover and location of the instrument. The location of a two level of meteorological station (denoted A) at 2 and 5 m heights, the Large Aperture Scintillometer (LAS) (BLS-900) system (denoted B) at 1.8 m height, and the EC system (denoted C with the black star) at 3 m height are shown. The dashed line

arrow (east- west) represents the beam of the scintillometer between the transmitter and receiver units. The number 1-5 represent the location of soil temperature measurements under different surface cover (1= barley, 2 and 4= fallow, 3= grass, 5=fallow field under EC station). The square dot line represent the central part of the LAS fluxing area.....183

Figure 4-2 Statistics of wind speed and direction during 7 July to 13 August 2013 at the FEF site.....184

Figure 4-3 Time-series composite of the 30-min average of local soil heat flux at the EC site (G_{local}) and the area-weighted averaged across the farmland (G_{large}). The samples size is 624 points.....184

Figure 4-4 Time-series composite of sensible heat fluxes 30-min average for H_{local} and H_{large}.....185

Figure 4-5 Time-series composite 30-min average diurnal cycles of Latent Heat at local and area average scales. LE_{local} and LE_{large}.....186

Figure 4-6 Statistical distribution of the Latent Heat flux difference between local and area average closure. Time-series contain 624 number of points based 30-min average eddy-covariance and large-aperture scintillometry.....187

Figure 4-7 Energy Balance Closure scatterplots. Top panels are based on local closure in sensible heat and latent heat estimation based on PM (a) and PT (b). Lower panel represents large scale closure in sensible heat and latent heat estimation based on PM (c) and PT (d) $H_{large} + LE_{PT}$ vs. $R_{net} - G_{large}$.....188

Figure 5-1 Scheme of the computational grid with the driving force terms (temperature, soil water potential and soil vapor concentration), the soil conductivities and the resistances involved

at the soil–atmosphere interface (Adapted from Bitelli et al., 2008). The red dot is the mass balance for heat flow and water flux at a node.....218

Figure 5-2 Global radiation, relative humidity, air temperature, and wind speed measured in the Atmospheric Surface Layer from top to bottom at the experimental plot during the dry period (left panel; 26 July-4 August 2013[Julian day 207-215]) and wet period (right panel; 18-31 August 2013 [Julian 230-242]).....219

Figure 5-3 Simulated and measured hourly data of net radiation during the dry and wet period as a function of time. (a) Dry period from 26 July to 3 August 2013 (Julian day 207-216), (b) wet period from 25-30 August 2013 (Julian day 237-242).....220

Figure 5-4 Comparison between the hourly observation of net radiation (Rnet obs) and the simulation of net radiation (Rnet mod) during the dry and wet period. (a) Dry period from 31 July to 3 August 2013 (Julian day 210-215) and during the wet period (b) from 25-30 August 2013 (Julian day 237-242).....221

Figure 5-5 Solar radiation as a function of time during dry and wet periods. (a) Dry period from 26 July to 3 August 2013 (Julian day 207-215) and (b) Wet period from 25-30 August 2013 (Julian day 237-242).....222

Figure 5-6 Evapotranspiration time series observed and modeled. (a) Dry period from 26 July to 3 August 2013 (Julian day 207-216), (b) wet period from 25-30 August 2013 (Julian day 237-242).....223

Figure 5-7 Simulated and observed cumulative evapotranspiration for the dry (a) and wet period (b).....224

Figure 5-8 Time series of simulated and estimated ground heat flux. (a) Dry period from 29 July to 2 August 2013 (Julian day 210-214), (b) wet period from 26 -30 August 2013 (Julian day 238-242).....225

Figure 5-9 Time-series composite of hourly diurnal variation of sensible heat flux during (a) dry and (b) wet period.....226

Figure 5-10 Coupled model simulation output for soil water content, soil water potential, and soil temperature as function of depth (from top to bottom) during dry (left panel) and wet (right panel) periods.....227

LIST OF TABLES

Table 2-1 Summary of instrumentation installed at the FEF site.....73

Table 2-2 The volumetric soil moisture content (convert from gravimetric moisture content by multiplying the bulk density) before and after harvesting with in lysimeter experiment.....74

Table 2-3 Properties of soil from different site in the farmland.....74

Table 2-4 Average air temperature, soil temperature, and soil moisture at different sites in the farm.....75

Table 3-1 Instrumentation utilized in the UAF AFES Fairbanks Experiment Farm in summers of 2012 and 2013.....128

Table 3-2 Instrumentation.....129

Table 3-3 Seasonal means of major microclimate variables at FEF during the growing seasons under study.....130

Table 3-4 Monthly mean meteorological parameters measured at the FEF.....131

Table 3-5 Seasonal means of surface energy partitions, Bowen ratio (β), vapor pressure deficit (VPD), Priestley Taylor alpha coefficient (α) and energy balance closure (CF) at the FEF...132

Table 3-6 Mean summer values of the energy balance partitioning for Arctic and subarctic ecosystems calculated and/or collected from various published data sources.....133

Table 3-7 A summary of weekly ET by water balance in comparison with the ET by energy balance during intermediate development phase (10 - 23 July, 2013) and maturity phase (20 - 27 August, 2013) of crop under wet conditions.....134

Table 3-8 The annual and summer hydrological balance characteristics for Arctic and sub-arctic regions compiled from various published data sources.....135

Table 4-1 Instruments during the Field Experiment.....189

Table 4-2 Half hourly mean of meteorological and hydrological condition during the period of study. 190

Table 4-3 Statistical Analysis between measured and estimated surface fluxes at two scales local and area-averaged measurement (sensible heat, latent heat fluxes and available energy).....191

Table 4-4 Agroecosystems energy balance closure, correlation, error and number of points at local and large scale and evapotranspiration fluxes approach.....192

Table 5-1 Soil properties within lysimeter.....228

Table 5-2 Initial setting for model simulation.....228

Table 5-3 Main meteorological conditions, soil properties and surface characteristics at during periods under study.....229

ACKNOWLEDGEMENTS

I express my most sincere appreciation and gratitude to my two major advisors, Elena Bautista. Sparrow and Gilberto Javier Fochesatto for accepting to be my advisors, for providing me with numerous opportunities to grow and become a research scientist, for their patience, guidance, encouragement, constant enthusiastic support, and many kindnesses extended especially during some seemingly interminable periods of this research and my graduate study. A big thank you also goes to my committee members William Schnabel and Mingchu Zhang, for providing thoughtful advice and challenging questions as well as encouragement and suggestions throughout my research. I am also grateful for William Schnabel's help with the lysimeter study setup.

I extend my sincere thanks to these people who have helped me in my research and dissertation in many ways:

- Stephen Sparrow for his help, advice, and support for the entire study
- Yongwon Kim for equipment support and thoughtful suggestions on my research
- David Valentine for all his constructive comments on my research
- Bob Van Veldhuizen for all soil techniques, support in the laboratory and field experiment
- Darleen Masiak for all her personalized help in the field and laboratory, helpful suggestions on my research and getting me accustomed to living in Alaska
- John Fox , for his thought provoking and friendly discussions
- Nicole Swenson for sharing her soil moisture data
- My colleagues Allen and Somnuk Wiggs and her family, Andrew David and Cherrywan Gryska, Pananya and Rene Guevara, and other Thai people in Fairbanks for their help, support, and provision of Thai food throughout my study.
- And for the many others who have also helped me in various ways, such as Alan Tonne, Nancy Tarnai, Deborah Cushing, David Verbyla, Martha and Bill Kopplin, Ketsiri Leelasakultum, Bindu Gadamsetty, Derek Starkenburg, Soumik Basu, Vinay Kayetha, Peter A Bieniek, Lola Oliver, John Yarie, Joshua Greenberg, Peter Fix, Carol Holz, Yurie and Abel Bul-Ito, Deborah Bennett and family, Marilis and Jim Bennett, and, Josie Wooding, I am also very grateful.

Further thanks go to Suratthani Rajabhat University in Thailand for financial support during my doctoral study and Alaska EPSCOR (OIA 1208927- Alaska Adapting to Changing Environments), and to the GLOBE Seasons and Biomes Program (NSF Grant GEO-0627941) and team for inspiring me to obtain a Ph.D. I also want to extend gratitude to the Natural Resources and Sustainability program, and the School of Natural Resources and Extension, and its talented and dedicated faculty and staff. I am very proud of being part of such a great school which has enhanced my learning as well as love for all of my Alaska experience.

Finally I express my appreciation and thanks to my family and my friends in Thailand for their unfailing love, care, and constant encouragement which gave me the ability to withstand the setbacks experienced along the way and the energy needed to successfully complete this dissertation and my doctorate.

CHAPTER 1

1.1 General introduction

Current climate change impacts are likely to be more pronounced in the Arctic and adjacent subarctic regions than other parts of the world (Chapin et al., 2000a; Grunzweig et al., 2004; ACIA, 2005; Chapin et al., 2005; Serreze and Francis, 2006; Christensen et al., 2007; IPCC, 2007a,b,c; MacDonald, 2010; Walsh et al., 2014). In particular, Alaska has been experiencing warming more than twice faster than the rest of the United States, with the average annual air temperature increasing by approximately 1.5 °C in the past 60 years, and substantial year-to-year and regional variability over the past several decades (Stewart et al., 2013; Chapin et al., 2014). Several environmental changes documented in response to this warming include lengthening of the growing season (Smith et al., 2004; Euskirchen et al., 2006; Shulski and Wendler, 2007; SNAP, 2008; Euskirchen et al., 2009), decline in snow cover duration and extent (Stone et al., 2002; Euskirchen et al., 2006; Euskirchen et al., 2007), permafrost degradation (Jorgenson et al., 2010), drier landscapes, increased ecosystem productivity, and shifts in seasonal fire regimes (Rupp et al., 2007). Associated with these changes are direct and indirect effects on terrestrial ecosystems; for example, modifications to the water and energy balance regimes resulting in feedbacks to the climate system (McFadden et al., 1998; Chapin et al., 2000b; Beringer et al., 2005; Chapin et al., 2005). One of the most considerable and direct impacts of climate change will be on agricultural and food systems (Battisti and Naylor, 2009). In this sense, it is projected that with the increase in average temperatures, the global potential for food production will decrease (IPCC, 2007b). To meet future demands and conduct sustainable agriculture, considerable growth in food production must be coupled with reduction in the environmental impacts from agriculture (Peltonen-Sainio, 2012).

However, agriculture activity can become vulnerable under changing climate because of its strong connection to meteorological, hydrological and climatological variability. Change in local climate variables such as temperature, humidity, snow melt, precipitation, and soil moisture affect crop development and farming activities. Future changes in these variables and their regimes configure new challenges for farmers which may increase vulnerability of farming activity and add uncertainty in production, particularly in Alaska where the region is more susceptible and sensitive to climate change than other regions. Agriculture in Alaska exists as an underdeveloped natural resource-based industry that has been shaped by historical and developmental processes and continually influenced by environmental and socioeconomic factors (Stevenson et al., 2014a). According to the report of the Natural Resources Conservation Service (NRCS) of the United States Department of Agriculture (USDA), Alaska has more than 16 million hectares of arable soil and climate suitable for agriculture (Figure 1-1). However, it has only 762 farms in the state in 2012 and among these are 212 farms located in Fairbanks (U.S. Census-Bureau, 2010; USDA, 2014). The Interior Alaska along with the area of Tanana River is considered to be a major agricultural area in Alaska (Juday et al., 2005). Agriculture in this region consists mostly of cool-season forage crops, cool-season vegetables, and small grains; raising traditional livestock (cattle, sheep, goats, pigs, poultry); and herding reindeer (Juday et al., 2005). Crop land accounts for about 10% of Alaska's farmlands, 83.5% is ranged land, and 6.5% is reserved for other uses (USDA, 2014). Perennial hay and grains are the majority of what is grown on agricultural lands while potatoes, carrots, green vegetables such as broccoli and cabbage and other crops are also important (Stevenson et al., 2014a).

The agriculture industry in Alaska makes up less than 1% of revenues earned compared with other resource industries in the state (UAF-CES, 2006). Local agriculture accounts for only

5% or less of Alaska's food demand and about 95% or more is imported (UAF-CES, 2006; Consenstein, 2010; Helfferich, 2010; Helfferich and Tarnai, 2010). This means food production is limited in this region. Hence, Alaskan residents generally depend more heavily on imported food resources because the state is isolated from the lower 48 contiguous states where the main nation's food supply is available. Under a crisis scenario, Alaska will become highly vulnerable to food insecurity. In addition, there is uncertainty for wild food on whether there will always be enough to be harvested, processed, and stored to satisfy the needs of all communities or to provide nutritious foods throughout the long winter in the future (White et al., 2007). Therefore, increasing agriculture will be essential for producing a more food-secure state, especially in view of uncertainty in availability of wild food sources (Stevenson et al., 2014a).

In addition, there is a limited time available for development and implementation of adaptation that are essential to improve resilience and adaptive capacity of the northern agricultural sector under rapid change of climate (Peltonen-Sainio et al., 2009). On the other hand, climate change may offer new opportunities for agriculture in the northern high latitude regions, which is currently limited by the short growing season (Juday et al., 2005; Peltonen-Sainio et al., 2009). A warmer climate will extend the thermal growing season and the physiologically effective part of it (Peltonen-Sainio et al., 2009). This means it could enhance the regional agricultural capacity as well as increase practice for larger scale agricultural systems in the future (Juday et al., 2005; Hatch, 2010).

Major environmental challenges compete against sustainable agriculture in Alaska and they are generally linked to high latitudes climate including strong seasonality, a short growing season, relatively cold temperatures and unpredictable frosts (Stevenson et al., 2014b). Long hours of sunshine in this region may cause bolting (the failure of a plant to properly form a head

because of excessively rapid stem elongation or leaf twisting), particularly in crops such as lettuce, cabbage, or spinach. Bolting can also be exacerbated by long days and warm temperature exposure. In the summer solstice, the Interior Alaska receives almost 22 hours of direct sunlight that influences photosynthetic periods and light intensity requirements that can vary significantly among different crops and cultivars. For example, lettuce can increase dry mass substantially, sometimes doubling in weight and having other positive effects when day length increased from 16 to 24 hours (Kitaya et al., 1998). Moreover, the effects of long summer days on plants are often positive and can produce large and fully mature crops that can also be produced in a relatively short time (Stevenson et al., 2014b). Additional challenges from climate change posed for sustainable agriculture in the Interior Alaska include changes in the abundance or type of pests, diseases, and invasive species (ACIA, 2005). Finally it must be noted that the actual signs of climate change verify different trends depending upon the area of Alaska under consideration; some are becoming warmer and drier, while others are becoming cooler or wetter, or both (Osterkamp, 2007), leading to an overall decrease in freshwater supply (Alessa et al., 2008).

In the U.S. about 70% of the freshwater is used for agriculture (WRI, 2000). Water is thus becoming more of an increasing concern for agriculture production during the growing season because major water availability through precipitation decline would encourage switching over to irrigation. In the coming decades, adaptation should mainly consist of adopting cultivars that are more resistant to higher temperatures and to water shortage, but irrigation will certainly become a more common practice putting even more pressure on local water resources (Parent and Anctil, 2012). Water stored on the land is the main variable controlling numerous processes and feedback loops within the local climate system (Seneviratne et al., 2010; Lahoz and De Lannoy, 2014). Water stored underneath in the unsaturated zone can be referred to as soil

moisture (Seneviratne et al., 2010; Lahoz and De Lannoy, 2014). The soil moisture has a significant impact on the partitioning of water and heat fluxes (latent heat and sensible heat), thereby connecting the hydrological (i.e., water) cycle with the energy cycle, including exchange of carbon dioxide in agroecosystems. It directly affects crop development (Lahoz and De Lannoy, 2014) and other processes in the subsurface. It also is a source of water for atmosphere through evapotranspiration from lands.

Although, Alaska has abundant supplies of freshwater and relatively low overall use for agriculture purpose (Kenny et al., 2009; Alessa et al., 2011), Alaskans may not have easy or affordable access to sufficient water. Many farmers in the Interior Alaska, even though they may live on the road system, may not have access to city water (Stevenson et al. 2014b). Thus, in some situations, water can be a factor limiting farming activities. Additionally, water stress occurs frequently during the growing season in the Subarctic. According to Sharratt (1994) irrigation can reduce water stress and support crop production in nearly 50% in all cases.

The most important variable that connects agroecosytem sustainability and climate change at all scales in space and time is evapotranspiration (ET). ET is a major component of the hydrological cycle, as it returns more than 60% of annual land precipitation back to the atmosphere (L'vovich and White, 1990; Shiklomanov, 1993; Trenberth et al., 2009; Miralles et al., 2011; Mu et al., 2011) and is the factor modulating moisture gradients and soil dryness (Ruairuen et al., 2014). Furthermore, ET is central to earth system science because it governs interactions (e.g., energy exchange and biogeochemical cycling) between the atmosphere and terrestrial ecosystems (Mu et al., 2007; Wang et al., 2010; Katul et al., 2012; Wang and Dickinson, 2012; Liu et al., 2013) as well as the major pathway for water loss from the surface in the Arctic and subarctic (Kane and Yang, 2004) as well as in agroecosystems. Despite of this

central role it is one of the least understood components of the Arctic hydrologic cycle (Kane et al., 1989; Kane et al., 1992; Vörösmarty et al., 2001; Woo et al., 2008) and in the energy balance cycle. Accurate ET estimation is fundamental to determine water management practices, design of irrigation systems, developing irrigation regimes, calculating crop yield (Allen et al., 1998), and sustaining agriculture. Therefore, better understanding of the ET cycle in high latitude agroecosytems can help determine whether irrigation practices can be improved so that available water can be used more productively (Kite, 2000; Zhao et al., 2013)

According to the limited availability of water on the surface become a major problem for agriculture activities. Then, irrigation becomes an important component of a sustainable agricultural system. However, the ability of agricultural production to successfully continue will depend on the availability of water for irrigation as well. Therefore, there is a need for experimental determination of ET and its components to understand the dynamics of ET and energy partitioning at a given site that would inform what resilience-based management practices to use particularly during the growing season, when pronounced changes are expected to occur.

Furthermore, future water resources for agriculture are being strained and threatened from a rapid increase in water demand mainly from population growth. Episodic events of extreme drought may compound the problem of increased demand and this may interact with projected climate change in unforeseen and potentially worrisome ways (Wang et al., 2012). This information will be used to develop some practices to cope with the change and conserve water such as improve water harvesting and irrigation schedule or technologies, manage soil and crops to increase water use efficiency and reduce the evaporation, introducing adapted crop varieties to future climate conditions, and using more diverse cropping systems in order to increase their resilience to climate change. These practices can be improved to maintain the sustainability of

agriculture for this region. Besides understanding the direction and the magnitude of changes in surface energy balance, it is essential to study whether agriculture activities alter surface energy budgets that potentially can influence future climate change and to provide an opportunity to better inform models and water management decisions.

1.2 Dissertation overview

This dissertation aims at understanding the evapotranspiration (ET) cycle and its components in a subarctic agroecosystem as well as examining the use of models to estimating ET and related parameters. Little is known about what the ET role is in the agroecosystem and how a rate change will affect the ecosystem, agriculture activities and sustainability, local or regional climate system under changing climate conditions in high latitudes. To achieve these goals, the field experiments were conducted to measure the meteorological, hydrological and micrometeorological parameters in the agroecosystem that are needed to calculate and estimate ET. Laboratory experiments and modeling studies related to ET were also conducted. Numerous approaches including simple methods, complicated techniques, and empirical modelling were applied to measure and estimate the ET in this study. Chapter 2 describes the field experiment and instrumentation which include hydrological, meteorological and micrometeorological measurements over the summer season. The site characteristics, climatology, hydrology are also described. Several methodologies which are widely used to study ET were also explained. The in-situ measurements of physical parameters of air temperature, rainfall, wind speed and direction, soil temperature (0-15cm), and soil moisture under three different surface cover are described.

Chapter 3 is the experimental determination of ET rates and the fractioning of energy in an agroecosystem during the 2012 and 2013 growing seasons. The energy partitioning and water

mass balance measured in this agroecosystem was then compared to different natural ecosystems across the pan-Arctic that raises questions of what the changes in land use in terms of converting from natural to agricultural ecosystems might entail for high latitude regional climate disturbance and feedback.

In terms of quantifying ET regionally or at large scales there is a need to use atmospheric models or a combination of them with satellite remote sensing information but the problem is that model parameterization occurs at local scales. Therefore, Chapter 4 is about a study designed with special instrumental arrangement to consider this spatial scale problem to show for the first time how in a very simple landscape and where flows are in steady-state ET estimates depends on the scale in which it is considered. This scale gaps are important to prepare future studies about the regional and landscape influence of ET.

Trying to advance ET, soil moisture and soil temperature determination across agricultural landscapes a model was adapted and implemented based on measured and calculated parameters during field experiments. Chapter 5 introduced the adaptation and implementation of a coupled numerical model of heat, water vapor and liquid water fluxes to estimate parameters related to ET and compare their performances for the estimation of ET in Alaskan soils. Description of the coupled model is detailed in Appendix-B with the model adaptation for this particular ecosystem. Model testing has been done through two different conditions (dry and wet periods) in summer 2013 by using the measured meteorological data and soil properties.

This dissertation presents the quantification of ET in field experiments that allows hypothesizing about a new climate scenario based on land use change from conversion of natural ecosystems to an agroecosystem. By communicating these results to those with stewardship responsibilities (i.e. policy makers, and land managers) or to modelers, Alaskan agriculture may

increase its capacity to respond and adapt with appropriate and scientifically informed actions and planning processes to sustain the agricultural resources and shape the trajectory of change in the social-ecological system (Chapin et al. 2009). In the conclusion Chapter 6, major findings were summarized including the potential of this research to provide a basis for preparing sustainable Alaskan agriculture under changing climate.

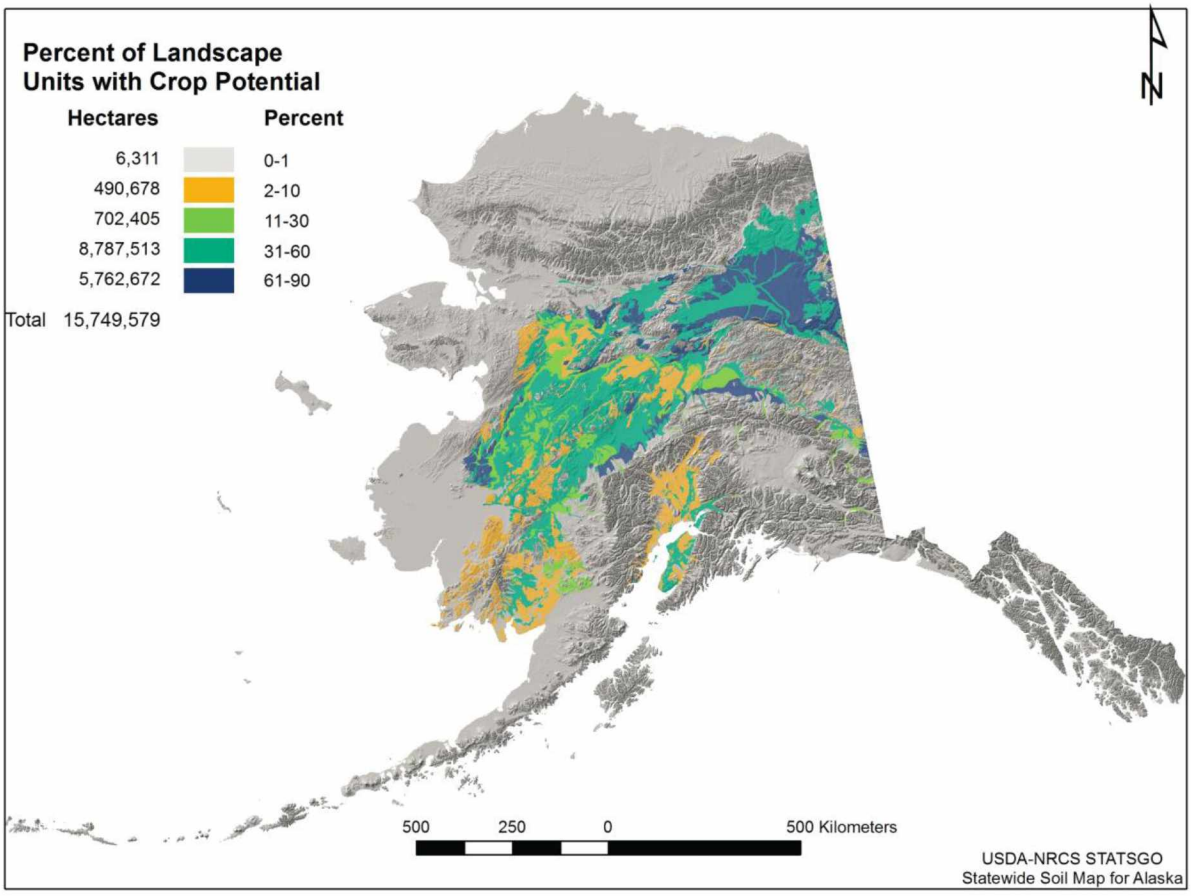

Figure 1-1 Percent of landscape units with soils of agricultural potential for Alaska adapted from Stevenson et al. (2014)

1.3 References

ACIA (Arctic Climate Impact Assessment), 2005. Arctic Climate Impact Assessment: Scientific report. Cambridge University Press, pp. 21-60.

Alessa, L., Altaweel, M., Kliskey, A., Bone, C., Schnabel, W. and Stevenson, K., 2011. Alaska's Freshwater Resources: Issues Affecting Local and International Interests. Journal of the American Water Resources Association, 47(1): 143-157.

Alessa, L., Kliskey, A., Busey, R., Hinzman, L. and White, D., 2008. Freshwater vulnerabilities and resilience on the Seward Peninsula: Integrating multiple dimensions of landscape change. Global Environmental Change-Human and Policy Dimensions, 18(2): 256-270.

Allen, R.G., Pereira, L.S., Raes, D. and Smith, M., 1998. Crop evapotranspiration - Guidelines for computing crop water requirements. FAO Irrigation and drainage paper 56, Rome.

Battisti, D.S. and Naylor, R.L., 2009. Historical Warnings of Future Food Insecurity with Unprecedented Seasonal Heat. Science, 323(5911): 240-244.

Beringer, J., Chapin, F.S., III, Thompson, C.C. and McGuire, A.D., 2005. Surface energy exchanges along a tundra-forest transition and feedbacks to climate. Agricultural and Forest Meteorology, 131(3-4): 143-161.

Chapin, F.S., III, Eugster, W., McFadden, J.P., Lynch, A.H. and Walker, D.A., 2000a. Summer differences among Arctic ecosystems in regional climate forcing. Journal of Climate, 13(12): 2002-2010.

Chapin, F.S., III, McGuire, A.D., Randerson, J., Pielke, R., Baldocchi, D., Hobbie, S.E., Roulet, N., Eugster, W., Kasischke, E., Rastetter, E.B., Zimov, S.A. and Running, S.W., 2000b. Arctic and boreal ecosystems of western North America as components of the climate system. Global Change Biology, 6: 211-223.

Chapin, F.S., III, Sturm, M., Serreze, M.C., McFadden, J.P., Key, J.R., Lloyd, A.H., McGuire, A.D., Rupp, T.S., Lynch, A.H., Schimel, J.P., Beringer, J., Chapman, W.L., Epstein, H.E., Euskirchen, E.S., Hinzman, L.D., Jia, G., Ping, C.L., Tape, K.D., Thompson, C.D.C., Walker, D.A. and Welker, J.M., 2005. Role of land-surface changes in Arctic summer warming. Science, 310(5748): 657-660.

Chapin, F.F., III, Kofinas, G., and Folke, C., 2009. Principles of ecosystem stewardship: Resilience for based resource management in a changing world. Springer. New York, NY

Chapin, F.S., III, Trainor, S.F., Cochran, P., Huntington, H., Markon, C., McCammon, M., McGuire, A.D. and Serreze, M., 2014. Chapter 22: Alaska. In: J.M. Melillo, T. Richmond, (T.C.), and Yohe, G.W. (Editors), Climate change Impacts in the United States: The Third National Climate Assessment, U.S. Global Change Research Program pp. 514 - 536.

Christensen, J.H., Hewitson, B., Busuioc, A., Chen, A., Gao, X., Held, I., Jones, R., Kolli, R.K., Kwon, W.T., Laprise, R., Magaña Rueda, V., Mearns, L., Menéndez, C.G., Räisänen, J., Rinke, A., Sarr, A. and Whetton, P., 2007. Regional Climate Projections. In: Solomon, S. et al. (Editors), Climate Change 2007: The Physical Science Basis. Contribution of Working Group I to the Fourth Assessment Report of the Intergovernmental Panel on Climate Change. Cambridge University Press, UK.

Consenstein, D., 2010. Framers put high-quality food on tables, Anchorage Daily News, September 27.

Euskirchen, E.S., McGuire, A.D., Kicklighter, D.W., Zhuang, Q., Clein, J.S., Dargaville, R.J., Dye, D.G., Kimball, J.S., McDonald, K.C., Melillo, J.M., Romanovsky, V.E. and Smith, N.V., 2006. Importance of recent shifts in soil thermal dynamics on growing season length, productivity, and carbon sequestration in terrestrial high-latitude ecosystems. Global Change Biology, 12(4): 731-750.

Euskirchen, E.S., Mcguire, A.D. and Chapin, F.S., 2007. Energy feedbacks of northern high-latitude ecosystems to the climate system due to reduced snow cover during 20th century warming. Global Change Biology, 13(11): 2425-2438.

Euskirchen, E.S., McGuire, A.D., Chapin, F.S., Yi, S. and Thompson, C.C., 2009. Changes in vegetation in northern Alaska under scenarios of climate change, 2003-2100: implications for climate feedbacks. Ecological Applications, 19(4): 1022-1043.

Grunzweig, J.M., Sparrow, S.D., Yakir, D. and Chapin, F.S., III, 2004. Impact of agricultural land-use change on carbon storage in boreal Alaska. Global Change Biology, 10(4): 452-472.

Hatch, E., W., 2010. Micro-hardiness Agriculture Zones in the North Star Borough, Alaska: Past and Future Scenarios, University of Alaska Fairbanks.

Helfferich, D., 2010. The local food movement in Alaska. The Statewide Voice, May (44).

Helfferich, D. and Tarnai, N., 2010. Alaska's food (in) security. Agroborealis, 41(1): 23 - 27.

IPCC (Intergovernmental Panel on Climate Change), 2007a. Climate Change 2007: Impacts, Adaptation and Vulnerability. Contribution of Working Groups II to the Fourth Assessment Report of the Intergovernmental Panel on Climate Change, Geneva, Switzerland.

IPCC, 2007b. Climate Change 2007: Synthesis Report. Contribution of Working Groups I, II and III to the Fourth Assessment Report of the Intergovernmental Panel on Climate Change, Geneva, Switzerland.

IPCC, 2007c. Climate Change 2007: The Physical Science Basis. Contribution of Working Groups I to the Fourth Assessment Report of the Intergovernmental Panel on Climate Change, Geneva, Switzerland.

Jorgenson, M.T., Romanovsky, V., Harden, J., Shur, Y., O'Donnell, J., Schuur, E.A.G., Kanevskiy, M. and Marchenko, S., 2010. Resilience and vulnerability of permafrost to climate change. Canadian Journal of Forest Research-Revue Canadienne De Recherche Forestiere, 40(7): 1219-1236.

Juday, G.P., Barber, V., Vaganov, E., Rupp, S., Sparrow, S., Yarie, J. and Linderholm, H., 2005. Chapter 14 - Forests, Land Management, Agriculture, Arctic Climate Impact Assessment. Arctic Council. Cambridge University Press, pp. 781-862.

Kane, D.L., Hinzman, L.D., Benson, C.S. and Everett, K.R., 1989. Hydrology of Imnavait Creek, an Arctic Watershed. Holarctic Ecology, 12(3): 262-269.

Kane, D.L., Hinzman, L.D., Woo, M. K. and Everett, K.R., 1992. Arctic hydrology and climate change. In: Chapin, F.S., III, Jeffries, R.L., Reynolds, J.E., Shaver, G.R., and Svoboda, J. (Editors), Arctic Ecosystem in a Changing Climate, San Diego, CA, pp. 35-57.

Kane, D.L. and Yang, D., 2004. Overview of water balance determinations for high latitude watersheds In: Kane, D. L., and Yang, D. (Editors), Northern Research Basins Water Balance, Oxfordshire, UK, pp. 1-12.

Katul, G.G., Oren, R., Manzoni, S., Higgins, C. and Parlange, M.B., 2012. Evapotranspiration: A Process Driving Mass Transport and Energy Exchange in the Soil-Plant-Atmosphere-Climate System. Reviews of Geophysics, 50.

Kenny, J.F., Barber, N.L., Hutson, S.S., Linsey, K.S., Lovelace, J.K., Maupin, M.A., 2009. Estimated use of water in the United States in 2005. U.S. Geological Survey Circular 1344, 52.

Kitaya, Y., Niu, G.H., Kozai, T. and Ohashi, M., 1998. Photosynthetic photon flux, photoperiod, and CO_2 concentration affect growth and morphology of lettuce plug transplants. Hortscience, 33(6): 988-991.

Kite, G., 2000. Using a basin-scale hydrological model to estimate crop transpiration and soil evaporation. Journal of Hydrology, 229 (1-2): 59-69.

L'vovich, M.I. and White, G.F., 1990. Use and transformation of terrestrial water systems In: Turner, B.L., II, Clark, W. C., Kates, R.W., Richards, J.F (Editors), The Earth as Transformed by Human Action on. Cambridge University Press, Cambridge, UK, pp. 235-252.

Lahoz, W.A. and De Lannoy, G.J.M., 2014. Closing the Gaps in Our Knowledge of the Hydrological Cycle over Land: Conceptual Problems. Surveys in Geophysics, 35(3): 623-660.

Liu, S.M., Xu, Z.W., Zhu, Z.L., Jia, Z.Z., and Zhu, M.J., 2013. Measurements of evapotranspiration from eddy-covariance systems and large aperture scintillometers in the Hai River Basin, China. Journal of Hydrology, 487: 24-38.

MacDonald, G.M., 2010. Global warming and the Arctic: a new world beyond the reach of the Grinnellian niche? Journal of Experimental Biology, 213(6): 855-861.

McFadden, J.P., Chapin, F.S. and Hollinger, D.Y., 1998. Subgrid-scale variability in the surface energy balance of arctic tundra. Journal of Geophysical Research-Atmospheres, 103(D22): 28947-28961.

Miralles, D.G., Holmes, T.R.H., De Jeu, R.A.M., Gash, J.H., Meesters, A.G.C.A. and Dolman, A.J., 2011. Global land-surface evaporation estimated from satellite-based observations. Hydrology and Earth System Sciences, 15(2): 453-469.

Mu, Q., Heinsch, F.A., Zhao, M. and Running, S.W., 2007. Development of a global evapotranspiration algorithm based on MODIS and global meteorology data. Remote Sensing of Environment, 111(4): 519-536.

Mu, Q.Z., Zhao, M.S. and Running, S.W., 2011. Improvements to a MODIS global terrestrial evapotranspiration algorithm. Remote Sensing of Environment, 115(8): 1781-1800.

Osterkamp, T.E., 2007. Characteristics of the recent warming of permafrost in Alaska. Journal of Geophysical Research-Earth Surface, 112(F2).

Parent, A.C. and Anctil, F., 2012. Quantifying evapotranspiration of a rainfed potato crop in South-eastern Canada using eddy covariance techniques. Agricultural Water Management, 113: 45-56.

Peltonen-Sainio, P., Jauhiainen, L. and Laurila, I.P., 2009. Cereal yield trends in northern European conditions: Changes in yield potential and its realisation. Field Crops Research, 110(1): 85-90.

Peltonen-Sainio, P., 2012. Crop production in a northern climate, FAO/OECD Workshop: Building Resilience for Adaptation to Climate Change in the Agriculture Sector, Rome, Italy.

Ruairuen, W., Zhang, M., Fochesatto, J., Sparrow, E.B. and Schnabel, W., 2014. Evapotranspiration from Subarctic Agricultural Ecosystems. In: S. Seefeldt and D. Helfferich (Editors), Sustainable Agriculture and Food Security in the Circumpolar North, Gridwood, Alaska.

Rupp, T.S., Chen, X., Olson, M. and McGuire, A.D., 2007. Sensitivity of simulated boreal fire dynamics to uncertainties in climate drivers. Earth Interactions, 11.

Seneviratne, S.I., Corti, T., Davin, E.L., Hirschi, M., Jaeger, E.B., Lehner, I., Orlowsky, B. and Teuling, A.J., 2010. Investigating soil moisture-climate interactions in a changing climate: A review. Earth-Science Reviews, 99(3-4): 125-161.

Serreze, M.C. and Francis, J.A., 2006. The Arctic on the fast track of change. Weather-March, 61(3): 65-69.

Sharratt, B.S., 1994. Observations and Modeling of Interactions between Barley Yield and Evapotranspiration in the Sub-Arctic. Agricultural Water Management, 25(2): 109-119.

Shiklomanov, I.A., 1993. World fresh water resources. In: P.H. Gleick (Editor), Water in Crisis: A Guide to the World's Fresh Water Resources. Oxford University Press, New York and Oxford, pp. 13-24.

Shulski, M., Wendler, G., 2007. The Climate of Alaska. University of Alaska Press

Smith, N.V., Saatchi, S.S. and Randerson, J.T., 2004. Trends in high northern latitude soil freeze and thaw cycles from 1988 to 2002. Journal of Geophysical Research-Atmospheres, 109(D12).

SNAP, 2008. Preliminary report to the Governor's subcabinet on climate change. SNRAS Pub. No. MP2008-06, University of Alaska Fairbanks.

Stevenson, K.T., Alessa, L., Kliskey, A.D., Rader, H.B., Pantoja, A. and Clark, M., 2014a. Sustainable Agriculture for Alaska and the Circumpolar North: Part I. Development and Status of Northern Agriculture and Food Security. Arctic, 67(3): 271-295.

Stevenson, K.T., Rader, H.B., Alessa, L., Kliskey, A.D., Pantoja, A., Clark, M. and Smeenk, J., 2014b. Sustainable Agriculture for Alaska and the Circumpolar North: Part II. Environmental, Geophysical; Biological and Socioeconomic Challenges. Arctic, 67(3): 296-319.

Stewart, B.C., Kunkel, K.E., Stevens, L.E., Sun, L. and Walsh, J.E., 2013. Regional climate trends and scenarios for the U.S. National Climate Assessment: Part 7. Climate of Alaska. NOAA Technical Report NESDIS 142-7.

Stone, R.S., Dutton, E.G., Harris, J.M. and Longenecker, D., 2002. Earlier spring snowmelt in northern Alaska as an indicator of climate change. Journal of Geophysical Research-Atmospheres, 107(D10).

Trenberth, K.E., Fasullo, J.T. and Kiehl, J., 2009. Earth's Global Energy Budget. Bulletin of the American Meteorological Society, 90(3): 311-323.

U.S. Census-Bureau, 2010. 2010 census data. http://www.census.gov/2010census/data/.

UAF-CES, 2006. The agricultural industry in Alaska: A changing and growing industry – Identification of issues and challenges. University of Alaska Fairbanks, Fairbanks.

USDA, 2014. 2012 census of agriculture: Alaska State and area data. Part 2. Geographic Area Series, 1(AC-12-A-1): 365.

Vörösmarty, C.J., Hinzman, L.D., Peterson, B.J., Bromwich, D.H., Hamilton, L.C., Morison, J., Romanovsky, V.E., Sturm, M. and Webb, R.S., 2001. The hydrologic cycle and its role in Arctic and global environmental change: A rational and strategy for synthesis study. Arctic Res. Consortium of the US, Fairbanks, AK: 84.

Walsh, J., Wuebbles, D., Hayhoe, K., Kossin, J., Kunkel, K., Stephens, G., Thorne, P., Vose, R., Wehner, M., Willis, J., Anderson, D., Doney, S., Feely, R., Hennon, P., Kharin, V., Knutson, T., Landerer, F., Lenton, T., Kennedy, J. and Somerville, R., 2014. Chapter 2: Our Changing Climate. In: J. Melillo, M.,, T.T.C. Richmond and G.W. Yohe (Editors), Climate Change Impacts in the United States: The Third National Assessment, U.S. Global Change Research Program, pp. 19 - 67.

Wang, K.C. and Dickinson, R.E., 2012. A Review of Global Terrestrial Evapotranspiration: Observation, Modeling, Climatology, and Climatic Variability. Reviews of Geophysics, 50.

Wang, K.C., Dickinson, R.E., Wild, M. and Liang, S.L., 2010. Evidence for decadal variation in global terrestrial evapotranspiration between 1982 and 2002: 2. Results. Journal of Geophysical Research-Atmospheres, 115.

Wang, S.Y., Gillies, R.R. and Reichler, T., 2012. Multidecadal Drought Cycles in the Great Basin Recorded by the Great Salt Lake: Modulation from a Transition-Phase Teleconnection. Journal of Climate, 25(5): 1711-1721.

White, D.M., Gerlach, S.C., Loring, P., Tidwell, A.C. and Chambers, M.C., 2007. Food and water security in a changing arctic climate. Environmental Research Letters, 2(4).

Woo, M.K., Kane, D.L., Carey, S.K. and Yang, D.Q., 2008. Progress in permafrost hydrology in the new millennium. Permafrost and Periglacial Processes, 19(2): 237-254.

WRI, 2000. World resources 2000 – 2001: People and ecosystems – The fraying web of life. WRI, Washington, DC, pp. 389.

Zhao, L.L., Xia, J., Xu, C.Y., Wang, Z.G., Sobkowiak, L. and Long, C.R., 2013. Evapotranspiration estimation methods in hydrological models. Journal of Geographical Sciences, 23(2): 359-369.

CHAPTER 2

An overview of methodology, field experiments and data collection in a subarctic agroecosystem in Interior Alaska

Abstract

Evapotranspiration (ET) from land surfaces is a key component of the hydrological cycle and is the only term that links water mass and energy balance. ET plays a major role in the energy and nutrient exchange in agroecosystems and affects many other ecological processes. The estimation of ET in agroecosystem is not often done in subarctic region but it is important and a basic tool to calculate water balance as well as to estimate water availability and requirements in the context of climate change. The purpose of this chapter is to describe the methodologies and field experiments that have been used to determine evapotranspiration particularly in subarctic region. The Fairbanks Experiment Farm at the University of Alaska Fairbanks, Agricultural and Forestry Experiment Station (AFES) was selected as a study site. The site is considered a baseline for Interior Alaska agricultural research conducted in the subarctic region and considered to be representative of floodplain Interior Alaska growing conditions. Meteorological and hydrological parameters were observed over the growing season 2011-2014. Several methods to measure and estimate ET ranged from sophisticated techniques to the simplest ones such as eddy covariance, energy balance, Bowen ratio, Penman-Monteith, Priestley-Taylor, lysimetry, and evaporation pan. The temporal series of hydro-meteorological variables for observing ET and data availability are also indicated. A comparative analysis of performance of the methodologies is presented here.

Keywords: Evapotranspiration, agroecosystem, subarctic, meteorological, hydrological, Penman-Monteith, Priestley-Taylor, lysimetry, eddy covariance

2.1 Introduction

Subarctic agroecosystem in Alaska lies between latitude 63° and 65° N. The environmental variables that influence crop growth and yield in this region are tightly linked to larger scale climatic forcing operating on a global scale which are then manifested regionally in several time-periods and under different hydro-meteorological configurations, climate, weather events, cloud cover, precipitation and humidity. Further influences on northern microclimates include topography and land formations (e.g. mountains, hills, and valleys), land and water cover. With climate change at high latitudes future temperatures are expected to rise even more in this region than elsewhere (Chapin et al., 2005, 2009; Walsh et al., 2008; Wolken et al., 2011). Additionally, evidence from remote sensing, ecosystem models, and surface observations have shown that the high latitude warming has increased growing seasons with changes in species composition, photosynthetic activity, and ecosystem respiration in boreal and arctic terrestrial ecosystems (Piao et al., 2008; Elmedorf et al., 2012; Xu et al., 2013; Gray et al. 2014). The response of agroecosystem to this change is uncertain and has not been forecasted.

Under changing climate, water supply for agricultural production may be impacted where 50% - 80% of water supply for human activities and agricultural production rely on snow melt water (Wand and Au, 2009) in the northern high latitudes. Specifically, the period of no precipitation, for example during summer would increase water stress and reduce agricultural production (Shratt, 1994) in subarctic region. However, a significantly longer growing season with increased soil temperature would have a positive impact on agriculture. In the meantime, it may require more water to successfully conduct farming activities. Therefore, water becomes one of the most concerning and limiting factors in agriculture.

Evapotranspiration (ET) plays a crucial role in landscapes, surface characteristics and micrometeorological factors (Drexler et al., 2004) impacting water loss from land to atmosphere in agriculture and other terrestrial ecosystems. The rate of ET depends on the water availability at the surface and the existing vegetation. The measurement of ET is essential for many applications in agriculture, hydrology and meteorology and some aspects of its role remains to be understood or has not yet been fully investigated. Because of, the large potential area for agriculture in Interior region across the area of Tanana River, there is a need for a better understanding of the hydrologic cycle and the substantial changes in ET, thermal, and moisture regime response to climate change. Therefore, the Fairbanks Experiment Farm (FEF) at the University of Alaska Fairbanks (UAF), Agricultural and Forestry Experiment Station (AFES) was selected to measure ET and other parameters over the growing seasons. A previous study has reported an average rate of 2.4 mm day^{-1} and 3.01 mm day^{-1} ET in non-irrigated and irrigated crop fields respectively in this area (Braley, 1980).

The Fairbanks Experiment Farm (FEF) at the University of Alaska Fairbanks was established by the United States Department of Agriculture (USDA) as an Agricultural Experiment Station to conduct research and promote agriculture in Interior Alaska. This site has a long history of research from a variety of disciplines. The following aspects of the FEF site make it similar to a farmland among other existing sites in the Interior of Alaska region and can be used as a baseline data for agriculture development according to: (1) geographical characteristics: FEF lies on a flat topography in the Tanana Valley, which is a large, and open basin where the main agriculture land is present; (2) the area is representative of a long history of agricultural land that has been conventionally farmed (3) Replicated experimental plots containing different land surface types were selected for studying the soil and air conditions; (4)

Existing site instrumentation through collaborations from faculties of School of Natural Resources and Extension (SNRE), College of Natural Science and Mathematics (CNSM) and Institute of Northern Engineering (INE) available on the study site included an automated meteorological station, soil temperature, soil moisture, pan evaporation, Large Aperture Scintilolometer (LAS), and an eddy covariance tower.

The aim of this chapter is to provide an overview of methodologies and field experiment, data collection, laboratory techniques that have been used to study the ET in an agroecosystem. A detailed field experiment installation as well as the description for estimating and/or measuring evapotranspiration and other related variables are presented, and the assumptions and limitations are highlighted. The meteorological and hydrological measurements during the summer growing season are also illustrated here.

2.2 Site descriptions

2.2.1 Location

The Fairbanks Experiment Farm (FEF) site is located on West Tanana Drive of the University of Alaska Fairbanks (UAF) Agricultural and Forestry Experiment Station (AFES) Fairbanks Alaska, USA (64° 51′ 16.6 ″N, 147° 51′ 36.4″ W, 150 m above sea level). It includes approximately 1.05 km^2 of cropland and 0.2 km^2 of forest land for research and demonstration projects. Figure 2-1 shows the deployment site of this study. A summer aerial photo is shown of the experiment site is located in an open, south facing plain at the base of foothills (Figure 2-1). The central field covers about 700 m in the north-south direction, and more than 1 km in the west-east direction (Fochesatto et al., 2013). This site provides physiographical and geomorphological similarity to other lowland farms in Interior Alaska but the soil characteristics do not precisely represent each farming location in the Tanana Valley in terms of aspect, slope,

soil type and management. The growing degree-days which is the heat accumulation used to estimate plant development range from 1930 to 1950 (Swenson, 2013). Figure 2-1 also illustrates the locations of the instruments used to monitor the growing condition as well as soil parameter across the croplands. The instrumentation used as well as the installation process is shown in Figure 2-2. More information about the study site can be found in (Ruairuen et al., 2015)

2.2.2 History

The research site was part of the Alaskan Boreal forest comprised mainly of black spruce [*Picea mariana* (Mill.) B.S.P.] species and cleared to be cultivated before 1952 (Sharratt, 1990). The site has a long history of agricultural management and research conducted for more than 100 years. In the past, large quantities of manure have been used as a supplement nutrient (Van Veldhuizen and Knight, 2004); as well the land had long term tillage and crop residue management practices (Sharratt, 1998).

2.2.3 Climate

The research area experiences a continental subarctic climate, with long, cold winters and short, warm summers. The climate is characterized by large daily and annual temperature ranges, low humidity, and relatively low precipitation. Thirty-year (1981-2010) meteorological data recorded at nearby station indicated that the long-term mean air temperature was -0.5°C during spring (March, April, and May), 15°C during summer (June, July, and August), -4.5°C during fall (September, October, and November), -18°C during winter (December, January, and February), and -2.4°C during the full year. The coldest month is January having -25°C average of temperature, while the warmest month is July having an average temperature of 22 °C. Mean precipitation was 10 mm $month^{-1}$ during spring, 46 mm $month^{-1}$ during summer, 22 mm $month^{-1}$ during fall, 14 mm $month^{-1}$ during winter, with about 1,651 mm $year^{-1}$ of snow fall (The Alaska

Climate Research Center; http://climate.gi.alaska.edu/Climate/Normals). Snow covers the area continuously from mid- or late October to mid-April or early May. Daylight hours vary from under 4 hours in the winter to approximately 22 hours in the midsummer (Shulski and Wendler, 2007). Break up for the area rivers is around the end of April or first week of May, with green-up for vegetation coming during the second week of May. The growing season is about 115 days long and the abundance of daylight allows for vegetables that can grow to impressive sizes. The end of the growing season is around early September (Shulski and Wendler, 2007). Winds are generally quite light in this area but high winds can be found in the summer months however surface winds average less than 2±0.5 m s^{-1} (Calculated from a 3 year data in this study). The prevailing wind is from northwest over the summer month.

2.2.4 Soil

The soils were cleared of black spruce vegetation in the 1940s at Fairbanks (Sharatt 1994). According to soil surveys, the soil in the farmland is classified as a Tanana silt loam (loamy, mixed, nonacid Pergelic Cryaquept) and contains alluvial soil in the flood plains of the Tanana River (Mulligan, 2004). This soil has a water storage capacity of 0.25 m^3 m^{-3} for the 0 to 10 cm depth and 0.2 m^3 m^{-3} below 10 cm (Sharatt, 1994). The value of field measured of thermal conductivity at field capacity (-0.3 bars) was 0.9 W m^{-1} °K and at wilting (-15 bars) was 0.6 W m^{-1} °K with an estimated saturated hydraulic conductivity was approximately 0.002 cm s^{-1} at 2-8 cm depth (Sharratt, 1990). In addition, soils contain a relatively high concentration of calcium carbonate and calcium sulfate at the surface (Van Veldhuizen and Knight, 2004). High organic matter content is found at the plow layer (at 0-15 cm depth) and decreases rapidly below this depth (Mulligan, 2004). A perched water table above the permafrost is about 8 m deep while the main water table is located about 20 m deep (Van Veldhuizen and Knight, 2004). The

existing soil moisture comes from the snow melt or residual moisture from the previous year that is need for successful seed germination and seeding establishment in the experiment site (Van Veldhuizen and Knight, 2004).

2.2.5 Vegetation

The farm field has three main vegetation types: woodland, grassland and crops, combined with fallow (bare land). Crops were planted into soil that had been summer fallowed the previous season. Some vegetables crops are usually grown under irrigation to improve and control crop growth allowing better use of the available plant nutrients (Van Veldhuizen and Knight, 2004). Most of the vegetation in the farm is uniformly spaced according to established crop management practices and planted on the same day. For example, barley (*Hordeum vulgare*) is planted in a 1 m wide swath of 6 rows about 15 cm apart, resulting in a closed canopy (Swenson, 2013). Smooth bromegrass (*Bromus inermis* Leyss.) is an important perennial forage grass and dominant in the farmland under no till management. The young black spruce trees are around the corner of the field at the northern-east and southern-east direction and represent a very small fraction of the total farm area.

2.3 Field instrumentations and environmental measurements

2.3.1 Calibration

Calibration of a given instrument can be obtained by collocating the instrument against another of known accuracy under the same environmental conditions or by measuring a physical process in which all his properties are perfectly know for example at all times. In addition basic checks can be carried out to detect any major failure of sensors, such as a visual check anemometer/wind vane, rain collector, and cleaning the instrument before installing in the field. Calibration temperature sensor was done by comparing the value recorded from the sensor with

the reading from a calibrated thermometer. The nominal accuracy in such sensor must be known and this must be greater than the sensor being calibrated. The thermometer the sensor can be calibrated in an isolated chamber together with the sensor from which the calibration is known. Starting the processes of acquiring data to produce the calibration curve has obtained after the sensor thermalization. Other sensors from the meteorological station can be done the same approach or by comparing the recorded data with standard weather station nearby. In addition, the sonic anemometer was calibrated by the manufacture before using in the field.

2.3.2 Meteorological data collection

The main meteorological station in this study is located in the central part of the FEF, which is shown in Figure 2-1. The automatic meteorological stations used to measure the atmospheric parameters is the Davis Instrument Vantage Pro2 weather station (http://www.davisnet.com). It includes display console/receiver, Integrated Sensor Suite (ISS), and mounting hardware. The ISS combines a rain collector, temperature and humidity sensors, and anemometer all into one package (Davis Hayward, CA). Data measurement are given in Table 2-1. Details about the setting can be found in Ruairuen et al. (2015).

Additionally, three micrometeorological stations over barley field, smooth bromegrass, and fallow field have been equipped with three replicate stations to provide air temperature above the ground 1.5 m, surface temperature, and soil temperature at 5, and 15 cm depths. Monitoring the soil temperature at these two depths are related to the requirement of germination and root growth for crops (Gilessman, 2007).

A standard weather bureau Class A evaporation pan (122 cm diameter by 25 cm height) located approximately 5 m away from agro-meteorological station was used to measure manually (hook gage) and determine daily time series of potential evaporation (E_P). The water level in the

pan was maintained within 7.5-12.5 cm of the lip. The evaporation pan is made of aluminum and rests on a wooden platform 12 cm above the ground over non-irrigated grass around the area. Daily Ep measurements were collected at 0800 (Alaska Standard Time (AKST)) systematically every-day from 20 June to 5 September 2013 and corrected by wind observations atop the pan evaporation in which the anemometer has integrated counter.

2.3.3 Eddy covariance installation

An eddy covariance (EC) is considered the most reliable and advanced method of measuring local scale surface energy fluxes. In this study, EC instrument is installed at the research site (Figure 2-1). The EC instrument was installed at 3 m above ground with a three-dimensional (3D) sonic anemometer (RMYoung 81000) mounted at 3.5 m above the ground to measure turbulence, the three components of the wind flow vector (u, w, v) and temperature. The EC tower was installed in the middle of LAS path approximately 500 m away from the LAS-receiver. Data was sampled at 20 Hz frequency and fluxes were calculated for a 30-min eddy-covariance average period. In addition, two temperature probes (PT 107 Campbell Scientific) also mounted to EC tower at 1 m and 3 m above the ground to determine air temperature (Table 2-1). Micrometeorological variables such as net radiation (R_{net}) was measured by a net radiometer (NRLite net radiometer) mounted at 3 m above the soil surface and oriented to the south to avoid shade at all times. A barometer (CS106, Campbell Scientific) was placed 30 cm above the ground surface for measuring the air pressure. A CR1000 logger (Campbell Scientific, Inc, Logan, UT) data logger was used to recorded data from EC system. Micrometeorological variables were sampled on a data logger every 1 minute and then averaged every 30 minutes. Additionally, two soil temperature probes were used to record every minute soil temperature at 15 and 30 cm depths in summer 2012 while four probes were buried at 5, 10, 20, and 30 cm

depths in summer 2013 and summer 2014 at EC station (Table 2-1). The soil temperature is used to estimate the ground heat flux at the EC station.

2.3.4 Large aperture scintillometer installation

The Scintec BLS-900 LAS was deployed at the FEF in summer 2012 and 2013 (Figure 2-1). This instrument uses a combination of a pulsed eye-safe near-infrared diodes system emitting at 880 nm wavelength and a refractive telescope receiver located 1 km distance. The LAS beam was placed in the orientation east-west across the farmland. The LAS receiver collects temporal variations of the optical pulses as they travels through the turbulent medium. The presence of gradient temperature in the surface layer introduces changes in the refractive index of the air at the emission wavelength causing space and time fluctuations of the optical intensity known as scintillations. These scintillations are measured in the mean and standard deviation to then be converted into turbulent refractive index structure $C_N^2(m^{-\frac{2}{3}})$ (Gruber and Fochesatto, 2013; Fochesatto et al., 2013). This integrated value across spatial scales allows calculating the area-averaged H in the atmosphere by using the equation defined by the Monin-Obukhov Similarity Hypothesis (Sorbjan 1989). The heights of the LAS emitter and receiver were set to 1.8 m over a flat grass-covered surface.

2.3.5 Doppler acoustic sounder

A doppler sodar, Remtech model PA2 was used to determine the vertical structure and flows in the surface boundary layer (SBL) during some periods of this present study. The sodar works at the central frequency of 2 kHz and consists of a monostatic antenna of 196 speakers over ~1.7 m^2 of effective collection area. The acoustic backscattering is measured continuously at a 10-m resolution, with a 10- to 15-min integration period above 20 m height. The sound wave time-of-flight back to the antenna indicates the height at which the backscatter occurred. This

intensity depends on the turbulent structure of the atmospheric boundary layer (ABL) and, due to the instrument's monostatic configuration, is only sensitive to the thermal structure of turbulence (C_T^2) depicting the ABL structure in great detail (Holmgren et al., 1975; Neff, 1975; Brown and Hall, 1978). The top height of the stable inversion layers and other elevated inversion layers (Mayfield and Fochesatto, 2013) can be retrieved by processing the sodar backscatter profiles (C_T^2) and searching for the 50 % decay of the backscatter pulse intensity above the maximum of thermal turbulence intensity according to Beyrich and Weill (1993) and Emeis and Türk (2004).

2.3.6 Lysimetry installation

The lysimeter approach is widely used for field work, especially for agronomic research (Verstraeten et al., 2008). The lysimeters are used to measure ET from vegetated surfaces and bare soil during summer 2012 and 2013 at the FEF. The lysimeters were constructed and installed since 2009 at the farmland adjacent to grass fields. Each lysimeter was built of a 62 cm length, 62 cm width, and a depth of 62 cm. The bottom of these lysimeters were perforated with 0.5 cm diameter holes to allow for drainage of any exceed moisture. A geofabric was placed over these holes to prevent the loss of soil particles. The base layers 15 cm of stones, gravel and mixture of sand-silt is then placed with layer of geofabric above to separate the soil from the filter layer. The base layer kept the soil from spilling into the drainage, helped to drain water during heavy rains or irrigation events, and reduced bias resulting from capillary effects in the drainage system. A pipe collected the drainage from the lysimeter bottom. Twelve of these lysimeters were filled with the lawn mix soils (sandy loam; 66% of sand, 29% of silt, and 5 % of clay) were filled and tamped for each 10 cm of soil profile in the lysimeters in the summer 2012. To bring the soil moisture status at field capacity (FC), drip irrigation was then applied to all lysimeters until continuous drainage occurred.

2.3.6.1 Lysimeter studies in summer 2012

A total of two 10HS soil moisture sensor (S-SMD-M005, Decagon Devices Inc., Pullman, WA) were deployed at 15 and 30 cm in six lysimeters to measure the soil volumetric moisture content (θ_{ly}). The lysimeter profiles in summer 2012 are depicted in Figure 2-3a. The 10HS has two 14.5 cm long prongs, spaced 3.3 cm, while ECH_2O EC-5 has two 8.9 cm long prongs, spaced 1.8 cm. The soil moisture sensor is capable of measuring volumetric saturations between 0% - 57% of θ with an accuracy of $\pm$ 0.033 m^3 m^{-3} ($\pm$ 3 %) (Decagon Devices, 2012). Data were then recorded by a HOBO U30 station data-logger (Onset Computer Corporation, Bourne, MA) with a sample rate of 1 second and record interval of 15 minutes. Data were averaged to 1 hour for the analysis. The soil water potential called watermarks 200ss sensor (Irrometer Co., Inc., Riverside, CA) was also installed parallel with soil moisture sensor in each lysimeter at 15 cm depth.

Only two lysimeters have been set with two watermark sensors at 15 and 30 cm depths. Data was recorded every 15-minutes by a Watermark monitor 900M data logger (Irrometer Co., Inc., Riverside, CA). The S-TMB-M006 soil temperature probes (Decagon Devices Inc., Pullman, WA) and HOBO 12-Bit Temp Smart Sensor (Onset Computer Corporation, Bourne, MA) were installed at 5 and 15 cm depths below the soil surface in lysimeter number four as well as at 15 cm and 30 cm depths in lysimeter number nine. The lysimeters were direct seeded with lettuce (*Lactuca sativa*) on 8 June 2012. Soil moisture content in each lysimeterr was maintained at or near field capacity throughout the growing season. This corresponded to a moisture content of 50% percent. This was accomplished by reading from watermark. The amount of drainage collected was measured from all lysimeter weekly or after heavy precipitation events. Drip irrigation was performed within all lysimeters throughout the 2012

growing season. The change in soil moisture storage, the drainage and any precipitation and irrigation was determined to be the evapotranspiration loss from the lysimeter based on the energy balance approach.

Gravimetric soil moisture measurements by means of the oven drying method (Gardner, 1986) was used as a standard calibration against the measurement by sensor at the 0-30 cm depths before planting and after harvesting in summer 2012. This method is widely used for directly determining soil moisture content (Schmugge et al., 1990). The gravimetric sample was collected with the gouge auger (diameter 0.19 cm, length 60 cm). A total of three soil samples were collected from lysimeter plot and placed in the metal cans with tight fitting lids. These samples were transferred to the laboratory for analysis. The samples were weighed immediately and then placed in a drying oven at 105 °C with the lid off, and dried for 24 hour, and re-weighed to determine the mass of water and mass of the soil solids. The water content is calculated by subtracting the oven dry weight from the initial field soil weight (Lunt et al., 2005). When multiplied by 100 and divided by the soil oven dry weight, this becomes the percentage of water in the sample on a dry-mass (dry weight) (Appendix A-1).

2.3.6.2 Lysimeter studies during summer 2013

During 2013 growing season, two treatments of lysimeter were used to determine the loss of evapotranspiration from irrigated lysimeter. Each treatment was replicated on three lysimeters. The use of three lysimeters allows obtaining replication of same observations in order to ensure the quality of data by reducing missing-data and instrumental malfunctioning errors. The plot treatments were: (i) vegetated lysimeter (VL) and (ii) unvegetated lysimeter (UVL). A total of three 10HS soil volumetric moisture sensors were installed at 5, 10, and 20 cm depths to measure the volumetric soil profile moisture in VL treatment (Figure 2-3b). Data were recorded by a

HOBO U30 station data-logger (Onset Computer Corporation, Bourne, MA) with a sample rate of 1 minute and record interval of 30 minutes. While ECH$_2$O EC-5 moisture sensor (S-SMC-M005; Decagon Devices Inc., Pullman, WA) were deployed at the same depth in UVL treatments with the data collected by a HOBO Micro Station H21-002 data logger (Onset Computer Corporation, Bourne, MA). This soil moisture sensor is capable of measuring volumetric saturations between 0-0.55 m^3m^{-3} with an accuracy of ± 0.031 m^3m^{-3} (± 3%) (Decagon Devices Inc., 2012). Soil temperatures (S-TMB-M006) probes were measured at 5 and 10 cm depths within VL.

The soil water potential instruments were also placed parallel with soil moisture sensor in each treatment at 5 and 10 cm depths. Oak leaf lettuce (*Lactuca sativa*) was transplanted at the five to six-leaf stage within VL on 1 June, 2013. The UVL was maintained without any weed or plant in the lysimeter throughout the period of study. Weekly drainage was collected from each lysimeter. Drip irrigation was performed throughout the 2013 growing season in both treatments with the same water level in order to maintain the system in the same water condition. Irrigation amount ranged from 5.5 mm to 20 mm. Gravimetric soil moisture was also determined before planting and after harvesting this 2013. (Table 2-2).

2.3.7 Soil volumetric water content and temperature in the farmland

In the farm field, 10HS and ECH$_2$O EC-5 (S-SMC-M005; Decagon Devices Inc., Pullman, WA) sensors were installed at soil depths 15 cm in summer 2011-2012 and at 5, 10, and 20 cm depths in summer 2014 in the barley, bromegrass, and fallow field (Table 2-1). The number of soil moisture sensors installed was 3 sensors per plot, giving a total of 9 sensors for the 3 plots in 2011-2012. The data were collected by HOBO U30 station and HOBO Micro Station H21-002 data logger (Onset Computer Corporation, Bourne, MA) with a record interval

of 1 hour in summer 2011-2012 and 30 minute in summer 2014.The sensors had been calibrated for this soil by using a conventional method as described in section 2.3.1. The volumetric measurement was also validated with the gravimetric measurements. Soil moisture monitoring started in May and ended in September. In addition, biweekly soil gravimetric moisture across the farmland also obtained at 0- 30 cm in summer 2011 (Appendix A-2).

The soil temperature collected in each plot was used to investigate the ground heat flux from different surface types. The soil temperature sensors (S-TMB-M006, Onset Computer Corporation, Bourne, MA) were installed at surface and soil depths 5, 15, and 30 cm during summer 2011 - 2013. The number of soil temperature sensors installed was 9 sensors per plot, giving a total of 27 sensors for the 3 plots. Data loggers (HOBO U12-006 4-channel External data logger) were installed to record and store data automatically at 1- hour interval. On the other hand, the soil temperature sensors were installed at the surface and soil depths 5, 10, 20 cm with the data recording of 30-min intervals in summer 2014. Soil temperature monitoring commenced in May and ended in September, covering the summer periods in this region.

2.3.7 Determination of soil bulk density

Bulk densities (ρ_b) is the ratio of the mass of dry soil to the bulk volume of the soil. It was determined through the use of soil core sampler method as described by Blake and Hartge (1986) with 17 cm in diameter and 14 cm deep (with a volume of about 3176 cm^3). While lysimeter soil samples were collected using cores with a volume of about 154 cm^3. In this method, a cylindrical metal sampler is pressed downward or driven into the soil to the desired depth. The sampler core is carefully removed to preserve a known volume of sample. A shovel, alongside and under the sampler are required to remove the sample without disturbance. The three replications at 0-30 cm were collected from three experimental plots in the farmland.

Samples were kept in sealed plastic cases and transported to the laboratory for analysis. The soil cores were oven-dried at 105 °C for 48 h to determine the bulk density (Table 2-3), the ratio of the mass of dry soil and volume of the cylinder determined (Blake and Hartge, 1986). Soil sampling in all plots was done in August in summer 2012 growing season for the determination of soil bulk density.

2.3.8 Soil texture

Soil texture was determined using particle-size analysis with a hydrometer (Gee and Bauder, 1986). The method allows for nondestructive sampling of suspensions undergoing settling. The hydrometer method has multiple measurements on the same suspension. Therefore, the detailed distribution of particle-size can be obtained. The soil texture of three replicate samples at 0-15 cm from each plot were determined using a Bouyoucos hydrometer with 50g of suspended sediment in 990 mL of water and 10 mL of sodium- hexametaphosphate. . Details of the procedure can be found in Gee and Bauder (1986). Soil texture is one of the most stable soil characteristics and is expected to be similar throughout management types (Gliessman, 2007). The soil texture data from different sites are shown in Table 2-3.

2.3.9 Soil water characteristic analysis

2.3.9.1 The soil water characteristic at field capacity

The field capacity (FC) represents the upper limit of soil moisture used by plants in well-drained soils. It is approximately equal to the water retained by a soil at a soil moisture tension of 0.3 bars or 1/3 atmosphere (0.03 MPa). Falcon 7013 filtration apparatus w/rubber gaskets and filter cups were used to determine the soil moisture at field capacity (0.3 bars). Air dried soil at a constant weight was used for this experiment. Soil samples are oven dried at a maximum of 60 °C until constant weight is attained. Soil was sieved through a 2 mm screen to remove all large

rocks, roots and other organic matter. The sieved soil sample is mixed to make as homogenous a sample as possible. Soil samples are brought to FC using a Falcon 7013 filtration apparatus with Millipore membrane filter paper (47 mm diameter) shinny side up. A representative 100 g sample of soil is added onto a filter apparatus, 75 mL of distilled water added bringing the soil to saturation, gently tapped to remove any air bubbles, and let sit for 1 hour. Hook up the vacuum line to the manifolds and turn on the pump set at 9.75 psi on the gauge (20 in Hg, 0.3 bars), and let it run for 3 hours. Continually check for soil drying out and cracking. Remove any filter apparatus from the manifold when the soil stops dripping. Replace the filter with a plug in the Tygon tubing to maintain vacuum pressure on the remaining filters. Once the soil is at field capacity, let the filter with soil sit overnight. The gravimetric method is used to determine the soil moisture content at FC.

2.3.9.2 The soil water characteristic at 1, 5 and 15 bars

The pressure plate and pressure membrane apparatus methods (Cassel and Nielsen, 1986; Klute, 1986) were used to determine the soil water characteristic. The pressure plate apparatus contains a pressure chamber enclosing a water saturated porous plate, which allows only water flow through its pores. The bottom of the porous plate is at atmospheric pressure condition, while the top surface is under condition the applied pressure of 1 bar, 5 bars, and 15 bars (wilting point) to the chamber.

The ten soil samples from lysimeter plots were used to determine the SWC curve. First, air dry soil samples to a constant weight for a week, and oven dry at a maximum 60 °C until a constant weight is attained. Sieve all soil samples through 2 mm screen, place in retaining rings in contact with the porous plate and allow saturating by immersion in water. The porous plate with saturated soil samples is then placed in the chamber and a known air gas pressure is applied

to force water out of the soil through the plate. Water flows out of the soil until equilibrium between the force exerted by the air pressure and the force by which soil water is being held by the soil- the matric potential is attained. The soil samples are removed from the apparatus after equilibrium between soil matric potential and the applied air pressure. Weigh the wet soil and dry in the oven at 105 °C for 24 hours and re-weigh the dried soil to determine the mass water content gravimetrically. These values were then converted to volume water contents through the bulk density. Then, two levels of nonlinear relationship (fit option: Levenberq-Marquardt) were applied to determine the SMC curve over the range 0.3 -15 bars.

2.3.11 Soil thermal properties

Soil thermal properties include thermal conductivity and resistivity, specific heat and thermal diffusivity are required to conduct analysis and modeling associated with numerous agricultural application. Thermal conductivity is one of the important thermal properties know to vary a function of soil moisture content. In this study, a Decagon Devices KD2 Thermal Properties Analyzer was used to record all thermal properties of the soil under different plots in the farmland. The KD2 Analyzer consists of a handheld controller and sensors that can be inserted into the soil medium. The handheld controller has a LCD display and key pad, which allows the user to test manually or automatic reading. This sensor is a 60-mm length with a diameter of 0.9 mm sensor. The single-needle sensor is capable of measuring thermal conductivity, thermal resistivity, and thermal diffusivity in the same time. Data of thermal properties is shown in Table 2-2.

2.3.12 Other Data

Amounts of organic carbon and nitrogen in the soil samples from lysimeters (Table 2-3) were determined by a TruSpec CN Carbon/Nitrogen Determinator (LECO Corporation, USA).

The soil samples which were sieved through 2 mm size screen were dropped into a 950 °C hot furnace and flushed with oxygen for very rapid complete combustion. Oxygen was mixed with the combustion gases, and then purged through a CO_2 infrared detector. When the gases equilibrated, carbon was measured as carbon dioxide by a CO_2 detector. The gases were transferred to a helium carrier flow and swept through hot copper to remove oxygen, changed NO_X to N_2, and removed carbon dioxide and water. A thermal conductivity cell was used to determine the nitrogen content.

Furthermore, weekly leaf area index (LAI) data, which is an estimate of the ratio between the total leaf surface area and the surface area of the ground it overlays, were collected with the AccuPAR Par80 linear PAR/LAI ceptometer of Decagon Devices (Table 2-1). LAI measurements were acquired weekly once plant emergence had occurred. The AccuPAR Par80 has 80 photosynthetic active radiation sensors along a 1m wand. Each week three consecutive measurements were collected and averaged across all 80 sensors. These measurements produced weekly average from 9 sample average for each plot (Appendix A-3).

2.4 Methods to measure and estimate evapotranspiration

ET is the water transferred from the land surface to the atmosphere by the combined processes of evaporation (E) from the bare soil and plant surface, surface water bodies, sublimation of snow and ice, etc. and transpiration from vegetation or any other moisture-containing living specie (Verstraeten et al., 2008). Consistently estimation of ET is important to determine the management of water resources efficiently, design irrigation systems and irrigation regimes, and calculate crop yield (Allen et al., 1998; Kool et al., 2014) in agriculture. Because of, water use for irrigation practices in agriculture land accounts for about 70% water use on the global basis (Bates et al., 2008).

A number of methodologies have been developed to measure ET or components of ET. The ET can be measured directly using weighing lysimeter or by means of the eddy covariance technique (Ivans et al., 2006), or indirectly from change in soil moisture or via the surface energy balance such as Bowen ratio (Fritschen and Simpson, 1985; Angus and Watts, 1984), respectively. In addition, there are techniques to estimate either evaporation (E), such as soil heat pulse analysis and surface chamber systems (Denmead, 1984) or transpiration (T), including sap flow methods (Wilson et al., 2001; Wullschleger and King, 2000), plant chamber systems, and isotopic tracers (Denmead, 1984), etc.

ET can also be estimated indirectly using empirical models. Based on the working principle or driving meteorological variables, the current ET models are categorized into Monin-Obukhov similarity hypothesis (Wang and Dickinson, 2012), temperature based approaches (Hargreaves equation) (Hargreaves and Allen 2003), radiation based approaches (Priestley-Taylor) (Priestly and Taylor 1972), and combination equations including resistance type approaches (Penman_Monteith equation) (Bormann, 2011).

Furthermore, there has been significant interest in and progress towards deducing area-average values of surface fluxes for large scale areas. Large-scale flux measurement methods include scintillometry (e.g. De Bruin et al., 1995), thermography using remotely sensed radiometric surface temperature measurements, airborne eddy correlation (Shuttleworth, 1991; Savige et al,. 2005) ground and airborne lidar (light detection and ranging) (e.g., Eichinger and Cooper, 2007).

The following methods (direct and indirect measurements of ET) were applied to estimate the ET rate in this study.

2.4.1 Drainage lysimeters *(*Hydrological approach)

A lysimeter is a method to determine ET directly. The lysimeter are tanks buried in the ground to measure the percolation of water through the soil layer. This method has been used extensively to provide baseline information for development, calibration, and validation of ET methods (Doorenbos and Pruitt, 1977; Wright, 1982; Allen et al., 1989; Jensen et al., 1990). However, lysimeter measurements of ET are sensitive to environmental factors, many of which are often poorly understood or have been ignored in practice. Lysimeter measurements are point measurements, representing measurements of ET from areas generally ranging from 0.05–40 m^2 and a common usage of it has been to characterize ET for large areas.

Drainage lysimeter (or non-weighting lysimeter) operate on the principle of conservation of mass in one dimension and on the principle that ET is equal to the amount of precipitation and irrigation water added to the system, minus percolation, runoff and soil moisture changes. To calculate the ET using lysimeter, the soil water balance equation is required to be applied:

$$ET = P + I + C_r - D - R \pm \Delta S \qquad \text{Eq. (1)}$$

where ET is evapotranspiration (or latent heat) that include canopy interception or wet canopy evaporation and plant transpiration (i.e. dry canopy transpiration), P is precipitation, I is irrigation, C_r is capillary raise (contribution from water table upward), D is the drainage, R is the runoff and, ΔS is the soil water storage in the soil layer. All terms are expressed in millimeter of water in the crop root zone per unit time (C_r and R were supposed to equal zero). Mass balance requires precipitation as the primary input and consequently the ET estimate can only be as accurate as the precipitation estimate. Soil water storage between two dates (i and f) is:

$$\Delta S = S_f - S_i \qquad \text{Eq. (2)}$$

where S_f is the soil water content at day two and S_i the initial soil water content (day one).

This approach's lack of precise ET measurements because it is difficult to accurately measure all the term of Eq. (1). However, this method is applicable to small plot or large basin and may cover from a week to a year (Rana and Katerji, 2000).

Beside precipitation, the irrigation term is another input in agricultural land which can be obtained from the measurement by the instrument while all other term in Eq. (1) need to be measured or estimated. Runoff term R can be neglected (e.g. Holmes, 1984) in arid and semi-arid region with a flat terrain, however, it depends on the occurrence and characteristics of precipitation (amount, duration, and intensity) and can only be neglected for a particular type of soil (Jensen et al., 1990), i.e. coarse (sand and loamy sand) and moderately coarse (sandy loam). On the other hand, drainage (D) is the most unknown term in Eq. (1) and it depends on the soil depth, slope, permeability and surface storage (Jensen et al., 1990; Parkes and Yuanhua, 1996), the climate and weather. A weekly or greater scale of D is suggested by Allen et al. (1991) to estimate ET. In general, this method strongly depends on time and scales of the soil moisture measurements (Burrough, 1989) and on the representativeness of the soil sampling (Leenhardt et al., 1994).

2.4.2 Evaporation pan

Evaporation pans (Ep) have been used to measure evaporation for over a century. The pan is regularly filled to a specified height, and the water loss (equal to evaporation) noted. The Class-A pan is considered to be the standard international pan. Daily evaporation pan is derived from a mass balance equation, Eq. (3)

$$E_p = D_{t-1} - D_t + P - L \pm e \quad \text{Eq. (3)}$$

where D_t is current day depth of water in the pan and D_{t-1} is previous day depth of water, measured from the top; P is precipitation over the pan; L is other losses such as animal consumption; and e is errors.

The rate of evaporation depends on the type of pan, type of pan environment, method of operating the pan, exchange of heat between pan and ground, solar radiation, air temperature, wind, and temperature (Jones, 1992). The Ep rates are different from evapotranspiration rates. Allen et al. (1998) relate the reference evapotranspiration to the Ep using an empirically derived pan coefficient (Kp).

This value depends on the type of pan as well as the environment that the pan is located. The pan coefficient for a US Class A pan is ~0.7 (Stanhill, 1976). Therefore this Kp value is applied to this study. The Ep values were used for the determination of potential of evapotranspiration for the study site.

2.4.3 Penman –Monteith equation

The most widely applied combination equation based ET model is the Penman-Monteith (PM) equation, which is based on meteorological data, aerodynamic resistance and canopy resistance. This methodology measures the latent heat flux using the vapor pressure deficit (VPD), the slope of the saturated vapor-pressure curve and aerodynamic resistance to heat, and canopy resistance, soil heat flux, and sensible heat flux. The measurements of air temperature, relative humidity, and wind speed are needed to determine these variables. However, obtaining reliable values of canopy resistance is complicated and therefore for certain situations limits application of the PM equation (Jarvis and McNaughton, 1986).

According to Allen et al. (1998), Eq. (4) describes the Penman-Monteith (PM) method to estimate ET over a vegetation stand.

$$\lambda ET = \frac{\Delta(R_{net} - G) + \rho_a C_p (e_s - e_a)/r_a}{\Delta + \gamma(1 + \frac{r_s}{r_a})} \quad \text{Eq. (4)}$$

where ET is the latent heat flux of evapotranspiration (mm h^{-1} or mm day^{-1}), λ is latent heat of vaporization (kJ kg^{-1}), Δ is the slope of saturation vapor pressure versus temperature curve (kPa $°C^{-1}$), R_{net} is net radiation flux (W m^{-2}), G is ground heat flux (W m^{-2}), ρ_a is the air density (kg m^{-3}), C_p is the air mass specific heat (kJ kg^{-1} $°C^{-1}$) at constant pressure, e_s is the saturation vapor pressure at ambient air temperature (k Pa), e_a is the actual vapor pressure of the air mass (k Pa), $e_s - e_a$ is the vapor pressure deficit (VPD) (kPa), γ is the psychometric constant (kPa $°C^{-1}$), r_a is the aerodynamic resistance (sm^{-1}), and r_s is the bulk surface resistance to vapor transport (sm^{-1}).

A convenient, empirical equation for computing the saturation vapor pressure from temperature is given by,

$$e_s(T) = 0.6108 exp\left(\frac{17.27\,T}{T + 237.3}\right) \quad \text{Eq. (5)}$$

$$e_a = e_s(T)\frac{RH}{100} \quad \text{Eq. (6)}$$

where T is air temperature (°C) and RH is relative humidity in (%)

The slope of the saturation vapor pressure (Δ) curve is also a function of temperature and can be calculated based on Eq. (7).

$$\Delta = \frac{4098\left[0.6108 exp\left(\frac{17.27\,T}{T + 237.3}\right)\right]}{(T + 237.3)^2} \quad \text{Eq. (7)}$$

The vapor pressure deficit is the difference in vapor pressure between saturated and ambient air,

$$VPD = e_s(T) - e_a = \frac{e_a}{RH} - e_a \quad \text{Eq. (8)}$$

The psychometric constant (γ) in $Eq.(4)$ is a function of atmospheric pressure (which varies slightly over time and altitude) and is given by Eq. (9):

$$\gamma = \frac{C_p P}{\varepsilon \lambda} \quad \text{Eq. (9)}$$

where C_p is the specific heat at constant pressure, equal to 1.013 (MJ kg^{-1} °C^{-1}), λ is the latent heat of vaporization 2.45 (MJ kg^{-1}), ε is the ratio of molecular weight of water vapor/dry air = 0.622, and P is the ambient air pressure (kPa).

The difficulty in using Eq. (4) is related to the derivation of r_a and r_s which already emphasized.

The aerodynamic resistance (r_a) is evaluated by the following formula Allen et al.(1998), assuming that r_a is equal to the conductance for momentum, and the wind speed profile in the atmosphere is close to neutral,

$$r_a = \frac{ln\frac{(z_m - d)}{z_{om}} ln\frac{(z_h - d)}{z_{oh}}}{k^2 u_z} \quad \text{Eq. (10)}$$

where r_a is aerodynamic resistance (sm^{-1}), z_m (m) is height of the wind speed measurements, z_h (m) is the height of temperature and humidity measurement, k is von Kármán constant (0.41), u_z (m s^{-1}) is wind speed measurement at z_m, d (m) is zero plane displacement height of wind profile, z_{om} (m) is roughness parameter for momentum, z_{oh} (m) is roughness parameter for heat and water vapor. Reference values recommended in the literature are $d = 2/3h_c$, where h_c crop height in meters is; $z_{om}$is $0.123h_c$, and z_{oh} is 0.1 (Allen et al., 1998). The Eq. (4) is restricted

for neutral stability conditions, i.e. where temperature, atmospheric pressure, and wind speed velocity distribution follow nearly adiabatic condition (no heat exchange). The equation of short time period (hourly or less) may require the correction for stability.

The bulk surface resistance (r_s) describes the resistance of vapor flow through the transpiration of plant leaves and evaporation from the soil surface and it is one of the most diffuse methods of estimating. During the period of vegetation not completely covering the soil, the resistance factor will include the effects of soil evaporation and if the vegetation is not transpiring at the potential rate, the resistance depends also on water availability for vegetation, and in this case it is proposed the use of the following approximation:

$$r_s = \frac{r_l}{LAI_{active}} \qquad \text{Eq. (11)}$$

where LAI_{active} is 0.5 times the measured leaf area index, rl is bulk stomatal resistance which is the average resistance of an individual leaf and can be measured using an instrument called a porometer.

Another way it can be estimated is through the inversion of the Penman-Monteith equation using:

$$r_s = \frac{\rho_a C_p (e_s - e_a) + r_a(\Delta(R_{net} - G) - \Delta\lambda ET - \gamma\lambda ET)}{\gamma\lambda ET} \qquad \text{Eq. (12)}$$

Here, the notation are as described earlier. However, this method cannot be used for determination of ET.

The bulk surface resistance can also be calculated using the Bowen ratio incorporation with the inversion of the Penman-Monteith equation as follow:

$$r_s = r_a\left(\frac{\Delta s}{\gamma}\beta - 1\right) + \frac{\rho_a C_p (e_s - e_a)}{\gamma\lambda ET} \qquad \text{Eq. (13)}$$

Accurate prediction of r_s requires a good estimate of the Bowen ratio.

To perform the evapotranspiration calculation using the Penman-Monteith equation, the following daily data are required: mean air temperature, the relative humidity or mean dew point (or dry and wet bulb temperature), measurement of net radiation or measurement of sunshine hours and cloud cover (from which net radiation can be modelled), aerodynamic and bulk surface resistance terms for the crop being analyzed, mean wind velocity at a standard height (if required for the aerodynamic resistance term), and ground heat flux. Unfortunately, it is not possible to directly measure the resistance terms, so use of the Penman-Monteith equation is mainly restricted to research studies in which the resistance terms are derived as functions of canopy characteristics and wind profile.

2.4.4 Priestley-Taylor model

Because of, the frequent unavailability of the meteorological variables needed for PM calculations. Priestley and Taylor (1972) proposed an empirical equation for calculating ET. This method is radiation-based model which neglects the aerodynamic which can be written as:

$$\lambda ET = \alpha \frac{\Delta}{\Delta + \gamma}(R_{net} - G) \qquad \text{Eq. (14)}$$

where α is an empirical coefficient relating actual evaporation to equilibrium evaporation with an average value of 1.26 (Priestley and Taylor, 1972). The other notations are described earlier. The Priestley–Taylor (PT) approach neglects the influence of vapor deficit on the evapotranspiration, relying on the assumption that ET depends only on solar radiation and temperature. The PT data requirement does not include some hard to obtain meteorological variables as wind speed or relative humidity. Hence this ET can be computed in places where PM calculations cannot be performed due to data lacking.

To perform the evapotranspiration calculation using any of the Priestley-Taylor variations, the following data are required: mean air temperature, measurement of net radiation or

measurement of sunshine hours and cloud cover (from which net radiation can be modeled), the ground heat flux, and ambient air pressure.

2.4.5 Crop evapotranspiration: The FAO approach

The FAO approach is a well-known method and very useful for the estimation of ET for single crop when the reference condition are available. Crop evapotranspiration (ETc), is known as a main component of the water consumption in agriculture fields, therefore estimating accurate value of ETc is important. ETc under standard conditions which refer to crops grown under condition of no limitations are placed on crop growth, disease-free, well-fertilized crops, grown in large fields, under optimum soil water conditions, and achieving full production under given climatic conditions (Allen et al., 1998). The crop evapotranspiration differs from reference evapotranspiration (ETo) and ET as the ground cover, canopy properties and aerodynamic resistance of crop from grass are integrated into the crop coefficient (Kc). The ETc can be calculated by multiplying ETo by the crop coefficient (K_c), as determined.

$$ET_c = K_c\, ET_0 \qquad \text{Eq. (15)}$$

where ETc is crop evapotranspiration (mm d^{-1}), Kc is crop coefficient (dimensionless), and ETo is reference crop evapotranspiration (mm d^{-1}).

The crop coefficient (K_c) varies predominately with the specific crop characteristic and only to a limited extent with climate and it can be expressed as a single coefficient, or it can be split into two factors, one describing the effect of evaporation and the other the effect of transpiration. The reference ET (ETo) is defined and calculated using the Penman-Monteith equation (previous section). The Kc is the ratio of the crop ETc to the ETo, and it represents an integration of the effects of four primary characteristics (crop height, albedo, canopy resistance, and evaporation from soil) that distinguish the crop from the reference grass (see FAO# 56 by

Allen et al. 1998). In the single crop coefficient approach, the effect of crop transpiration and soil evaporation are combined into a single Kc coefficient.

$$K_s = K_{cb} + K_e \quad \text{Eq. (16)}$$

where K_{cb} is the basal crop coefficient, K_e is the soil evaporation.

Under soil water stress condition, the effects can be accounted for by a crop water stress coefficient (Ks) as follows:

$$ET_{c\,adj} = K_s K_c ET_o \quad \text{Eq. (17)}$$

K_s describes the effect of water stress on crop transpiration. For soil water limiting condition, K_s<1 and K_s= 1 when there is no soil water stress. K_s is given by:

$$K_s = \frac{TAW - D_r}{(1-p)\,TAW} \quad \text{Eq. (18)}$$

where K_s is a dimensionless transpiration reduction factor dependent on available soil water (0-1), D_r is root zone depletion (mm), TAW is total available soil water in root zone (mm), p is fraction of TAW that a crop can extract from the root zone without suffering water stress. More information about crop evapotranspiration can be found in FAO Irrigation and Drainage Paper No. 56 (Allen et al., 1998).

2.4.6 The energy balance and Bowen ratio method

Evapotranspiration can be considered as the energy employed for transferring water from leaves and plant organs to the atmosphere as vapor in agriculture lands. In this case it is called "latent heat" (λET, with λ is latent heat of vaporization) and it is measured as energy flux density (W m^{-2}). The latent heat flux can be calculated from the measurement of the energy budget over the land surface and it is the main used part of available energy due to the radiation balance. All the energy related in the evapotranspiration component must satisfy the closure of the energy

balance. The surface energy balance equation with an exemption of neglected the residual term is generally expressed in the following form:

$$\lambda ET = R_{net} - G - H \quad \text{Eq. (19)}$$

where λET = latent heat flux (energy consumed by ET) (W m^{-2}), R_{net} is the surface net radiation flux (W m^{-2}), G is conductive heat flux into or out of the ground (W m^{-2}), H is the sensible heat flux (W m^{-2}), λ is the latent heat of vaporization (kJ kg^{-1}). The latent heat of vaporization is defined as the amount of energy required to convert 1 gram of liquid water to vapor at constant temperature. λET is the latent heat flux (W m^{-2}). In some cases no storage term is considered since the vegetative canopy is very simple.

Sensible heat flux (H) can be obtained from the measurement using eddy covariance and a large scintillometer technique (more details can be found in Chapter 4)

Ground heat flux (G) was determined by integrating the gradient of soil temperature from soil temperature profiles.

$$G = -k \int_0^{z_s} \frac{\partial T_s}{\partial t} \quad \text{Eq. (20)}$$

where k is soil thermal conductivity, t is time, z_s is the soil depth that responds to temperature change and T_s is soil temperature.

The Bowen ratio is defined as $\beta = \frac{H}{\lambda E}$. Then, Eq. (19) can be rearranged to,

$$\lambda ET = \frac{R_{net} - G}{1 + \beta} \quad \text{Eq. (21)}$$

β can be obtained by the ratio of the air temperature at the two levels (ΔT) and the vapor pressure difference (Δe), with e (kPa) air vapor pressure, measured at the same two levels. With

assumptions of turbulent transfer coefficients for heat (K_h) and water vapor (K_v) are identical and the two levels at which temperature and humidity are measured must be within the layer of the airflow that has adjusted to that surface so that there is an absence of horizontal gradients of temperature and humidity. β will be defined as:

$$\beta = \gamma \frac{\Delta T}{\Delta e} \quad \text{Eq. (22)}$$

Bowen ratio method has been proven as a standard method in semi-arid environments (Dugas et al. 1991) and is widely used in a variety of field conditions.

2.4.3.1 The aerodynamic method

The latent heat flux by aerodynamic approach can be determined by means of the dimensional scaling factors u_* and q_*, with q specific air humidity (kg kg^{-1}).

$$\lambda ET = -\lambda \rho u_* q_* \quad \text{Eq. (23)}$$

where ρ is density of air (kg m^{-3}) and u_* is friction velocity (m s^{-1}) derived from the wind speed profile measurement:

$$u_* = \frac{ku}{ln\left(\frac{z-d}{z_0}\right) - \zeta_m} \quad \text{Eq. (24)}$$

where k =0.4 is the von Karman constant, d(m) is the zero plane displacement height, z_0 (m) is the roughness length of the surface and ζ_m is the stability correction function for momentum transport. q_* is determined similarly from the humidity profile measurement:

$$q_* = \frac{k(q - q_0)}{ln\left(\frac{z-d}{z_0}\right) - \zeta_v} \quad \text{Eq. (25)}$$

where q_0 is the air humidity extrapolated at z= d+z_0 and ζ_v is the correction function for non-neutrality for the case of latent heat transport.

The major difficulty for this technique is the correct measurement of the vapor pressure at different heights above the vegetation. According to this reason λET can be derived indirectly by the energy balance Eq. (19) if the sensible heat flux (H) is obtained by the flux-gradient relation:

$$H = -\rho c_p u_* \theta_* \qquad \text{Eq. (26)}$$

where θ_* is deduced from the air temperature profile:

$$\theta_* = \frac{k(\theta - \theta_0)}{\ln\left(\frac{z-d}{z_0}\right) - \zeta_h} \qquad \text{Eq. (27)}$$

where θ_0 is the temperature extrapolated at z= d+z_0 and ζ_h is the correction function for the heat transport. By using this form, the main advantage of the aerodynamic technique is avoiding the humidity measurements. The accuracy depends on the number of measurement levels of temperature and wind speed profiles. This techniques has good results when stability correction functions were applied (Pieri and Funchs, 1990). However, the aerodynamic approach does not work well on tall crops (Thom et al., 1975).

2.4.7 The eddy covariance

The transport of heat and vapor, CO_2, and momentum in the low atmosphere in contact with the canopies is mostly governed by air turbulence. The fluxes from surface can be measured correlating the vertical wind fluctuations from the mean (w') with the fluctuations from the mean in concentration of the transported admixture. Therefore, the latent heat can be obtained following the covariance of vertical wind speed (m s^{-1}) and vapor density (q' in g m^{-3}):

$$\lambda ET = \lambda\overline{w'q'} \quad \text{Eq. (28)}$$

To measure ET directly by this method, vertical wind fluctuation has to be measured and acquired contemporary to the vapor density. The error in eddy covariance method can add to problems of the sensors configuration and meteorological characteristics (Foken et al. 2008)

To avoid some problems linked to the humidity fluctuations measurements, theoretical λET can be obtained indirectly as a residue of the energy balance Eq. (19) when the sensible heat flux is defined as:

$$H = -\rho c_p \overline{w'\theta'} \quad \text{Eq. (29)}$$

2. 5 Meteorological and hydrological parameter measurements during the summer season

A number of methods to estimate and measure ET have been introduced in the previous sections. It is useful to review input data from the experiment which include the meteorological and hydrological factors during the summer season, with the aim of identifying an appropriate framework for evapotranspiration calculations across this agroecosystem. All of the methodologies require suitable meteorological and hydrological data. Sufficient and high quality data from experiments are needed to estimate the ET. Data requirement as well as some examples of these data is included in this section.

2.5.1 Micrometeorological parameters

The micrometeorological parameters (net radiation, air temperature at 1 and 3 m height, ambient air pressure, soil temperature and ground heat flux at 15 and 30 cm depths) at the EC station were obtained for 42 days and 72 days in summer 2012 and 2013 respectively. These data ranged from 13 July to 7 September in summer 2012 and 6 July to 4 October in summer 2013 with the resolution of 1 minute interval. Data are missing for 8 days (27 August to 3 September)

in 2012 and for 10 days (17-26 September) in 2013. Net radiation (Rnet) and two levels of air temperature at EC site were represented by 69,276 points in summer 2012 and 114,157points in summer 2013 (Figure 2-4). Ambient air pressures record had 45,115 and 114,132 data points in summer 2012 and 2013, respectively. Soil temperature and calculated ground heat fluxes records were 103,102 and 113,855 data points in 2012 and 2013, respectively (Figure 2-5).

In general, average Rnet of 148 ±128 Wm^{-2} was found in both years. The air temperature ranged from -1.3 to 27.9 °C with average of 14°C in 2012, and ranged from -2.4 to 32.0 °C with an average of 15 °C in 2013 respectively. Mean soil temperature integrated from 15 -30 cm soil depth was 14°C in 2012 and an average soil temperature integrated from5 -30 cm was 13°C in 2013.

2.5.2 Meteorological parameters

The meteorological parameters included air temperature, relative humidity, air pressure, wind speed and direction, and precipitation at 2 m and 5 m above the ground were obtained at 1 minute intervals. These data ranged from 31 May to 9 September in summer 2012 and 10 June to 30 September in summer 2013. For a total of 79 days in 2012, 113,845 data points were recorded at 2 m height while only 98,169 points were recorded at 5 m height. On the other hand, for a total of 97 days with 136,900 data points at 2 m height and 140,442 at 5 m height were recorded in 2013. There were only three periods of missing data at 2 m height and two periods at 5 m height detected which accounted to 20% of data capturing. Temporal variations of these meteorological factors are depicted in Figure 2-6. Wind speed and direction are also presented for summer 2012 to 2014 (Figure 2-7). The prevailing wind directions were from west to north sectors with an average wind speed of 2-3 m s^{-1} during the summer.

The refractive index structure parameter (C_n^2) was determined represented by 20,160 data points (14 days) in 2012 and 109,440 points (76 days) in 2013 (Figure 2-8). Class A pan evaporation data were collected from June 20 to September 8 in summer 2013 to determine the potential evapotranspiration (Ep) in the farm. In Figure 2-9 the Ep in summer 2013 is compared to ten years average of Ep from NOAA meteorological station which is located at the Fairbanks Agricultural Experiment station (about 1000 m away from the meteorological station of this study).

In Figure 2-10 the Doppler SODAR- measured wind speed, wind direction, boundary development and vertical velocity are shown under different conditions. Specific days were chosen to depict at this site, strong wind speed larger than 10 m s^{-1} at upper layer on 29 July 2013 and average wind speed (2 m s^{-1}) on 5 August 2013.

2.5.3 Hydrological parameters

2.5.3.1 The soil water characteristic curve

The soil moisture water characteristic curve (SMC) can be obtained by using the two levels of nonlinear relationship (fit option: Levenberq-Marquardt) over the air pressure range 0.3 -15 bars. In Figure 2-11 the SMC curve (blue line) for sandy loam soil in lysimeter, the gravimetric soil moisture (green square color), volumetric moisture content measured by 10HS sensor (red color) from lysimeter, and the soil volumetric moisture at different air pressure (black dot) from the experiment were illustrated. The figure also showed the 10HS sensor- recorded moisture content was around field capacity (FC) while the gravimetric moisture ranged from below and above the FC. However, the SMC curve generated from nonlinear function underestimated the soil moisture during some periods.

2.5.3.2 Soil moisture, soil water potential and soil temperature in the lysimter plot

The soil moisture and temperature (within two lysimeters) were measured at 15- minutes intervals for about 55 days (5,277 data points) with the water potential (WP) of 110 days (10,654 data points) during summer 2012. These data ranged from June 6 to July 27 for nine lysimeters, while more data were obtained within only three lysimeters during 5-19 September, 2012. Sensor failure caused missing data. However, WP was measured from 6 June to 6 September, 2012.

As for summer 2013, the soil moisture data for 30-min resolution at 5, 10 and 20 cm depths in vegetated and unvegetated lysimeter were collected for about 83 days (1,996 data points). On the other hand, WP was obtained for ~110 days with 2,632 data points for both treatments. These data were collected from 14 June to 16 September, 2013. However, missing data was detected in some periods during the field experiment. There was a noticeable increase in moisture content and decrease of WP after the precipitation and irrigation events. Sample temporal variations of these data in vegetated and unvegetated lysimeters are illustrated in Figure 2-12.

2.5.3.3 Spatial variation of soil moisture and temperature under different surface cover

Soil temperature was measured and recorded hourly under annual barley (*Hordeum vulgare*), a perennial bromegrass (*Bromus inermis*), a bare (fallow) in summer 2011-2014, while the soil moisture was not collected in summer 2013. There were two types of data collected from each plot. Soil temperature and air temperature in each plots was measured for 137, 151, 114, and 100 days in summer 2011, 2012, 2013 and 2014 respectively. Generally, these data are collected over the growing season of each year. The hourly average of air temperature, soil

temperature, and soil temperature in each site during 2011-2013 is shown in Table 2-4. Temporal and spatial variation of measured parameters is presented in Figure 2-13.

2.6 Summary

Understanding evapotranspiration particularly across the farmland in agroecosytems in high latitudes is a difficult task because it depends on the availability of input data and accurate measurements. Thus, it is essential to measure hydro-meteorological variables, such as radiation, precipitation, soil moisture, water vapor, wind speed, surface water and runoff, vegetation state, albedo and surface temperature, etc. Such measurements are required not only for the purposes of determining ET but also to improve knowledge of components of the water cycle and its variability, both spatially and temporally, as well as to characterize the coupling between the land and atmospheric interaction of the water cycle. Quantifying this interaction is of utmost importance because this coupling may influence and simultaneously be influenced by climate variability and predictability. In this study, field sampling has been extensively used to measure hydro-meteorological variables and estimate evapotranspiration during summer season. Parallel to these measurements were monitoring soil temperature and moisture to investigate the interconnection between surface and atmosphere in different land cover. However, if larger heterogeneities occur over vast land surface scaling to regional estimates from field observations may be limited.

Several important methods of measuring and modelling evapotranspiration were also explained. These techniques are mainly based on site (field)-measurements and many of those techniques are dependent on a variety of model parameters that is very difficult to know. Therefore, some methods are more suitable than others in terms of convenience, accuracy or cost for the measurement of ET at different space and time scale. Furthermore, field measurements of

hydro-meteorological variables were also presented mainly from summer 2012 and 2013 which have large amounts of data available. Data collected for the purposes of carrying out this research may also be of use in other research applications in this region such as for a ground base calibration of the satellite data and modelling developing, monitoring of the changes and assessment of future changes as consequences of climate fluctuations and climate changes in the region; study of agrometeorological weather-crop model and weather-plant model, study of climate extremes and meteorological phenomena causing greatest damages in agriculture and their consequences (drought, extremely high and low air temperatures, storms with hail), etc.

Many techniques and field studies have been used to estimate ET in this site, and some issues can occur throughout the field experiment period which will affect the accuracy of ET estimation. Some problems mainly associated with instruments have been addressed. Some deployments based on inexpensive devices have required a lot of attention so at least one person needed to work on these; and commercially available instruments required a lot of experience for a person to install, set- up and maintain the instruments and a team effort was applied. The heterogeneity of equipment and data loggers from different manufacturers may introduce difficulties in compiling the entire information, so systems maintenance was important in the operation such as eddy covariance, LAS and SODAR. Some measurements required manual daily readings at the same time in the morning such as evaporation pan but that was done faithfully. Integrated data management from different field plots could be challenging to ensure data quality control for usability, detecting instrument failure from an unexpected factor in the environment such as presence of wild animals. Finally, and maybe the most relevant aspect, is ensuring high spatial and temporal resolution, not only within a single deployment, but also among different deployments both in the same and different sites.

There is a real need for field measurements and modelling to investigate and predict in a reliable manner the variations in the ET cycle which is central in contributing to the improvement of water governance, the mitigation of water-related damage to crops and to sustainable agriculture development.

Figures

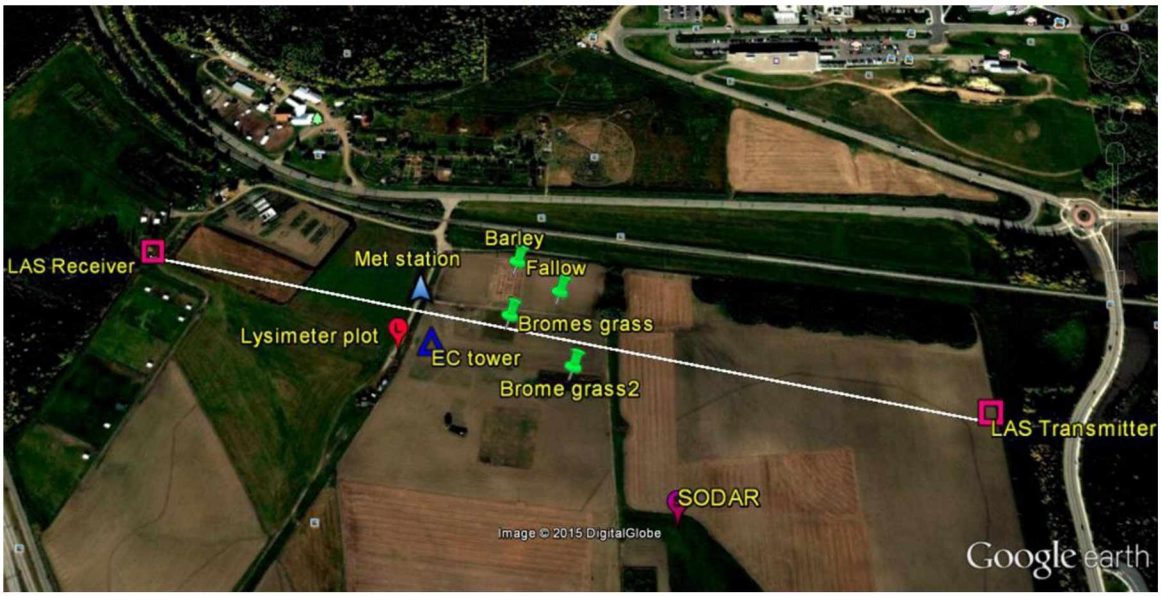

Figure 2-1. Experimental site at the FEF during summer season. The location of the instrumentation is illustrated. The farm is more than 1 kilometer from East-West and about 600 m North - South. This figure was obtained from Google Earth on 9 September 2012

Figure 2-2. Micrometeorological and Soil Moisture sensing. EC, LAS, soil potential data logger including picture of the installation process in the lysimeter plots, pan evaporation, with two treatments of the lysimeter study shown.

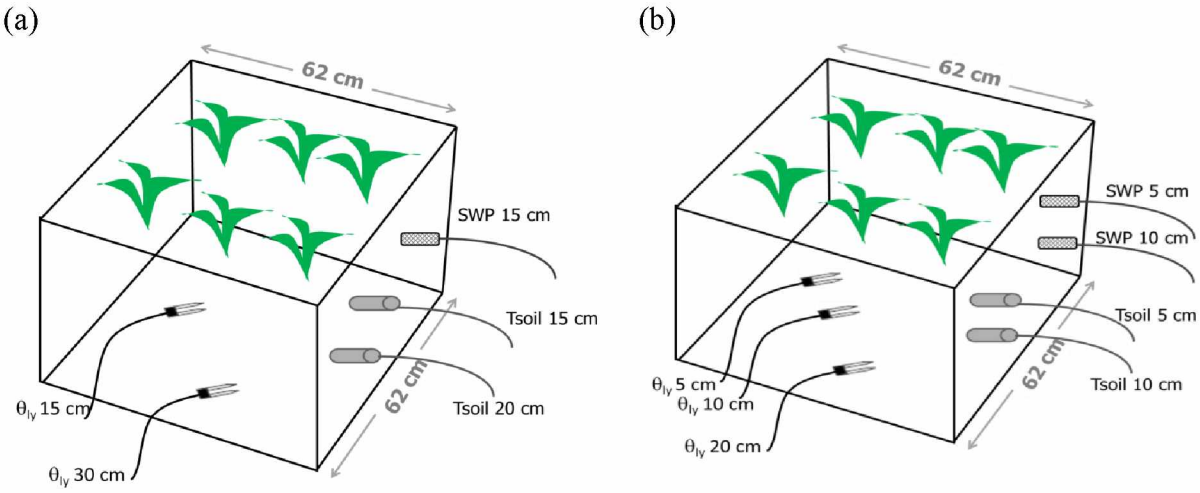

Figure 2-3. Instrumentation of the lysimeter plot; (a) summer 2012 and (b) summer 2013. (Tsoil = soil temperature sensor, SWP=soil water potential sensor, θly=soil moisture sensor)

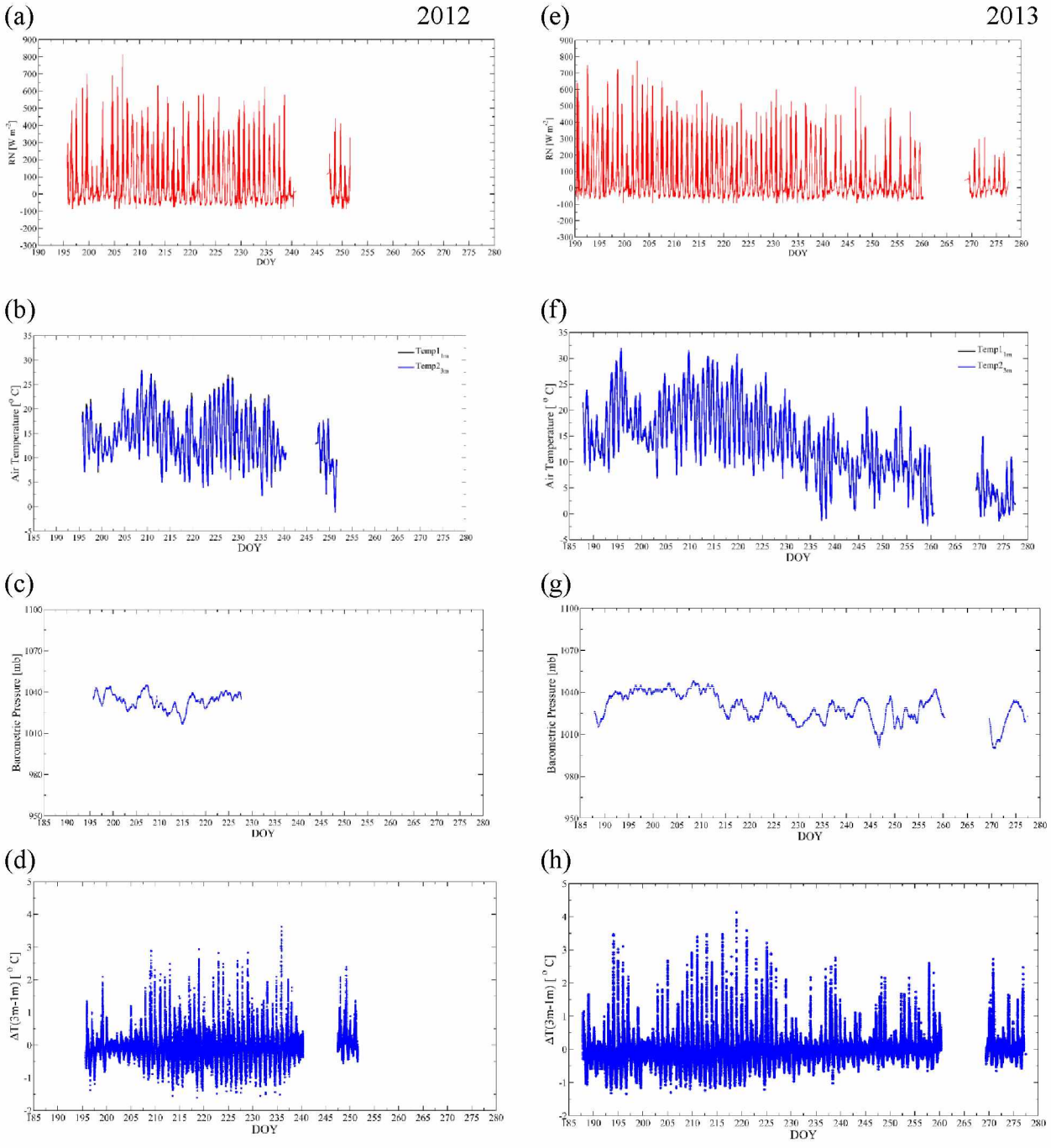

Figure 2-4. Micrometeorological conditions during the growing season; (a)- (h) represent the net radiation (at 3 m height), air temperature (at 1 and 3 m height), barometric air pressure, and static stability parameter for summer 2012 (left panel: a-d) and 2013 (right panel: e-h) respectively. Blank spaces in the graphs indicate missing data.

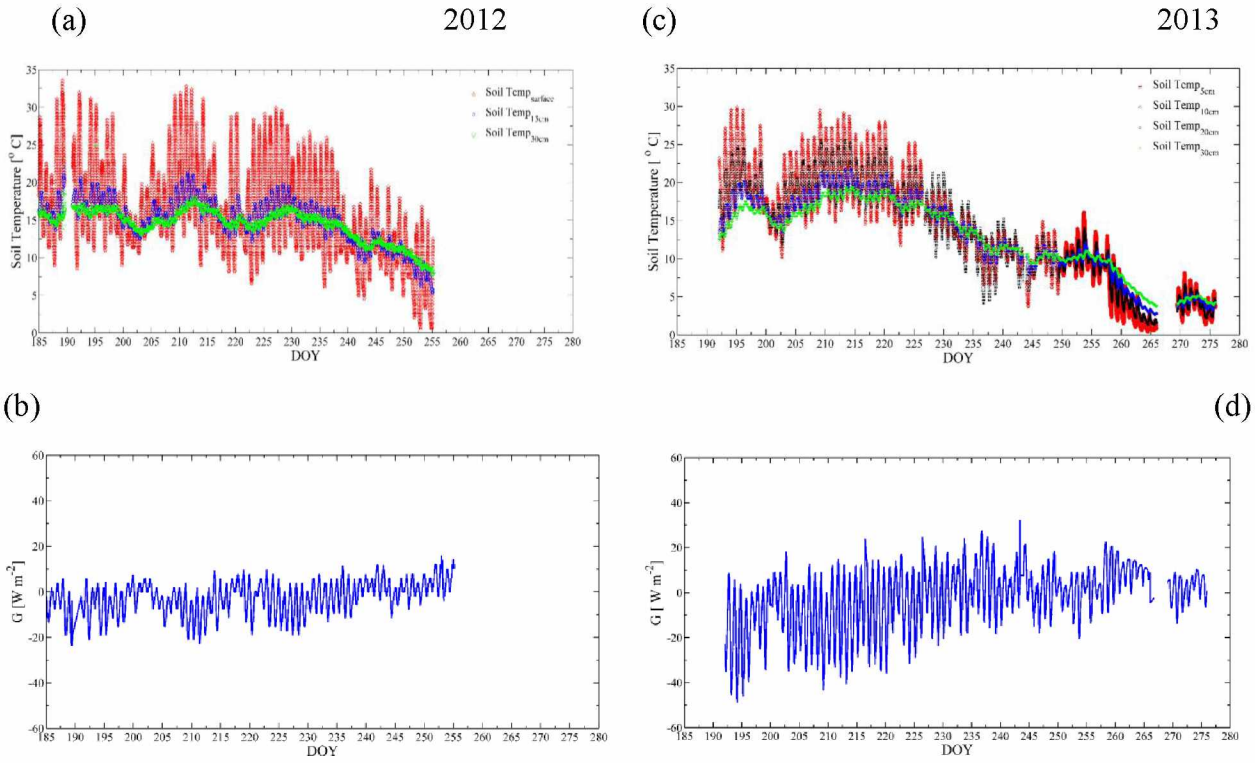

Figure 2-5. Soil Temperature and ground heat flux at EC tower location in summer 20 12 (left panel) and 2013 (right panel). (a) soil temperature at surface (red), at 15 cm (blue), and 30 cm (green) soil depths; (b) Calculated ground heat flux (G) in 2012; (c) soil temperature at 5cm (red), 10 cm (black), 20 cm (blue), and 30 cm (green) soil depths; and (d) Calculated ground heat flux (G) in summer 2013.

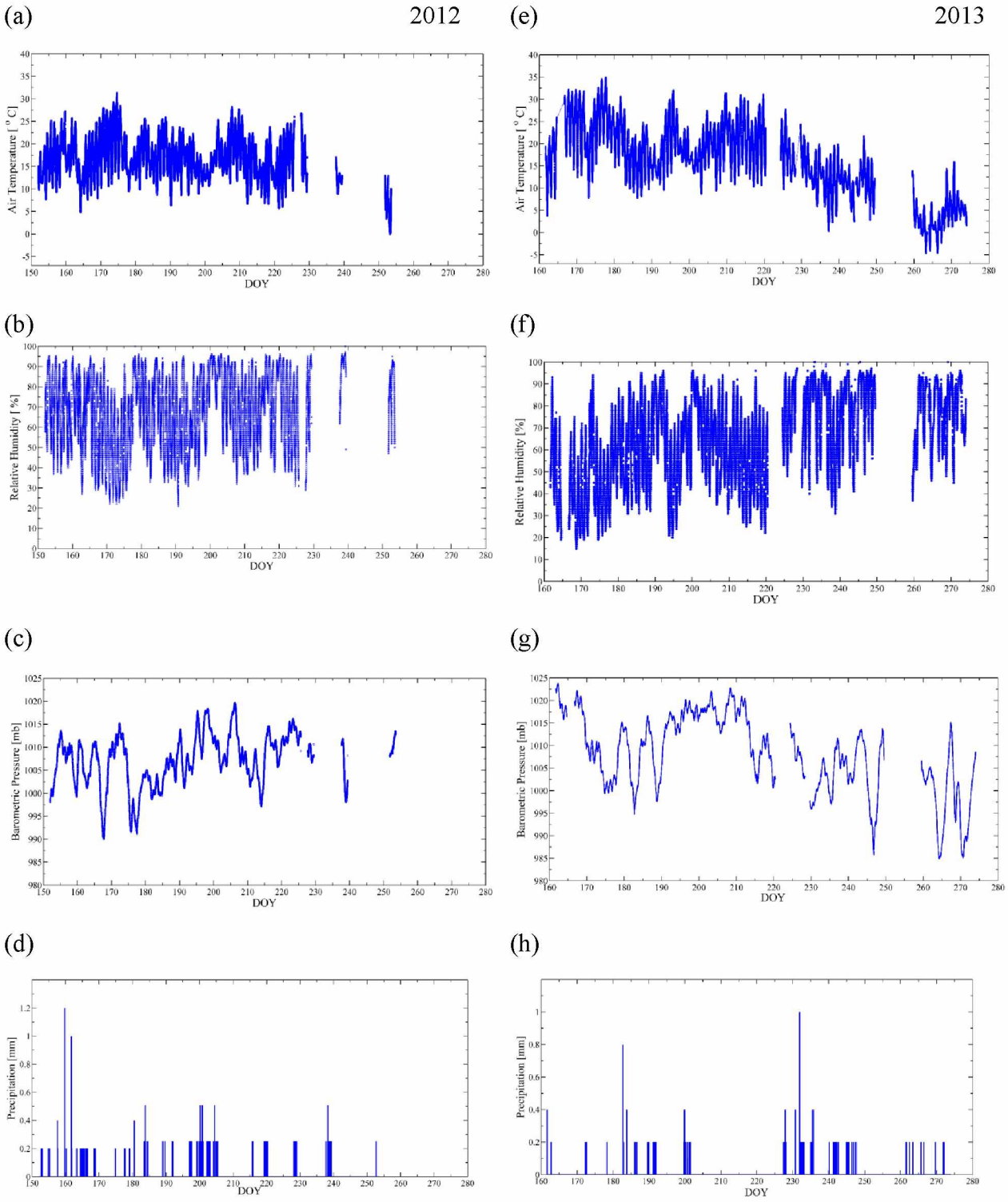

Figure 2-6. Meteorological condition during summer 2012 (left panel) and 2013 (right panel). (a)-(d) and (e)-(h) are one- minute records of air temperature, relative humidity, pressure, and precipitation at 2 m height in summer 2012 and 2013 respectively. Blank spaces indicate missing or no data.

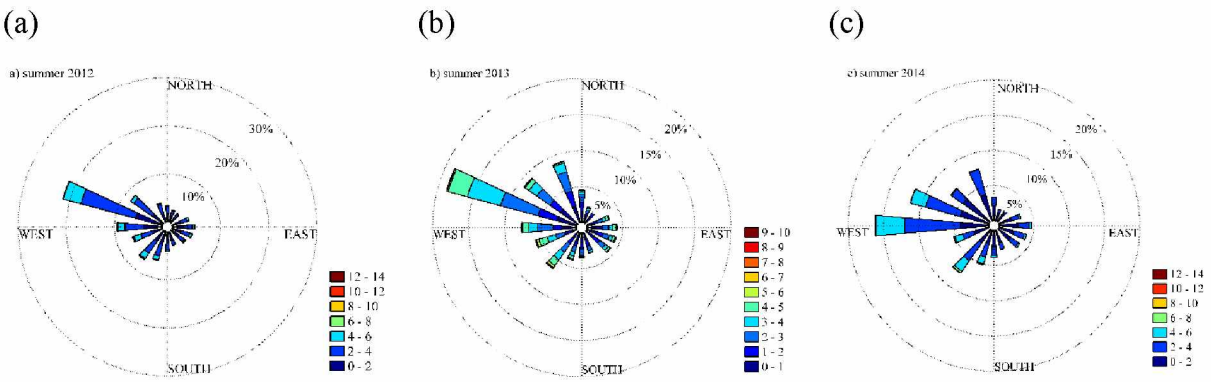

Figure 2-7. Histograms of wind speed and direction from June to September over the three summer growing seasons; (a) 2012 wind speed ranges from 0.4-12.5 m s^{-1}, prevailing wind direction is north-west, (b) 2013 wind speed ranges from 0.4-9.8 m s^{-1}, prevailing wind direction is north-west sector, and (c) 2014 wind speed ranges from 0.4-13 m s^{-1}, prevailing wind direction is west sector.

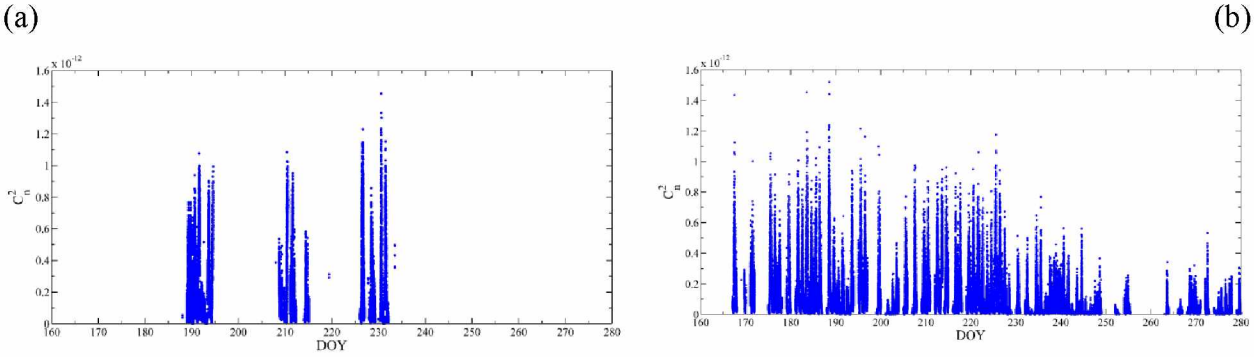

Figure 2-8. Refractive index structure parameter (C_n^2). (a) summer 2012 and (b) summer 2013 Blank spaces in the graphs indicate missing data.

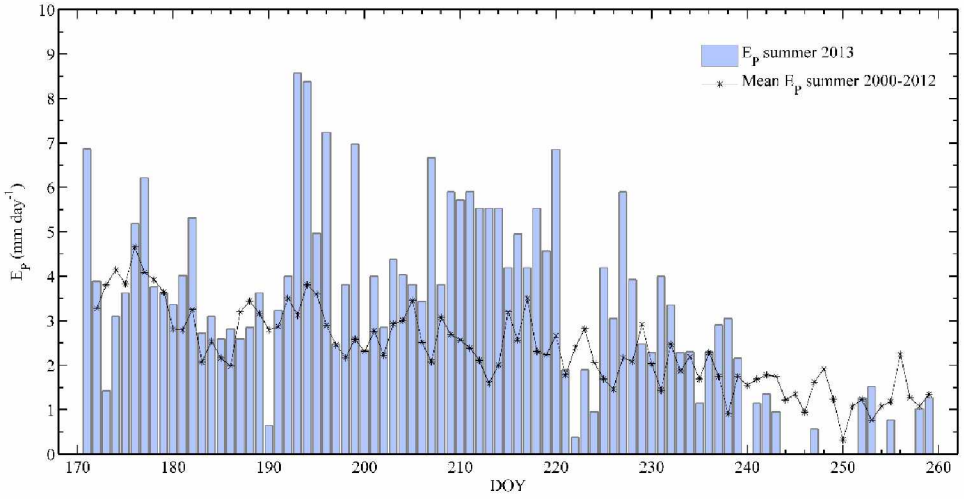

Figure 2-9. Class A pan evaporation data in summer 2013. Evaporation pan (Ep) in the study site versus the evaporation pan at NOAA meteorological station located at the Fairbanks Agricultural Experiment station (1000 m away) from the study site.

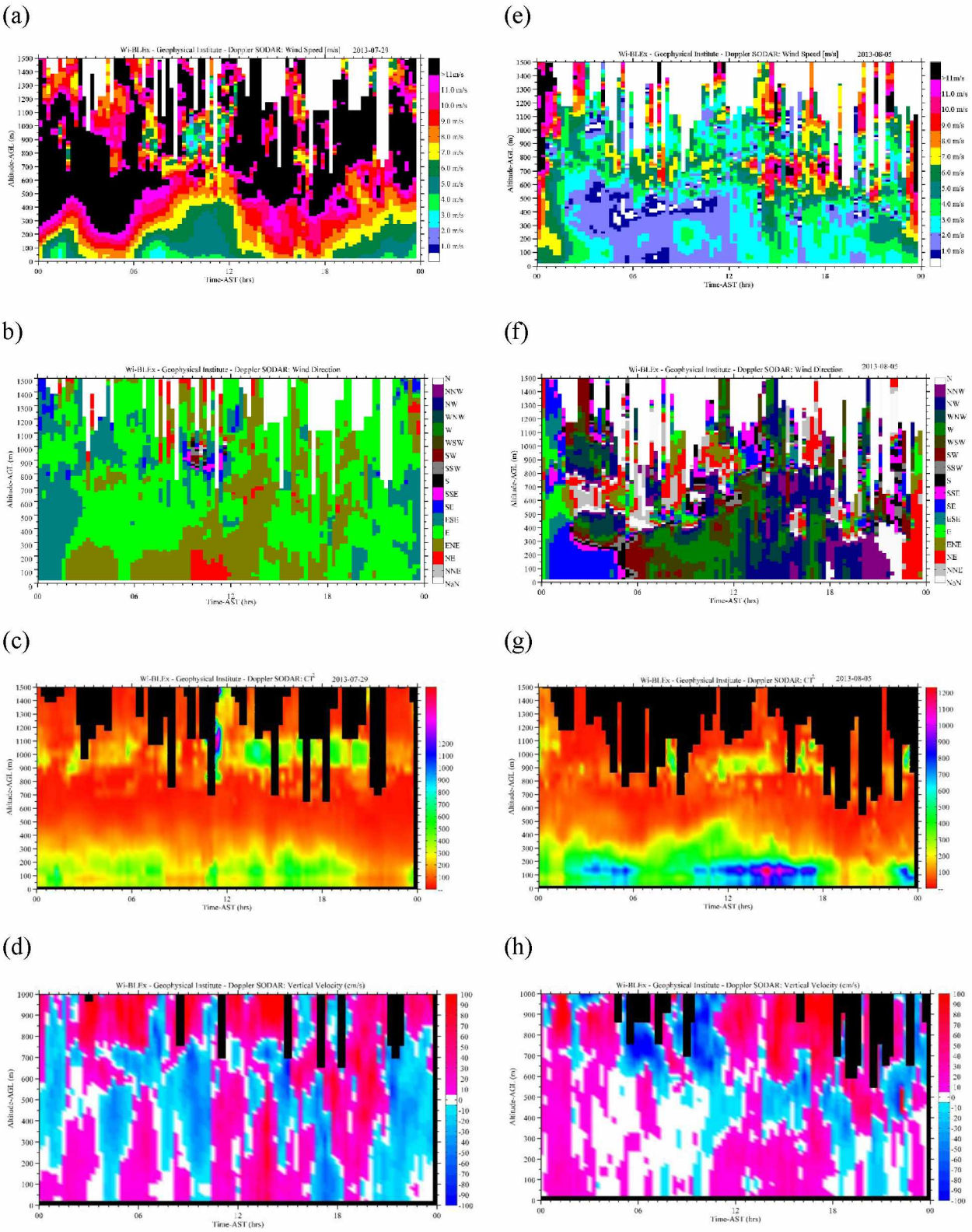

Figure 2-10. Doppler SODAR measured wind speed (a, e), wind direction (b, f), boundary development (c, g), and velocity (d, h) during July 29, 2013 and 5 August 2013 respectively.

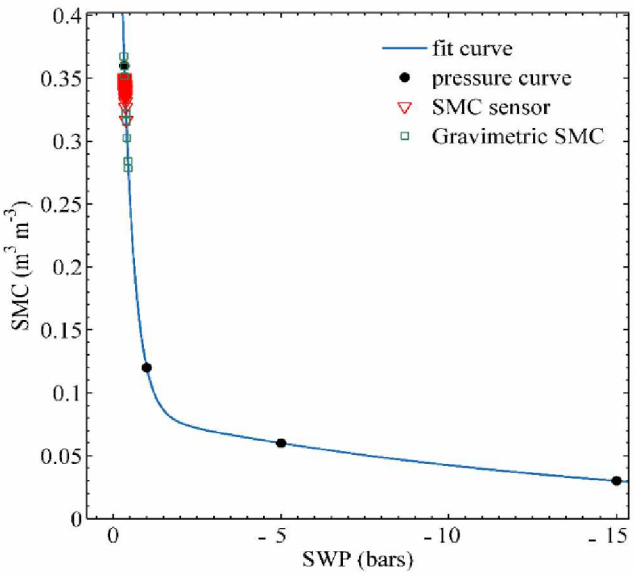

Figure 2-11. Soil moisture characteristic curve from the lysimeter soil sample; blue line represent the SMC curve for the nonlinear relationship fitting, the black dot is the moisture content at different air pressures, the red triangle is the moisture content measuring by 10HS sensor, and the green square is the gravimetric moisture content.

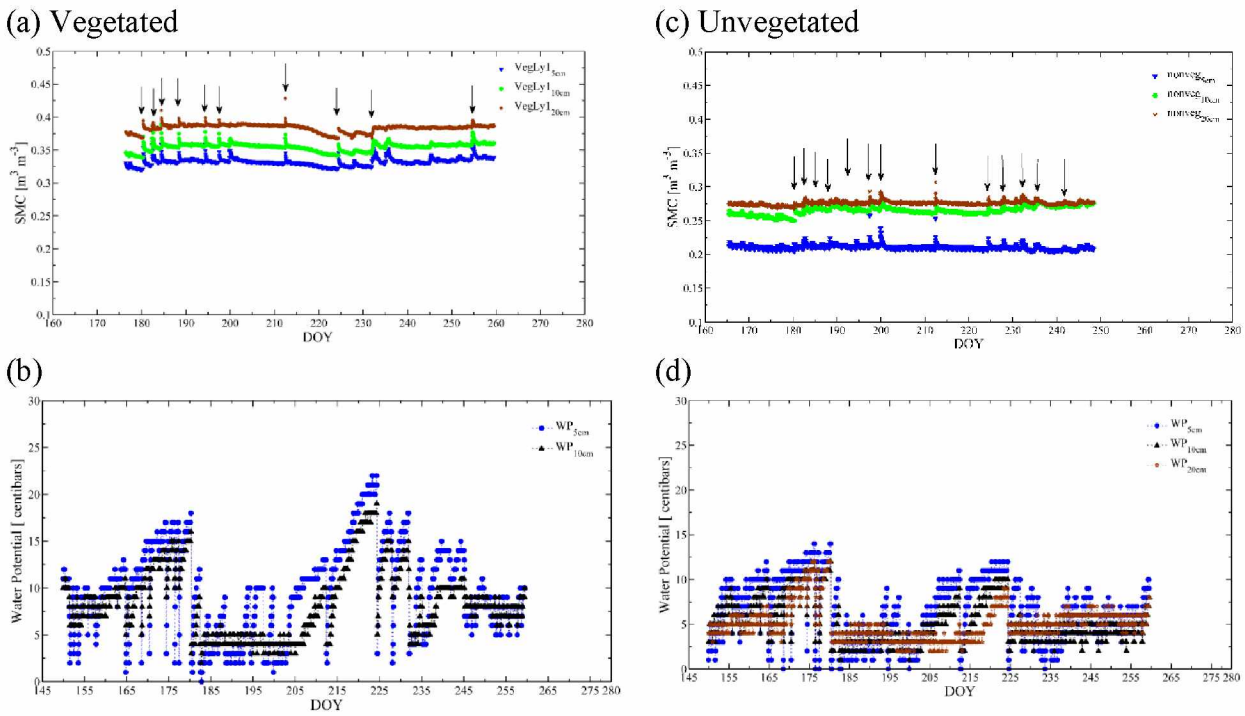

Figure 2-12. Sample data of soil moisture content and water potential within vegetated and unvegetated lysimeters in summer 2013; (a) soil moisture in vegetated lysimeter, (b) water potential in vegetated lysimeter, (c) soil moisture content in unvegetated lysimeter, and (d) water potential in unvegetated lysimeter. The arrows represent the precipitation and irrigation events.

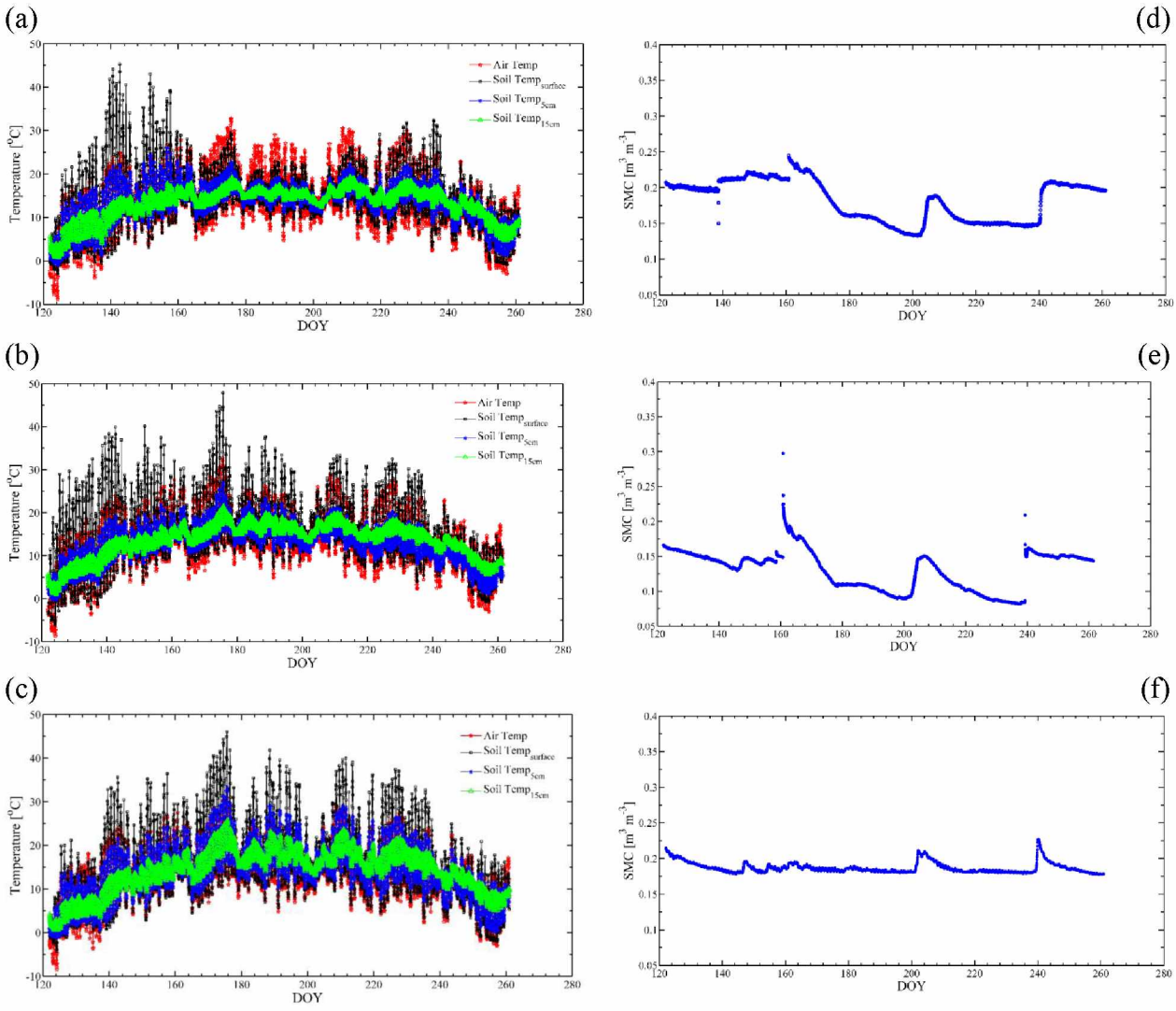

Figure 2-13. Sample data of soil temperature and soil moisture under different fields in the farm during summer 2012; (a) –(c) soil temperature at barley field, bromegrass, and fallow field, and (d) – (f) soil moisture (SMC) at barley, bromegrass, and fallow field, and (d) – (f) soil moisture (SMC) at barley , bromegrass, and fallow field respectively.

Tables

Table 2-1 Summary of instrumentation installed at the FEF site

Parameter	Sensor heights (m)	Model and Sensor maker	Sensor location	Growing season	Resolution
Air temperature	2 and 5	Integrated Sensor Suite (ISS) , Davis Hayward, CA	Met station	2012-2014	1 min
Air temperature	1 and 3	PT 107, Campbell Scientific	EC tower	2012-2014	1 min
Air temperature	1.5	ECT, Decagon Devices, Inc.	Barley, brome grass and bare fields	2012-2013	Hourly
Barometric pressure	0.30	CS 106, Campbell Scientific.	EC tower	2012-2013	1 min
Barometric Pressure	2 and 5	ISS , Davis Hayward CA	Met station	2012-2014	1 min
Net radiation	3	NRLite, Campbell Scientific	EC tower	2012-2013	1 min
Shortwave down welling	2	Piranometer CM3, Holland	Bare fields	2013	30 min
Wind speed and direction	2 and 5	Anemometer, Davis Hayward CA	Met station	2012-2014	1 min
Three-dimensional velocity	3	RMYoung 8100 VRE	EC tower	2012-2013	1 min
Precipitation	2 and 5	ISS, Davis Hayward, CA	Met station	2012-2014	1 min
Relative humidity	2 and 5	ISS, Davis Hayward, CA	Met station	2012-2014	1 min
Soil moisture	-0.15 ,-0.30	10HS, Decagon Devices, Inc.	Lysimeter plot	2012	15 min
Soil moisture	-0.05, -0.10, -0.20	10HS and ECH$_2$O EC-5, Decagon Devices, Inc.	Lysimeter plot	2013	30 min
Soil moisture	-0.05, -0.10,-0.30	10HS and ECH$_2$O EC-5, Decagon Devices, Inc.	Barley, fallow, and brome grass fields	2014	30 min
Surface temperature	0	S-TMB-M006., Onset Computer Corporation, Bourne, MA	barley, fallow, and brome grass fields	2011-2012	Hourly
Soil temperature	-0.01,-0.15,-0.30	S-TMB-M006, Onset Computer Corporation, Bourne, MA	Lysimeter plot	2012	15 min
Soil temperature	-0.05,-0.10,-0.20,-0.30	S-TMB-M006, Onset Computer Corporation, Bourne, MA	EC tower	2013	1 min
Soil temperature	-0.05,-0.10,-0.20	S-TMB-M006, Onset Computer Corporation, Bourne, MA	Lysimeter plot	2013	30 min
Soil temperature	-0.05,-0.15,-0.30	5TM, Decagon Devices, Inc.	Barley, bare, brome grass fields	2011-2013	Hourly
Soil temperature	-0.15,-0.30	S-TMB-M006, Onset Computer Corporation, Bourne, MA ,	barley, fallow, and brome grass fields	2014	30 min
A Doppler sodar	20	Remtech model PA2	SODAR site	2013	1 min
Soil water potential	-0.15,-0.30	200ss, Irrometer Co., Inc., CA	Lysimeter plot	2012	15 min
Soil water potential	-0.05,-0.10	200ss, Irrometer Co., Inc., CA	Lysimeter plot	2013	30 min
Soil water potential	-0.05,-0.10,-0.20	200ss, Irrometer Co., Inc., CA	Barley and bare fields	2014	30 min
Gravimetric soil moisture	-0-0.15, -0.15-0.30	Core sampling	Lysimeter plot	2012-2013	3 samples/plot
Soil thermal properties	-0.06	KD2, Decagon Device, Inc.	barley, fallow, and brome grass fields	2014	3 times/plot
Lysimeter	0.62	Drainage lysimeter	Lysimeter plot	2012-2013	Weekly
Refractive index structure parameter (Cn^2)	1.8	BLS-900, Scintec AG, Rottenburg, Germany	Across the farm	2012-2013	1 min
Potential evapotranspiration	Class A evaporation pan		Lysimeter plot	2013	Daily
Leaf area index		AccuPAR Par80 linear PAR/LAI ceptometer, Decagon Device, Inc.	barley, brome grass	2012	Weekly
			Lysimeter plot,	2012	3 times
Stomatal resistance		Porometer, Decagon Device, Inc.	Lysimter plot, barley, brome grass	2013	3 times

Table 2-2 The volumetric soil moisture content (convert from gravimetric moisture content by multiplying the bulk density) before and after harvesting with in lysimeter experiment.

Soil depth	Before planting (mean±std)	After harvesting (mean±std)
Growing season 2012		
Vegetated lysimeter (0-15 cm)	0.3600±0.0554[a]	0.3376±0.0452[a]
Vegetated lysimeter (15-40 cm)	0.3468±0.0817[a]	0.3471±0.0294[a]
Growing season 2013		
Vegetated lysimeter (0-20 cm)	0.3634±0.0238[b]	0.3732±0.0243[b]
Unvegetated lysimeter (0-20 cm)	0.2584±0.0497[b]	0.2466±0.0318[b]

[a] Average from twelve lysimeter

[b]Average from 3 lysimeters and integrated from 0-20 cm

Table 2-3 Properties of soil from different site in the farmland

Soil properties	Lysimeter	Barley	Brome	Bare
% clay	5	16	13	12
% Sand	66	14	17	16
%Silt	29	70	70	72
Bulk Density (g/cm3)	0.70	0.74	0.83	0.87
Saturated moisture content (θs) ($m^3\ m^{-3}$)	0.61	0.56[a]	NA	NA
pH	NA	6.91	6.86	6.86
% Carbon	5.41	3.04	3.50	3.60
% Nitrogen	0.17	0.26	0.28	0.31
Saturated hydraulic conductivity; K_{gs} ($m\ s^{-1}$)	3.41×10^{-5}	7.20×10^{-6}	7.20×10^{-6}	7.20×10^{-6}
Thermal conductivity ($Wm^{-1}\ C^{-1}$)	0.75[d]	0.78[b]	0.73[c]	0.48[d]
Thermal resistivity ($mC\ W^{-1}$)	1.20[d]	1.26[b]	1.36[c]	2.08[d]
Thermal diffusivity (ms^2s^{-1})	0.20[d]	0.21[b]	0.19[c]	0.16[d]

[a] The Saturated hydraulic conductivity (Sharratt, 1990)

[b] soil temperature = 8.3 °C, [c] soil temperature = 9.5°C, [d] soil temperature =9.5°C, [d] soil temperature =8.0°C

Table 2-4 Average air temperature, soil temperature, and soil moisture at different sites in the farm.

Site	Soil Temperature (°C)			Soil Moisture (m^3 m^{-3})	
	2011	2012	2013	2011	2012
Barley					
➢ **Air temp**	14.37 ± 6.52	13.81 ± 7.06	16.38 ± 7.26	-	-
➢ **Surface**	14.54 ± 6.71	14.33 ± 7.19	17.98 ± 8.48	-	-
➢ **5 cm**	13.66 ± 4.23	13.41 ± 4.68	15.91 ± 6.29	-	-
➢ **15 cm**	13.25 ± 2.88	13.13 ± 2.86	16.34 ± 4.61	0.15 ± 0.03	0.18 ± 0.03
Brome grass					
➢ **Air temp**	14.21 ± 6.42	13.47 ± 6.74	16.26 ± 7.36	-	-
➢ **Surface**	15.98 ± 9.24	15.35 ± 8.09	20.92 ± 9.06	-	-
➢ **5 cm**	13.92 ± 4.13	12.75 ± 4.67	15.67 ± 4.58	-	-
➢ **15 cm**	13.67 ± 2.95	13.51 ± 3.95	14.41 ± 3.27	0.11 ± 0.02	0.13 ± 0.03
Bare					
➢ **Air temp**	14.60 ± 6.28	13.42 ± 6.71	16.38 ± 7.47	-	-
➢ **Surface**	16.15 ± 8.78	15.32 ± 8.84	17.31 ± 8.64	-	-
➢ **5 cm**	15.11 ± 5.67	14.05 ± 6.30	16.31 ± 6.18	-	-
➢ **15 cm**	14.37 ± 3.41	14.07 ± 5.00	15.51 ± 4.39	0.14 ± 0.01	0.18 ± 0.01

2.7 References

Allen, R.G., Jensen, M.E., Burman, R.D., 1989. Operational estimates of reference evapotranspiration. Agronomy Journal, 81, 650-662.

Allen, R.G., Howell, T.A., Pruitt, W.O., Walter, I.A. and Jensen, M.E., 1991. Lysimeters for evapotranspiration and environmental measurements. In: R.G. Allen, T.A. Howell, W.O. Pruitt, I.A. Walter and M.E. Jensen (Editors), Proceeding of the International Symposium on Lysimetry. ASCE Publication, Honolulu, HI.

Allen, R.G., Pereira, L.S., Raes, D. and Smith, M., 1998. Crop evapotranspiration - Guidelines for computing crop water requirements. FAO Irrigation and drainage paper 56, Rome.

Angus, D.E. and Watts, P.J., 1984. Evapotranspiration—how good is the Bowen ratio method? . Agricultural Water Management., 8: 133–150.

Braley, W., 1980. Estimates of evapotranspiration from barley and rapeseed in interior Alaska, Thesis, University of Alaska Fairbanks.

Bates, B., Kundzewicz, Z.W., Wu, S. and Palutikof, J., 2008. Climate Change and Water, IPCC Technical Paper VI of the Intergovernmental Panel on Climate Change, IPCC Secretariat, Geneva, Switzerland.

Beyrich, F. and Weill, A., 1993. Some Aspects of Determining the Stable Boundary-Layer Depth from Sodar Data. Bound-Lay Meteorol, 63(1-2): 97-116.

Blake, G.R. and Harge, K.H., 1986. Bulk density. Methods of soil analysis Part 1. Agronomy. 9. American Society of Agronomy and Soil Science Society of America, Madison, Wisconsin.

Bormann, H., 2011. Sensitivity analysis of 18 different potential evapotranspiration models to observed climatic change at German climate stations. Climatic Change, 104(3-4): 729-753.

Brown, E.H. and Hall Jr., F.F., 1978. Advances in atmospheric acoustics. Reviews of Geophysics and Space Physics, 16: 47–110.

Burrough, P.A., 1989. Matching spatial databased and quantitative models in land resources assessment. Soil Management, 5: 3-8.

Cassel, D.K. and Nielsen, D.R., 1986. Field capacity and available water capacity Methods of soil analysis Part 1. 2nd. Agronomy. 9. American Society of Agronomy and Soil Science Society of America, Madison, Wisconsin. .

Chapin, F.S., III, Folke, C. and G.P., K., 2009. Principles of Ecosystem Stewardship. A framework for understanding change. Springer New York, NY, 401 pp.

Chapin, F.S., III, Sturm, M., Serreze, M.C., McFadden, J.P., Key, J.R., Lloyd, A.H., McGuire, A.D., Rupp, T.S., Lynch, A.H., Schimel, J.P., Beringer, J., Chapman, W.L., Epstein, H.E., Euskirchen, E.S., Hinzman, L.D., Jia, G., Ping, C.L., Tape, K.D., Thompson, C.D.C., Walker, D.A. and Welker, J.M., 2005. Role of land-surface changes in Arctic summer warming. Science, 310(5748): 657-660.

De Bruin, H., van den Hurk, B. and Kohsiek, W., 1995. The scintillation method tested over a dry vineyard area. Boundary-Layer Meteorol, 75: 25-40.

Decagon Devices Inc, 2012. EC-5 Soil Moisture Sensor. Decagon Devices, Inc., Pullman WA, 19 pp.

Denmead, O.T., 1984. Plant physiological methods for studying evapotranspiration: Problems of telling the forest from the trees. Agricultural Water Management, 8: 167-189.

Doorenbos, J. and Pruitt, W.O., 1977. Guidelines for predicting crop water requirements. Irrig. and Drain. Paper No. 24. United Nations FAO, Rome, Italy.

Drexler, J.Z., Snyder, R.L., Spano, D. and Paw, K.T.U., 2004. A review of models and micrometeorological methods used to estimate wetland evapotranspiration. Hydrological Process, 18(11): 2071-2101.

Dugas, W.A., Fristchen, L.J., Gay, L.W., Held, A.A., Matthias, A.D., Reicosky, D.C., Steduto, P., and Steiner, J.L., 1991. Bowen ratio, eddy correlation, and portable chamber measurement of sensible and latent heat flux over irrigated spring wheat. Agricultural Forest Meteorology, 56: 1-20.

Eichinger, W.E. and Cooper, D.I., 2007. Using lidar remote sensing for spatially resolved measurements of evaporation and other meteorological parameters. Agronomy Journal, 99(1): 255-271.

Emeis, S. and Türk, M., 2004. Frequency distributions of the mixing height over an urban area from SODAR data. Meteorologische Zeitschrift, 13(5): 361-367.

Fochesatto, G.J., Mayfield, J.A., Starkenburg, D.P., Gruber, M.A. and Conner, J., 2013. Occurrence of shallow cold flows in the winter atmospheric boundary layer of interior of Alaska. Meteorology and Atmospheric Physics, doi: 10.1007/s00703-013-0274-4

Foken, T., 2008. The energy balance closure problem: An overview. Ecological Applications, 18(6): 1351-1367.

Fritschen, L.J., Simpson, J.R., 1985. Evapotranspiration from forests: measurement and modeling. Advances in Evapotranspiration. American Society of Agricultural and Biological Engineers, MI, USA.

Gardner, W.H., 1986. Water content. In: A. Klute (Editor), Methods of soil analysis Part 1. Agronomy. American Society of Agronomy and Soil Science Society of America, Madison, Wisconsin., pp. 493-541.

Gee, G.W. and Bauder, J.W., 1986. Particle-size analysis. Methods of soil analysis Part 1. Agronomy. 9. American Society of Agronomy and Soil Science Society of America, Madison, Wisconsin.

Gliessman, S.R., 2007. Field and laboratory investigations in agroecology. Taylor and Francis Group, Boca Raton, FL.

Gray, J.M., Frolking, S., Kort, E.A., Ray, D.K., Kucharik, C.J., Ramankutty, N. and Friedl, M.A., 2014. Direct human influence on atmospheric CO_2 seasonality from increased cropland productivity. Nature, 515(7527): 398-+.

Gruber, M. and Fochesatto, G.J., 2013. A New Sensitivity Analysis and Solution Method for Scintillometer Measurements of Area-Averaged Turbulent Fluxes. Boundary-layer Meteorology, 149(1): 65-83.

Hargreaves, G.H. and Allen, R.G., 2003. History and evaluation of Hargreaves evapotranspiration equation. Journal of Irrigation and Drainage Engineering -ASCE, 129(1): 53-63.

Holmes, J.W., 1984. Measuring evapotranspiration by hydrological methods. Agricultural Water Management, 8: 29-40.

Holmgren, B., Spears, L., Wilson, C. and Benson, C.S., 1975. Acoustic soundings of the Fairbanks temperature inversions.Climate of the Arctic. In: G. Weller and S.A. Bowling (Editors), Climate of the Arctic: Proceedings of the AAAS-AMS Conference, Fairbanks, Alaska, 1973, University of Alaska Fairbanks, pp. 293–306.

Ivans, S., Hipps, L., Leffler, A.J. and Ivans, C.Y., 2006. Response of water vapor and CO2 fluxes in semiarid lands to seasonal and intermittent precipitation pulses. Journal of Hydrometeorol, 7(5): 995-1010.

Jarvis, P.G. and Mcnaughton, K.G., 1986. Stomatal Control of Transpiration - Scaling up from Leaf to Region. Advances in Ecological Research, 15: 1-49.

Jensen, M.E., Burman, R.D. and Allen, R.G., 1990. Evapotranspiration and irrigation water requirements. ASCE Manuals No. 70, 332 pp.

Jones, F.E., 1992. Evaporation of water. Lewis, Chelse, MI.

Klute, A., 1986. Water retention: laboratory methods Methods of soil analysis Part 1. 2nd. Agronomy. 9 American Society of Agronomy and Soil Science Society of America, Madison, Wisconsin.

Kool, D., Agam, N., Lazarovitch, N., Heitman, J.L., Sauer, T.J. and Ben-Gal, A., 2014. A review of approaches for evapotranspiration partitioning. Agricultural and Forest Meteorology, 184: 56-70.

Leenhardt, D., Voltz, M. and Bornand, M., 1994. Propagation of the Error of Spatial Prediction of Soil Properties in Simulating Crop Evapotranspiration. European Journal of Soil Science, 45(3): 303-310.

Lunt, I.A., Hubbard, S.S. and Rubin, Y., 2005. Soil moisture content estimation using ground-penetrating radar reflection data. Journal of Hydrology, 307(1-4): 254-269.

Mayfield, J.A. and Fochesatto, G.J., 2013. The Layered Structure of the Winter Atmospheric Boundary Layer in the Interior of Alaska. Journal of Applied Meteorology and Climatology, 52(4): 953-973.

Mulligan, D., 2004. Soil Survey of the Greater Fairbanks Area, Alaska, United States Department of Agriculture, Washington, D.C

Neff, W.D. and Coulter, R.L., 1988. Acoustic remote sensing. Probing the Atmospheric Boundary Layer.

Parkes, M., and Yuanhua, L., 1996. Modeling mobile water flow. In. Camp, C.R., Sadler, E.J., Yoder, R.E. (Ediors). Evapotranspiration and Irrigation Scheduling. Proceedings of the International Conferences, November 3-6, San Antonio, TX, pp. 509-515.

Piao, S.L., Sitch, S., Ciais, P., Friedlingstein, P., Peylin, P., Wang, X.H., Ahlstrom, A., Anav, A., Canadell, J.G., Cong, N., Huntingford, C., Jung, M., Levis, S., Levy, P.E., Li, J.S., Lin, X., Lomas, M.R., Lu, M., Luo, Y.Q., Ma, Y.C., Myneni, R.B., Poulter, B., Sun, Z.Z., Wang, T., Viovy, N., Zaehle, S. and Zeng, N., 2013. Evaluation of terrestrial carbon cycle models for their response to climate variability and to CO_2 trends. Global Change Biology, 19(7): 2117-2132.

Pieri, P. and Fuchs, M., 1990. Comparison of Bowen-Ratio and Aerodynamic Estimates of Evapotranspiration. Agricultural and Forest Meteorology, 49(3): 243-256.

Priestley, C.H.B. and Taylor, R.J., 1972. On the assessment of surface heat flux and evaporation using large-scale parameters. Monthly Weather Review, 100(2): 81-92.

Rana, G., Katerji, N., Mastrorilli, M., ElMoujabber, M. and Brisson, N., 1997. Validation of a model of actual evapotranspiration for water stressed soybeans. Agricultural and Forest Meteorology, 86(3-4): 215-224.

Ruairuen, W., Fochesatto, J., Sparrow, E.B., Zhung, M., Schanabel, W. and Kim, Y., 2015. Evapotranspiration Cycles in a High Latitude Agroecosystem: Potential Warming Role. In review PLOSONE. Submitted on 6 February 2015.

Savige, C.L., French, A.N., Western, A.W., Walker, J., Abuzar, M., Hacker, J.M. and Kalma, J.D., 2006. Remote Sensing Estimates of Actual Evapotranspiration in an Irrigation District Australian Journal of Water Resources: 207-212.

Schmugge, T., 1990. Remote Sensing of Biosphere Functioning. Measurements of surface soil moisture and temperature Springer-Verlag, New York.

Sharratt, B.S., 1990. Water retentiion, bulk density, particle size, and thermal and hydraulic conductivity of arable soils in Interior Alaska, Bulletin. University of Alaska Fairbanks.

Sharratt, B.S., 1994. Observations and Modeling of Interactions between Barley Yield and Evapotranspiration in the Sub-Arctic. Agricultural Water Management, 25(2): 109-119.

Sharratt, B.S., 1998. Barley yield and evapotranspiration governed by tillage practices in interior Alaska. Soil and Tillage Research, 46(3-4): 225-229.

Shulski, M. and Wendler, G., 2007. The Climate of Alaska. University of Alaska Press.

Shuttleworth, W.J., 1991. Insight from Large-Scale Observational Studies of Land Atmosphere Interactions. Surveys in Geophysics, 12(1-3): 3-30.

Sorbjan, Z., 1989. Structure of the Atmospheric Boundary Layer. Prentice-Hall, New Jersey, 316 pp.

Stanhill, G., 1976. The CIMO International Evaporimeter Comparisons, World Meteorological Organisation, Geneva.

Swenson, N.Y., 2013. Modeling changes in the length of the agricultural growing season in Interior Alaska, University of Alaska Fairbanks.

Thom, A.S., 1975. Momentum, mass and heat exchange. Vegetation and the Atmosphere, 1. Academic Press, London, U.K.

Van Veldhuizen, R.M. and Knight, C.W., 2004. Performance of agronomic crop varieties in Alaska 1978-2002. AEFF Bulletin. University of Alaska Fairbanks.

Verstraeten, W.W., Veroustraete, F. and Feyen, J., 2008. Assessment of evapotranspiration and soil moisture content across different scales of observation. Sensors, 8(1): 70-117.

Walsh, J.E., Chapman, W.L., Romanovsky, V., Christensen, J.H. and Stendel, M., 2008. Global Climate Model Performance over Alaska and Greenland. Journal of Climate, 21(23): 6156-6174.

Wang, K.C. and Dickinson, R.E., 2012. A Review of Global Terrestrial Evapotranspiration: Observation, Modeling, Climatology, and Climatic Variability. Reviews of Geophysics, 50.

Wang, Y. and Au, S.K., 2009. Spatial distribution of water supply reliability and critical links of water supply to crucial water consumers under an earthquake. Reliability Engineering & System Safety, 94(2): 534-541.

Wilson, K.B., Hanson, P.J., Mulholland, P.J., Baldocchi, D.D. and Wullschleger, S.D., 2001. A comparison of methods for determining forest evapotranspiration and its components: sap-flow, soil water budget, eddy covariance and catchment water balance. Agricultural Forest Meteorology, 106(2): 153-168.

Wolken, J.M., Hollingsworth, T.N., Rupp, T.S., Chapin, F.S., Trainor, S.F., Barrett, T.M., Sullivan, P.F., McGuire, A.D., Euskirchen, E.S., Hennon, P.E., Beever, E.A., Conn, J.S., Crone, L.K., D'Amore, D.V., Fresco, N., Hanley, T.A., Kielland, K., Kruse, J.J., Patterson, T., Schuur, E.A.G., Verbyla, D.L., and Yarie, J., 2011. Evidence and implications of recent and projected climate change in Alaska's forest ecosystems. Ecosphere, 2(11): 124.

Wright, J.L., 1982. New evapotranspiration crop coefficients. Journal of Irrigation and Drainage Engineering, 108(1): 57-74.

Wullschleger, S.D. and King, A.W., 2000. Radial variation in sap velocity as a function of stem diameter and sapwood thickness in yellow-poplar trees. Tree Physiology, 20(8): 511-518.

Xu, L., Myneni, R.B., Chapin, F.S., Callaghan, T.V., Pinzon, J.E., Tucker, C.J., Zhu, Z., Bi, J., Ciais, P., Tommervik, H., Euskirchen, E.S., Forbes, B.C., Piao, S.L., Anderson, B.T., Ganguly, S., Nemani, R.R., Goetz, S.J., Beck, P.S.A., Bunn, A.G., Cao, C. and Stroeve, J.C., 2013. Temperature and vegetation seasonality diminishment over northern lands. Nature Climate Change, 3(6): 581-586.

CHAPTER 3

Evapotranspiration cycles in a high latitude agroecosystem: Potential warming role[1]

[1] Ruairuen, W., Fochesatto, J., Sparrow, E.B., Zhang, M., Schanabel, W. and Kim, Y., 2015. Evapotranspiration Cycles in a High Latitude Agroecosystem: Potential Warming Role. In review PLOSONE. Submitted on 6 February 2015.

Abstract

Climate change is expected to have a profound influence on agroecosystems in Alaska. Over time as the acreages of agricultural lands increase, unexpected changes in surface energetics and evapotranspiration (ET) rates may arise consequently affecting regional climate regimes. The objective of this study was to evaluate summertime ET dynamics and surface energy processes in a subarctic agricultural farm in Interior Alaska. The study includes micrometeorological and hydrological data. Results covering the period from June to September 2012 and 2013 indicated consistent energy fractions: LE/R_{net} (64%), G/R_{net} (5%), H/R_{net} (27%) where LE is latent heat flux, R_{net} is the surface net radiation, G is ground heat flux and H is the sensible heat flux. Additionally actual surface evapotranspiration fraction from potential evaporation was found to be in the range of 59 to 66 %. After comparing these rates with those of most prominent high latitude ecosystems it is argued here that if agricultural lands and agroecosystem in high latitudes become an emerging feature, the regional surface energy balance may significantly shift in comparison to existing Arctic natural ecosystems.

Keywords: Evapotranspiration, agroecosystem, micrometeorology, surface energy, latent heat, sensible heat, subarctic

3.1 Introduction

Recent warming in high-latitudes has significantly impacted Alaska's ecosystems (Chapin et al., 2005a; Chapin et al., 2014). These impacts have affected a broad spectrum of ecological, physical and societal systems of the Arctic (Serreze and Hurst, 2000; Overland et al., 2004; Stow et al., 2004; Chapin et al., 2005a, 2005b; Hinzman et al., 2005; Euskirchen et al., 2006a; Serreze and Francis 2006). In this context agroecosystem and food related economic activities may be highly impacted by climate change over the next decades (Lobell et al., 2008; Battisti and Naylor 2009). Consequently, improvements in production efficiency and strategic utilization of agricultural and natural resources are important assets to cope with the increasing population, urbanization and therefore unprecedented demands for food (Foley et al., 2011).

Agroecosystem in Alaska currently represent only a small fraction of the entire landscape consisting mainly of boreal forests and tundra. Two current trends are supporting re-invigoration of Alaskan agriculture. First, desire for local food production and concerns about food security and second, lengthening of the growing season, higher surface temperatures and greater precipitation rates (Zhou et al., 2001; Chapin et al., 2005a; Bunn et al., 2007; Walsh et al., 2008; Wendler and Shulski, 2009; Euskirchen et al., 2012). To substantiate these current trends the expected changes at the end of the current century in mean surface temperature will range from 1.5 to 4.5 °C (Euskirchen et al., 2006b). Summer warming in the Alaskan Arctic has been observed to accelerate at rates from 0.3 °C to 0.4 °C per decade (Chapin et al., 2005a) peaking in the snow-free season (0.4 °C to 0.6 °C per decade) (Hammond and Yarie, 1996; Overpeck et al., 1997; Serreze and Hurst, 2000; Chapin et al., 2011). As a consequence of this warming trend, Arctic and Subarctic areas are experiencing longer growing seasons which in turn will favor the

implementation of large scale agriculture, as indicated by Juday et al. (2005) and Hatch (2011), albeit not in all areas (Slingo et al., 2005).

According to future scenarios of growing degree days (Juday, 2005; Hatch, 2011) the increasingly favorable conditions for developing agricultural lands may also expand crop variety including cash crops such as corn or canola. However there are major environmental challenges in high latitude settings that may have a counteracting influence on sustainable agriculture and expansion. Some of such elements are strong seasonal variation, cold soils, unpredictable frosts (Holloway, 1993; Loring and Gerlach, 2009; Stevenson et al., 2014) and precipitation events and low amounts of accumulated heat energy throughout the growing season (Van Veldhuizen and Knight, 2004). Nevertheless, Interior of Alaska provides a unique growing region that combines atmospheric radiation, warm air temperatures, agricultural and natural resources and water availability over a short and intensive growing season.

Soil surveys in Alaska indicate that more than 16 million hectares are suitable for agriculture where the largest and more productive area is localized in the Interior along the Tanana River Valley (Juday et al., 2005; STATSGO, 2011). Hence, Alaska may become more attractive as agriculture in the contiguous US becomes threatened (e.g., increasing drought). However, if agricultural demands in Alaska were to increase then part of the boreal forest would be at risk of being cleared for agricultural production purposes. Such land use change would likely have an important effect on surface-energy balance as well as water cycling potentially leading to local and regional climate changes and feedback (Bolle, 1990; Chapin et al., 2000; Pielke et al., 2007; Randerson et al., 2011; Wolken et al., 2011). Specifically this conversion would alter the seasonal albedo, surface roughness, moisture fluxes, and leaf area index (Pielke et al., 2007). Similarly, agricultural production could be limited by water availability and therefore increase in production

would increase the need for irrigation. This in turn would drive land surface-climate interactions by artificially modifying surface water and energy budget (Adegoke et al., 2003; Haddeland et al., 2006; Evans and Zaitchik, 2008; Ozdogan et al., 2010). Several observational and modeling studies have shown these effects on both ET and other atmospheric variables. The effects of irrigation are not only restricted to increase of ET over irrigated land (Suyker and Verma, 2009; Lei and Yang, 2010), but also to increase cloud formation, surface cooling and precipitation in nearby non-irrigated areas, and potentially induce changes in mesoscale circulation (Segal et al., 1998; Adegoke et al., 2007; Cook et al., 2011). In Alaska, however, the presence of agricultural land and its potential influence or feedback to regional climate is still unknown.

Evidence of changes in surface energy fluxes (Eugster et al., 2000) and water balance (Kane and Yang, 2004a) in Arctic ecosystem has been already documented. However, to the authors' knowledge, the case of agroecosystem in high latitude has not yet been systematically assessed. Here we provide measurements of surface energy balance over two growing seasons in summer of 2012 and 2013 from an agricultural land in Interior Alaska. Previous estimates of potential ET and actual ET have been carried out by other researchers in the same site using various methods (Patric and Black, 1968; Tanana Valley Irrigation Study Team, 1972). They found annual values of potential ET to be 467 mm and between 360 to 460 mm for Fairbanks (Patric and Black, 1968; Tanana Valley Irrigation Study Team, 1972). For the growing season (14 June to 31 August), the total ET of 223 mm for irrigated barley field, 113 mm for non-irrigated barley field, and 110 mm for fallow field were reported from experiments in the same site of the present study (Braley, 1980).

The objectives of this study are to determine the seasonal cycle of ET and to examine the energy fractioning in high latitude agroecosystem. A comparative assessment is then provided

between agroecosystems and representative natural ecosystems to highlight the importance and potential influence in climate projections. This information may be important to understand future possibilities for sustainable agricultural, local and regional climate change and feedbacks in the regional climate.

3.2 Materials and methods

3.2.1 Experimental site

The field experiment was conducted at the Fairbanks Experiment Farm (FEF) on West Tanana Drive of the University of Alaska Fairbanks (UAF) Agricultural and Forestry Experiment Station (AFES), in Fairbanks, Alaska, USA (64° 51′ 16.6″ N, 147° 51′ 36.4 ″ W, 150 m above sea level) (Figure 3-1). Experimental data were collected during the summer season from June to September of 2012 and 2013. The length of the growing season in the subarctic can be defined as the number of days between the last frost of spring and the first frost of fall. In this period of time the air temperature never drops below the freezing point (Sharatt, 1992). Based on meteorological data covering the period 1906-2006, the length of the growing season in Interior of Alaska, has increased over the last century by about 45% from 85 to 123 days (Shulski and Wendler, 2007).

The experimental site is characterized by an almost flat topography of the valley floor of the Chena and Tanana River basin. The area is sheltered on three sides from the northwest to the northeast by nearby hills rising to an elevation of 300-500 m, with another barrier about 250 km south the Alaska Range (Mayfield and Forchesatto, 2013; Fochesatto et al., 2013). The site has three main vegetation types: woodland, grassland and crops, combined with bare land. The research area has a continental subarctic climate with long, cold winters and short, warm summers. Summer comprises the months of June, July, and August where air temperature average 15°C. On the other hand, winter months of November through March have average air temperatures of

-18°C. Considering the central months of the two major seasons, the thirty-year (1981-2010) average air temperature in Fairbanks for July was 22°C with extreme temperatures rising above 32°C and decreasing down to -40°C in the month of December with continuous snow cover ground (Mulligan, 2004; ACRC, 2014). Precipitation is relatively low with the average annual accumulation for the period 1981-2010 about 263 mm, which mostly occurs during the summer months of July and August (ACRC, 2014). In general, daylength during the summer month rises up to 22 hours, which leads to a swing in temperature above 27°C for around 13 days. The range of frost free days, (i.e. air temperatures above 0°C) is approximately from 86 to 144 days with a median value of 115 days (ACRC, 2014).

Approximately one hundred years ago the research site was part of the Alaskan Boreal forest comprised mainly of *Picea mariana* specie and was cleared to be cultivated after 1906. In the past, large quantities of manure have been used as a supplement nutrient (Van Veldhuizen and Knight, 2014). The land had long term tillage and crop residue management practices (Sharratt, 1998). The site contains alluvial soil in the flood plains of the Tanana River. It is classified as a Tanana silt loam (Mulligan, 2004) with an approximate composition of 70% of silt, 8% of clay, and 22% of sand that has been conventionally farmed for about 80 years. It also contains a relatively high concentration of calcium carbonate and calcium sulfate at the soil surface (Van Veldhuizen and Knight, 2014). A perched water table above the permafrost is about 8 m deep while the main water table is located about 20 m deep (Van Veldhuizen and Knight, 2014). Crops were planted into soil that had been summer fallowed the previous season. Some vegetables crops are usually grown under irrigation practice to improve and control crop growth allowing better use of the available plant nutrients (Mulligan, 2004). As mentioned earlier this site was utilized by

Braley (1980) to estimate rates of ET from barley *(Hordeum vulgare L)* and rapeseed (*Brassica rapa*) fields during 1978 and 1979.

The research site for this study is considered a baseline for Interior Alaska agricultural research under the UAF AFES FEF research unit and considered to be representative of floodplain Interior Alaska growing condition.

3.2.2 Instrumentation

3.2.2.1 Lysimeter setup

The experiment deployed several drainage lysimeters (Figure 3-2a-b) during the two growing seasons in 2012 and 2013 (June to September). Each lysimeter was built 62 cm long, 62 cm wide and 62 cm high. A lawn mix soil consisting mostly of sandy loam (66% sand, 29% silt, and 5 % clay) was added to each lysimeter up to 10 cm from the top of each lysimeter prior to the summer of 2012. The lysimeters were installed on a flat land area over a leveled horizontal plane. The bottom of each lysimeter had a 15 cm filter layer that consisted of stones, gravel and sand with a layer of geofabric above and beneath. The geofabric separates the soil from the filter layer. The filter layer kept the soil from spilling into the drainage and helped to drain water during heavy rains or irrigation events. A pipe collected the drainage from the lysimeter bottom.

In 2012, the experiment in lysimeter plots was conducted from 6 June to 16 September. A set of six drainage lysimeters were used to measure ET for lettuce (*Lactuca sativa*) after direct seeding on 8 June, 2012. Sensors for soil volumetric moisture content (θ_{ly}) in the root zone were deployed at 15 and 30 cm depth in the lysimeters with a sample rate of 1 minute and record interval of 1 hour (Table 3-1). Soil temperature at 15 and 30 cm depths was measured with sensors in the lysimeter (Figure 3-2a). The lysimeters were irrigated throughout the, 2012 growing season. The observations were complemented by a multilevel 1, 2, 3 and 5 m meteorological observations,

along with measurements of net radiation (R_{net}), turbulent velocities (u, v, w), and sonic temperature (T_{sonic}) operating from 16 July to 9 September, 2012. Additionally, soil volumetric moisture content under barley, bromegrass *(Bromus inermis* Leyss.*)*, bare field (θ_{FEF}) and soil temperature (T_{soil}) at 15 cm depth were measured from 1 June to 30 September at the experiment site.

The intensive period of measurements during summer, 2013 was from 14 June to 16 September, with two treatments in which ET was measured. The plot treatments (three replicates) were: (i) vegetated lysimeter and (ii) unvegetated lysimeter. A total of three soil moisture sensors were installed at 5, 10 and 20 cm depths in the vegetated lysimeters (θ_{ly}) and unvegetated lysimeters (θ_{unly}) treatments (Figure 3-2b). The soil temperature was measured at 5 and 10 cm depth in each lysimeter. Oak leaf lettuce (*Lactuca sativa*) at the five to six-leaf stage was transplanted into vegetated lysimeters on 1 June, 2013. Irrigation was done throughout the, 2013 growing season in both treatments by adding the same amount of water to each lysimeter. Irrigation amount ranged from 5.5 mm to 20 mm. Data from measurements in both lysimeters treatments were used three weeks after set up to allow the soil to settle. Observations during summer, 2013 incorporated turbulent flux measurements derived from 3 m high sonic anemometer tower (operating from 7 July to 11 September, 2013) and a large aperture scintillometer (LAS), which was operated from 7 July to 30 August. These observations were complemented by subsoil measurements (T_{soil}) in barley, bromegrass and bare plots at 15 cm depth (operating from 1 June to 17 September) (Table 3-1). All soil moisture and subsoil temperature profiles were recorded on dedicated data loggers (Table 3-2).

3.2.2.2 Micrometeorological instrumentation

An eddy covariance (EC) instrument and meteorological station (Met station) were installed at the research site (Figure 3-1 and Table 3-1). The EC instrument was installed at 3 m above ground with two temperature probes (T_{air}) mounted at 1 m and 3 m above the ground to determine air temperature. Data were collected at 20 Hz frequency and fluxes were calculated for a 30-min eddy-covariance average period. With the aim to foster further studies a LAS was also installed on site (Figure 3-1). R_{net} sensor was mounted at 3 m oriented to the south to avoid shade at all times. A barometer (P) was placed at the surface to determine the ambient air pressure. All data sensors were centralized in a single data logger (Table 3-2). Similarly, two different levels of meteorological stations were mounted at 2 and 5 m above the ground surface to measure air temperature, relative humidity (RH), air pressure, wind speed (U), wind direction, and precipitation at 1-minute sampling rate. Data redundancy ensured a fairly continuous rate of data collection.

3.2.2.3 Pan evaporation

A standard weather bureau Class A evaporation pan (E_P) (122 cm diameter by 25 cm height) located 5 m away from the lysimeter plots was used to measure manually (hook gage) and determine daily time series of potential evaporation (E_P). The water level in the pan was maintained within 7.5-12.5 cm of the lip. The evaporation pan is made of aluminum and rests on a wooden platform 12 cm above the ground over non-irrigated grass around the area. Daily Ep measurements were collected at 0800 AM systematically every-day from 20 June to 5 September, 2013 and corrected by wind observations atop the pan evaporation (Table 3-1).

3.2.2.4 Surface energy balance

The surface energy balance is established based on Eq. (1). As described previously the FEF sits on an almost flat surface terrain with no aerodynamic obstacles on the central section of the farm covering 1 km East-West and approximately 700 m North-South direction.

$$R_{net} - G = H + LE + Res \quad \text{Eq. (1)}$$

where R_{net} is the surface net radiation flux (W m^{-2}), G is conductive ground heat flux (W m^{-2}), H is the sensible heat flux (W m^{-2}), LE is the latent heat flux (W m^{-2}) and Res is the residual closure component. In this case no storage term is considered since the vegetative canopy is very simple.

In Eq. (1) the net radiation term R_{net}, was measured directly. Ground heat flux (G) was calculated based on subsoil thermistors over different vegetation covers such as bromegrass field, barley field and fallow field. Sub-soil temperatures depths were 5 and 15 cm in summer 2012 experiment and 5, 15, 20 and 30 cm for the summer, 2013. Eq. (2) for conductive heat on the ground was utilized to calculate fluxes.

$$G = -k.\frac{\partial T}{\partial z} \quad \text{Eq. (2)}$$

where $T(z)$ is the soil temperature profile (°C) at specified depths z (cm) and k is the soil thermal conductivity. The k value in this study is treated as constant at 0.9 W $(m°C)^{-1}$ (ACRC, 2014). The H component was measured based on meteorological data and compared to eddy covariance procedure. The latent heat term (LE) was estimated using ET method described in following subsections.

Energy balance partitioning is used to determine the total available energy at the surface among the energy balance components by calculating the ratios LE/R_{net}, H/R_{net} and G/R_{net}.

These ratios indicated the relative magnitudes of LE, H and G in the surface energy balance. The ratio of H/LE flux is the Bowen ratio (β).

3.2.2.5 Energy balance closure

Based on independent measurements and determinations of R_{net}, LE, H and G the surface energy balance was established. Since Eq. (1) combine radiative fluxes with turbulent fluxes averaged in space and time; still an energy closure was estimated characterizing the site in terms of the surface-atmosphere interactions. The closure fraction C_F was therefore deduced based on Eq. (3).

$$C_F = \frac{LE + H}{R_{net} - G} \qquad \text{Eq. (3)}$$

3.2.3 Estimation of evapotranspiration

3.2.3.1 Penman-Monteith

A number of approaches can be used to estimate ET based on energy balance measurements Penman-Monteith (Monteith, 1965, PM hereafter), Priestley-Taylor (Priestley and Taylor, 1972) and Bowen ratio energy balance method (Dugas et al., 1991; Dugus, 1993). Of these, the PM method is the more widely used in advanced ET models (Goyal and Harmsen, 2014). This method estimates ET on the basis of surface aerodynamic properties and physiological characteristics of vegetation. Variables used in the PM method are net radiation, soil heat flux, air temperature, relative humidity, wind speed, and environment-specific variables related to vegetation cover. The aerodynamic and physiological properties of the vegetation are the two main drivers in the PM model. The study from López-Urrea et al. (2006) showed that the PM method verified the best performance approach to estimate ET using lysimeter observation in a semiarid climate among

seven other methods under comparison in a region of Spain. In this present study, the PM method has been chosen.

The general form of the Penman-Monteith ET estimate is defined in Eq. (4).

$$\lambda ET = \frac{\Delta(R_{net} - G) + \rho_a C_p (e_s - e_a)/r_a}{\Delta + \gamma(1 + \frac{r_s}{r_a})} \quad \text{Eq. (4)}$$

where ET is the latent heat flux of evapotranspiration (mm h^{-1} or mm day^{-1}), λ is latent heat of vaporization (kJ kg^{-1}), Δ is the slope of saturation vapor pressure versus temperature curve (kPa $°C^{-1}$), R_{net} is net radiation flux (W m^{-2}), G is ground heat flux (W m^{-2}), ρ_a is the air density (kg m^{-3}), C_p is the air mass specific heat (kJ kg^{-1} $°C^{-1}$) at constant pressure, e_s is the saturation vapor pressure at ambient air temperature (k Pa), e_a is the actual vapor pressure of the air mass (k Pa), $e_s - e_a$ is the vapor pressure deficit (VPD) (kPa), γ is the psychometric constant (kPa $°C^{-1}$), r_a is the aerodynamic resistance (sm^{-1}), and r_s is the bulk surface resistance to vapor transport (sm^{-1}). The recommendation of r_s equal 50 s m^{-1} is used for hourly time steps in this study (Allen et al., 2006). As indicated in Eq. (4) the PM method requires information on net radiation, air temperature, air humidity, wind speed, and ground heat flux that can be obtained and deduced from meteorological and radiation observations. In this case the vapor pressure deficit (VPD; $e_s - e_a$) can be calculated as a function of measured air temperature and relative humidity using Eq. (5) and Eq. (6).

$$e_s(T) = 0.6108 exp\left(\frac{17.27\,T}{T + 237.3}\right) \quad \text{Eq. (5)}$$

$$e_a = e_s(T)\frac{RH}{100} \quad \text{Eq. (6)}$$

where T is air temperature (°C) and RH is relative humidity in (%)

The slope of the saturation vapor pressure (Δ) curve is also a function of temperature and can be calculated based on Eq. (7).

$$\Delta = \frac{4098\left[0.6108exp\left(\frac{17.27\,T}{T+237.3}\right)\right]}{(T+237.3)^2} \quad \text{Eq. (7)}$$

The psychometric constant (γ) in Eq. (4) is a function of atmospheric pressure (which varies slightly over time and altitude) and is given by Eq. (8).

$$\gamma = \frac{C_p P}{\varepsilon\lambda} \quad \text{Eq. (8)}$$

where C_p is the specific heat at constant pressure, equal to 1.013 (MJ kg^{-1} °C^{-1}), λ is the latent heat of vaporization 2.45 (MJ kg^{-1}), ε is the ratio of molecular weight of water vapor/dry air = 0.622, and P is the ambient air pressure (kPa).

The aerodynamic resistance (r_a) under neutral conditions is calculated from Eq. (9) following Allen et al. (1998):

$$r_a = \frac{ln\frac{(z_m-d)}{z_{om}}\,ln\frac{(z_h-d)}{z_{oh}}}{k^2 u_z} \quad \text{Eq. (9)}$$

where r_a is aerodynamic resistance (sm^{-1}), z_m (m) is height of the wind speed measurements, z_h (m) is the height of temperature and humidity measurement, k is von Kármán constant (0.41), u_z (m s^{-1}) is wind speed measurement at z_m, d (m) is zero plane displacement height of wind profile, z_{om} (m) is roughness parameter for momentum, z_{oh} (m) is roughness parameter for heat and water vapor. Reference values recommended in the literature are $d = 2/3h_c$, where h_c is crop height in meters; $z_{om}$is $0.123h_c$, and z_{oh} is 0.1 (Smith et al., 2004).

3.2.3.2 Priestley-Taylor coefficient

Priestley and Taylor (1972) model (PT) calculates ET based on the measurements of equilibrium evapotranspiration via an empirical coefficient α. This coefficient varies according to the surface and vegetation type. A constant value of 1.26 is generally used in landscapes where vegetation cover is almost complete and for saturated surface conditions (Priestley and Taylor, 1972; Engstrom et al., 2002). The PT equation can be applied for unsaturated water surfaces provided α is adjusted to each conditions type (Flint and Childs, 1991). The PT model has been shown to provide acceptable accuracy for predicting daily evaporation in Arctic ecosystems if the value of α is known (Kane et al., 1990). The equation Eq. (10) describes the PT approach.

$$\alpha = \frac{\lambda ET}{\frac{\Delta}{\Delta + \gamma}(R_{net} - G)} \qquad \text{Eq. (10)}$$

where α is an empirical coefficient relating actual evaporation to equilibrium evaporation; Δ is the slope of the saturation vapor pressure and air temperature curve (kPa°C^{-1}); γ is the psychrometric constant (kPa°C^{-1}); R_{net} is net radiation (W m^{-2}); and G is ground heat flux (W m^{-2}).

3.2.3.3 Mass balance approach

The ET estimated from lysimeters usually derives from applying the mass balance equation as a closed system including measurement of the soil water budget and some meteorological variables. The mass balance method is largely used in agriculture especially in crop productions that use irrigation input (Allen et al., 1998; Jalota and Arora, 2002; Allen et al., 2005; Sun et al., 2006). The mass balance equation is indicated in Eq. (11) (Doorenbos and Kassam, 1986; Malek and Bingham, 1993).

$$P + I + C_r = ET + D + R \pm \Delta S \qquad \text{Eq. (11)}$$

where P is precipitation, I is irrigation, C_r is capillary rise, ET is evapotranspiration that includes canopy interception or wet canopy evaporation and plant transpiration (i.e. dry canopy transpiration), D is drainage, R is runoff and, ΔS is the change in water storage (all terms expressed in mm) in both the unsaturated and saturated soil zones.

In lysimeter systems, the runoff component R is not considered and the capillary rise C_r is assumed to be negligible. The mass balance for the study can thus be expressed according to Eq. (12):

$$P + I - D \pm \Delta S = ET \qquad \text{Eq. (12)}$$

To calculate the lysimeter water storage the devices were divided into different layers for which measurements are available by depth, assuming that each soil moisture sensor was installed in a sampling depth layer within the lysimeter. According to Lewan and Jansson (1996) on a similar setup measurements at 5 cm depth were considered to represent 0-7.5 cm layer; 10 cm depth representing 7.5-15 cm layer, and 20 cm corresponding to 15 cm down to the bottom of the soil profile. Then, the value of the soil water storage was obtained per layer after integrating the volumetric soil water content in the specific depth. The total soil water storage was determined by the sum of the storage in each layer Eq. (13).

$$S = \int_0^D \theta dz \cong \sum \theta \Delta z = \theta D \qquad \text{Eq. (13)}$$

where S represent the storage (mm), θ the volumetric soil water content ($m^3\ m^{-3}$), and D the considered soil depth (mm). The change in soil moisture can be obtained by the change in soil moisture content over depth and time as indicated in Eq. (14).

$$\Delta S = \int_0^z \int_{t_1}^{t_2} \theta dt dz \qquad \text{Eq. (14)}$$

where ΔS is the soil water storage, θ is the volumetric soil moisture content (m^3 m^{-3}), t is the time, and z is depth (cm). Hence, the soil water storage variation profile was determined by the difference between the values of the soil moisture content obtained in the final and initial time of each considered period (daily or weekly), using Eq. (15).

$$\Delta S = S_f - S_i \quad \text{Eq. (15)}$$

where ΔS is the soil water storage variation (mm), S_f the final soil water storage (mm), and S_i the initial soil water storage (mm).

Two phases of crop developments (intermediate phase and maturity phase) were selected for the comparison between ET derived from mass balance and energy balance. The period of 5 weeks after planting was identified as the intermediate phase, which started from 10 July to 23 July, 2013. While the maturity phase is when the canopy is fully developed starting from 14 August to 27 August, 2013.

3.3 Results

3.3.1 Meteorological and hydrological conditions

During the growing season, the average 30-min net radiation (R_{net}) in summer, 2013 was slightly higher than 2012 (Table 3-3), with the daytime average of 156±122 Wm^{-2} in 2013 and 149±123 Wm^{-2} (Figure 3-3a) in 2012. Conductive ground heat fluxes (G) at the site were calculated according to Eq. (2) and found to be mostly proportional to R_{net} and following a diurnal cycle. On average G in summer, 2013 resulted to be similar to 2012 (Figure 3-3b). The mean air temperature during the growing season was found to be on average 16.6°C in 2012 ranging from 0.2°C to 31.0°C and 18.2°C in 2013 with a variability range from -4.3°C and 34.9°C (Table 3-4). The growing season 2013 included ~5 days (44 hours) of negative air temperatures. However, the mean

air temperatures in both years were higher than the 30-year average. The maximum air temperature reached to 31.0°C and 34.9°C during the month of June, 2012 and 2013 respectively, while the normal (over 30 years) mean maximum was only 21.2°C (Table 3-4). This increase in maximum air temperature indicated a slightly warmer growing season in this high latitude agroecosystem. Conversely, the minimum air temperature occurred in September with the minimum value of -4.3°C recorded in 2013.

The relative humidity (RH) of the experimental site averaged 69±19 % for 2012 compared to 66±21 % for 2013. High values of RH were correlated to lower air temperatures (Figure 3-3d) as well as to increased precipitation events. Half-hourly mean vapor pressure deficit (VPD) varied during the growing season as depicted in Figure 3-3e. The mean midday VPD was 0.6±0.5 and 1.2±0.9 kPa with the maximum VPD of 3.4 and 4.3 kPa in June 2012 and 2013, respectively (Table 3-3).

The precipitation field was found to be very variable and significantly different from long term averages. Collected values at the experimental site for both years (Figure 3-3f) resulted in much lower amounts than those from 30-year average 165.3 mm (Table 3-4). On the other hand, comparing side-by-side both summers it was found that August 2013 (56.2 mm) verified larger amounts than August, 2012 (30.5 mm) while the normal monthly average precipitation is (47.7 mm). Similarly, the driest period in the past 30 years was verified to be June of every year (mean precipitation of 34.8 mm); however, June 2013, showed in the study area, a precipitation of 4.4 mm that was below the 30-year average. In contrast, the amount of precipitation in June 2012 (53 mm) was higher than the normal average of June. In addition, precipitation decreased about 6% during the summer season of 2012 when compared to the long-term 30 years mean for this area (Wendler and Shulski, 2009). A decreasing rate of more than 28% was found in the summer 2013

resulting in abnormally dry conditions. In terms of T_{soil}, there has not been significant differences on average T_{soil} measured at 15 cm depth at the experiment site when comparing the growing season of 2012 and 2013 (Figure 3-4; Table 3-3).

The soil volumetric water content (θ_{ly}) in the lysimeters in the layer 0-15 cm (2012) and in the 0-20 cm depth (2013) varied greatly over the growing season. The variability of θ_{ly} depended on irrigation practice (i.e., irrigation quota and timing) and precipitation events. An average θ_{ly} was 0.3851±0.0174 (6 June to 27 July 2012) and 0.3685±0.0245 m^3 m^{-3} (1 June to 6 September 2013) while an average θ_{FEF} in the farm field with no irrigation was 0.1700±0.0197 m^3 m^{-3} average accounting for farm diversity of land surface type (e.g., crop land, grass land and bare land) (Table 3-3).

The frequency distribution of surface wind direction and wind speed is shown during the period of study for the 2012 (Figure 3-5a) and 2013 (Figure 3-5b). Based on 30-min average temporal series wind data illustrated that the prevalent wind direction was from northwest sector variable from WNW to NNW and occurred about 30 % and 36 % of the time in 2012 and 2013 respectively. Additionally the occurrence of surface winds from southwest was 22 % for both years and from the southeast was 18 % and 17 % in 2012 and 2013, respectively. Wind speed, on the other hand, showed relatively steady values with an average value of 1.9±1.2 m s^{-1} and 2.0 ± 1.0 m s^{-1} with maximum at 6.7 m s^{-1} and 5.7 m s^{-1} in the 2012 and 2013 growing season, respectively.

In terms of the thermodynamic state of the surface atmospheric layer and soil conditions small differences were found in average air temperature, soil temperature, soil moisture, VPD, and wind speed during both years. However in terms of preseason difference it has to be noted that the snow melt in 2013 extended to the 18 May while it reached only up to mid-March and melted on 22 April in 2012 (NOAA, 2012, 2013).

3.3.2 Surface Energy Balance

3.3.2.1 Energy closure at half-hour time-scale

The energy balance closure is defined as the ratio between the resulting turbulent fluxes manifested at the surface and the total energy available (Twine et al., 2000; Farahani et al., 2007; Foken, 2008). In this study, the energy balance closure was evaluated for the entire dataset 1,540 thirty-minute daytime intervals. There is a strong linear relationship between the sum of the 30-min average latent heat (LE) and sensible heat (H) plotted against the available energy (R_{net}- G) for the summer 2013 growing season (Figure 3-6). A slope of 0.97 and an intercept of 10 W m^{-2} was obtained. These values indicate that on average the turbulent heat fluxes are slightly underestimated (by ~ 3%) neglecting the storage term in the energy balance equation due to the short canopy across the farm landscape (i.e., less than 0.50 m on average; see Figure 3-1). Similar results were found in Li et al. (2008) over maize farmland in Northwestern region of China. While Parent and Anctil (2012) obtained 0.79 in a farmlands at Saint-Ubalde, South-Eastern Canada. Moreover in grasslands, energy balance closure values generally ranged from 0.70 to 0.80 (Twine et al., 2000), 0.70 in prairie (Ma et al., 2009), 0.74 in olive orchard field (Martinez-Cob and Faci, 2010), 0.77 in switchgrass field (Wagle and Kakani, 2014), and 0.85 in an alfalfa field (Liu et al., 2010). However in terrestrial ecosystems, particularly including forest (Vourlitis and Oechel, 1999; Wilson et al., 2002; Grunwald and Bernhofer, 2007; Foken, 2008; Moderow et al., 2009; Sánchez et al., 2010) the energy balance closure was found to range from 0.50 to 0.96 due to the complexities of the canopy architecture.

Therefore it is concluded that giving the surface and atmospheric flow conditions of the experiment (Figure 3-1) the energy balance closure was established and being highly reliable to examine energy partitioning among all energy fluxes.

3.3.2.2 Energy balance and energy partitioning

Diurnal patterns. An example of diurnal cycle of energy fluxes in the 2013 growing season is shown in Figure 3-7. In this case a clear sky day is shown in the central part of the growing stage (on 30 July, day of the year 211). The diurnal variation of LE flux was larger than the one for H flux. The values of LE gradually increased in the morning until it reached the peak value of 296 W m^{-2} around midday, basically following the time-variation of R_{net}. Then, LE rapidly decreased to zero at 2100 Alaska Standard Time (AKST) when transition in the atmospheric surface layer started. On the same day, H flux slowly rose from 0 to a value of 180 W m^{-2}, when R_{net} peaked at 385 W m^{-2}, then H declined steadily to zero at 1900 AKST indicating the changes in stability conditions in the atmospheric surface layer. The midday fraction of available energy $(R_{net} - G)$ into H was about 37 %. On the same day, the G flux was the smallest compared with the rest of fluxes and became positive at 1000 AKST. The peak magnitude of G was 38 W m^{-2} and occurred at roughly 1600 AKST. Later on G dropped below zero about 2200 AKST ~two hours after R_{net}turned negative. The calculated Bowen ratio (β) around middday was 0.6.

Monthly Energy Balance. The monthly midday averages on the energy balance components (R_{net}, LE, H, G) for two years were calculated, and these results are illustrated in Figure 3-8. The data were acquired in the period June to September of each growing season. The summer mean R_{net} flux input for both years peaked in June (reaching ~ 244 W m^{-2} in 2012 and 264 W m^{-2} in 2013) and dropped-off gradually in August below 31-35 % and September below 56-64 % from the seasonal maximum (Figure 3-8). The amounts of R_{net} for both years were slightly different, with ~20 W m^{-2} in 2012 being lower than in 2013. When the midday means were considered over the period of the study, the mean LE was 114 W m^{-2} and 131 Wm^{-2}, the mean H was 70 W m^{-2}, 57 W m^{-2}, and the mean G was 18.8 W m^{-2} and 16.7 W m^{-2}, respectively, for summer 2012 and 2013.

On average, LE in 2013 was about 17 W m^{-2} greater than in 2012; the maximum difference between both years was 57 W m^{-2} in July. In this subarctic farm, from June to September, the monthly mean of LE was greater than H and G, with a declining trend illustraed in July of each year. On the other hand, the maximum monthly mean of H occurred in July for both years and was approximately 80 W m^{-2}, or about one half of the seasonal peak of LE. G is the smallest term in the energy balance equation. G was the largest in June 2013 (number of times G positive was 582 times from 698 times or ~ 83% positive) and July 2012 (number of G positive was 773 times from the total 1193 times or ~ 65% positive) and slowly decreased after July until it appraoched around zero or negative number in September.

Energy Partition. Summertime energy balance partitioning was calculated based on the obtained experimental values. The mean values per variable during each year and the overall average for the entire two-years experiment are shown in Column 2, 3 and 4 respectively in Table 3-5. The fraction of the incoming R_{net} distributed across the variables in the energy balance components at the FEF during four months (June to September) of 2012 and 2013 growing seasons are shown in Figure 3-9. A similar pattern was observed in the time evolution of enegy fractions LE/R_{net} and G/R_{net}. However H/R_{net} during 2012 exhibited some divergence when compared with LE/R_{net}. The values of LE/R_{net} ranged from 0.57 to 0.74 with an average of 0.64 for two growing seasons. The maximum of LE $/R_{net}$ illustrated in June 2012 (Figure 3-9a) and July 2013 when the vegetation was fully developed (Figure 3-9a-b) slightly decreased after this month in both years following vegetation senescence as well as gradually decreased VPD in August 2012. The variations of VPD directly relate to LE and show a decreasing pattern after the greening period (June).

On the other hand, it was observed over the two years that the major portion of surface energy balance was attrributed to LE in the period June to September behaving similarly to that in tundra and wetlands in Arctic and Subarctic sites (Table 3-6). Nevertheless, LE/R_{net} value is comparable to the lower range variability of that obtained from maize and soybean farmland, Nebraska, USA (0.6 to 0.9) (Suyker and Verma, 2008) and are close to the value of 0.68 obtained in commercial farms near Flora city, Florida USA (Sumner and Jacobs, 2005). In addition, the value of H/R_{net} ranged from 0.28 to 0.37 (mean 0.33) and 0.20 to 0.30 (mean 0.25) of R_{net} in 2012 and 2013, respectively. In comparison to other farmlands the ratio of H/R_{net} in this study was found slightly higher than in soybean and maize (0.2 to -0.2) according to experiments carried out in Nebraska (Suyker and Verma, 2008) considering only periods of fully-developed canopies.

At all instances the Bowen ratio (β) in the experiment site during the summer 2012 and 2013 was found to be systematically less than unity and ranging from 0.3 to 0.9 with an average of 0.56 in 2012 and 0.38 in 2013 (Table 3-5). On the other hand, G/R_{net} ranged from 0.05 to 0.11 in 2012 (mean 0.06) and 0.01 to 0. 08 (mean 0.07) in 2013 of R_{net}. Large values of G are typically found in subarctic landscapes (Eaton et al., 2001) with the exception of boreal forests (Starkenburg et al., 2014). Nevertheless, the ratios of H/R_{net} and G/R_{net} were in the interval of observed values from wetlands and shrub tundra (H/R_{net} near 28%, G/R_{net} ranges from 6-12%) from the Western and Central Canadian Subarctic (Eaton et al., 2001).

In terms of evaluating the general trends on ET associated with changes in vegetation, soil moisture, and meteorological parameters (Engstrom et al., 2002) the Priestley-Taylor coefficient (α) was calculated. High values of α are associated with a high-energy partition of LE/R_{net}, while low value represents the opposite. Stewart and Rouse (Stewart and Rouse, 1977) found that the theoretical value of α=1.26 is generally applied to saturated surfaces in high latitude. However, in

the present study α=0.91 was the average from two years while α ranging from 0.40 to 1.22 is reported for Arctic and boreal ecosystems (Eugster et al., 2000). The average value of 0.91 in this study is consistent with values reported by Eaton et al. (2001) in upland tundra. This variable range of α depends on the specific ecosystems under consideration for example, Liljedahl et al. (2011) reported mean midday α=1.08 (offshore) and 0.95 (onshore) in Arctic coastal wetland.

3.3.4 Evapotranspiration from water balance equation

3.3.4.1 ET by mass balance from irrigated lysimeters versus ET by energy balance

ET based on energy balance was obtained using Penman-Monteith (ET_{PM}) approach. ET_{PM} was computed based on available meteorological variables collected at the site (Figure 3-3), Eq. (4) according to Monteith (1973). The cumulative ET from mass balance obtained by Eq. (12) was applied to the irrigated vegetated (ET_{VL}) and unvegetated (ET_{UVL}) lysimeters. The measurements of precipitation (P), irrigation (I), drainage (D), and change in storage (ΔS) allowed estimating ET.

Comparing ET rates among different treatments on lysimeters, the results showed ET_{VL} having from 5 to 25 % larger cumulative ET compared to ET_{UVL}. When considering ET_{PM} as reference of a larger evaporative area, the ratios ET_{VI}/ ET_{PM} and ET_{UVI}/ ET_{PM} verified a lower fraction than 1 during the first week. While, for the rest of the experiment, it resulted in a ratio larger than or fairly close to 1 (Table 3-7). Similar results were obtained by Braley (1980) based upon their study within irrigated lysimeter and non-irrigated lysimeter in 1979. On the other hand, the ratio of ET_{VI}/ ET_{PM} was found to be slightly higher than ET_{UVL}/ ET_{PM} (Table 3-7). Nevertheless, on average ET mass balance was mostly higher than ET energy balance due to additional water input from irrigation. The average ratios of ET_{VI}/ ET_{PM} and ET_{UVI}/ ET_{PM} were

found to be 1.12 and 0.97, respectively. However, the ratio of ET from mass balance to the measurement of pan evaporation averaged 0.59 and 0.66 for ET_{UVL} and ET_{VL}, respectively.

Additionally, the ET estimate from water mass balance approach provided higher rates than from energy balance approaches, and this difference was accentuated as the vegetation fully developed (Table 3-7). However, ET from energy balance method can be used as a reference ET for an agroecosystem especially in the sparse vegetation landscape.

In order to compare and benchmark the hydrological rates in agricultural lands, Table 3-8 shows the annual and summer hydrological balance characteristics among various ecosystems in Arctic and subarctic regions. Based on, the total precipitation of 65 mm and irrigation 41.2 mm during this study period, the ET_{VL} was almost 97% while the ET_{UVL} was approximately 88% of precipitation and irrigation. In contrast, lower percentages indicated in Imnavait Creek Basin in North Slope of Alaska reported that 50% of precipitation went through the ET process and only 36% was found in the Upper Kuparuk Alaskan watershed (Kane et al., 2004b). In addition, 76% of precipitation was found to be evaporated from the permafrost in the boreal forest at Caribou-Poker Creek Watershed in Interior Alaska (Bolton et al., 2004). Nevertheless, other studies have also shown a lower ratio of precipitation being evaporated through ET process when compared to this present study (Ishii et al., 2004; Marsh et al., 2004; Quinton et al., 2004; Seuna and Linjama, 2004; Thorne and Hawkins, 2004; Vasilenko, 2004; Zhuravin, 2004; Table 3-8).

3.3.4.2 Penman- Monteith evapotranspiration (ET_{PM}) and pan evaporation (E_P)

Potential ET was measured with a Class A evaporation pan (E_P). Daily pan evaporation determinations (E_P) were manually made at 0800 AKST and no later than 0815 AKST every day. The E_P fraction is defined as the potential evaporation rate for a given location. E_P in this study ranged from 0 to more than 8.57 mm per day under clear skies conditions with daily average of

3.44±2.15 mm per day. Because manual E_P measurements were made at one given time everyday the temporal series of ET_{PM} was then compiled for a similar time interval for daily estimates comparison. There were about 89 measured values of E_P available and only 69 values were used for comparison with ET_{PM} because of sensor malfunctioning (Table 3-1). On the other hand, during the study period, relatively high rates of ET_{PM} were recorded in the month of July, while a declining trend was shown in September (Figure 3-10). Daily values of ET_{PM} ranged from less than 1 mm to more than 4 mm and the daily average was 2.27±1.40 mm day^{-1}. This average value is slightly higher than values obtained by Braley (1980) for the same site. The results showed that overall daily values of E_P exceeded ET_{PM}. Regression analysis was used to relate ET_{PM} to E_P and a correlation (R^2 = 0.69) was found, while a very poor relation (R^2 = 0.38) between those values was documented in other environments Florida, USA (Sumner and Jacobs, 2005).

3.4 Discussion

This study investigated the energy and water mass balance during 2012 and 2013 growing season at the UAF AFES FEF representative of high latitude agricultural lands in Interior Alaska. The summertime climatic characteristics at the site during both years were examined. An increase in the mean air temperature of +2.2°C and +3.7°C was observed in 2012 and 2013, respectively, when compared the temporal series to the 30-year average mean air temperature. Nevertheless, the mean air temperature regime during 2012 resulted within the normal range of variability for 30-year climatological data (Table 3-4). It is worth mentioning, that the mean values during 2013 verified a temperature excursion larger than one standard deviation when compared with the 30-year climatological mean. This warmer mean air temperature observed in summer 2013 is consistent with recent results indicating an increase in air temperatures of 1.4°C for Interior Alaska during the last 100-year record (2009). On the other hand, summer precipitation for 2012 remained

approximately within the range of the 30-year average (165.35 mm); while, precipitation for 2013 was ~26 mm below the normal average. After statistical examination of time series of R_{net} values it was concluded that no major differences were found (Table 3-3 and Figure 3-8).

In terms of turbulent flux regimes, the sensible heat verified no major variations with an average of ~ 80 W m^{-2}. However latent heat fluxes increased by ~ 22 W m^{-2} during summer 2013. This slight positive trend could only be explained by the change in pre-season conditions that made the sub surface to be wetter through an extended snowmelt period than in the other year (2012), (NOAA, 2012; Twine et al., 2000).

The value of energy balance closure C_F found in the field experiment reached levels of ~0.97 (Figure 3-6). This value is considered to be representative of energy closure in agricultural fields because often the topography characterizing such systems is close to ideal conditions (i.e., flat terrain covered by short grass). In comparison we found this value in good agreement to closure levels 0.70 to 0.99 observed at Fluxnet sites including several agricultural lands (Grunwald and Bernhofer, 2007). Still, a small residual term was found ~3%. This term is generally attributed to systematic methodological errors, systematic instrument bias, neglected energy sinks, and unrepresentativeness of the G term (Culf et al., 1993; Stannard et al., 1994; Mahrt, 1998; Aubinet et al., 2000; Zhuravin, 2004; Farahani et al., 2007; Grunwald and Bernhofer, 2007; Sánchez et al., 2010). After a careful revision of all terms intervening in the energy balance the residual term, can only arise from surface patches containing different crops (e.g., bare land, grass land and wooden trees). Therefore, an evaluation of G was conducted over the mentioned surface patches and it was observed to vary 3-6% (Table 3-3). This attribution is in agreement with other reports (Sánchez et al., 2010; Land et al., 2014) in which G was found to dominate the relative uncertainty on the

surface energy balance closure reaching up to 20% in agriculture sites (Heusinkveld et al., 2004; Meyers and Hollinger, 2004).

The energy partitioning of R_{net} into H, LE and G is strongly influenced by changes in surface conditions such as dynamics of vegetation growth, changes in of soil moisture and surface temperature affected by precipitation (Blanken and Rouse, 1995; Baldocchi et al., 1997; Wever et al., 2002). In particular the relationship between LE and soil moisture is complex, variable in space and time and verifies nonlinear relationships with the energy balance terms. For example, LE/R_{net} was found practically similar in dry and wet soils constrained in the case by VPD<0.30 kPa in Arctic coastal wetland (Liljedahl et al., 2011).

In the present study, the energy ratio of LE/R_{net} was found to be systematically larger than the same ratio for H/R_{net} and G/R_{net} consistently also with $\beta < 1$ (Table 3-5). Likewise, several ecosystems in Arctic and subarctic have larger $LE\ /R_{net}$ than H/R_{net} (Harazono et al., 1998; McGuire et al., 1998, Eugster, 2000; Rouse, 2000; Eaton et al., 2001; Kane and Yang, 2004a; Beringer et al., 2005; Nakai et al., 2013; Table 3-6). Alternatively, we have found that in comparison to some Arctic ecosystems (Eugster, 2000; Eaton et al., 2001; Boike et al., 2008; Langer et al., 2011b; Liljedahl et al., 2011) this ratio $LE\ /R_{net}$ is largest amongst the other fractions. However, we have to point out that this ratio is still on the lower range interval when compared to mid-latitude agricultural fields (Lloyd et al., 2001).

The monthly trends of energy fractions accounting for their seasonal evolution were observed to maximize around the middle of the summer to then trend negatively to the end of the season (Figure 3-9). This behavior is verified in the case of G/R_{net} and LE/R_{net}. However, the energy ratio associated to H/R_{net} is observed to fluctuate at the end of the season in 2012. These variations in H/R_{net} are consistent to changes in the thermodynamics of the air mass as indicated

in Figure 3-4. Similarly the energy fraction associated to $LE\ /R_{net}$ verifies a positive trend during the decaying phase of the season demonstrating an increasing response to monthly precipitation during August 2012 (Table 3-4).

With the aim to identify agricultural land energy fractions in the framework of natural ecosystems in high latitudes, Table 3-6, reports a comprehensive comparison among these systems across the panArctic. For Arctic and Subarctic wetlands, $LE/R_{net}$was reported to be larger than 0.57 according to the studies of Moore et al. (1994), Harazono et al. (1998), and Rouse (2000). In contrast, a lower value of LE/R_{net} in Arctic coastal wetlands was observed. In this case, a different environmental forcing due to the presence of onshore wind constantly offsets the energy partitioning (Liljedahl et al., 2011). While on the other hand, the reported values in literature of H/R_{net} and G/R_{net} are similar to the ones in the present study.

Furthermore the energy partitioning in tundra ecosystem verifies in comparison mostly a lower LE/R_{net}ranging from 0.36 to 0.67 (Rouse et al., 1997; Harazono et al., 1998; Eugster et al., 2000; Beringer et al., 2005; Grunwald and Bernhofer, 2007). On the other hand, H/R_{net} in the present study compares well with the lower range reported from the mentioned studies in the range 0.26 to 0.40. Finally the energy fractions obtained in this study correspond well with the results obtained in upland tundra ecosystems reported by Eugster et al. (2000) in which LE was the dominant component of surface energy balance. Conversely, energy balance studies in Alaskan coniferous boreal forest (i.e, composed mainly of white and black spruce trees) have found that H dominated the energy balance (Beringer et al., 2005; Lui et al., 2005; Starkenburg et al., 2014) with the exception of the study of Nakai et al. (2013) in the Poker Flat Research Range which indicated LE slightly dominant on a sparser canopy over discontinuous permafrost.

In terms of evaluating the ET rates, this study produced two different approaches based on mass balance (i.e., lysimeters based) and energy balance (i.e., micrometeorological based). These two approaches have definitively different spatial and temporal scales in terms of their environmental interactions (Alfieri et al., 2012) and therefore their ET rates were slightly different owing to the vegetation development and the spatial scale representation. In order to evaluate the potential for environmental interaction of agricultural land the lysimeter experiment was conducted based on irrigation practices over two treatments: vegetated and unvegetated. Overall this study found that ET_{VL} was higher than ET_{UVL} while ET_{UVL} was similar across the season to ET_{PM} (Table 3-7). However, it is important to note that if ET_{PM} is taken as the reference, the ratios ET_{VL}/ET_{PM} and ET_{UVL}/ET_{PM} verified a lower fraction in the first week due to the development phase of the vegetation. On the other hand, the fraction ET_{UVL}/ET_{VL} represented the percentage of ET due to vegetation growth and interception ranging from 75 to 94% (Table 3-7).

To give a prospective of the impact of agricultural lands in the framework of high latitude environments, Table 3-8 brings similar data records from ten sites around the pan-Arctic and they are compared to the findings of this study. Establishing the ratio ET/P allows the evaluation of the percentage of precipitation input that is sent back to the atmosphere through ET. Based on the synthesis of Arctic basins hydrology study by Kane and Yang the ET/P ratio is well-correlated to latitude in Arctic natural ecosystems and basically accounts for 36-75% of the mass balance (Table 3-8) (Bolton et al., 2004; Ishii et al., 2004; Kane et al., 2004; Marsh et al., 2004; Quinton et al., 2004; Seuna and Linjama, 2004; Thorne and Hawkins, 2004; Vasilenko, 2004; Zhuravin, 2004). Whereas, in this study this fraction ranged much higher from 87% to 97%; only comparable to the ones obtained by Thorne and Hawkins (2004) calculating 80% return (Table 3-8). This differences in ET and ET/P ratios are due to availability of energy for fluxes at the surface (Lu et al., 2003;

Stoy et al., 2006), precipitation distribution and rate as well as topography (Sun et al., 2002), forest canopy interception capacity associated to tree species and leaf area index (Swank and Douglass, 1974). It is therefore concluded here that the fraction of ET returned to the atmosphere in agricultural lands represent a much larger fraction of what has been reported for boreal forest at approximately the same latitude (Starkenburg et al., 2014) and also larger than the fractions obtained in Arctic tundra.

3.5 Conclusions

We found that the ET cycles represent a large portion of surface energy balance partitioning accounting for approximately 64% of the net radiation. Additionally we found the ratio of ET obtained by water mass balance related to the measured potential ET ranging from 0.59 to 0.66 for evapotranspiration rates based on unvegetated and vegetated lysimeters respectively. Conversely, ET was responsible for removing 97% and 88% of the moisture added to the vegetated and non-vegetated lysimeters, respectively.

Northern high latitudes are characterized by diverse ecosystems where wetlands and tundra dominate Arctic regions while subarctic locations are populated by boreal forest with coniferous and deciduous trees. This work puts in perspective and compares the surface energy fraction on agricultural land in the context of boreal forests, Arctic wetlands and tundra (Tables 3-6 and 3-8). The results indicated that the energy fluxing regime in terms of ET/R_{net} of agroecosystem in the subarctic exhibits similar characteristics to the tundra ecosystem in the Arctic; however they were found to be in contrast to those in boreal forest with coniferous and deciduous trees. Agroecosystems are an important land surface process which impact ET/R_{net} in the quantification of energy fluxes since subarctic regions are vastly populated by boreal forest and dotted by small-scale agricultural farms. Hence, differential fluxes manifested between these two clearly indicate

that different land surface features can drive small-scale circulation creating an additional imbalance term in the energy budget. Therefore, this study indicates that the presence and further development of agroecosystems in northern high latitudes may lead to an uncontrolled intensification of the ET cycle during the growing season in comparison with natural existing ecosystems.

Consequently, replacing native ecosystems to promote agricultural development and economic activities may result in significant changes in surface energy regimes, balance and new interactions that will need to be considered further. Moreover, these changes can collectivelly upscale to shift seasonal magnitude and temporal partitioning of regional fluxes introducing a positive feedbak to regional climate; therefore altering temperature and precipitation patterns which in turn may affect larger atmospheric scales.

Finally, on the basis of a changing climate scenario manifested through increasing air temperatures, lengthening of growing season and changes in vegetation gradients in northern high latitudes conjugated with agricultural lands and other developments, may lead to an overturning of the ET cycles (water vapor return to the atmosphere) with unexpected and yet unpredicted consequences given the nature of the changes and the nonlinear interactions characterizing the surface-atmosphere system.

3.6 Acknowledgements

The authors thank the Agricultural and Forestry Experiment Station (AFES) School of Natural Resources and Extension, the University of Alaska Fairbanks. Also, the authors are indebted to Alan Tonne, Darleen Masiak, Bob Van Veldhuizen, Stephen Sparrow, for help in facilitating the field experiment of this study. Ms Watcharee Ruairuen was funded by Suratthani Rajabhat University, Thailand. Gilberto J. Fochesatto was supported by the Geophysical Institute,

University of Alaska Fairbanks. Elena B. Sparrow was supported by the International Arctic Research Center and Alaska EPSCOR.

Figures

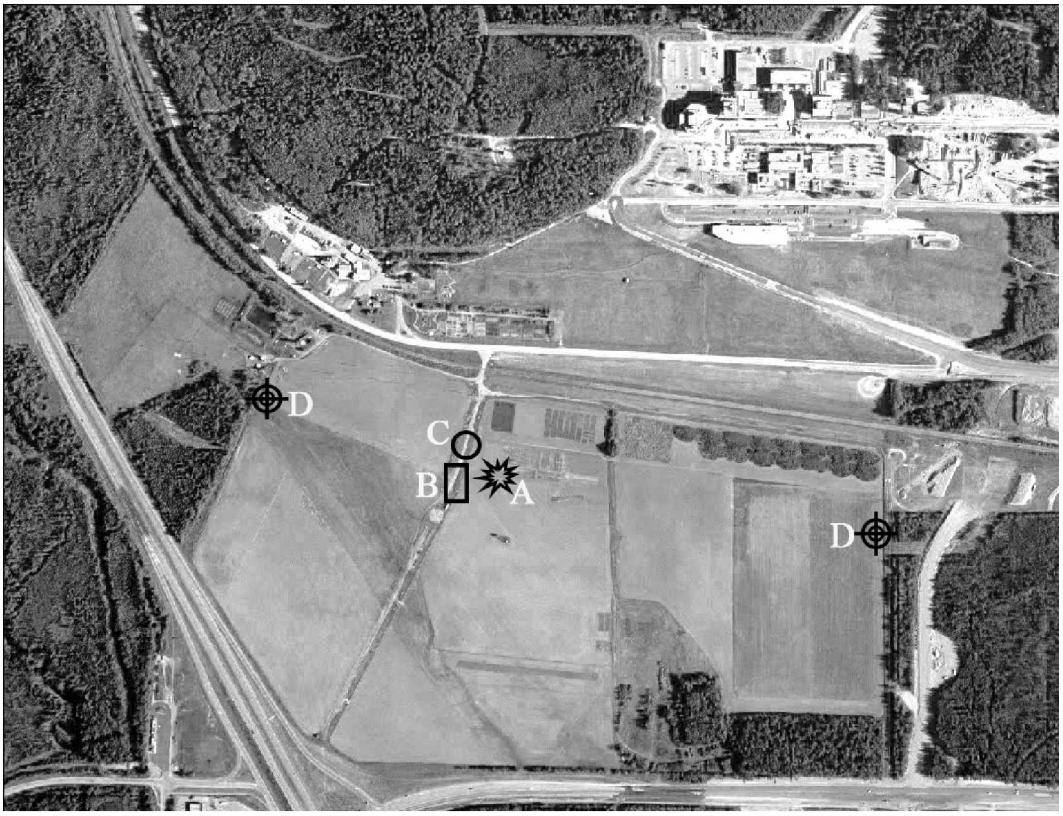

Figure 3-1 Fairbanks Experiment Farm (FEF) site at the UAF AFES. The location of the instrumentation is illustrated. The farm dimensions are: more than 1 kilometer on East to West and about 600 m North to South. EC tower (A), lysimeter plot (B), Meteorological station (C), LAS system (D).

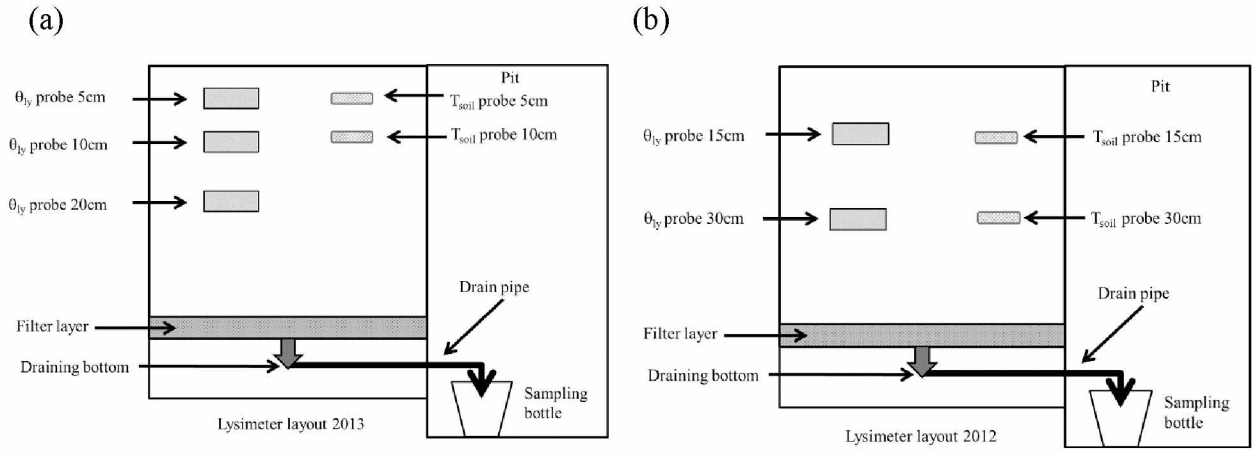

Figure 3-2 Ensemble instrumentation during intensive observing periods. Panel (a) – (b) represent the lysimeter setup including drainage system and installation probes layout for summer 2012 and 2013.

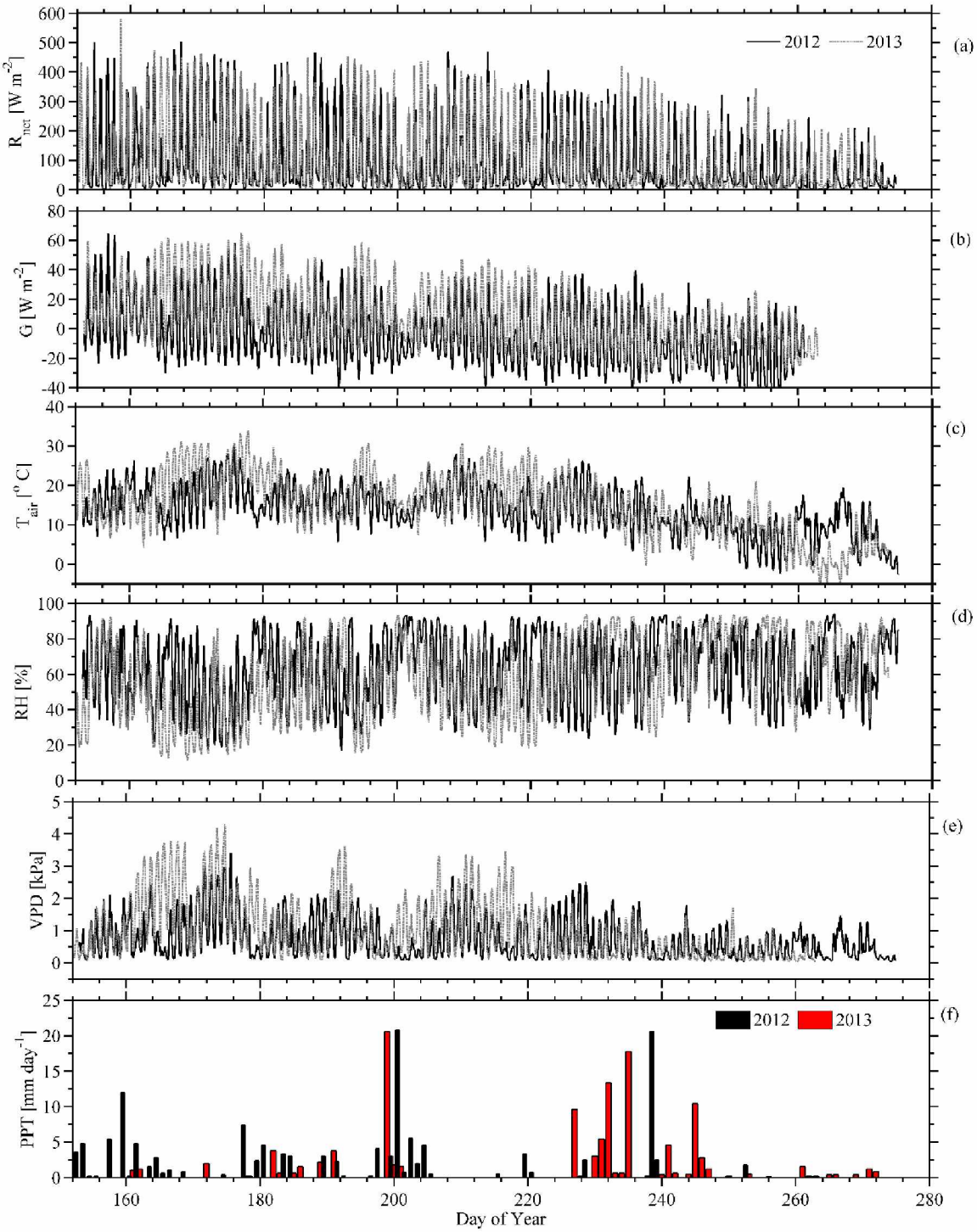

Figure 3- 3 Half hourly meteorological time series during growing seasons in 2012 and 2013 measured at the eddy-covariance tower. Panels: (a) net radiation R_{net} (W m^{-2}); (b) ground heat flux G (Wm^{-2}), (c) air temperature T_{air} (^{o}C); (c) relative humidity RH (%), (e) vapor pressure deficit VPD (kPa), and (f) precipitation (mm day^{-1}). The horizontal axis represents fractional Julian day in local Alaska Standard Time (AKST: UTC - 8 hrs).

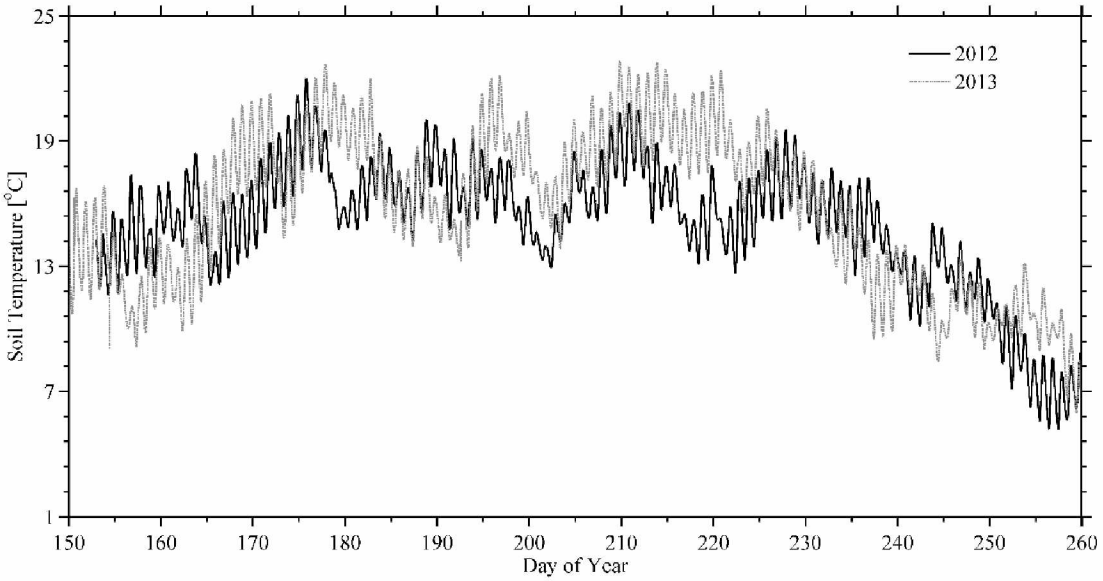

Figure 3-4 Time-series of soil temperatures. Soil temperature at 15 cm depth at the experiment site 1 June to 17 September in 2012 (black trace) and 2013 (gray trace). The horizontal axis represents fractional Julian day in local AKST.

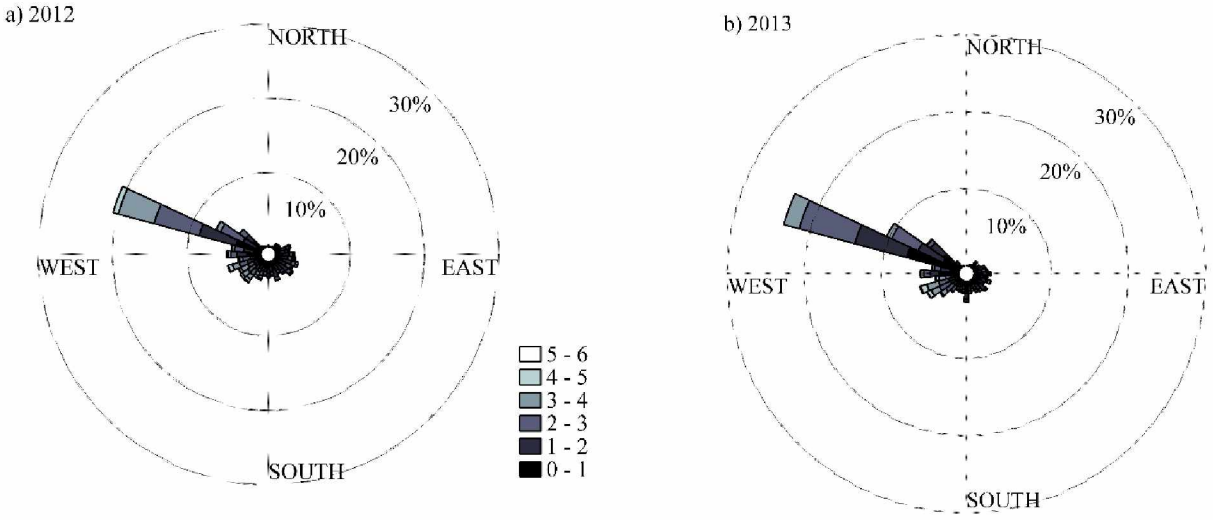

Figure 3-5 Frequency distribution of the wind speed and direction during summer. Panel (a) 2012 and (b) for 2013 at the experiment site during the period of study at 2 m height.

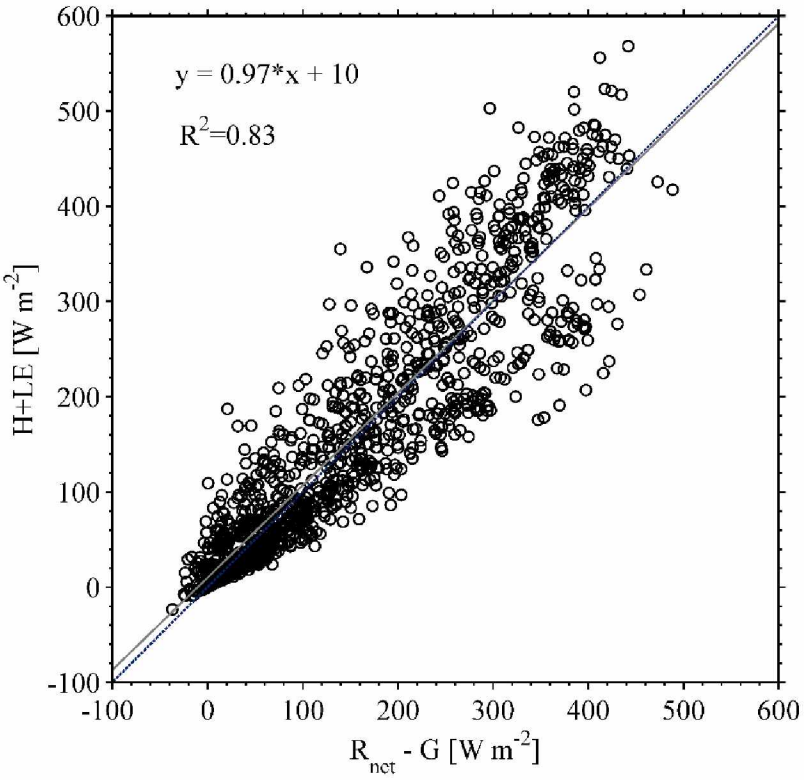

Figure 3-6 Scatterplot of energy balance closure. Horizontal axis is the available energy for fluxes (R_{net} - G) at the surface (W m^{-2}) and vertical axis of the sum of turbulent fluxes of sensible (H) and latent heat (LE). Period of study (11 July to 31 August, summer 2013). Values were obtained after 30 minute average under stationary conditions (1540 of points). Correlation coefficient was 97 % with an offset of 10 W m^{-2}.

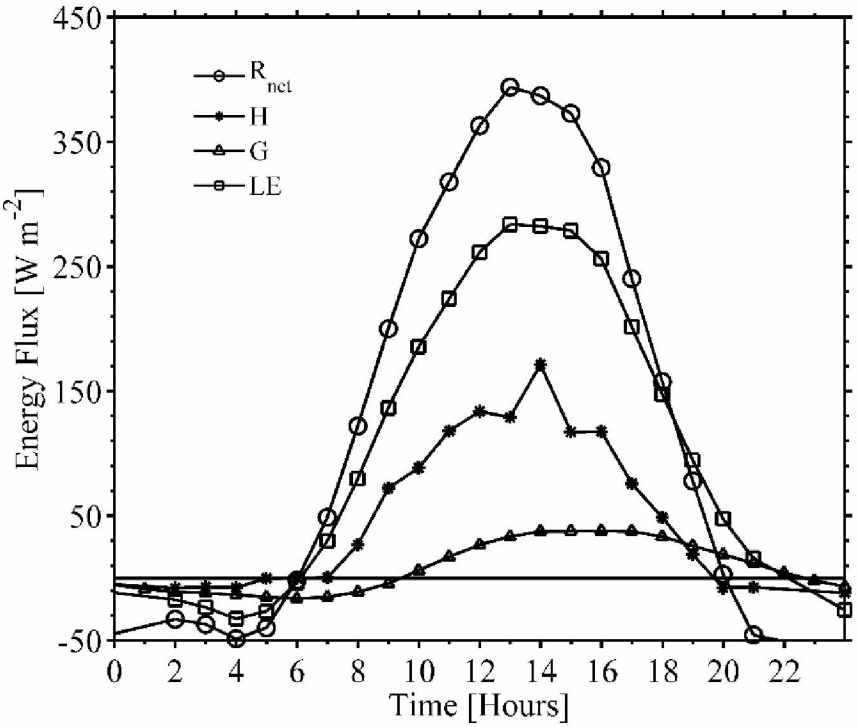

Figure 3-7 Diurnal cycle of radiative and turbulent fluxes during clear sky conditions. Case of July 30 (Day of Year 211) at the experiment site. Horizontal axis in AKST time in (hrs.) and vertical axis is in W m^{-2}. R_{net}=net radiation, LE=latent heat flux, H= sensible heat flux, G= ground heat flux.

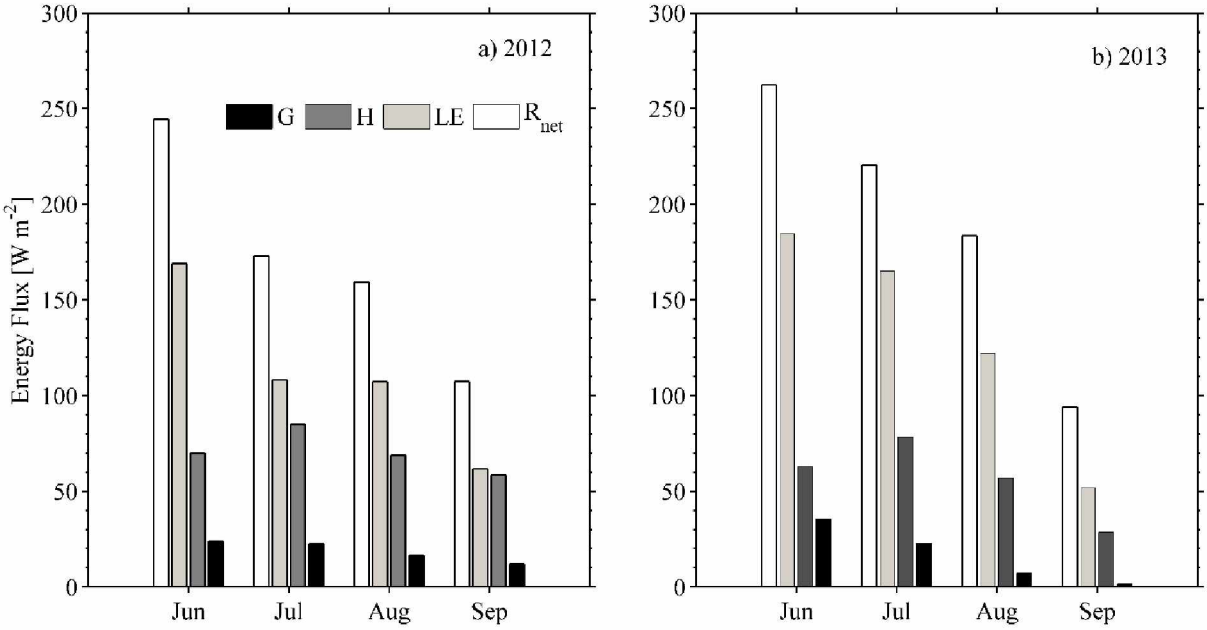

Figure 3-8 Monthly means estimates for the four components of the surface energy balance (R_{net}=net radiation, LE=latent heat flux, H= sensible heat flux, G= ground heat flux). The series covers from June to September of 2012 (panel-a) and 2013 (panel-b).

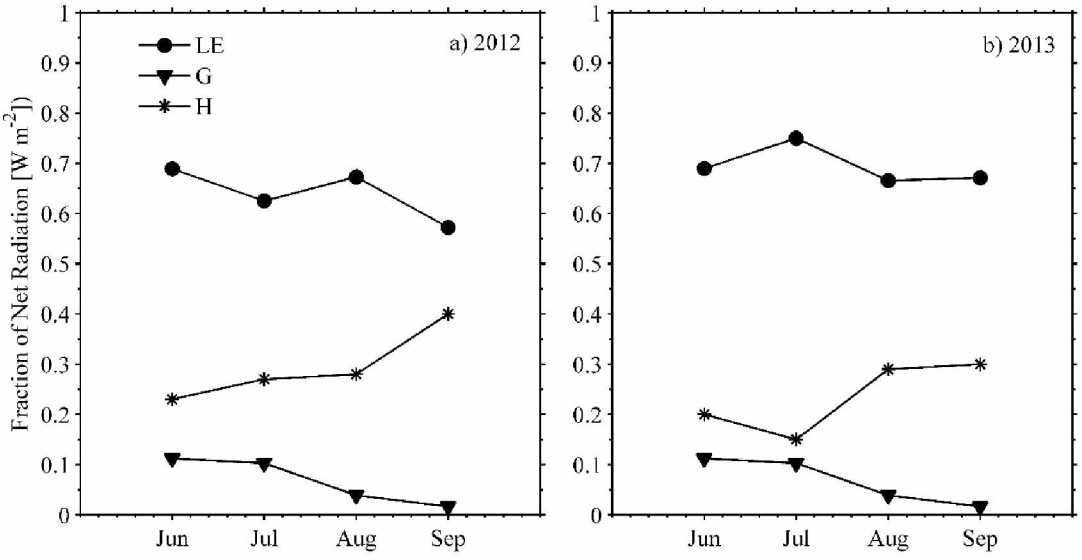

Figure 3-9 Monthly means estimates of energy partitioning. G, H and LE are referred to Rnet. Panel-a represents 2012 and panel-b 2013 during the growing season. Statistical values to define the series are based on midday energy partitioning computed as a mean over 5 hours centered in solar noon.

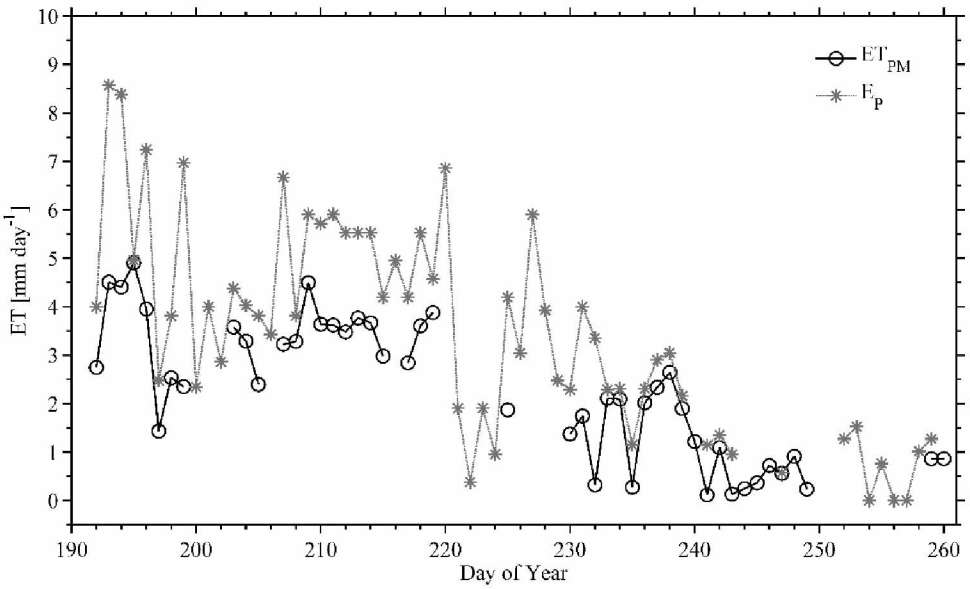

Figure 3-10 Daily means of evapotranspiration. Measured by pan evaporation (E_P) and estimated based on Penman Monteith (ET_{PM}) from 10 July to 16 September 2013. Some data gaps were caused by power interruptions and instrument failure and repair.

Table 3-1 Instrumentation utilized in the UAF AFES Fairbanks Experiment Farm in summers of 2012 and 2013.

Instruments & symbol	**Growing season - 2012**																**Growing season - 2013**															
	Jun				**Jul**				**Aug**				**Sep**				**Jun**				**Jul**				**Aug**				**Sep**			
T_{air}	-	-	-	-	-	-	-	-	-	-	-	-	-		-	-	-	-	-	-	-	-	-	-	-	-	-	-	-	-	-	-
RH	-	-	-	-	-	-	-	-	-	-	-	-	-		-	-	-	-	-	-	-	-	-	-	-	-	-	-	-	-	-	-
P	-	-	-	-	-	-	-	-	-	-	-	-	-		-	-	-	-	-	-	-	-	-	-	-	-	-	-	-	-	-	-
$\theta_{ly,unly}$		-	-	-	-	-	-						-	-				-	-	-	-	-	-	-	-	-	-	-	-			
θ_{FEF}	-	-	-	-	-	-	-	-	-	-	-	-	-	-	-	-																
T_{soil}	-	-	-	-	-	-	-	-	-	-	-	-	-	-	-	-	-	-	-	-	-	-	-	-	-	-	-	-	-	-	-	-
u_i,T																					-		-	-	-	-	-	-	-			
R_{net}	-	-	-	-	-	-	-	-	-	-	-	-	-	-	-	-	-	-	-	-	-	-	-	-	-	-	-	-	-	-	-	-
LAS						-	-			-	-											-		-	-	-	-	-	-	-	-	
PE																			-	-	-	-	-	-	-	-	-	-	-	-		

The observations were made during the growing season experiment (June-September). Timeline for involved instruments is indicated by shaded gray color in the table. Sensor description: T_{air} (ambient temperature sensors), RH (relative humidity probes 2 m and 5m), P (ambient pressure) probes, θ_{ly} and θ_{unly} (volumetric soil moisture sensor in lysimeter plot), θ_{FEF} (volumetric soil moisture sensor under barley, brome grass and bare field at FEF), T_{soil} (soil temperature sensors), sonic anemometer (u_i is u, v, w and T is sonic temperature), R_{net} (net radiation sensor), LAS (large aperture scintillometer) and PE (class A pan evaporation).

Table 3- 2 Instrumentation

Instrument & Symbol	Model	Variable Measured	Mounting Height [m]
u_i ,T	RMYoung 81000	u, v, w and sonic temperature	3
RH	Film capacitor element	relative humidity	2, 5
R_{net}	NRLite Campbell Scientific	solar radiation	1
T_{air}	PT 107 Campbell Scientific	air temperature	1, 3
Met station	Vantage Pro2 weather station, Davis Instruments	air temperature, barometric pressure, dew point temperature, rainfall, wind speed, wind direction	2, 5
Lysimeter	Drainage lysimeter	storage, drainage, ET	-0.62
θ_{ly} & θ_{unly}	10HS and ECH$_2$O EC-5, S-SMD-M005, Decagon Devices Inc.	soil moisture content	-0.15, -0.30 -0.05, -0.10, -0.20
θ_{FEF}	10HS ,S-SMD-M005, Decagon Devices Inc.	soil moisture content	-0.15
P	CS106 Campbell Scientific	barometric pressure	1
T_{soil}	S-TMB-M006 Onset Computer Corporation, Bourne, MA	soil temperature	-0.01, -0.15, -0.30 -0.05, -0.1, -0.2
PE	A standard weather bureau Class A evaporation pan	pan evaporation	0.12
LAS	The Scintec BLS-900 LAS	turbulent flux	1.8
CR1000	CR1000 Campbell Scientific	data logger for EC data	-
HOBO U30	HOBO U30 station , Onset Computer Corporation, Bourne, MA	data logger for soil moisture	-
HOBO Micro	HOBO Micro station, Onset Computer Corporation, Bourne, MA	data logger for soil moisture	-
HOBO 4 ext	HOBO 4 ext channels , Onset Computer Corporation, Bourne, MA	data logger for soil temperature	-

Table 3-3 Seasonal means of major microclimate variables at FEF during the growing seasons under study.

Parameters	Growing season in 2012	Growing season in 2013
R_{net}	149±123	156±122
G_{EC}	8.0±5.8	7.5±5.6
G_{bare}	21.1±18.8	13.1±8.7
G_{grass}	18.2±13.7	8.1±5.7
G_{barley}	20.0±16.9	21.5±18.8
VPD	0.6±0.5	1.15±0.92
θ_{ly}[a]	0.3851±0.0174[b]	0.3685±0.0245[c]
θ_{unly}[a]	-	0.2666±0.0659[d]
θ_{FEF}[a]	0.1700±0.0197	-
T_{soil} (°C)	13.6±4.1	15.4±4.0
U (m s^{-1})	1.9±1.15	2.0±1.0

R_{net}: net radiation (W m^{-2}), G_{EC}: ground heat flux (W m^{-2}) at EC site, bare field (G_{bare}), brome grass field (G_{grass}), and barley field (G_{barley}), LE: latent heat flux (W m^{-2}), VPD: vapor pressure deficit (kPa), θ_{ly}: volumetric soil moisture content (m^3 m^{-3}) in irrigated vegetated lysimeter at 15 cm depth average from three lysimeters in summer 2012 and averaged from 0-20 cm depths from three lysimeters in summer 2013, θ_{unly}: volumetric soil moisture content (m^3 m^{-3}) in unvegetated lysimeter in summer 2013, θ_{FEF}: an average volumetric soil moisture content (m^3 m^{-3}) at 15 cm depth from brome grass, barley and bare field, T_s: an average soil temperature (°C) at 15 cm from brome grass, barley and bare field, and U: wind speed (m s^{-1}) at 2 m height at meteorological station. First column represents the major variables measured, second and third column are mean ± standard error of each variable for the 2012 and 2013 growing season.

[a] More than two significant digits are needed for volumetric soil moisture content

[b] volumetric soil moisture content data were available from June –July 27, 2012

[c] volumetric soil moisture content in a vegetated lysimeter for 2013 growing season

[d] volumetric soil moisture content in an unvegetated lysimeter for 2013 growing season

Table 3-4 Monthly mean meteorological parameters measured at the FEF.

Month	Mean Temp. ± Std dev (°C)			Max Temp (°C)			Min Temp (°C)			Precipitation (mm)		
	Hist.	2012	2013	Hist.	2012	2013	Hist.	2012	2013	Hist.	2012	2013
Jun	15.8±5.4	17.6±4.9	22.7±6.3	22.0	31.4	34.9	9.6	4.9	3.8	34.8	53.0	4.4
Jul	16.9±5.1	17.0±4.2	19.1±4.8	22.6	28.2	32.0	11.3	6.3	7.8	54.9	53.6	36.6
Aug	13.2±5.3	14.9±4.6	15.9±5.9	18.8	26.8	31.1	8.0	5.7	0.3	47.7	30.5	56.2
Sep	6.4±6.7	5.6±3.2	5.9±5.2	12.6	12.8	21.3	1.7	0.2	-4.3	27.9	18.2	21.0
Growing season[c]	14.4±2.9	16.6±4.9	18.2±6.4	21.2	24.8	29.8	7.6	4.3	1.9	165.3	155.3	118.2

Monthly means calculated between June to September during the 2012[a] and 2013[a] growing season in comparison with historical data of the climate normal[b] in the 30-year time period from 1981-2010 for Fairbanks, Alaska, USA, provided by the National Climatic Data Center. Hist. represents the historical data of climatological in the 30-year average. The second-four columns indicate the mean of air temperature with standard deviation (Std dev) during two summer season compare to the 30-year average.

[a] Meteorological station at the study site

[b]The climate normal (a 30-year mean) at the Fairbanks International Airport (http://climate.gi.alaska.edu/Climate/Normals).

[C] Here the growing period is calculated from 1st June to 20th September

Table 3-5 Seasonal means of surface energy partitions, Bowen ratio (β), vapor pressure deficit (VPD), Priestley Taylor alpha coefficient (α) and energy balance closure (C_F) at the FEF.

Parameters	Entire growing season 2012	Entire growing season 2013	Two years Average
LE/R_{net}	0.58	0.65	0.64
H/R_{net}	0.33	0.25	0.27
G/R_{net}	0.06	0.07	0.06
β	0.56	0.38	0.45
α	1.03	0.77	0.91
C_F	0.97	0.97	0.97

Values are calculated between 1 June to 15 September in 2012 and 2013 growing season. Average midday (1100 -1500 AKST) energy balance energy partitioning obtained from a total 352 and 364 samples in 2012 and 2013 respectively. An average over two years period was calculated based on 716 data-points indicated in fourth column.

Table 3-6 Mean summer values of the energy balance partitioning for Arctic and subarctic ecosystems calculated and/or collected from various published data sources.

Terrain type	Location	LE $/R_{net}$	H $/R_{net}$	G $/R_{net}$	VPD	β	Methods	Source
Agricultural land	Alaskan subarctic farm, Interior Alaska	0.64	0.27	0.06	1.54	0.44	EC	Ruairuen et al. (this work)[a]
Wetland	Schefferville, Quebec	0.63	0.25	0.10	-	0.50	EC	Moore et al. (1994)
Wetland	Happy Valley, Alaska	0.57	0.29	0.09	-	0.50	EC	Harazono et al. (1998)
Wetland	Churchill, Manitoba	0.65	0.20	0.11	1.06	0.31	BREB	Rouse (2000)
Arctic coastal wetland	Barrow Alaska	0.28	0.35	0.15	0.12	1.25	EC	Liljedahl et al. (2011)
Moist tussock Tundra	Happy Valley Alaska	0.43	0.37	0.14	-	0.9	EC	Vourlitis and Oechel (1999)
Moist Tussock Tundra	Council on Seward Peninsula, Alaska	0.36	0.34	0.12	0.52	0.94	EC	Beringer et al. (2005)
Upland Tundra	Hudson Bay Coast, Ontario	0.57	0.29	0.09	-	0.51	BREB	Rouse et al. (1997)
Upland Tundra	Happy Valley, Alaska	0.49	0.40	0.16	0.81	0.82	EC	Harazono et al. (1998)
Upland Tundra	Ice Cut, Alaska	0.61	0.27	0.12	-	0.44	EC	Eugster et al. (2000)
Tundra (non-shrub wet fen)	Imnavait Creek, Alaska	0.67	0.26	0.07	-	0.39	EC	Eugster et al. (2000)
Tree line shrub tundra	Wiseman, Alaska	0.65	0.30	0.05	-	0.46	EC	Eugster et al. (2000)
Black Spruce forest	UAF	0.20	0.39	0.03	-	2.03	EC	Starkenburg et al. (2014)
White spruce forest	Council on Seward Peninsula, Alaska	0.37	0.44	0.05	0.39	1.22	EC	Beringer et al. (2005)
Black spruce forest	Delta Junction, Interior Alaska	0.24	0.58	0.03	-	2.42	EC	Lui et al. (2005)
Black spruce forest	Poker Flat, Interior Alaska	0.37	0.35	0.26	0.5	0.95	EC	Nakai et al. (2013)

First column represents the ecosystem types, second column is the location of measuring site, third to fifth columns are energy partitioning values for $LE\ /R_{net}, H\ /R_{net}, G\ /R_{net}$ (derived from daily midday flux averages), sixth column is VPD (kPa) for each ecosystem type, seventh column is the Bowen ratio (β), eigth column is the measuring method used for energy budget components measured, and nineth column is the reference for data.

EC=Eddy covariance methods, BREB= Bowen ratio-energy balance methods

[a]Average over two years growing season data in 2012 and 2013 from this present work during 1 June - 20 September.

Table 3-7 A summary of weekly ET by water balance in comparison with the ET by energy balance during intermediate development phase (10 - 23 July, 2013) and maturity phase (20 – 27 August, 2013) of crop under wet conditions.

Week-period	ET_{VL} (mm)	ET_{UVL} (mm)	ET_{PM} (mm)	ET_{VL}/ ET_{PM}	ET_{UVL}/ ET_{PM}
10 - 16 July, 2013	22.91	21.57	25.81	0.89	0.84
17 - 23 July, 2013	22.26	20.64	20.54	1.08	1.00
14 – 20 August, 2013	20.86	15.59	15.00	1.39	1.04
21 - 27 August , 2013	18.50	16.47	16.47	1.12	1.00

First column is time period covered by measurement (i.e., 10-16 July, 2013), second column is a weekly accumulated ET in the vegetated lysimeter (ET_{VL}), third column is a weekly accumulated ET in unvegetated lysimeter (ET_{UVL}), fourth column is a weekly accumulated ET by energy balance (ET_{PM}) derived using the Penman Monteith equation, fifth column is the ratio of ET_{VL}/ ET_{PM}, and sixth column is the ratio of ET_{UVL} / ET_{PM}.

Table 3-8 The annual and summer hydrological balance characteristics for Arctic and subarctic regions compiled from various published data sources.

	Location/latitude, longitude	P	Runoff	ET	ΔS	ET/P	Source
1	VL at the UAF AFES FEF, Alaska, USA (64. 5°N 147. 5° W)	106.2[a]	0	103.18	-0.07	0.97	Ruairuen et al. [This work][b]
2	UVL at the UAF AFES FEF, Alaska, USA (64. 5°N 147. 5° W)	106.2[a]	0	92.99	-0.93	0.87	Ruairuen et al. [This work][b]
3	Imnavait Creek (kuparuk), Alaska, USA (68. 6°N 149. 4° W)	359	181	179	-	0.50	Kane et al. (1990)
4	Upper Kuparuk, Alaska, USA (68. 6°N 149. 4° W)	376	237	140	-	0.37	Kane et al. (1973)
5	C2, Caribou-Poker Creek, Alaska,USA (65. 2°N 147. 5° W)	412	80	312	15	0.75	Bolton et al. (2004)
6	Tiksi, Russia (71. 7°N 128. 8° W)	98	144	54	-17	0.55	Ishii et al. (2004)[b]
7	Havikpak Creek, Canada (68. 3°N 133. 5° W)	283	110	134	-	0.47	Marsh et al. (2004)
8	Scotty Creek, Canada (61. 3°N 121. 3° W)	421	148	282	-	0.68	Quinton et al. (2004)
9	Dead Creek, Canada (50. 0°N 95. 0° W)	526	103	423	-	0.80	Thorne and Hawkins (2004)
10	Iittovuoma, Finland (68. 8°N 25. 4° E)	573	342	231	-	0.40	Seuna and Linjama (2004)
11	Filiper River (Mogot), Russia (56. 6°N 124. 9° E)	319	168	169	-8	0.53	Vailenko (2004)[b]
12	Kontakovy Creek, Russia (68.7. 3°N 133. 5° W)	405	296	137	0	0.34	Zhuravin (2004)
13	Trail Valley Creek, Canada (68.7. 3°N 133. 5° W)	231	118	110	4	0.48	Zhuravin (2004)

[a] Precipitation+Irrigation, [b] Summer hydrological balance

3.7 References

Adegoke, J.O., Pielke, R.A., Eastman, J., Mahmood, R., and Hubbard, K.G., 2003. Impact of irrigation on midsummer surface fluxes and temperature under dry synoptic conditions: A regional atmospheric model study of the U.S. high plain. Monthly Weather Review, 131: 55-564.

Adegoke, J.O., Pielke, R.S., and Carleton, A.M., 2007. Observational and modeling studies of the impacts of agriculture-related land use change on planetary boundary layer processes in the central U.S. Agricultural and Forest Meteorology, 142(2 – 4): 203 – 215.

Alaska Climate Research Center (ACRC), 2014. Climate Normal. University of Alaska, Fairbanks. Accessed: http://climate.gi.alaska.edu/Climate.

Alfieri, J.G., Kustas, W.P., Prueger, J.H., Hipps, L.E., Evett, S.R., Basara, J.B., Neale, C.M.U., French, A.N., Colaizzi, P., Agam, N., Cosh, M.H., Chavez, J.L., and Howell, T.A., 2012. On the discrepancy between eddy covariance and lysimetry-based surface flux measurement under strongly advective conditions. Advance in Water Resources, 50: 62-78.

Allen, R.G., Pereira, L.S., Raes, D., and Smith, M., 1998. Crop evapotranspiration guidelines for computing crop water requirements. FAO Irrigation and Drainage Paper 56, Rome.

Allen, R.G., Tasumi, M., Morse, A., and Trezza, R., 2005. A Landsat-based energy balance and evapotranspiration model in Western US water rights regulation and planning. Irrigation and Drainage Systems, 19: 251–268.

Allen, R.G., Pruitt, W.O., Wright, J. L., Howell, T.A., and Ventura, F., 2006. A recommendation on standardized surface resistance for hourly calculation of reference ET_o by the FAO56 Penman-Monteith method. Agricultural Water Management, 81: 1-22.

Aubinet, M., Grelle, A., Ibrom, A., Rannik, Ü., Moncrieff, J., Foken, T., Kowalski, A.S., Martin, P. H.,Berbigier, P., Bernhofer, C., Clement, R., Elbers, J.,Granier, A., Grünwald, T., Morgenstern, K., Pilegaard, K.,Rebmann, C., Snijders, W., Valentini, R., and Vesala, T., 2000. Estimates of the annual net carbon and water exchange of European forests: the EUROFLUX methodology. Advances in Ecological Research, 30: 114-175.

Baldocchi, D.D., Vogel, C.A., and Hall, B., 1997. Seasonal variation of carbon dioxide exchange rates above and below a boreal jack pine forest. Agricultural and Forest Meteorology, 83:147–170.

Battisti, D., and Naylor, R.L., 2009. Historical Warnings of future food insecurity with unprecedented seasonal heat. Science, 323(5911): 240.

Beringer, J., Chapin, F.S., III, Thompson, C.C., and McGuire, A.D., 2005. Surface energy exchange along a tundra-forest transition and feedbacks to climate. Agricultural and Forest Meteorology, 131: 143-161.

Blanken, P.D., and Rouse, W.R., 1995. Modelling evaporation from a high subarctic willow-birch forest. International Journal of Climatology, 15: 97–106.

Boike, J., Wille, C., and Abnizova, A., 2008. Climatology and summer energy and water balance of polygonal tundra in the Lena River Delta, Siberia. Journal of geophysical research. Biogeosciences, 113: G03025. doi: 10.1029/2007JG000540.

Bolle, H.J., 1990. The effect of land use change on net radiation and its partitioning into heat fluxes. In Bouwman, A.F., editor. Soils and the greenhouse effect. John Wiley and Sons, New York, New York, USA, pp. 329- 342.

Bolton, W.R., Hinzman, L., and Yoshikawa, K., 2004. Water balance dynamics of three small catchments in a Sub-Arctic boreal forest. In: Kane, D.L., Yang, D., (Editors). Northern Research Basins Water Balance. IAHS Publication 290. Wallingford, Oxfordshire, UK, pp. 213–223.

Braley, W.A., 1980. Estimates of evapotranspiration from barley and rapeseed in interior Alaska. M.Sc. Thesis, University of Alaska Fairbanks.

Bunn, A.G., Goetz, S.J., Kimball, J.S., and Zhang, K., 2007. Northern high-latitude ecosystems respond to climate change. EOS, 88: 333–334.

Chapin, S.F.III, Zavaleta, E.S., Eviner, V.T., Naylor, R.L., Vitousek, P.M., Reynolds, H.L., Hooper, D.U. , Sala, O.E., Hobbie, S.E., Mack, M.C., and Diaz, S., 2000. Consequences of changing biodiversity. Nature, 405: 234–242.

Chapin, F.S.III., Sturm, M., Serreze, M.C., McFadden, J.P., Key, J.R., 2005a. Role of land-surface changes in Arctic summer warming. Science, 310:657-660.

Chapin, F.S. III., Berman, M., Callaghan, T.V., Convey, P., Crépin, A.S., Danell, K., Ducklow, H., Forbes, G, Kofinas, G., McGuire, A.D., Nattall, M., Virginia, R., Young, O., and Zimov, S.A., 2005b. Polar systems. Polar Systems. In: Hassan, H., Scholes, R., Ash, N., editors. Ecosystems and Human Well-Being: Current State and Trends. Island Press, Washington, pp. 717-743.

Chapin, F.S. III., Matson, P.A., and Vitousek, P.M., 2011. Principles of terrestrial ecosystem ecology 2st ed. Springer, New York, pp. 447.

Chapin, F.S.III., Trainor, S.F., Cochran, P., Huntington, H., Markon, C., McCammon, M., McGuire, A.D., and Serreze, M., 2014. Chapter 22: Alaska. Climate Change Impacts in the United States. In: Melillo, J.M., Terese (TC), Richmond, and Yohe, G.W., (Editors). The Third National Climate Assessment: U.S. Global Change Research Program, pp. 514-536. Available: http://nca2014.globalchange.gov/report/regions/alaska

Cook, B.I., Puma, M.J., and Krakauer, N.Y., 2011. Irrigation induced surface cooling in the context of modern and increased greenhouse gas forcing. Climate Dynamics, 37:1587–1600.

Culf, A.D., Allen, S.J., Gash, J.H.C., Lloyd, C.R., and Wallace, J.S., 1993. Energy and water budgets of an area of patterned woodland in the Sahel. Agriculture and Forest Meteorology, 66: 65–80.

Doorenbos, J., and Kassam, A.H., 1986. Yield response to water. FAO Irrigation and Drainage Paper 33, Rome Italy.

Dugas, W.A., Fritschen, L.J., Gay, L.W., Held, A.A., and Matthias, A.D., 1991. Bowen ratio, eddy correlation, and portable chamber measurements of sensible and latent heat flux over irrigated spring wheat. Agricultural and Forest Meteorology, 56: 12-20.

Dugas, W.A., 1993. Micrometeorological and chamber measurements of CO_2 flux from bare soil. Agricultural and Forest Meteorology, 66: 115-128.

Eaton, A.K., Rouse, W.R., Lafleur, P.M., Marsh, P., and Blanken, P.D., 2001. Surface energy balance of the Western and Central Canadian subarctic: variations in the energy balance among five major terrain types. Journal of Climate, 14: 3692-3703.

Engstrom, R., Hope, A., Stow, D.A., Voulitis, G.L., and Oechel, W.C., 2002. Priestley-Taylor alpha coefficient: variability and relationship to NDVI in Arctic tundra landscapes. Journal of the American Water Resources Association, 38(6): 1647-1659.

Eugster, W., Rouse, W., Pielke Sr ,R., McFadden, J., Baldocchi, D., Kittel, T. G.F., Chapin, F.S., III, Liston, G., Vidale, P.L., Vaganov, E., and Chambers, S., 2000. Land–atmosphere energy exchange in Arctic tundra and boreal forest. Global Change Biology, 6: 84–115.

Euskirchen, E.S., McGuire, A.D., Kicklighter, D.W., Zhuang, Q., Clein, J.S., Dargaville, R.J., Dye, D.G., Kimball, J.S., McDonald, K.C., Melillo, J.M., Romanovsky, V.E. and Smith, N.V., 2006a. Importance of recent shifts in soil thermal dynamics on growing season length, productivity, and carbon sequestration in terrestrial high-latitude ecosystems. Global Change Biology, 12(4): 731-750.

Euskirchen, E.S., Pregitzer, K.S., and Chen, J., 2006b. Carbon fluxes in a young, naturally regenerating jack pine ecosystem. Journal of Geophysical Research, 111(D01101). doi:10.1029/2005JD005793.

Euskirchen, E.S., Bret-Harte, M.S., Scott, G.J., Edgar, C., and Shaver, G.R., 2012. Seasonal patterns of carbon dioxide and water fluxes in three representative tundra ecosystems in northern Alaska. Ecosphere, 3(1): 4. doi: 10.1890/ES11-00202.1

Evans, J.P., and Zaitchik, B.F., 2008. Modeling the large-scale water balance impact of different irrigation systems. Water Resources Research, 44 (W08448). doi: 10.1029/2007WR006671

Farahani, S.H.J., Howell, T.A., Shuttleworth, W.J., and Bausch, W.C., 2007. Evapotranspiration: progress in measurement and modeling in agriculture. Transactions of the ASABE, 50(50): 1627-1638.

Flint, A.L., and Childs, SW., 1990. Use of the Priestley-Talor evaporation equation for soil water limited conditions in a small forest clearcut. Agricultural and Forest Meteorology, 56: 247-260.

Fochesatto, G.J., Mayfield, J.A., Starkenburg, D.P., Gruber, M.A., 2013. Occurrence of shallow cold flows in the winter atmospheric Boundary layer of interior of Alaska. Meteorology and Atmospheric Physics, doi: 10.1007/s00703-013-0274-4.

Foken, T., 2008. The energy balance closure problem: An overview. Ecological Applications, 18(6): 1351-1367

Foley, J.A., Ramankutty, N., Brauman, K.A., Cassidy, E.S., Gerber, J.S., Johnston, M., Mueller, N.D., O'Connell, C., Ray, D.K., West, P.C., Balzer, C., Bennett, E.M., Carpenter, S. R., Hill, J., Monfreda, C., Polasky, S., Rockström, J., Sheehan, J., Siebert, S., Tilman, D., and Zaks, D.P.M., 2011. Solutions for a cultivated planet. Nature, 487: 337-342.

Goyal, M.R., and Harmsen, E.W., 2014. Evapotranspiration: Principle and Applications for Water Management. Apple Academic Press, NJ, USA.

Grunwald, T., and Bernhofer, C., 2007. A decade of carbon, water and energy flux measurements of an old spruce forest at the Anchor Station Tharandt. Tellus B, 59: 387–396.

Haddeland, I., Skaugen, T., and Lettenmaier, D.P., 2006. Anthropogenic impacts on continental surface water fluxes. Geophysical Research Letters, 33(L08406). doi: 10.1029/2006GL026047

Hammond, T., and Yarie, J., 1996. Spatial prediction of climate state factor regions in Alaska. Ecoscience, 3(4): 490-501.

Harazono, Y., Yoshimoto, M., Mano, M., Vourlitis, G., and Oechel, W.C., 1998. Characteristics of energy and water budgets over wet sedge and tussock tundra ecosystems at North Slope Alaska. Hydrological Processes, 12: 2163-2183.

Hatch, E., 2011. Micro-hardiness agriculture zones in the North Star Borough, Alaska Past and future scenarios. Senior Thesis, University of Alaska, Fairbanks.

Heusinkveld, B.G., Jacobs, A.F.G., Holtslag, A.A.M., and Berkowicz, S.M., 2004. Surface energy balance closure in an arid region: role of soil heat flux. Agricultural and Forest Meteorology, 122:21–37.

Hinzman, L.D., Bettez, N.D., Bolton, W.R. ., Chapin, F.S., Dyurgerov, M.B., Fastie, C.L., Griffith, B.., Hollister, R.D., Hope, A., Huntington, H.P., Jensen, A.M., Jia, G.J., Jorgenson, T., Kane, D.L., Klein, D.R., Kofinas, G., Lynch, A.H., Lloyd, A.H., McGuire, A.D.., Nelson, F.E., Oechel, W.C., Osterkamp, T.E., Racine, C.H., Romanovsky, V.E., Stone, R.S., Stow, D.A., Sturm, M., Tweedie, C.E ., Vourlitis, G.L., Walker, M.D., Walker, D.A., Webber, P.J., Welker, Winker, J.M., Kevin, S., and Yoshikawa, K., 2005. Evidence and implications of recent climate change in northern Alaska and other Arctic regions. Journal of Climate, 72: 251–298.

Holloway, P.S., 1993. The challenge of cultivating plants in cold soils, University of Alaska Fairbanks Agricultural and Forestry Experiment Station, Georgeson Botanical Notes N°, 12. Available: http://www.alaskaagresources.com/wp/wp-content/uploads/holloway_challenge_cultivating_plants_cold_soils_1993.pdf. Accessed 23 July 2014.

Ishii, Y., Kodama, Y., Sato, N., and Yabuki, H., 2004. Summer water balance in an Arctic tundra basin, eastern Siberia. In: Kane, D.L., Yang, D., (Editors). Northern Research Basins Water Balance. IAHS Publication 290. Wallingford, Oxfordshire, UK, pp. 50-64.

Jalota, S.K., and Arora, V.K., 2002. Model-based assessment of water balance components under different cropping systems in north-west India. Agricultural Water Management, 57: 75-87.

Juday, G.P., Barber, V., Duffy, P., Linderholm, H., Rupp, S., Sparrow, S., Vaganov, E., and Yarie, J., 2005. Forests, Land management and agricultural. Chapter 14th In: Arctic climate impact assessment (Ed) Arctic Council, Cambridge University Press, New York, NY, pp. 782-854.

Kane, D.L., Gleck, R.E., and Hinzman, L.D., 1990. Evapotranspiration from a small Alaskan Arctic watershed. Nordic Hydrology, 21: 253-272.

Kane, D.L., and Yang, D., 2004a. Overview of water balance determinations for high latitude watersheds. In: Kane, D.L., Yang, D. (Editors). Northern Research Basins Water Balance. IAHS Publication 290. Wallingford, Oxfordshire, UK, pp.1-12.

Kane, D., Gieck, R.E., Kitover, D.C., Hinzman, L.D., Mcnamara, J.P., and Yang, D., 2004b. Hydrological cycle on the North Slope of Alaska. In: Kane, D.L., Yang, D., (Editors). Northern Research Basins Water Balance. IAHS Publication 290. Wallingford, Oxfordshire, UK, pp. 224-236.

Land, M., Hansen, B.U., Pedersen, S.H., Stiegler, C., and Tamstorf, M., 2014. Characteristics of summer-time energy exchange in a high Arctic tundra health 2000-2010. Tellus B, 66: 21631.

Langer, M., Westermann, S., Muster, S., Piel, K., and Boike, J., 2011. The surface energy balance of a polygonal tundra site in northern Siberia Part 2: winter. Cryosphere, 5: 509524.

Lei, H., and Yang, D., 2010.Interannual and seasonal variability in evapotranspiration and energy partitioning over an irrigated cropland in the North China Plain. Agricultural and Forest Meteorology, 150(4): 581-589.

Lewan, E., and Jansson, P., 1996. Implications of spatial variability of soil physical properties for simulation of evaporation at the field scale. Water Resources Research, 32: 2067-2074.

Liljedahl, A.K., Hinzman, L.D., Harazano, Y., Zona, D., Tweedie, C.E., Hollister, R.D., Engstrom, R., and Oechel ,W.C., 2011. Nonlinear controls on evapotranspiration in arctic coastal wetlands. Biogeosciences, 8: 3375-3389.

Li, S., Shaozhong, K., Fusheng, L., and Zhang, L., 2008. Evapotranspiration and crop coefficient of spring maize with plastic mulch using eddy covariance in northwest China. Agricultural Water Management, 95: 1214-1222.

Liu, S., Bai, J., Jia, Z., Jia, L., Zhou, H., and Lu, L., 2010. Estimation of evapotranspiration in the Mu Us Sandland of China. Hydrology Earth System Science, 14: 573–584.

Lloyd, C., Harding, R., Friborg, T., and Aurela, M., 2001. Surface fluxes of heat and water vapour from sites in the European Arctic. Theoretical and Applied Climatology, 70: 19-33.

Lobell, D.B., Burke, M.B., Tebaldi, C., Mastrandrea, M.D., Falcon, W.P., and Naylor, R.L., 2008. Prioritizing climate change adaptation needs for food security in 2030. Science, 319(5863): 607–610.

Loring, P. A., and Gerlach, S. C., 2009. Food, culture, and human health in Alaska: an integrative health approach to food security. Environmental Science and Policy, 12: 466-478.

López-Urrea, R., Martín de Santa Olalla, F., Fabeiro, C., and Moratalla, A., 2006. Testing evapotranspiration equations using lysimeter observations in a semiarid climate. Agricultural Water Management, 85(1):15-26.

Lu, J., Sun, G., Amatya, D.M., and McNulty, S.G., 2003. Modeling actual evapotranspiration from forested watersheds across the Southeastern United States. Journal of American Water Resources Association, 39: 887–896.

Lui, H., Randerson, J.T., Lindfors, J., and Chapin, F.S., III, 2005. Change in the surface energy budget after fire in boreal ecosystems of interior Alaska: an annual perspective. Journal Geophysical Research, 110: D13101. doi: 10.1029/2004JD005158

Ma, Y., Wang, Y., Wu, R., Hu, Z.,Yang, K., Li, M., W. Ma, Zhong, L., Sun, F., Chen, X., Zhu, Z., Wang, S., and Ishikawa, H., 2009. Recent advances on the study of atmosphere-land interaction observations on the Tibetan Plateau. Hydrology Earth System Science, 13: 1103-1111.

Mahrt, L., 1998. Flux sampling errors for aircraft and towers. Journal of Atmospheric and Oceanic Technology, 15: 416–429.

Malek, E., and Bingham, G.E., 1993. Comparison of the Bowen ratio energy balance and the water balance methods for the measurement of evapotranspiration. Journal of Hydrology, 146: 209-220.

Marsh, P., Onclin, C., and Russell, M., 2004. A multi-year hydrological data set for two research basins in the Machenzie Delta region, NW Canada. In: Kane, D.L., Yang, D., (Editors). Northern Research Basins Water Balance. IAHS Publication 290. Wallingford, Oxfordshire, UK, pp. 205-212.

Martinez-Cob, A., and Faci, J.M., 2010. Evapotranspiration of a hedge-pruned olive orchard in a semiarid area of NE Spain. Agricultural Water Management, 97: 410-418.

Mayfield, J.A., and Fochesatto, G.J., 2013. The Layered Structure of the Winter Atmospheric Boundary Layer in the Interior of Alaska. Journal of Applied Meteorology and Climatology, 52(4): 953-973.

McGuire, J.P., Chapin, F.S.,III, and Hollinger, D.Y., 1998. Subgrid-scale variability in the surface energy balance of arctic tundra. Journal of Geophysical Research, 103: 28947-28961.

Meyers, T.P., and Hollinger, S.E., 2004. An assessment of storage terms in the surface energy balance of maize and soybean. Agricultural and Forest Meteorology, 125: 105–115.

Moderow, U., Aubinet, M., Feigenwinter, C., Kolle, O., Lindroth, A., Mölder, M., Montagnani, L., Rebmann, C., and Bernhofer, C., 2009. Available energy and energy balance closure at four coniferous sites across Europe. Theoretical and Applied Climatology, 98: 397–412.

Monteith, J.L., 1965. Evapotranspiration and environment. In: Proceedings of the 19th Symposium of the Society for Experimental Biology. Cambridge University Press, New York, NY, pp. 205-233.

Monteith, J.L., 1973. Principles of Environmental Physics. London, U.K.

Moore, K.E., Fitzjarrald, D.R., Wofsy, S.C., Daube, B.C., Munger, J.W., and Bakwin, P.S., 1994. A season of heat, water vapor, total hydrocarbon, and ozone fluxes at a subarctic fen. Journal of Geophysical Research, 99(D1): 1937-1952.

Mulligan, D., 2004. Soil Survey of the Greater Fairbanks Area, Alaska. Washington, D.C. United States Department of Agriculture, pp.101-103.

Nakai, T., Kim, Y., Busey, R.C., Suzuki, R., Nagai, S., Kobayashi, H., Kobayashi, H., Park, H., Sugiura, K., and Ito, A., 2013. Characteristics of evapotranspiration from a permafrost black spruce forest in interior Alaska. Polar Science, 7: 136-148.

NOAA Climatological Data, 2012. Climatological Data for Alaska 98. April 2012, pp. 4:34.

NOAA Climatological Data, 2013. Climatological Data for Alaska 99, May 2013, pp.5:34.

Overland, J.E., Spillane, M.C., and Soreide, N.N., 2004. Integrated analysis of physical and biological pan-Arctic change. Climate Change, 63: 291–322.

Overpeck, J., Hughen, K., Hardy, D., Bradley, R., Case, R., Douglas, M., Finney, B., Gajewski, K., Jacoby, G., Jennings, A., Lamoureux, S., Lasca, A., MacDonald, G., Moore, J., Retelle, M., Smith, S., Wolfe, A., and Zielinski, G., 1997. Arctic environmental change of the last four centuries. Science, 278: 1251-1256.

Ozdogan, M., Rodell, M., Beaudoing, H.K., and Toll, D.L., 2010. Simulating the effects of irrigation over the United States in a land surface model based on satellite-derived agricultural data. Journal of Hydrometeorological, 11:171–184.

Parent, A.C., and Anctil, F., 2012. Quantifying evapotranspiration of a rainfed potato crop in South-eastern Canada using eddy covariance techniques. Agricultural Water Management, 113: 45-56.

Patric, J.H., and Black, P.E., 1968. Potential evapotranspiration and climate in Alaska by Thornthwaite's classification. U.S. Department of Agricultural, Forest Service Research Report PNW 71.

Pielke, R.A.S., Degoke, J., Beltrán-Przekurat, A., Hiemstra, C.A., Lin, J., Nair, U.S., Niyogi, D., and Nobis, T.E., 2007. An overview of regional land-use and land-cover impacts on rainfall. Tellus, 59B: 587-601.

Priestley, C.H.B., and Taylor, R.J., 1972. On the assessment of surface heat-flux and evaporation using large-scale parameters. Monthly Weather Review, 100: 81-92.

Quinton, W.L., Hayashi, M., Blais, K.E., Wright, N., and Peitroniro, A., 2004. The water balance of wetland-dominated permafrost basin. In: Kane, D.L., Yang, D., (Editors). Northern Research Basins Water Balance. IAHS Publication 290. Wallingford, Oxfordshire, UK, pp. 186-194.

Randerson, J.T., Liu, H., Flanner, M.G., Chambers, S.D., Jin, Y., 2011. The Impact of Boreal Forest Fire on Climate Warming. Science, 314 (5802): 1130-1132.

Rouse, W.R., Mills, P.F., and Stewart, R.B., 1997. Evaporation in high latitudes. Water Resource Research, 13: 909-914.

Rouse, W.R., 2000. The energy and water balance of high latitude wetlands: controls and extrapolation. Global Change Biology, 6(1): 59-68.

Sánchez, J.M., Caselles, V., and Rubio, E.M., 2010. Analysis of the energy balance closure over a FLUXNET boreal forest in Finland. Hydrology Earth System Science, 14: 1487–1497.

Segal, M., Pan, Z., Turner, R.W., and Takle, E.S., 1998. On the Potential Impact of Irrigated Areas in North America on Summer Rainfall Caused by Large-Scale Systems. Journal of Applied Meteorology and Climatology, 37: 325–331.

Serreze, M.C., and Hurst, C.M., 2000. Representation of mean Arctic precipitation from NCEP–NCAR and ERA reanalyses. Journal of Climate, 13: 182–201.

Serreze, M.C., and Francis, J.A., 2006. The arctic amplification debate. Climate Change, 76: 241–64.

Seuna, P., and Linjama, J., 2004. Water balance of the northern catchments of Finland. In: Kane, D.L., Yang, D., (Editors). Northern Research Basins Water Balance. IAHS Publication 290. Wallingford, Oxfordshire, UK, pp. 111-119.

Sharatt, B.S., 1992. Growing Season Trends in the Alaskan Climate Record. Arctic, 45(2): 124-127.

Sharratt, B.S., 1998. Barley yield and evapotranspiration governed by tillage practices in interior Alaska. Soil and Tillage Research, 46(3): 225-229.

Shulski, M., and Wendler, G., 2007. The Climate of Alaska. University of Alaska Press.

Slingo, J.M., Challinor, A., Hoskins, B.J., Weeler, T.R., 2005. Introduction: food crops in a changing climate. Philosophical the Royal Society, 360: 1983-1989.

Smith, N.V., Saatchi, S.S., and Randerson, J.T., 2004. Trends in high northern latitude soil freeze and thaw cycles from 1988 to 2002. Journal of Geophysical Research: Atmospheres, 109(D1210). doi: 10.1029/2003JD004472

Stannard, D.I., Blanford, J.H., Kustas, W.P., Nichols, W.D., Amer, A., Schmugge, T.J., and Weltz, M.A., 1994. Interpretation of surface flux measurements in heterogeneous terrain during the Monsoon'90 experiment. Water resources research, 30: 1227–1239.

STATSGO, 2011. State soil geographic (STATSGO) data base. Alaska State geographic database. Washington, D.C.: U.S. Department of Agriculture, Natural Resources Conservation Service.

Starkenburg, D., Fochesatto, G.J., Cristóbal, J., Prakash, A., Gens, R., Alfieri, J.G., Nagona, H., Harazono, Y., Iwata, H. and Kane, D., 2014. Temperature regimes and turbulent heat fluxes across a heterogeneous canopy in an Alaskan boreal forest. Journal of Geophysical Research: Atmosphere, 120.

Stevenson, K.T., Rader, H. B., Alessa, L., Kliskey, A.D., Pantoja, A., Clark, M., and Smeek, J., 2014. Sustainable Agriculture for Alaska and the Circumpolar North: Part II. Environmental, Geophysical, Biological and Socioeconomic Challenges. Arctic. 2014; 296-319.

Stewart, R.B., and Rouse, W.R., 1977. Substantiation of the Priestley and Taylor parameter alpha=1.26 for potential evaporation in high latitudes. Journal of Applied Meteorology, 16: 649-650.

Stoy, P., Katul, G.G., Siqueira, M.B.S., Juang, J.Y., Novick, K.A., McCarthy, H.R., Oishi, A.C., Uebelherr , J., Kim, H ., and Oren, R., 2006. Separating the effects of climate and vegetation on evapotranspiration along a successional chronosequence in the southeastern US. Global Change Biology, 12: 2115–2135.

Stow, D., Hope, A., McGuire, A.D., Verbyla, D., and Gamon, J., 2004. Remote sensing of vegetation and land-cover changes in Arctic tundra ecosystems. Journal of Remote Sensing, 89: 281-308.

Sumner, D.M., and Jacobs, J. M., 2005. Utility of Penman-Monteith –Taylor, reference evapotranspiration, and pan evaporation methods to estimate pasture evapotranspiration. Journal of Hydrology, 308: 81-104.

Sun, G., McNulty, S.G., Amatya, D. M., Skaggs, R.W., Swift, L.W., Shepard, J.P., Riekerk, H., 2002. A comparison of the hydrology of the coastal forested wetlands/pine flat woods and the mountainous uplands in the southern US. Journal of Hydrology, 263: 92–104.

Sun, H.Y., Liu, C.M., Zhang, X.Y., Shen, Y.J., and Zhang, Y.Q., 2006. Effects of irrigation on water balance, yield and WUE of winter wheat in the North China Plain. Agricultural Water Management, 85: 211-218.

Suyker, A.E., and Verma, S.B., 2008. Interannual water vapour and energy exchange in an irrigated maize-based agroecosystem. Agricultural and Forest Meteorology, 148: 417-427.

Suyker, A.E., and Verma, S.B., 2009. Evapotranspiration of irrigated and rainfed maize–soybean cropping systems. Agricultural and Forest Meteorology, 149 (3-4): 443–452.

Swank, W.T., and Douglass, J.E., 1974. Stream flow greatly reduced by converting hard woods to pine. Science, 185: 857–859.

Tanana Valley Irrigation Study Team, 1972. Irrigation potential, Tanana river valley, Alaska. Report of a federal-state study team to the Fairbanks North Star Borough.

Thorne, G., and Hawkins, J., 2004. Hydrological processes and water balance for the Dead Creek watershed of southeastern Manitoba, 1982-1995. In: Kane, D.L., Yang, D., (Editors). Northern Research Basins Water Balance. IAHS Publication 290. Wallingford, Oxfordshire, UK, pp. 164-176.

Twine, E.T., Frustas, W.P., Norman, J.M., Cook, D.R., Houser, P.R., Meyers, T.P., Prueger, J. H., Starks, P.J., and Wesley, M.L., 2000. Correcting eddy-covariance flux underestimates over grassland. Agricultural and Forest Meteorology, 103: 279-300.

Van Veldhuizen, R.M., and Knight, C.W., 2004. Performance of agronomic crop varieties in Alaska 1978-2002. AEFF Bulletin, 111. Available: http://www.uaf.edu/files/snre/B111.pdf. Accessed 10 October 2014.

Vasilenko, N., 2004. Water balance of small Russian catchments in the Southern mountainous Taiga zone: "Mogot" case study. In: Kane, D.L., Yang, D., (Editors). Northern Research Basins Water Balance. IAHS Publication 290. Wallingford, Oxfordshire, UK, pp. 65-77.

Vourlitis, G.L., and Oechel, W.C., 1999. Eddy covariance measurements of net CO_2 flux and energy balance of an Alaskan moist-tussock tundra ecosystem. Ecology, 80(2): 686 -701.

Wagle, P., and Kakani, V.G., 2014. Growing season variability in evapotranspiration, ecosystem water use efficiency, and energy partitioning in switchgrass. Ecohydrology, 7: 64-72.

Walsh, J.E., Chapman, W.L., Romanovsky, V., Christensen, J.H., and Stendel, M., 2008. Global climate model performance over Alaska and Greenland. Journal of Climate, 21: 6156-6174.

Wendler, G., and Shulski, M.A., 2009. Century of Climate Change for Fairbanks, Alaska. Arctic, 62(3): 295-300.

Wever, L.A., Flanagan, L.B., Carlson, P.J., 2002. Seasonal and interannual variation in evapotranspiration, energy balance and surface conductance in a northern temperate grassland. Agricultural and Forest Meteorology, 112(1): 31–49.

Wilson, K., Goldstein, A., Falge, A., Aubinet M., Baldocchi, D., Berbigier, P., Bernhofer, C., Ceulemans, R., Dolman, H., Field, C., Grelle, A ., Ibrom, A., Law, B.E., Kowalski, A., Meyers, T., Moncrieff, J., Monson, R., Oechel, W., Tenhunen, J., Verma, S., and Valentin, R., 2002. Energy balance closure at FLUXNET sites. Agricultural and Forest Meteorology, 113: 223–243.

Wolken, J.M., Hollingsworth, T.N., Rupp, T.S., Chapin, F.S., Trainor, S.F., Barrett, T.M., Sullivan, P.F., McGuire, A.D., Euskirchen, E.S., Hennon, P.E., Beever, E.A., Conn, J.S., Crone, L.K., D'Amore, D.V., Fresco, N., Hanley, T.A., Kielland, K., Kruse, J.J., Patterson, T., Schuur, E.A.G., Verbyla, D.L., and Yarie, J., 2011. Evidence and implications of recent and projected climate change in Alaska's forest ecosystems. Climate Change, 72: 251-298.

Zhuravin, S., 2004. Features of forest-steppe small basins water balance: the Nizhedevitsk water balance station case study. In: Kane, D.L., Yang, D., (Editors). Northern Research Basins Water Balance. IAHS Publication 290. Wallingford, Oxfordshire, UK, pp. 78-90.

Zhou, L., Tucker, C.J., Kaufmann, R.K., Slayback, D., Shabanov, N.V., and Myneni, R.B., 2001. Variation in northern vegetation activity inferred from satellite data of vegetation index during 1981-1999. Journal of Geophysical Research, 106(D17): 20069-20083.

CHAPTER 4

Scale dependence of evapotranspiration estimates in a high latitude Alaskan agroecosystem[1]

[1]Manuscript prepared for submission to the Agricultural and Forest Meteorology

Abstract

Quantification of evapotranspiration (ET) in agroecosystems is important for water management especially in regions where water deficiency limits agricultural development. However different methodologies and approximations to estimate ET can lead to different results. In particular, methodologies to estimate turbulent fluxes representative of local scales might not be representative at all times and under all conditions to larger spatial scales typical of many remote sensing observations. This is due to surface heterogeneities that can dominate the energy balance closure even under atmospheric flows over flat areas without major aerodynamic obstacles.

In this study, a multi-scale turbulent heat flux experiment was carried out in a farm area in Fairbanks, Alaska during the summer of 2013. Area-average farm-scale sensible heat fluxes were found on average 34% larger than local scale estimates where this difference exceeded 45 W m^{-2} more than 46% of the time. As a result, ET observations based on local closure of energy balance overestimate by 19 Wm^{-2} more than 39% of the time when compared to large-scale area-averaged estimates. Furthermore, based on two independent methodologies to estimate ET, Penman-Monteith and Priestley-Taylor, a comparative analysis was established in terms of energy balance closure at local and large scale. A comparative analysis of energy balance closure was established under variable surface fluxing regime, stability and dynamical conditions in the atmospheric surface layer. Our results suggest that Penman-Monteith brings higher closure at local and large scales when flux levels are below 50 Wm^{-2} under all unstable conditions. While depending on flow forcing and particularly when friction velocity is larger than 0.2 ms^{-1} Priestley-Taylor performs better in terms of energy balance closure.

Keywords: Evapotranspiration, sensible heat, surface heterogeneity, large aperture scintillometer, Eddy covariance, agroecosystem

4.1 Introduction

Evapotranspiration (ET) is a major process in the water and energy cycle of terrestrial ecosystems (Rivas and Caselles, 2004; Burba and Verma, 2005; Sobrino et al., 2007; Lei and Yang, 2010; Fang et al., 2012) particularly in agroecosystem in northern latitudes (Ruairuen et al., 2015) because of extreme temperature and radiative fluxes regime and water availability. ET cycles are closely tied to water availability and energy exchange between surface and atmosphere at a given site, and thus it is one of the most critical factors affecting crop production during the growing season. ET is critically important since water resources in a region can become limited or difficult to estimate due to climate variability and change, seasonal shifts, population growth, drought, competition from other industrial water uses, and water quality degradation (Farahani et al., 2007; Suyker and Verma, 2009). The estimation of ET is also important in quantifying the responses and feedbacks of terrestrial ecosystem into dynamical changes at the regional and large scale climate (Churkina et al., 1999; Nemani et al., 2002). This central role of ET also applies to a wide range of problems in agriculture, hydrology, land management and water resources management (Samain et al., 2012). Moreover, knowledge of ET is imperative in developing mitigation strategies of water resources management for agriculture, monitoring and predicting drought periods (McVicar and Jupp, 1998; Mu et al., 2013) and in hydro-meteorological modelling (Evans et al., 2012).

The ET regime in high latitudes can be highly variable to an extent that, during the summers, it can exceed precipitation (Hinzman and Kane, 1992; Parka et al., 2008). This has been indeed reflected in specific studies carried out in agroecosystems where high latitude precipitation has been largely lost through ET (Sharratt, 1994; Ruairuen et al., 2015). Hence, due to this outstanding rate of ET against precipitation and soil moisture depletion water stress in crops is

often verified. However, measurements of ET in such ecosystems are still spatially limited to assess how changes in hydrological and energy balance impact agro-economic activities and climate system. Therefore, it is important to identify ET measurement techniques that are representative of a farm extension in scales ~1 km so that later on models and satellite remote sensing approaches can provide a more comprehensive assessment of regional trends in ET.

Several local-scale approaches have been used to estimate ET in large-scale field experiments such as lysimeters, Bowen ratio and eddy-covariance tower. In general, the eddy covariance (EC) method is often considered as a standard and advanced method for measuring the exchange of energy at the interface land surface-atmosphere. Despite the inevitable spatial heterogeneity of real landscapes, interpretation of results based on this technique needs to be carefully considered in particular when those observations are intended to be representatives of large areas composing farm lands (Pelgrum and Bastiaanssen, 1996; Su, 2002). Methodologies based on approximations to the surface fluxes notably Penman-Monteith evapotranspiration (ET_{PM}) method or pan evaporation (E_P) with empirically derived correction factors (vegetation and pan coefficients) are used frequently to estimate ET. ET_{PM} (Allen et al., 1998; Walter et al., 2000) had been widely used in agricultural hydrology and other ecosystems research activities. In this case, ET is derived from a hypothetical, well-watered crop while E_P is the potential evaporation from evaporation pan. The Priestley and Taylor (PT) model is a simplification of the Penman equation (Priestley and Taylor, 1972; Agam et al., 2010; Ding et al., 2010). The ET derived from PT is a product of the equilibrium evaporation (ET_{eq}) and PT coefficient (α), where ET_{eq} can be obtained from a combination of meteorological and radiation data including net radiation, ground heat fluxes, and air temperature. However, highly heterogeneous land surface properties including topographic and vegetation cover and gradients, soil properties, availability of water and

precipitation pattern, as well as climate variability challenge the use of the of mentioned ET fluxes estimation techniques (Friedl, 1996; Janowiak et al., 1998; Ruhoff et al., 2013).

Large Aperture Scintillometer (LAS) offers a useful perspective to overcome this problem for routine measurements of area-average sensible heat flux (H) under several terrain conditions (Chehbouni et al., 2000; Meijninger et al., 2002; Hemakumara et al., 2003; Meijninger et al., 2006; Ezzahar et al., 2009b). LAS instrumentation present considerable advantages compared to EC systems since it retrieves at all times the area-average integrated flux regime across an entire farm surface. Due to this instantaneous spatial scale integration LAS can be used to calculate fluxes at shorter time-scales (10-min) (Thiermann and Grassl, 1992) while maintaining the spatial footprint. This is a significant fundamental difference when compared to EC systems (Finnigan et al., 2003). Several studies reported the application of sensible heat flux measurement by LAS systems to estimate the ET rates (or latent heat). In all those studies, the latent heat flux (LE) was determined as the residual term of the energy balance Eq. (1).

$$LE = R_{net} - G - H \qquad \text{Eq. (1)}$$

In Eq. (1) R_{net} is the net radiation, G is conductive heat on the ground and H is the sensible heat flux. For example, Hemakumara et al. (2003) showed good agreement between LE derived from scintillometer and net radiometer against estimates obtained from a remote sensing based on a mixed vegetation canopy. Savage (2009) used the measured sensible heat from LAS while the net radiation and ground heat fluxes were obtained from the point location along the scintillometer path. In this case results showed a good correlation between the LAS-derived latent heat fluxes and LE obtained from Bowen ratio Energy Balance and EC along the path of LAS. The same approach have been used to estimate LE derived as the residual term of the energy balance equation through the combination of LAS over the path lengths 500, 600, and 1050 m with an estimate of

available energy ($R_{net} - G$) over three different vegetation types in agricultural fields. Results showed that combining LAS with an estimate of the available energy can provide reasonable large-scale ET estimates (Ezzahar et al., 2009a). Recently, Samain et al. (2012) compared the estimates of actual ET rate from the energy balance approach based on LAS measurements of sensible heat over 9.5 km path and point measurement of R_{net} and G for a heterogeneous catchment in Belgium including remote sensing based ET data. From the ET rates calculated per 10-day period, results show a good correspondence between remote sensing based estimates and LAS-derived ET rates with average differences of 3.5%. Therefore, LAS can be considered as a good method to determine area-averaged turbulent heat fluxes and therefore to establish energy balance closure at large scales.

This study aims to (i) evaluate ET derived as the residual term of the energy balance approach when local and large scale area-averaged measurements of sensible heat flux by EC and LAS instruments are available and (ii) to evaluate the performance of independent determination of ET based on Penman-Monteith and Priestley-Taylor in combination to scale dependent sensible heat fluxes estimates. This comparison was established under different atmospheric surface layer conditions to improve understanding of the energy balance closure and the spatial scales dependences of ET retrievals.

4. 2 Field experiment and methodologies

4.2.1 Study site and meteorological regime

The field experiment was carried out in the Fairbanks Experiment Farm (FEF), the University of Alaska Fairbanks (UAF) Agricultural and Forestry Experiment Station (AFES) Fairbanks Alaska, USA (64° 51′ 16.6 ″N, 147° 51′ 36.4″ W, 150 m above sea level), over a flat topography (Figure4-1). The research site is characterized by a continental subarctic climate, with large temperature variability, low humidity and relatively low precipitation. The total annual precipitation averages approximately 254 mm per year, with half of this amount falling during summer (Shulski and Wendler, 2007). The mean annual temperature is a few degrees below freezing at around -3°C, where the average summer temperature (June–August) is above 15 °C. The length of growing season is approximately 115 days in this region (Shulski and Wendler, 2007). The soil texture is a silt loam (silt 70%, clay 8% and sand 22%). The site was covered with 1.05 km^2 of cropland and 0.2 km^2 of forest land (along some sections on the outside edges of the farm). These surface covers are uniformly spaced due to the crop management practices. The central farm surface where overlapping fluxing areas occur is shown in Figure 4-1. This figure displays different plot of land cover in the FEF during growing season and the location of instrument installation. During the growing season, the smooth bromegrass (*Bromus inermis* Leyss.) ranged in height from about 0.30 m to 0.50 m, and was then clipped to a height no lower than 0.05 m twice per growing season (Sparrow and Masiak, 2008). Barley *(Hordeum vulgare L)* ranged in height from about 0.6-1.20 m and was not cut during period of this experiment. Further details about the site, soil and climate may be found in Ruairuen et al. (2015).

4.2.2. Experimental design

The experiment was established during summer 2013. Within the farm field, an automatic meteorological station (Met station) was wirelessly connected and mounted at 2 m and 5 m above the ground to measure air temperature, relative humidity, barometric pressure, precipitation, wind speed and direction (denoted "A"; Figure 4-1). The output data was stored at 1-min intervals. In addition, soil temperatures were monitored at the surface, 0.05, and 0.15 m depths over three parcel areas (Figure 4-1) to determine the area-weighted average of the ground heat fluxes (denoted G_{large}) together with air temperature at 1.5 m height above the ground. The area inside the dashed rectangular zone (Figure 4-1) is about 300 m x 500 m, which included several plots where different crops were grown. It was found that the fallow (bare land) constituted more than 55% of the surface area, barley 24%, the smooth bromegrass was about 10%, potatoes~3% forest ~6%, and the farm building and roads constituted less than 2% of the area. The available of data is listed in Table 4-1.

The BLS-900 large aperture scintillometer (LAS) was deployed across the farm field (denoted "B"; Figure 4-1) in the direction east-west. This instrument uses a pulsed eye-safe near-infrared light emitting diode system at 880 nm wavelength and a refractive telescope receiver located 1 km distance. Both transmitter and receiver have been installed on a 1.8 m height tower over a flat grass-covered surface. The LAS was set up along a 1 km path length L to derive a 1 minute spatial average of the coefficient of refractive index structure C_n^2 (spanning barley field, smooth bromegrass field, and fallow fields). Analysis of the wind direction pattern during the study period showed that the dominant wind direction 34% of the time is originated within an interval ranging from south-west to north-west sectors (see Figure 4-2).

In order to measure representative fluxes along the transect of the LAS, the EC system was installed in the center path of LAS, about 500 m away from the LAS receiver over the fallow field (denoted ''C") according to Figure. 4-1. The three-dimensional velocity (u, v, w) was measured using 3D ultrasonic anemometer (Table 4-1) mounted at 3 m above the surface. Air temperature fluctuations were obtained from the sonic anemometer and from two thermocouples at 1 m and 3 m height from the ground surface. Net-radiation budget (R_{net}) was also set at 3 m height at EC tower as well as ambient air pressure. The EC tower sits over a bare soil with spare grass. Raw data were sampled at a rate of 20 Hz with velocity threshold of 0.01 ms^{-1} and provide the three velocity components of the air flow (u, v, and w), as well as sonic temperature. Additionally, soil temperatures at 0.05 m, 0.10 m, 0.20 m, 0.30 m depths were collected at EC site for the ground heat fluxes estimation (denoted G_{local}). Description of the instruments incorporated in the farm can be found in Table 4-1.

Period of interest

The LAS and EC measurements were initiated on 15 June and 7 July 2013 in FEF, respectively. The period of present study is focused on the middle of growing season spanning from 7 July to 13 August 2013. For the purposes of comparison the analysis was performed only in a limited part of the available LAS and EC measurements whenever the instruments collected simultaneously. During this period an amount of 69.34 mm of precipitation was observed. The average hourly short wave downwelling was about 225 Wm^{-2}, air temperature was about 17.3 °C and soil temperature over the farm field was around 18.2 °C at 0.05 m (Table 4-2).

4.3 Data processing and methods

4.3.1 Eddy covariance

Based on the measurements of temperature and three dimensional velocity field which operate at a frequency of 20-Hz, turbulent flux H was estimated for 30-min eddy-covariance averaging period. The sonic measured temperature was calibrated based on Vaisala HTM-333 humicap sensor at 1 Hz and the barometric pressure in a laboratory chamber. The conversion was first applied to raw data of the sonic temperature and velocity. After that data was cleaned according to despiking procedure adapted from Vickers and Mahrt (1997). Anemometer signal dropouts were examined through the temporal series as proposed by Vickers and Mahrt (1997) that includes the formulation of the statistical distribution of data (i.e. means, standard deviation, minimum and maximum, and covariance) in a sliding window of 1 min (1200 points) to minimize errors in the computation of fluxes. An ultimate visual control is executed to ensure the turbulent time-series were free of spikes and dropouts.

Over an almost flat terrain the streamline coordinate rotation was applied in intervals of 30 minutes (Kaimal and Finnigan, 1994). Then, data ware corrected for sensor displacement and frequency response attenuation (Massman, 2000; Massman and Lee, 2002). To compute the sensible heat flux, the turbulent component of temperature (T') is calculated applying a mean by blocks (Lee et al., 2004), after converting sonic temperature into actual temperature and corrected for humidity effects according to Kaimai and Gaynor (1991). The sensible heat flux H (H_{local}) is then calculated based on Eq. (2) (Foken, 2008),

$$H_{local} = \rho c_p cov(w', T') \quad \text{Eq. (2)}$$

where ρ is the air density calculated overtime, c_p is the heat capacity of the air mass as dependent on the ambient pressure, and cov is the covariance in time of the turbulent parts of w and T.

4.3.2 Large aperture scintillometer

The area average large-scale turbulent sensible heat flux (H_{large}) was retrieved from LAS measurements installed across the field as indicated in Figure 4-1. Calculation of the sensible heat fluxes are based on the direct measurement of C_n^2 through optical intensity measurements of the optical beam scintillation as described in Eq. (3) (Tatarski, 1961), using local temperature and pressure measurements.

$$C_n^2 = 0.12 D^{-\frac{7}{3}} L^{-3} \sigma^2 (\ln(\frac{\sigma(I)}{\bar{I}})) \quad \text{Eq. (3)}$$

where L = 1000 m is the distance between emitter and receiver and D = 0.15 m is the laser disk separation in the laser emitter in this study, and $\sigma^2(\ln(\frac{\sigma(I)}{\bar{I}}))$ is the variance of the logarithmic ratio between the optical signal variation and the time average optical signal intensity (Kleissl et al., 2008). Then, the coefficient of thermal turbulence structure can be calculated C_T^2 through the following system of equation.

$$C_T^2 = \left(\frac{-0.78 \times 10^{-6}.P}{T^2}\right)^{-2} C_n^2 \quad \text{Eq. (4)}$$

where P is the ambient pressure (Pa) and T is air temperature in °K.

Once C_T^2 is known, the sensible heat flux (H_{large}) across the farmland can be derived from the set of Monin–Obukhov similarity relationships that included the C_T^2 coefficient,

$$\frac{C_T^2 (Z_{LAS} - d)^{2/3}}{T_*^2} = f_T(\zeta) \quad \text{Eq. (5)}$$

where d is the displacement height, Z_{LAS} the effective height of LAS beam above the surface, T_* is the temperature scale of turbulence defined as

$$T_* = \frac{-H_{large}}{\rho_{air} c_p u_*} \quad \text{Eq. (6)}$$

where u_* is friction velocity (m s^{-1}), ρ_{air} is the air density, c_p is the air heat capacity, and the Obukhov Stability length is given by:

$$L = -\frac{u_*^3 \rho_{air} c_p T}{kg H_{large}} \quad \text{Eq. (7)}$$

where g is the gravitational acceleration and and $k = 0.4$ is the von Kármán constant.

The right hand side of Eq. (5), $f_T(\zeta)$ are the universal stability functions as function of the Obukhov number ζ to correct the set of Eq. (6, 7) for unstable $\zeta < 0$ and stable $\zeta > 0$ conditions (De Bruin et al., 1995; Wyngaard et al., 1971). They are indicated in Eq. (8), where c_1 = 4.9, c_2 = 6.1, and c_3 = 2.2, and $\zeta = \frac{Z_{LAS} - d}{L}$ where ζ is the stability parameter.

$$f_T(\zeta) = \begin{cases} c_1 (1 - c_2 \zeta)^{-2/3} & \zeta < 0 \\ c_1 \left(1 + c_3 \zeta^{2/3}\right) & \zeta > 0 \end{cases} \quad \text{Eq. (8)}$$

Given an independent measurement of the friction velocity from either an eddy covariance station or a wind speed from meteorological station (Fochesatto et al., 2013), the system of Eq. (5) - (8) can be solved analytically to obtain the value of sensible heat flux for the agriculture field (Gruber and Fochesatto, 2013; Gruber et al., 2014).

4.4 ET methods

4.4.1 The energy balance

The energy balance requires determination of the amount of net radiation at the surface (R_{net}) and the ground heat fluxes as well estimation of turbulent heat fluxes. The observations of R_{net} can be considered to have a large scale representation for most of the cases except those circumstances where localized cloudiness affects the energy balance. On the other hand, it has to be pointed out that generally ground heat is obtained by a series of observations distributed around the area where the turbulent fluxes are being measured. However in the presence of a landscape where surface and vegetative gradients may introduce soil moisture regimes will be reflected on surface heterogeneities that can significantly affect the development of turbulent heat fluxes. Therefore in this study G measurements representative of local scale, nearby the EC tower, and across the agricultural farm have been carried out based on local measurements on different plots (see Figure 4-1).

Therefore to calculate LE as the residual term of the energy balance equation two assumptions can be made according to the spatial scale being used: local and large scale closure according to Eq. (9) – (10).

The energy balance budget at the local scale:

$$R_{net} - G_{local} = LE_{local} + H_{local} \qquad \text{Eq. (9)}$$

and the energy balance budget at the area-average scale (or large scale) is defined as:

$$R_{net} - G_{large} = LE_{large} + H_{large} \qquad \text{Eq. (10)}$$

where the R_{net} (W m^{-2}) is net radiation, G_{local} (W m^{-2}) is the ground heat fluxes nearby the EC site, and G_{large} (W m^{-2}) is the area-weighted average of the ground heat fluxes calculated from

Eq. (11), LE (Wm^{-2}) is derived latent heat for the local and area averaged (large scale), H_{local} and H_{large} (Wm^{-2}) are sensible heat fluxes density from EC tower and LAS, respectively.

Area-weighted averaged of ground heat flux was calculated based on Eq. (11).

$$G_{large} = \sum_{n} \frac{A_n}{A_T} G_n \qquad \text{Eq. (11)}$$

where A_n is the area of each surface patch, A_T is total area of patches which can be obtained from $A_T = \sum_n A_n$, G_n is the ground heat fluxes from each patch, and n is number of patches.

Therefore based on these two scale dependent equations we can deduce two estimates for the LE according to Eq. (12).

$$LE_{local,large} = R_{net} - G_{local,large} - H_{local,large} \qquad \text{Eq. (12)}$$

However, in the case that each component of energy balance equation has been estimated independently then, an analysis of the energy balance closure for local and large scale can be performed. In this case and based on the available meteorological and radiation observations two estimates are normally used based on the Penman-Monteith and Priestley-Taylor approximation. For the evaluation energy balance closure, the derivation of linear regression coefficients of available energy ($R_{net} - G_{local,large}$) and the dependent flux ($LE_{PM,PT} + H_{local,large}$) are used according to Eq. (13).

$$\left(LE_{PM,PT} + H_{local,large}\right) = a + b * (R_{net} - G_{local,large}) \qquad \text{Eq. (13)}$$

where $LE_{PM,PT}$ is the estimation of LE based on Penman-Monteith and Priestley-Taylor described in more detail in the following section, a is constant value, and b is the closure fraction.

4.4.2 Penman-Monteith (PM)

The Penman-Monteith (PM) method has long been extensively used in hydrological, atmospheric and environmental modeling for estimating latent heat flux ($\lambda \mathrm{ET}\ or LE$). The PM method computes relatively accurate LE in different meteorological and surface conditions when the correct parameterizations are applied. The PM formulation describes the physical process of LE from a vegetative surface which include the aerodynamic (r_a) and bulk surface resistance (r_s). The PM equation can be written in terms of LE (W m^{-2}) as:

$$LE = \frac{\Delta(R_{net} - G) + \rho_a C_p (e_s - e_a)/r_a}{\Delta + \gamma(1 + \frac{r_s}{r_a})} \qquad \text{Eq. (14)}$$

where Δ is the slope of saturation vapor pressure versus temperature curve (kPa $°C^{-1}$), R_{net} is net radiation flux (Wm^{-2}), G is ground heat flux (Wm^{-2}), ρ_a is the air density (kg m^{-3}), c_p is the air mass specific heat (kJ kg^{-1} $°C^{-1}$) at constant pressure, e_s is the saturation vapor pressure at ambient air temperature (k Pa), e_a is the actual vapor pressure of the air mass (k Pa), $e_s - e_a$ is the vapor pressure deficit (VPD) (kPa), γ is the psychometric constant (kPa $°C^{-1}$), r_a is the aerodynamic resistance (sm^{-1}), and r_s is the bulk surface resistance to vapor transport (sm^{-1}). The conversion from latent energy fluxes (LE, W m^{-2}) to ET (mm s^{-1}) is ET = LE /λ, where λ is latent heat of vaporization (kJ kg^{-1}).

4.4.3 Priestley-Taylor (PT)

Priestley-Taylor approach to determine LE was proposed based on an empirical equation for calculating the reference evapotranspiration (Priestley and Taylor, 1972), which can be expressed as:

$$LE = \alpha \frac{\Delta}{\Delta + \gamma}(R_{net} - G) \qquad \text{Eq. (15)}$$

where α is an empirical constant coefficient and is a variable according to different underlying surfaces and the rest of variables have been previously defined. This method assumes that latent heat flux depends upon the temperature and solar radiation (Utset et al., 2004). The coefficient α is typically assumed to be equal to 1.26 (Priestley and Taylor, 1972; McAneney and Itier, 1996) for saturated surfaces or freely evaporating surface (Priestley and Taylor, 1972; Stewart and Rouse, 1977). In this study we use the α value to be 1.26.

4.5 Results and discussion

In this section, we first compare the ground heat fluxes at the local scale (G_{local}) against the area-weighted averaged ground heat (G_{large}) (section 4.5.1). Second, we establish a comparison between sensible heat fluxes retrieved by EC systems and LAS (section 4.5.2). Then, based on these two different estimates of G and H we derive two scale-dependent estimates of LE. One of them will be representative of local scale and the other will be an estimate of LE based on the use of large scale area-average observations (section 4.5.4). Moreover based on well-known methodologies for ET determination (PM and PT) an analysis of energy balance closure was performed. This analysis combined the scale dependent estimates of H and G to determine what combination of methodologies offers the best closure argument in agriculture fields that is of special application in northern regions. In this study, we will mostly be concerned with daytime observation rather than nighttime with half-hourly time scale to account for periods where soil moisture depletion occurs. In this case, the daytime period the agroecosystem will be considered from 0600 until 2100 Alaska Standard Time (AKST), which is UTC-8hrs. This analysis is further

complemented by indicating conditions in the atmospheric flow, atmospheric surface layer stability and development of mechanical turbulence.

4.5.1 Comparison of the ground heat fluxes at the local and area-averaged scale

The ground heat flux is important, highly variable and very difficult to estimate when on-site field observations are lacking. Nevertheless the ground heat flux comprises approximately 5-11% of net radiation in the agriculture land (Ruairuen et al., 2015). Nonetheless, it could reach more than 40% of the net radiation in dry land areas (Heusinkveld et al., 2004) and more than 50% of the net radiation in a bare soil (Idso et al., 1975) in daytime periods.

In this study, the ground heat fluxes as calculated from the temperature gradient methods at the EC site (G_{local}) and area-weighted averaged (G_{large}) (as showed in Figure 4-1) are compared. Figure 4-3 shows the composite of time-series of average half-hourly diurnal ground heat fluxes for the 13 days (624 points) from two different scales. Here it is evident that the G_{large} resulted to be larger than G_{local} during the day time and lower than G_{local} during the nighttime. The onset of conductive heat on the ground for G_{large} was approximately 7 hours earlier than G_{local}, and the time-offset was delayed compared to G_{local} by almost 3 hours. To examine the differences between G_{large} and G_{local}, all half-hourly periods for positive ground heat fluxes were isolated because these periods correspond with an onset of conductive heat on the ground. In total, 363 and 148 half-hourly periods for G_{large} and G_{local}, respectively met this condition. Results show that G_{large} has positive values about 58% (or ~42% for negative) of the time, while only 23% (or ~77% of negative) of the time for G_{local} that was positive. On average, the G_{large} has the maximum of 11 Wm^{-2} whereas the maximum of 4 Wm^{-2} was found in G_{local} during the daytime. The maximum difference between G_{large} and G_{local} was nearly 28 Wm^{-2} at 0630 (AKST) during

the daytime and more than 30 Wm^{-2} at 0400 at nighttime. These results clearly show the effect of heterogeneous surfaces on an agricultural field that is almost flat across all directions.

Variations in soil physical properties can be caused by management practices on the farm land during the growing season. In this study site, the soil around the EC station was not tilled or processed for about two years, while the rest of the field has been tilled after harvesting the year before as well as before planting. Crop residue management and tillage can influence soil physical properties as a direct result of altering the soil physical matrix or indirectly by altering surface energy partitioning, microbial activity, and soil chemical composition. In subarctic, a silt loam soil was more stable and wetter at the time of sowing in spring with seven years of no tillage compared with intensive tillage (Sharratt, 1996). High moisture content and penetration resistance was found in no tillage soil than intensive tillage in a subarctic agriculture field (Sharratt et al., 2006). Thus, we conclude that the area-weighted averaged ground heat flux is important to be estimated because it provides a more representative value of the variability across landscape and therefore it configures a better representation of ground heat exchange over the heterogeneous surface in the agriculture field.

4.5.2 Comparing the sensible heat fluxes from EC-based and LAS-based

A comparison between LAS-based estimate of sensible heat flux and EC method was performed. In this comparison we only consider periods where the surface atmospheric layer is under unstable conditions (i.e. $L < 0$). The sensible heat flux from LAS was obtained according to Eq. (5) – (8). In general, when studies of this nature are realized the sensible heat flux of EC result lower than the one derived based on LAS. This has been reported in several studies (Ezzahar et al., 2007; Hoedjes et al., 2007; Ezzahar et al., 2009a; Ezzahar et al., 2009b; Samain et al., 2011; Evans et al., 2012; Samain et al., 2012). The sensible heat fluxes obtained from EC (H_{local}) against

LAS (H_{large}) for agricultural field in the northern high latitude are compared in this section. The statistical results are shown in Table 4-3 and display a correlation between H_{local} and H_{large} with R^2 of 0.60, and RMSE of 36 Wm^{-2}. The H_{large} shows systematically higher values than H_{local} by about 40% during the unstable condition. Similarly the fraction of large scale fluxes captured by H_{local} was about 58%. From this comparison, the H_{large} on average was higher than H_{local} with the maximum of 248 Wm^{-2} and the mean of 93 Wm^{-2}, while H_{EC} has the maximum of 201 Wm^{-2} and 60 Wm^{-2} for the mean (Table 4-2). This comparison illustrate an important difference that can only be explained by the landscape heterogeneity, differences in vegetation types and cover, soil temperature and soil moisture regimes. These results suggest that even under practically ideal conditions respect to aerodynamic distortions and stationary conditions of the flow the H_{local} can only arrive to capture certain fraction of the agriculture land flux when we compare against the fluxes provided by the LAS.

Furthermore, time-series composite of half-hourly diurnal variation of sensible heat fluxes from both scales are illustrated for the period under study (Figure 4-4). Mean half-hourly of H_{large} developed between 0530 and 0600, about 1 hour in advance compared with respect to H_{local}, then it peaked between 1300 and 1500 with the maximum values of 145 W m^{-2}. However, the H_{large} transitioned basically at the same pace as H_{local} at 2200. This time differences observed in the transitions of scale dependent fluxes has been observed in a similar experiment in boreal forest and has been demonstrated to occur due to highly heterogeneous canopies and complex surfaces (Starkenburg et al., 2013; Starkenburg et al., 2015). According to comparisons of sensor types and data quality showed accuracies of sensible heat flux values ranging from 10 W m^{-2} to 30 Wm^{-2} (Mauder et al., 2006), therefore to determine the differences between H_{large} and H_{local}, all half-hourly periods when the heat flux at both instrument exceeded 10 W m^{-2} was applied. This resulted

in a total of 288 half-hourly periods falling within this condition. Results show that the difference exceeded 34% of the measured fluxed about 46% of the time. The maximum difference of more than 46 Wm^{-2} occurred at 1330 AKST between H_{large} and H_{local}. On average H_{large} was larger than H_{local} about 30 W m^{-2} during the daytime periods. These differences are explained by the ground heat fluxes variance across the landscape in the LAS source area

These results agree well with several studies that have been reported differences in the sensible heat fluxes measured by LAS and EC. For example, Schüttemeyer et al. (2006) have reported the differences between the LAS and EC measurements caused from the heterogeneity of the underlying surface in a mixed vegetation area. Ezzahar et al. (2007) have proposed the differences between the two measurements could be explained by the closure failure of the energy balance of the EC and differences of the source areas of the LAS and EC. Su et al. (2009) have proposed that the difference between the two measurements may be attributed to the sensitivity of the H_{large} to the aerodynamic roughness length and different footprint in grass land and forest. While Liu et al. (2011) concluded the differences between the two fluxes caused by the energy balance closure of EC, the heterogeneity of the underlying surfaces and the difference between the source areas of the EC and LAS measurements.

4.5.3 Retrieval of ET based on energy balance equation

In this case we are interested in the determination of *LE* fluxes based on energy balance closure at the corresponding spatial scales. This approach allowed estimating *LE* as the residual term when storage terms can be considered to be negligible since the canopy is short enough. In this case we consider Eq. (12) – (13) and we use ground heat and *H* fluxes at different scale.

The estimation of *LE* at local scale (LE_{local}) was calculated as the residual of the energy balance using Eq. (12). Similarity, an area-average of *LE* in the larger scale (LE_{large}) was obtained

from Eq. (13). Then, the estimation of LE from both scales estimates LE_{local} and LE_{large} was compared. A maximum of 334 W m^{-2} with an average of 150 W m^{-2} was found in LE_{local} while the maximum of 303 W m^{-2} with the mean of 103 W m^{-2} was indicated in LE_{large} (Table 4-2). The mean half-hourly diurnal variation of LE at both scales is depicted in Figure 4-5. The LE_{large} developed at 0700 about 1 hour delay compared with LE_{local}, while it collapsed before LE_{local} approximately 1 hour in the evening. This corresponded with the cycle of H_{large}. The LE_{large} is positive about 50% of the time while LE_{local} was approximately 65% of the time overestimating LE_{large} about 30%.

The diurnal cycle of these two fluxes is significantly different during the onset and mid-day steady-state regime while a minor difference can be verified at the decaying stage of the surface fluxes. At the onset of surface fluxes this difference is dominated by differential thermal heating on each parcel in the landscape ought to soil moisture and temperature regimes. This leads to the developing of localized internal boundary layers while the fluxing is still low. However, when the fluxing level increases, the ASL in general reaches a level of horizontal homogenization; but still not sufficient in this case to blend all parcels and therefore large-scale LE resulted different from local-scale LE. At the decaying phase the surface fluxes are dominated by a temperature gradient that is horizontally homogenous on the air temperature as a result of the developed atmospheric boundary layer diurnal cycle.

To summarize, the differences of the 30-min average between LE_{local} and LE_{large} are shown in Figure 4-6. This results illustrated that the differences over 10, 20, 30, and 40 Wm^{-2} occurred more than 48%, 40%, 30%, and 25% respectively of the time with the maximum different 171 Wm^{-2} was reported.

Moreover, the statistical analysis of time series also shows that LE_{large} agrees with LE_{local}, with a regression slope of 0.83, R^2 of 0.73, and RMSE of 38 Wm^{-2} (Table 4-3). This result is lower than the values of Samain et al. (2012) where R^2 of 0.87 and RMSE values of 15.7 Wm^{-2} was found between LE derived from LAS versus the remote sensing in a heterogeneous catchment in Belgium and another results by the study of Teixeira et al. (2009) with R^2 of 0.93, RMSE of 33.8 Wm^{-2} between Surface Energy Balance Algorithm for Land estimates the field measurement in the semi-arid region of the Low-Middle São Francisco River basin, Brazil. We conclude that based on energy balance approach LE_{local} becomes overestimated by 37 Wm^{-2} more than 27% of the diurnal cycle evapotranspiration compared with LE_{large} with the ratio of LE_{large}/LE_{local} was 0.66±0.27.

4.5.4 Energy balance closure at local and large scale using independent observations

According to the existing difference between H_{large} and H_{local}, illustrating the heterogeneous conditions of the agricultural farm which under the assumption of energy balance leads to an important overestimation in LE as demonstrated in previous sections, in this section we provide an independent way to evaluate LE and we analyze the scale dependent energy balance equation to determine the degree of closure on each of the formulations.

According to description of methodologies in section 4.4, PM method is widely used to estimate reference evapotranspiration by combining the surface energy balance with resistance-based approximation to model exchange processes and has been incorporated in many land surface and atmosphere models (Liang et al., 1994; Sellers et al., 1996). On the other hand, PT method requires less meteorological parameter than the PM method. Therefore, on the basis of the simplicity presented by these methodologies we have estimated LE and then formulated the closure

fraction under different scales condition to benchmark which combination of methodologies improves the closure fraction and under what conditions on the surface-atmospheric interaction.

The estimation of evapotranspiration based on Penman-Monteith (LE_{PM}) and Priestley-Taylor (LE_{PT}) are now being used as independent measure of latent heat in Eq. (9) – (10). After that, the performance and the energy balance closure fraction (CF) is analyzed by using the scale-dependent energy balance equation. For comparison purposes the algorithms are only applied to a limited section of the available data where all instruments have been working for the entire diurnal cycle basically from 7 July to 13 August 2013. In order to examine the CF we have considered an extra cluster upon the time-series to extract only the periods where the sensible heat flux at local and area-average are positive (H_{local} and $H_{large} > 0$). A regression analysis is then performed between the available energy ($R_{net} - G_{local,large}$) and the sum of estimated latent heat fluxes (LE_{PM} and LE_{PT}) and measured sensible heat fluxed (H_{local} and H_{large}) and combination thereof.

The results are illustrated in Figure 4-7. At the local scale, the higher CF value was found when the PM-based (CF=0.98) formulation is used than PT-based (CF=0.86), with a slight difference in R^2. While, the RMSE from PT-based (44 Wm^{-2}) was lower compared with the PM-based (53 Wm^{-2}) for the local scale (Table 4-4). Thus, during the unstable periods of the atmospheric surface layer (ASL) diurnal cycle the PM-based tend to perform better when the local scale energy balance (EB) is considered than the PT-based indicating that local fluxes are well-represented and integrated in the overall unstable phase. Similar result was obtained when the EB equation was formulated at the large scale, where the higher CF from PM-based (1.00) was reported, with the same R^2 and slightly higher value of RMSE compared with the PT-based. This

result suggested that overall PM-based estimates help closing the EB at higher fractions than PT-based.

To conclude, under unstable conditions in the ASL an overall agreement was found in terms of using large area-averaged observations to improve the EB closure fraction. Similar results were obtained by Schüttemeyer et al. (2006) in terms of reaching a higher EB closure when LAS based measurements were used instead of EC during the daytime in semi-arid terrain in West Africa. Nevertheless, it seems worthwhile to point out that the unstable condition in the ASL includes surface patches of heterogeneous land surface that have no functional relationship to each other when the fluxing level is relatively low basically close to transitions in the atmospheric boundary layer (ABL). Therefore the integration of the turbulent fluxes from individual surface patches to the large scale area-averaged has to be treated separately. In other words, the fluxing level of a given patchy-heterogeneous surface below certain threshold compromises its large scale aggregation and large scale representation. This has been demonstrated recently in a parallel study on an area no far from the actual experimental farm ~2 km in a complex heterogeneous surface on boreal forest (Starkenburg et al., 2015).

It is worth noticing that based on statistical arguments the comparison of turbulent fluxes (section 4.5.2) returned robust correlation values given the fact that a large percentage of the population data contain large population of low level fluxes. This facts are also reflected in the R^2 and RMSE quantities because no significant different between local and large scale can be appreciated.

Generally, the turbulent fluxes under consideration H and LE fluxes relate to many variables in the surface soil and vegetative factors, environmental conditions and nature of fluxing vegetative patterns during the day. Then, clustering data is needed to firmly establish the scale

behavior or scaling of *LE* and therefore establish which *LE* formulation is more reliable for local and large scale *LE*. Therefore, the criteria used in this analysis as well as the results are described in the following section.

4.5.4.1 Determination the CF as function of sensible heat flux level

In this case we seek to evaluate the CF as function of the level of *H* flux. Here *H* is used as a measure of turbulent flux activity and of indication of "interconnectivity" of individual patches to aggregate to the large scale flux. Previous studies reported how sensible heat fluxes changes across landscape over highly heterogeneous surface on a nearby experiment we concluded that a fluxing level above 50 Wm^{-2} (Starkenburg et al., 2015). Based on this criterion, a low and high flux regime was applied to test the dataset. The low flux regimes is referred to the period that sensible heat lower than 50 Wm^{-2}. According to this criterion, the total of 1,054 half-hourly periods met this condition. The results show that PM-based is more appropriate to determine the local scale *LE* than PT-based, with the higher value of CF (Table 4-4). Besides, the PM-based is also performing well for the large scale *LE* than PT-based.

Furthermore, when we consider the high fluxes regimes period based on the sensible heat flux larger than 50 Wm^{-2} this fluxing level correspond to unstable conditions in which case we can hypothesize that individual patch level flux becomes large enough to blend across space becoming more representative of the farmland scale. As a result of 233 half-hourly periods met this condition. Results clearly show that the CF, R^2 improve for the PT-based with a lower RMSE at the local scale. Similarly, at the large scale closure PT-based provided a better result than the PM-based. Therefore, the PT-based is likely a better approach to estimate the local and large scale *LE* under high surface flux regime (Table 4-4).

4.5.4.2 Determination of CF as function of the Obukhov Stability Length (L)

In this case the criterion was based on the one given by Barthlott et al. (2007) to identify the atmospheric stability classes and Obukhov stability length L (Table 4-4). The region defined to be unstable is $-1000 < L \leq -200$ and the one for very unstable conditions is ranging $-200 < L < 0$. The unstable condition usually occur during the initial and terminal periods phases of the ABL convective development daytime but the very unstable condition mostly occur around midday (solar noon) when the fluxes are very strong and higher than the unstable condition.

In the case of very unstable a total of 631 half-hourly periods were included in the analysis. Results for the local scale CF fraction improved when LE is retrieved using PM-based while they verified the same R^2 with slightly different RMSE (Table 4-4). Same results have been verified for the case of large scale closure; resulting also the same R^2 and without significant difference in term of RMSE. This result suggested that the PM-based is more reliable for LE at local and large scales during very unstable conditions.

Conversely, under unstable condition total 173 half-hourly periods. The result for the small scale indicated that the PT-based performed better than the PM-based with R^2 of 0.80 and RMSE of 45 Wm^{-2}. However, a small difference in the CF fraction was observed between the two approximations (Table 4-4). In contrast, the CF fraction and R^2 seem to favor the PM-based than PT-based for the large scale formulation of the energy balance with RMSE difference about 10 W m^{-2} was found (Table 4-4). Therefore, it is concluded here that the PM-based formulation of LE retrieval is more suitable for large scale LE retrieval.

4.5.4.3 Determination of CF as function of the kinematic conditions of the flow

In order to establish this criterion the data was preselected based on the most prevalent wind direction (south-west and north-west sectors) over the site and for wind speeds (U) greater than 2 ms^{-1}. This wind direction sector includes the prevailing wind direction during the study (Figure 4-2) and is free from all aerodynamic obstructions such as meteorological tower and the sonic anemometer themselves. According to this selection criterion, 289 cases containing 30-min data periods were included in this analysis. Table 4-4 on the section surface wind speed shows that the PM-based outperform the PT-based at both scales with small differences in the CF fraction. Moreover, within these datasets, two intervals of friction velocity were selected (u_*) (Table 4-4) to determine which methodology work best in terms of development of mechanical turbulence. This study found that for cases where $u_* > 0.2$ m s^{-1} both methodologies reached approximately similar CF values while the RMSE from PT-based approach is lower at both scales. Conversely, for the cases in which $u_* < 0.2$ m s^{-1}, the PM-based methodology shows higher CF values at both scales.

4.6 Conclusions

In this study experimental evidence of scale-dependence of turbulent heat fluxes and consequently in the fluxing rate of the estimated evapotranspiration was demonstrated. This difference in the integrated amount of evapotranspiration is important from many aspects of agricultural system, climate implications as well as for business sustainability and long term economic projections. The results have been obtained from the summer 2013 growing season but given the fundamental characteristics of the deduced variables they are also valid in general.

The study found an important difference in the conductive ground heat flux between local and area-weighted averaged estimates that rises to approximately 30 Wm^{-2}. This difference is

important and is manifested in forcing of turbulent heat fluxes at local and large scales that has been verified to reach levels of 45 Wm^{-2} on average in the central part of the diurnal cycle.

Multiscale observations of diurnal cycle of sensible heat fluxes from EC measurements captured about 58% of sensible heat fluxes from LAS. This ratio rises to 0.80±0.68 under conditions of sensible heat flux >50Wm^{-2} at both scales. This means that despite introduction of a high fluxing level the local scale fluxes samples still average the 80% of the large scale fluxes. This scale ratio was calculated based in the ensemble mean times series and represent a considerable difference giving the fact that the terrain is almost flat and under stationary flows.

Based on energy balance approach, evapotranspiration derived from local scale measurements resulted an overestimation of 37 W m^{-2} more than 27% of the diurnal cycle when compared to determinations based on LAS. This difference may occur from different sources of latent heat associated to ground heat fluxes and soil moisture across the landscape that indicate the extent to which surface heterogeneities introduce changes in the surface layer fluxing regime. Nevertheless, under unstable conditions in the atmospheric surface layer, the use of large scale evapotranspiration observations clearly improve the energy balance closure fraction.

In addition, the study of the energy balance closure fraction in terms of scales and turbulent flux regimes, atmospheric surface layer stability and conditions for development of mechanical turbulence lead to conclude that: PM-based retrieval for evapotranspiration works best under low flux regime and low friction velocity while, PT-based methodology, works best under high fluxing regime and high friction velocity larger than 0.2 ms^{-1} and basically under all unstable conditions. It must be pointed out here that the majority of cases during the unstable phases were found to be on the very unstable phase L>-200 m.

We conclude that spatial variation in soil thermal and moisture regimes greatly influence the sensible heat fluxes across scales within the agricultural land in northern latitude even though flat topographies and smooth surfaces were considered. We also conclude that this spatial variations of turbulent fluxes impose an ultimate limitation in the accuracy by which modeling and satellite remote sensing retrievals of surface fluxes can be obtained whenever the pixel size or model scale represent larger areas than the surface patches characterizing the landscape heterogeneities. Since the existence of different and localized thermodynamic regimes depends upon natural characteristics or agriculture management it becomes important to consider in the future extra information related to soil moisture for example through modeling of the coupled heat and water transport at the surface-atmosphere interface.

4.7 Acknowledgements

The authors thank the Agricultural and Forestry Experiment Station (AFES) School of Natural Resources and Extension, the University of Alaska Fairbanks. Also, the authors are indebted to Alan Tonne, Darleen Masiak, Bob Van Veldhuizen, Stephen Sparrow, for help in facilitating the field experiment of this study. Ms Watcharee Ruairuen was funded by Suratthani Rajabhat University, Thailand. Gilberto J. Fochesatto was supported by the Geophysical Institute, University of Alaska Fairbanks. Elena B. Sparrow was supported by the International Arctic Research Center and Alaska EPSCOR.

Figures

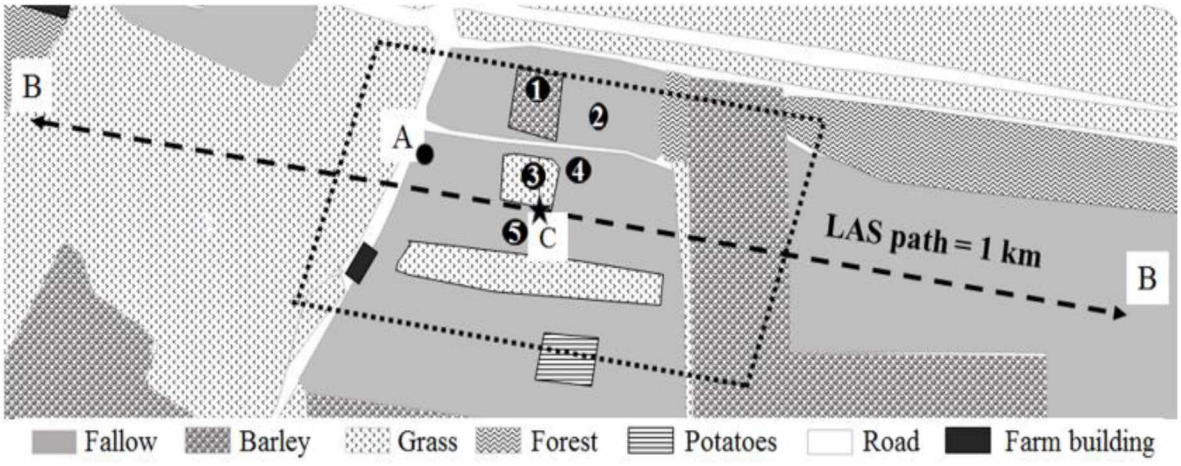

Figure 4-1 Diagram of the field experimental site at the Fairbanks Experiment Farm (FEF), University of Alaska Fairbanks (UAF) Agricultural and Forestry Experiment Station (AFES) Fairbanks Alaska, USA. The experimental site display different surface cover and location of the instrument. The location of a two level of meteorological station (denoted A) at 2 and 5 m heights, the Large Aperture Scintillometer (LAS) (BLS-900) system (denoted B) at 1.8 m height, and the EC system (denoted C with the black star) at 3 m height are shown. The dashed line arrow (east-west) represents the beam of the scintillometer between the transmitter and receiver units. The number 1-5 represent the location of soil temperature measurements under different surface cover (1= barley, 2 and 4= fallow, 3= grass, 5=fallow field under EC station). The square dot line represent the central part of the LAS fluxing area.

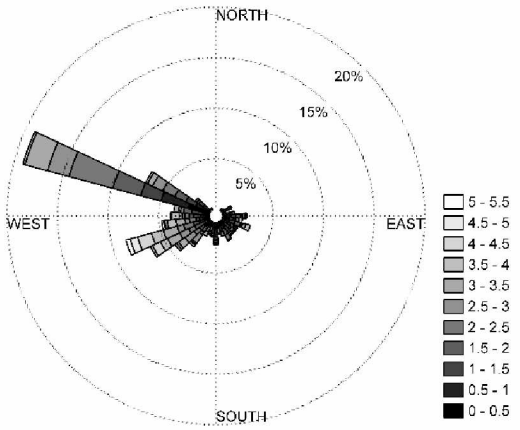

Figure 4-2 Statistics of wind speed and direction during 7 July to 13 August 2013 at the FEF site.

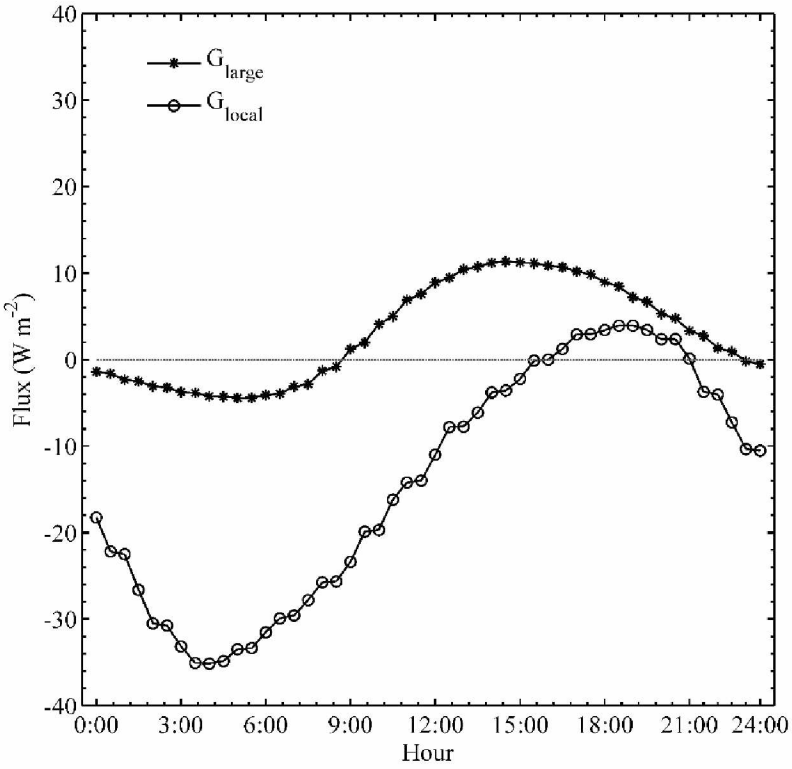

Figure 4-3 Time-series composite of the 30-min average of local soil heat flux at the EC site (G_{local}) and the area-weighted averaged across the farmland (G_{large}). The samples size is 624 points.

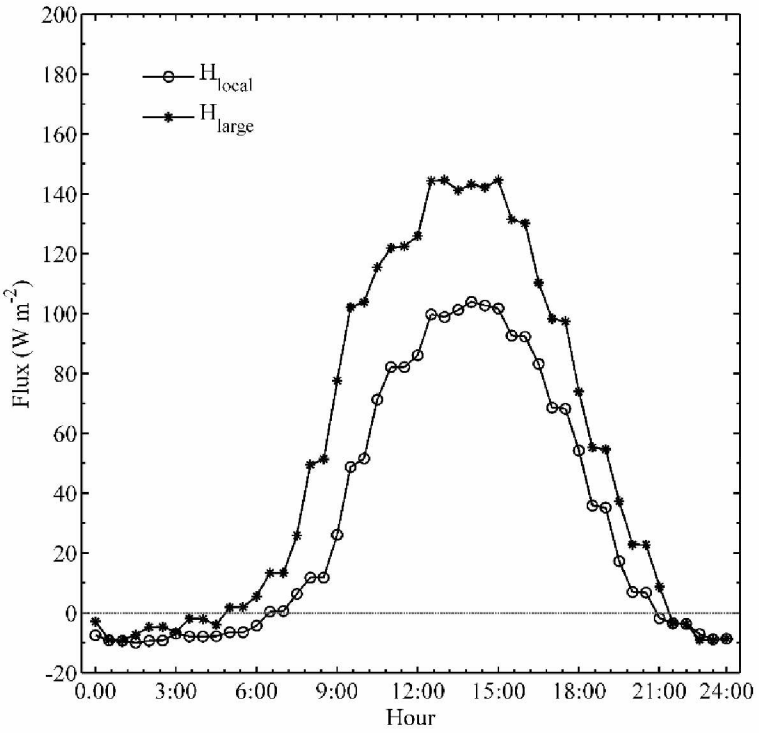

Figure 4-4 Time-series composite of sensible heat fluxes 30-min average for H_{local} and H_{large}.

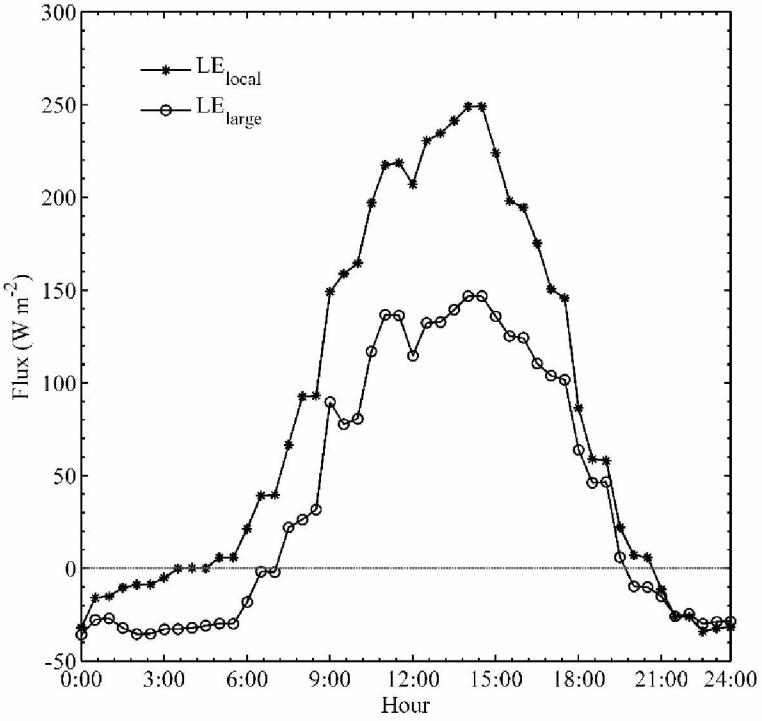

Figure 4-5 Time-series composite 30-min average diurnal cycles of Latent Heat at local and area average scales. LE_{local} and LE_{large}

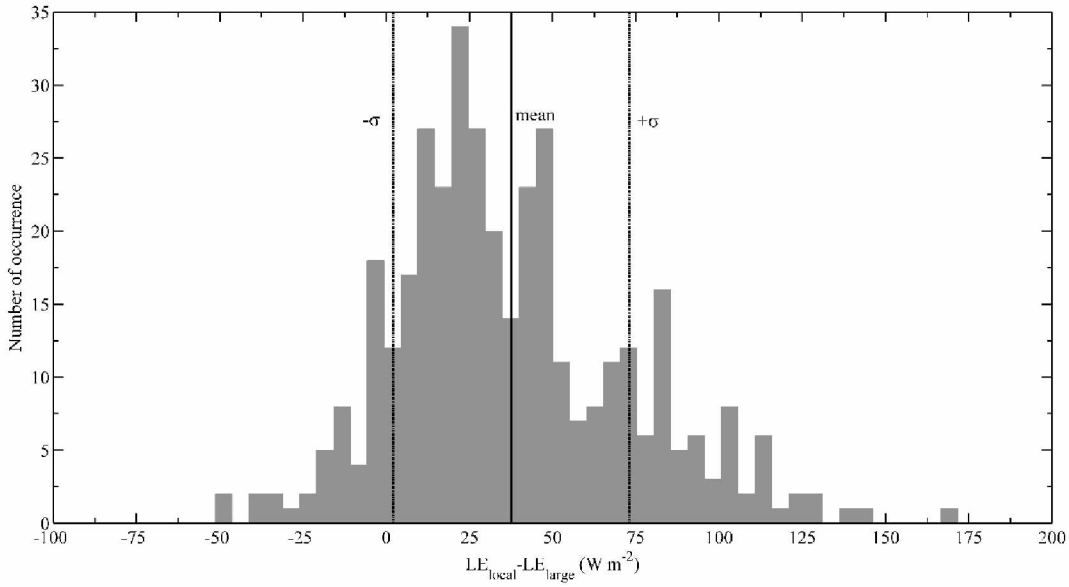

Figure 4-6 Statistical distribution of the Latent Heat flux difference between local and area average closure. Time-series contain 624 number of points based 30-min average eddy-covariance and large-aperture scintillometry.

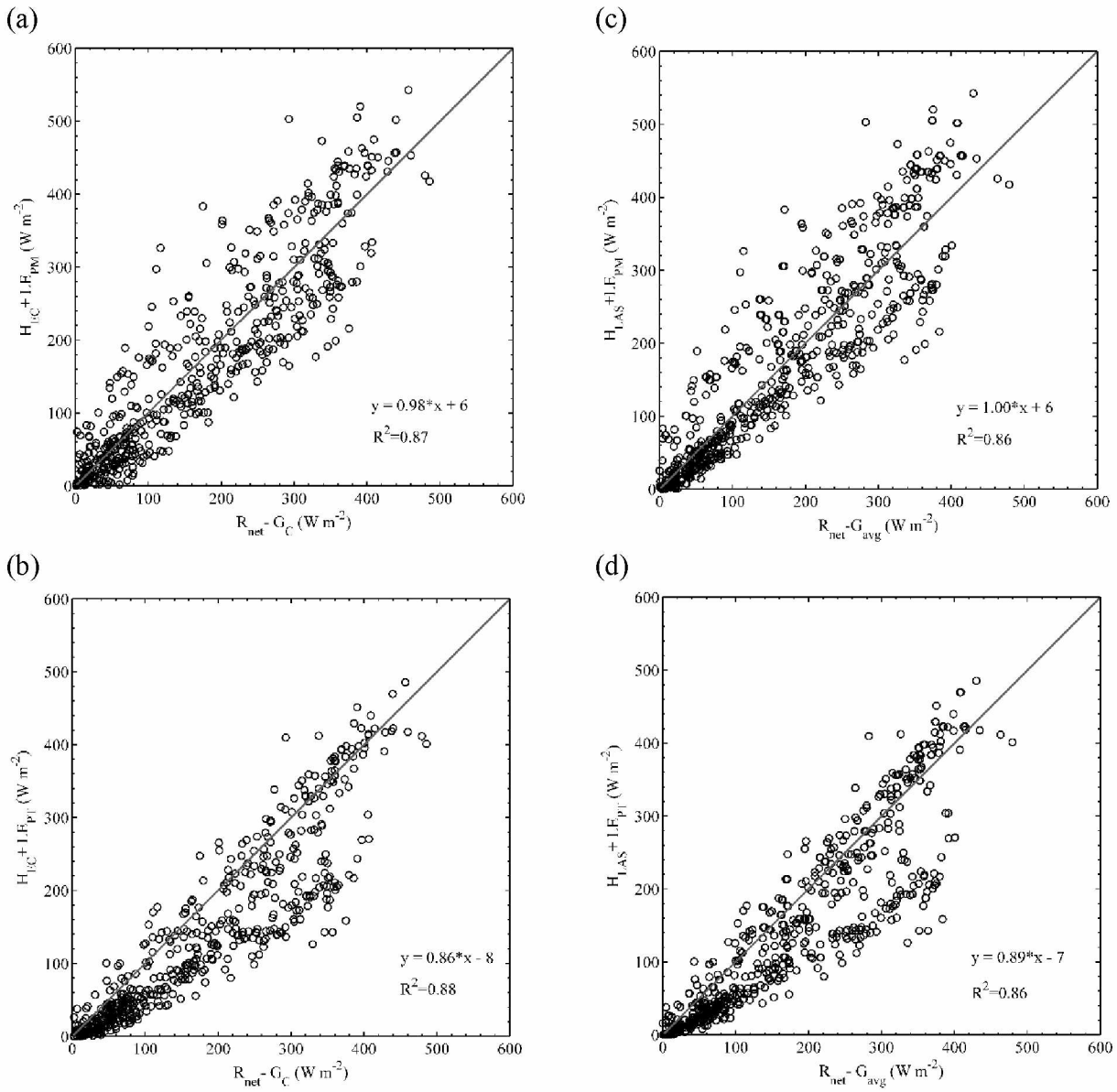

Figure 4-7 Energy Balance Closure scatterplots. Top panels are based on local closure in sensible heat and latent heat estimation based on PM (a) and PT (b). Lower panel represents large scale closure in sensible heat and latent heat estimation based on PM (c) and PT (d) $H_{large} + LE_{PT}$ vs. $R_{net} - G_{large}$.

Table 4-1 Instruments during the Field Experiment

Instrument	Variable	Sensor	Height/Depth (m)	Period
EC	Sonic anemometer	R.M. Young 81000	3	7 July-13 August
	Net radiation	NRLite net radiometer	3	
	Air temperature	PT 107, Campbell Scientific	1, 3	
	Air pressure	CS106, Campbell Scientific	0.20	
LAS	C_n^2	BLS, Scintec900	1.8 (path length 1000 m)	7 July-13 August
Met station	Air temperature	Integrated Sensor Suite, Davis Hayward, CA	2, 5	5 June-20 September
	Wind speed	Integrated Sensor Suite, Davis Hayward, CA	2, 5	
	Relative humidity	Integrated Sensor Suite, Davis Hayward, CA	2, 5	
	Short wave radiation	CM3 Pyranometer, Holland	2	
	Barometric pressure	Integrated Sensor Suite, Davis Hayward, CA	2, 5	
	Soil temperature	S-TMB-M006, Decagon Devices Inc	-0.05, -0.15	
	Precipitation	Tipping-bucket	2, 5	
Barley field	Soil temperature	S-TMB-M006, Decagon Devices Inc	0, -0.05, -0.15	1 June-20 September
	Air temperature	ECT, Decagon Devices Inc.	1	
Smooth brome grass	Soil temperature	S-TMB-M006, Decagon Devices Inc	0, -0.05, -0.15	1 June-20 September
	Air temperature	ECT, Decagon Devices Inc.	1	
Fallow field	Soil temperature	S-TMB-M006, Decagon Devices Inc	0, -0.05, -0.15	1 June-20 September
	Air temperature	ECT, Decagon Devices Inc.	1	
Vegetation Height	Barley field: 1 m max. Smooth brome grass: 0.2-0.4 max.			

Table 4-2 Half hourly mean of meteorological and hydrological condition during the period of study

Parameters	Mean	Median	Std	Maximum	Minimum
Ta (°C)	17.3	16.6	5.4	31.0	4.5
Ts (°C)	18.2	17.6	4.3	29.2	7.6
VPD (kPa)	0.82	0.59	0.72	3.17	0.04
Rnet (W m^{-2})	163	138	129	487	0
G_{local} (W m^{-2})	5.5	3.4	5.1	12.0	-44.2
G_{large} (W m^{-2})	7.5	6.6	4.7	17.7	-7.3
SW_{down} (W m^{-2})	225	183	197	739	0
RH (%)	69	71	19	97	22
P (kPa)	103	103	9	105	101
Wind speed (m s^{-1})	1.18	1.71	1.2	5.7	0
u_* (m s^{-1})	0.1	0.09	0.09	0.44	0
Rainfall (mm)(sum)	69.34	-	-	-	-
H_{local}	59	49	48	201	-21
H_{large}	94	88	58	248	-33
LE_{local}	150	156	90	334	-32
LE_{large}	103	92	86	303	-50
$R_{net} - G_{large}$	175	164	117	435	-94

T_a air temperature 1 m height at EC station; T_s is soil temperature at 0.05 m depth; VPD is vapor pressure deficit; R_{net} is net radiation; G_{local} is the ground heat flux at the EC station (positive mean warming the surface and negative sign mean cooling the surface); G_{large} is the area-weighted average soil heat flux; SW_{down} is shortwave down welling; RH is humidity; P is ambient air pressure; u_* is friction velocity; Rainfall is the accumulation of rainfall during the period of the study, H_{local} is sensible heat from EC measurement, H_{large} is sensible heat from LAS measurement, LE_{local} is latent heat flux as a residual term of the energy balance equation derived from EC measurement, LE_{large} is latent flux as a residual term of the energy balance equation derived from LAS measurement, and $R_{net} - G_{large}$ is the available energy fluxes at large scale.

Table 4-3 Statistical Analysis between measured and estimated surface fluxes at two scales local and area-averaged measurement (sensible heat, latent heat fluxes and available energy).

Parameter	**Slope**	**R^2**	**RMSE**	**Npoint**
Available energy ($R_{net} - G_{local}$ *vs.* $R_{net} - G_{large}$)	0.99	0.99	11	432
Ground heat flux *(G_{local} vs. G_{large})*	1.40	0.42	11	432
Sensible heat flux *(H_{local} vs. H_{large})*	0.64	0.60	30	357
Latent heat flux (LE_{large} *vs.* LE_{local})	0.83	0.73	38	198

Table 4-4 Agroecosystems energy balance closure, correlation, error and number of points at local and large scale and evapotranspiration fluxes approach.

Criteria		Closure	R^2	RMSE	Npoint
Surface Turbulent heat fluxes	**H > 0 W m^{-2}**				786
	$H_{local} + LE_{PM}$ vs. $R_{net} - G_{local}$	0.98	0.86	53	
	$H_{local} + LE_{PT}$ vs. $R_{net} - G_{local}$	0.86	0.88	44	
	$H_{loarge} + LE_{PM}$ vs. $R_{net} - G_{large}$	1.00	0.86	54	
	$H_{large} + LE_{PT}$ vs. $R_{net} - G_{large}$	0.89	0.86	48	
	H < 50 W m^{-2}				433
	$H_{local} + LE_{PM}$ vs. $R_{net} - G_{local}$	0.64	0.76	24	
	$H_{local} + LE_{PT}$ vs. $R_{net} - G_{local}$	0.52	0.86	14	
	$H_{loarge} + LE_{PM}$ vs. $R_{net} - G_{large}$	0.68	0.81	22	
	$H_{large} + LE_{PT}$ vs. $R_{net} - G_{large}$	0.54	0.85	15	
	H > 50 W m^{-2}				233
	$H_{local} + LE_{PM}$ vs. $R_{net} - G_{local}$	0.82	0.57	58	
	$H_{local} + LE_{PT}$ vs. $R_{net} - G_{local}$	0.89	0.68	48	
	$H_{loarge} + LE_{PM}$ vs. $R_{net} - G_{large}$	0.78	0.44	69	
	$H_{large} + LE_{PT}$ vs. $R_{net} - G_{large}$	0.83	0.53	62	
Atmosphere stability	**Very unstable condition**				
	-200 < L_{obv} < 0				631
	$H_{local} + LE_{PM}$ vs. $R_{net} - G_{local}$	0.98	0.90	49	
	$H_{local} + LE_{PT}$ vs. $R_{net} - G_{local}$	0.88	0.90	43	
	$H_{loarge} + LE_{PM}$ vs. $R_{net} - G_{large}$	1.03	0.88	54	
	$H_{large} + LE_{PT}$ vs. $R_{net} - G_{large}$	0.92	0.88	49	
	Unstable condition				
	-1000 < L_{obv} <=-200				172
	$H_{local} + LE_{PM}$ vs. $R_{net} - G_{local}$	0.87	0.76	61	
	$H_{local} + LE_{PT}$ vs. $R_{net} - G_{local}$	0.72	0.80	45	
	$H_{loarge} + LE_{PM}$ vs. $R_{net} - G_{large}$	0.88	0.62	86	
	$H_{large} + LE_{PT}$ vs. $R_{net} - G_{large}$	0.72	0.60	73	
Surface wind speed	**U > 2 & 200< Wind direction <340**				289
	$H_{local} + LE_{PM}$ vs. $R_{net} - G_{local}$	1.04	0.91	45	
	$H_{local} + LE_{PT}$ vs. $R_{net} - G_{local}$	0.92	0.94	34	
	$H_{loarge} + LE_{PM}$ vs. $R_{net} - G_{large}$	1.22	0.92	52	
	$H_{large} + LE_{PT}$ vs. $R_{net} - G_{large}$	1.09	0.94	39	
	u_*> 0.2 m s^{-1}				425
	$H_{local} + LE_{PM}$ vs. $R_{net} - G_{local}$	1.14	0.85	69	
	$H_{local} + LE_{PT}$ vs. $R_{net} - G_{local}$	1.11	0.88	53	
	$H_{loarge} + LE_{PM}$ vs. $R_{net} - G_{large}$	1.11	0.87	63	
	$H_{large} + LE_{PT}$ vs. $R_{net} - G_{large}$	1.10	0.91	56	
	u_*< 0.2 m s^{-1}				134
	$H_{local} + LE_{PM}$ vs. $R_{net} - G_{local}$	1.03	0.90	31	
	$H_{local} + LE_{PT}$ vs. $R_{net} - G_{local}$	0.96	0.93	23	
	$H_{loarge} + LE_{PM}$ vs. $R_{net} - G_{large}$	1.10	0.85	25	
	$H_{large} + LE_{PT}$ vs. $R_{net} - G_{large}$	0.64	0.90	15	

4.8 References

Agam, N., Kustas, W.P., Anderson, M.C., Norman, J.M., Colaizzi, P.D., Howell, T.A., Prueger, J.H., Meyers, T.P. and Wilson, T.B., 2010. Application of the Priestley-Taylor Approach in a Two-Source Surface Energy Balance Model. Journal of Hydrometeorology, 11(1): 185-198.

Allen, R.G., Periera, L.S., Raes, D. and Smith, M., 1998. Crop Evapotranspiration: Guidelines for Computing Crop Requirements,Irrigation and Drainage Paper No. 56, Rome, Italy, 300 pp.

Barthlott, C., Drobinski, P., Fesquet, C., Dubos, T. and Pietras, C., 2007. Long-term study of coherent structures in the atmospheric surface layer. Boundary-Layer Meteorology, 125(1): 1-24.

Burba, G.G. and Verma, S.B., 2005. Seasonal and interannual variability in evapotranspiration of native tallgrass prairie and cultivated wheat ecosystems. Agricultural and Forest Meteorology, 135(1-4): 190-201.

Chehbouni, A., Watts, C., Lagouarde, J.P., Kerr, Y.H., Rodriguez, J.C., Bonnefond, J.M., Santiago, F., Dedieu, G., Goodrich, D.C. and Unkrich, C., 2000. Estimation of heat and momentum fluxes over complex terrain using a large aperture scintillometer. Agricultural and Forest Meteorology, 105(1-3): 215-226.

Churkina, G., Running, S.W. and Schloss, A.L., 1999. Comparing global models of terrestrial net primary productivity (NPP): the importance of water availability. Global Change Biology, 5: 46-55.

De Bruin, H.A.R., Van Den Hurk, B.J.J.M. and Kohsiek, W., 1995. The scintillation method tested over a dry vineyard area. Boundary-Layer Meteorology, 76(1-2): 25-40.

Ding, R.S., Kang, S.Z., Li, F.S., Zhang, Y.Q., Ling, T. and Sun, Q.Y., 2010. Evaluating eddy covariance method by large-scale weighing lysimeter in a maize field of northwest China. Agricultural Water Management, 98(1): 87-95.

Evans, J.G., McNeil, D.D., Finch, J.W., Murray, T., Harding, R.J., Ward, H.C. and Verhoef, A., 2012. Determination of turbulent heat fluxes using a large aperture scintillometer over undulating mixed agricultural terrain. Agricultural and Forest Meteorology, 166: 221-233.

Ezzahar, J., Chehbouni, A., Hoedjes, J.C.B., Er-Raki, S., Chehbouni, A., Boulet, G., Bonnefond, J.M. and De Bruin, H.A.R., 2007. The use of the scintillation technique for monitoring seasonal water consumption of olive orchards in a semi-arid region. Agricultural Water Management, 89(3): 173-184.

Ezzahar, J., Chehbouni, A., Er-Raki, S. and Hanich, L., 2009a. Combining a large aperture scintillometer and estimates of available energy to derive evapotranspiration over several agricultural fields in a semi-arid region. Plant Biosystems, 143(1): 209-221.

Ezzahar, J., Chehbouni, A., Hoedjes, J., Ramier, D., Boulain, N., Boubkraoui, S., Cappelaere, B., Descroix, L., Mougenot, B. and Timouk, F., 2009b. Combining scintillometer measurements and an aggregation scheme to estimate area-averaged latent heat flux during the AMMA experiment. Journal of Hydrology, 375(1-2): 217-226.

Fang, X.Q., Ren, L.L., Li, Q.F., Liu, X.F., Yuan, F., Zhao, D.Z. and Zhu, Q.A., 2012. Estimating and validating basin-scale actual evapotranspiration using MODIS images and hydrologic models. Hydrology Research, 43(1-2): 156-166.

Farahani, H.J., Howell, T.A., Shuttleworth, W.J. and Bausch, W.C., 2007. Evapotranspiration: Progress in measurement and modeling in agriculture. Transactions of the Asabe, 50(5): 1627-1638.

Finnigan, J.J., Clement, R., Malhi, Y., Leuning, R. and Cleugh, H.A., 2003. A re-evaluation of long-term flux measurement techniques - Part I: Averaging and coordinate rotation. Boundary-Layer Meteorology, 107(1): 1-48.

Fochesatto, G.J., Mayfield, J.A., Starkenburg, D.P., Gruber, M.A. and Conner, J., 2013. Occurrence of shallow cold flows in the winter atmospheric boundary layer of interior of Alaska. Meteorology and Atmospheric Physics, doi: 10.1007/s00703-013-0274-4.

Foken, T., 2008. The energy balance closure problem: An overview. Ecological Applications, 18(6): 1351-1367.

Friedl, M.A., 1996. Relationships among remotely sensed data, surface energy balance, and area-averaged fluxes over partially vegetated land surfaces. Journal of Applied Meteorology, 35(11): 2091-2103.

Gruber, M. and Fochesatto, G.J., 2013. A New Sensitivity Analysis and Solution Method for Scintillometer Measurements of Area-Averaged Turbulent Fluxes. Boundary-Layer Meteorology, 149(1): 65-83.

Gruber, M.A., Fochesatto, G.J., Hartogensis, O.K. and Lysy, M., 2014. Functional derivatives applied to error propagation of uncertainties in topography to large-aperture scintillometer-derived heat fluxes. Atmospheric Measurement Techniques, 7(7): 2361-2371.

Hemakumara, H.M., Chandrapala, L. and Moene, A.F., 2003. Evapotranspiration fluxes over mixed vegetation areas measured from large aperture scintillometer. Agricultural Water Management, 58(2): 109-122.

Heusinkveld, B.G., Jacobs, A.F.G., Holtslag, A.A.M. and Berkowicz, S.M., 2004. Surface energy balance closure in an arid region: role of soil heat flux. Agricultural and Forest Meteorology, 122(1-2): 21-37.

Hinzman, L.D. and Kane, D.L., 1992. Potential Response of an Arctic Watershed during a Period of Global Warming. Journal of Geophysical Research-Atmospheres, 97(D3): 2811-2820.

Hoedjes, J.C.B., Chehbouni, A., Ezzahar, J., Escadafal, R. and De Bruin, H.A.R., 2007. Comparison of large aperture scintillometer and eddy covariance measurements: Can thermal infrared data be used to capture footprint-induced differences? Journal of Hydrometeorology, 8(2): 144-159.

Idso, S.B., Aase, J.K. and Jackson, R.D., 1975. Net radiation-soil heat flux relations as influenced by soil water variations. Boundary-Layer Meteorology, 9: 113–122.

Janowiak, J.E., Gruber, A., Kondragunta, C.R., Livezey, R.E. and Huffman, G.J., 1998. A comparison of the NCEP-NCAR reanalysis precipitation and the GPCP rain gauge-satellite combined dataset with observational error considerations. Journal of Climate, 11(11): 2960-2979.

Kaimai, J.C. and Gaynor, J.E., 1991. Another Look at Sonic Thermometry. Boundary-Layer Meteorology, 56(4): 401-410.

Kaimal, J.C. and Finnigan, J.J., 1994. Atmospheric Boundary Layer Flows: Their Structure and Measurement. Oxford University, New York., 289 pp.

Kleissl, J., Gomez, J., Hong, S.H., Hendrickx, J.M.H., Rahn, T. and Defoor, W.L., 2008. Large aperture scintillometer intercomparison study. Boundary-Layer Meteorology, 128(1): 133-150.

Lee, X., Massman, W.J. and Law, B., 2004. Handbook of Micrometeorology. Kluwer Academic Publishers, the Netherlands, 238 pp.

Lei, H.M. and Yang, D.W., 2010. Interannual and seasonal variability in evapotranspiration and energy partitioning over an irrigated cropland in the North China Plain. Agricultural and Forest Meteorology, 150(4): 581-589.

Liang, X., Lettenmaier, D.P., Wood, E.F. and Burges, S.J., 1994. A Simple Hydrologically Based Model of Land-Surface Water and Energy Fluxes for General-Circulation Models. Journal of Geophysical Research-Atmospheres, 99(D7): 14415-14428.

Liu, S.M., Xu, Z.W., Wang, W.Z., Jia, Z.Z., Zhu, M.J., Bai, J. and Wang, J.M., 2011. A comparison of eddy-covariance and large aperture scintillometer measurements with respect to the energy balance closure problem. Hydrology and Earth System Sciences, 15(4): 1291-1306.

Massman, W.J., 2000. A simple method for estimating frequency response corrections for eddy covariance systems. Agricultural and Forest Meteorology, 104(3): 185-198.

Massman, W.J. and Lee, X., 2002. Eddy covariance flux corrections and uncertainties in long-term studies of carbon and energy exchanges. Agricultural and Forest Meteorology, 113(1-4): 121-144.

Mauder, M., Liebethal, C., Gockede, M., Leps, J.P., Beyrich, F. and Foken, T., 2006. Processing and quality control of flux data during LITFASS-2003. Boundary-Layer Meteorology, 121(1): 67-88.

McAneney, K.J. and Itier, B., 1996. Operational limits to the Priestley-Taylor formula. Irrigation Science, 17(1): 37-43.

McVicar, T.R. and Jupp, D.L.B., 1998. The current and potential operational uses of remote sensing to aid decisions on drought exceptional circumstances in Australia: a review. Agricultural Systems, 57(3): 399-468.

Meijninger, W.M.L., Hartogensis, O.K., Kohsiek, W., Hoedjes, J.C.B., Zuurbier, R.M. and De Bruin, H.A.R., 2002. Determination of area-averaged sensible heat fluxes with a large aperture scintillometer over a heterogeneous surface - Flevoland field experiment. Boundary-Layer Meteorology, 105(1): 37-62.

Meijninger, W.M.L., Beyrich, F., Luedi, A., Kohsiek, W. and De Bruin, H.A.R., 2006. Scintillometer-based turbulent fluxes of sensible and latent heat over a heterogeneous land surface - A contribution to LITFASS-2003. Boundary-Layer Meteorology, 121(1): 89-110.

Mu, Q.Z., Zhao, M.S., Kimball, J.S., McDowell, N.G. and Running, S.W., 2013. A Remotely Sensed Global Terrestrial Drought Severity Index. Bulletin of the American Meteorological Society, 94(1): 83-98.

Nemani, R., White, M., Thornton, P., Nishida, K., Reddy, S., Jenkins, J. and Running, S., 2002. Recent trends in hydrologic balance have enhanced the terrestrial carbon sink in the United States. Geophysical Research Letters, 29(10).

Parka, H., Yamazaki, T., Yamamoto, K. and Ohta, T., 2008. Tempo-spatial characteristics of energy budget and evapotranspiration in the eastern Siberia. Agricultural and Forest Meteorology, 148(12): 1990-2005.

Pelgrum, H. and Bastiaanssen, W.G.M., 1996. An intercomparison of techniques to determine the area-averaged latent heat flux from individual in situ observations: A remote sensing approach using the European Field Experiment in a Desertification-Threatened Area data. Water Resources Research, 32(9): 2775-2786.

Priestley, C.H.B. and Taylor, R.J., 1972. On the assessment of surface heat flux and evaporation using large-scale parameters. Monthy Weather Review, 100(2): 81-92.

Rivas, R. and Caselles, V., 2004. A simplified equation to estimate spatial reference evaporation from remote sensing-based surface temperature and local meteorological data. Remote Sensing of Environment, 93(1-2): 68-76.

Ruairuen, W., Fochesatto, J., Sparrow, E.B., Zhung, M., Schanabel, W. and Kim, Y., 2015. Evapotranspiration Cycles in a High Latitude Agroecosystem: Potential Warming Role. . Submitted.

Ruhoff, A.L., Paz, A.R., Aragao, L.E.O.C., Mu, Q., Malhi, Y., Collischonn, W., Rocha, H.R. and Running, S.W., 2013. Assessment of the MODIS global evapotranspiration algorithm using eddy covariance measurements and hydrological modelling in the Rio Grande basin. Hydrological Sciences Journal-Journal Des Sciences Hydrologiques, 58(8): 1658-1676.

Samain, B., Ferket, B.V.A., Defloor, W. and Pauwels, V.R.N., 2011. Estimation of catchment averaged sensible heat fluxes using a large aperture scintillometer. Water Resources Research, 47.

Samain, B., Simons, G.W.H., Voogt, M.P., Defloor, W., Bink, N.J. and Pauwels, V.R.N., 2012. Consistency between hydrological model, large aperture scintillometer and remote sensing based evapotranspiration estimates for a heterogeneous catchment. Hydrology and Earth System Sciences, 16(7): 2095-2107.

Savage, M.J., 2009. Estimation of evaporation using a dual-beam surface layer scintillometer and component energy balance measurements. Agricultural and Forest Meteorology, 149(3-4): 501-517.

Schüttemeyer, D., Moene, A.F., Holtslag, A.A.M., De Bruin, H.A.R. and De Giesen, N.V., 2006. Surface fluxes and characteristics of drying semi-arid terrain in West Africa. Boundary-Layer Meteorology, 118(3): 583-612.

Sellers, P.J., Randall, D.A., Collatz, G.J., Berry, J.A., Field, C.B., Dazlich, D.A., Zhang, C., Collelo, G.D. and Bounoua, L., 1996. A revised land surface parameterization (SiB2) for atmospheric GCMs .1. Model formulation. Journal of Climate, 9(4): 676-705.

Sharratt, B., Zhang, M.C. and Sparrow, S., 2006. Twenty years of tillage research in subarctic Alaska - I. Impact on soil strength, aggregation, roughness, and residue cover. Soil & Tillage Research, 91(1-2): 75-81.

Sharratt, B.S., 1994. Observations and Modeling of Interactions between Barley Yield and Evapotranspiration in the Sub-Arctic. Agricultural Water Management, 25(2): 109-119.

Sharratt, B.S., 1996. Tillage and straw management for modifying physical properties of a subarctic soil. Soil & Tillage Research, 38(3-4): 239-250.

Shulski, M. and Wendler, G., 2007. The Climate of Alaska. University of Alaska Press.

Sobrino, J.A., Gómez, M., Jiménez-Muñoz, J.C. and Olioso, A., 2007. Application of a simple algorithm to estimate daily evapotranspiration from NOAA-AVHRR images for the Iberian Peninsula. Remote Sens. Environ. , 110: 139-148.

Sparrow, S.D. and Masiak, D.T., 2008. Second Harvest Timing and Cut Height of Forage Crops in Central Alaska. Agronomy Journal, 100(6): 1615-1621.

Starkenburg, D., Fochesatto, G.J., Prakash, A., Cristóbal, J., Gens, R. and Kane, D.L., 2013. The role of coherent flow structures in the sensible heat fluxes of an Alaskan boreal forest. J. Geophys. Res. Atmos., 118: 8140–8155.

Starkenburg, D., Fochesatto, G.J., Cristóbal, J., Prakash, A., Gens, R., Alfier, J.G., Nagona, H., Harazono, Y., Iwata, H. and Kane, D., 2015. Temperature regimes and turbulent heat fluxes across a heterogeneous canopy in an Alaskan boreal forest. J. of Geophys. Res. Atmos, 120.

Stewart, R.B. and Rouse, W.R., 1977. Substantiation of the Priestley and Taylor Parameter α =1.26 for Potential Evaporation in High Latitudes. Journal of Applied Meteorology 16: 649-650.

Su, Z., 2002. The Surface Energy Balance System (SEBS) for estimation of turbulent heat fluxes. Hydrology and Earth System Sciences, 6(1): 85-99.

Su, Z., Timmermans, W.J., van der Tol, C., Dost, R., Bianchi, R., Gomez, J.A., House, A., Hajnsek, I., Menenti, M., Magliulo, V., Esposito, M., Haarbrink, R., Bosveld, F., Rothe, R., Baltink, H.K., Vekerdy, Z., Sobrino, J.A., Timmermans, J., van Laake, P., Salama, S., van der Kwast, H., Claassen, E., Stolk, A., Jia, L., Moors, E., Hartogensis, O. and Gillespie, A., 2009. EAGLE 2006-Multi-purpose, multi-angle and multi-sensor in-situ and airborne campaigns over grassland and forest. Hydrology and Earth System Sciences, 13(6): 833-845.

Suyker, A.E. and Verma, S.B., 2009. Evapotranspiration of irrigated and rainfed maize-soybean cropping systems. Agricultural and Forest Meteorology, 149(3-4): 443-452.

Tatarski, V., 1961. Wave propagation in a turbulent medium. McGarw Hill, New York, 285 pp.

Teixeira, A.H.D.C., Bastiaanssen, W.G.M., Ahmad, M.D. and Bos, M.G., 2009. Reviewing SEBAL input parameters for assessing evapotranspiration and water productivity for the Low-Middle Sao Francisco River basin, Brazil Part A: Calibration and validation. Agricultural and Forest Meteorology, 149(3-4): 462-476.

Thiermann, V. and Grassl, H., 1992. The Measurement of Turbulent Surface-Layer Fluxes by Use of Bichromatic Scintillation. Boundary-Layer Meteorology, 58(4): 367-389.

Utset, A., Farre, I., Martinez-Cob, A. and Cavero, J., 2004. Comparing Penman-Monteith and Priestley-Taylor approaches as reference-evapotranspiration inputs for modeling maize water-use under Mediterranean conditions. Agricultural Water Management, 66(3): 205-219.

Vickers, D. and Mahrt, L., 1997. Quality control and flux sampling problems for tower and aircraft data. Journal of Atmospheric and Oceanic Technology, 14(3): 512-526.

Walter, I.A., Allen, R.G., Elliott, R., Mecham, B., Jensen, M.E., Itenfisu, D., Howell, T.A., Snyder, R., Brown, P., Echings, S., Spofford, T., Hattendorf, M., Cuenca, R.H., Right, J.L. and Martin, D., 2000. ASCE standardized reference evapotranspiration equation. In: R.G. Evans, B.L. Benham and T.P. Trooien (Editors), Proceedings of the National Irrigation Symposium. ASAE, Phoenix, AZ, pp. 209–215.

Wyngaard, J.C., Izumi, Y. and Collins, S.A., 1971. Behavior of the refractive-index-structure parameter near the ground. Journal of the Optical Society of America, 61(12): 1646-1650.

CHAPTER 5

Simulating the coupled transport equations to compute evapotranspiration[1]

[1]Manuscript prepared for submission to the Agricultural and Forest Meteorology

Abstract

Soil evaporation and soil moisture dynamics near the surface are key players in the mass and energy balance equations ultimately regulating energy fluxes of exchange between the soil and the atmospheric surface layer. Essential to this determination is the computation of fluxes in liquid and gas phase of water movement in the soil medium. However in the implementation of such coupled numerical model, including the transport equation for liquid and vapor phases, still remain under discussion is how to consider the soil surface resistance and soil surface temperature. In this case a non-isothermal solution of the vapor flux equation that accounts for the thermally driven water vapor transport and phase changes was implemented. The objective of this work was to adapt and evaluate the numerical simulation outputs of the fully coupled fluxes model against field measurements of soil temperature, heat flux, water content, and evaporation in an agroecosystem in northern latitudes. Two well-defined hydrometeorological situations were selected: dry and wet periods to fully test the model's ability to reproduce the soil medium dynamics and the resulting interface fluxes. Model forcing variables are incoming solar radiation and surface layer thermodynamic parameters (wind speed, ambient temperature, relative humidity, precipitation, soil temperature and moisture) while changing in depth and time soil parameters are considered dynamically adjusted boundary conditions for solving the set of coupled differential equations. Evaluation of simulation results according to the best found initialization and boundary conditions gives good agreement in the radiative fluxes and turbulent fluxes only for the dry period while, on the other hand, the wet periods perform poorly due to the lack of representation in the radiation field and differences in soil dynamics across the landscape.

Keywords: coupled fluxes, evaporation, soil dynamics, vapor transport, simulation

5.1 Introduction

Northern latitudes have been identified as a region where global climate change will have earlier and stronger impacts than in other regions of the world (Chapin et al., 2000; Serreze et al., 2000; Hinzman et al., 2005; Intergovernmental Panel on Climate Change, 2007). Most of the entire region is underlain by permafrost, or perennially frozen ground in which temperatures remain below 0°C for at least two consecutive years and an active layer on top of the permafrost. Seasonal thaws of this active layer is the primary dominant subsurface component of the land-atmosphere system (Mölders and Romanovsky, 2006). Under warming of climate much of this terrain would be vulnerable to subsidence, particularly in ice-rich areas of relatively warm, discontinuous permafrost, and shrinking ponds and lakes (Romanovsky et al., 2002; Yoshikawa and Hinzman, 2003; Hinzman et al., 2005; Smith et al., 2005; Osterkamp, 2007; Jorgenson et al., 2010). All these changes could potentially alter the exchange of surface energy, water, and carbon cycles in high latitude ecosystems (Mack et al., 2004; Chapin et al., 2005).

Soil moisture plays a critical role in the surface energy balance and water cycle in these regions (Chapin et al., 2000; Clein et al., 2000; McGuire et al., 2000). It is widely recognized that the soil moisture confined in a thin layer underneath the land surface influences the partitioning of the surface energy balance by modifying surface thermal conductance and rates of evaporation (McFadden et al., 2003). An example of such an important role is the control of precipitation transfer and the partitioning of incoming solar radiation into latent, sensible heat and ground heat fluxes (Hinzman and Kane, 1992; McFadden et al., 1998). In addition, soil moisture and temperature status affect biological processes such as soil microbial activity, seed germination and plant growth. They also affect water and nutrition absorption and solute transport in soil.

High latitudes will experience increased summer dryness as the warming climate progresses, changing therefore atmospheric vapor pressure conditions and thereby enhancing evapotranspiration rate. In terms of seasonal effect inadequate snowmelt infiltration or rainfall during spring and early summer often causes crop water stress and reduction in yield of small grains (Sharratt, 1994, 1998) in the subarctic agriculture. Therefore evapotranspiration becomes of absolute importance for plant growth because it mainly controls the available soil water and therefore is a limiting factor in agriculture productivity and sustainability. As a result, continuous monitoring of soil water content and soil temperature is very important in the fields of agronomy and hydrology (Banimahd and Zand-Parsa, 2013).

Several modeling studies have focused on soil carbon reservoirs (e.g. Zhuang et al., 2003; Euskirchen et al., 2006; Balshi et al., 2007) and permafrost degradation in natural ecosystems across the circumpolar region (Euskirchen et al., 2006; Lawrence et al., 2008), nevertheless agroecosystem has not been taken into consideration until now. Despite the mentioned complexities in the soil medium, similarities between high latitude and mid-latitude agricultural soils can be found during the growing season. This allows for making use of models that are currently in use for mid-latitude agricultural settings. In this case a fully coupled differential equation system solving for soil temperature and vertical soil moisture regimes is utilized to bring emphasis on the sub medium transport in contrast to most large-scale ecosystem models where one or two soil layers are used to simulate soil moisture dynamics in ecosystem models (e.g., Sitch et al., 2003).

In this study, we apply a well-developed numerical model which fully couples heat and water transport to deduce the coupled water and heat transport across the soil medium forced by radiation and meteorological conditions. As demonstrated in Bittelli et al. (2008), this approach enables

numerically stable, energy- and mass conservation equation solution in terms of the external forcing and boundary conditions. Such an approach requires a modeling framework that incorporates the interactions among meteorological variables (e.g. air temperature, relative humidity, precipitation, solar radiation) and soil properties (e.g. soil temperature, soil moisture, soil water potential) into the coupled numerical model. In section 5.2 the numerical model for computation of coupled heat, liquid water and vapor fluxes in the soil and at the soil–atmosphere interface in a real condition of agroecosystem is presented. Section 5.4 presents the comparison of model results through independent direct measurement of net radiation, sensible heat flux, soil moisture, and soil temperature as well as calculated evapotranspiration, and soil heat flux. Finally an assessment of scenarios modeling and future use of the model is provided.

5.2 Materials and Methods

5.2.1. Field Experiment

A field study was conducted at the Fairbanks Experiment Farm (FEF) of the University of Alaska Fairbanks (UAF) Agricultural and Forestry Experiment Station (AFES) Fairbanks Alaska, USA (64° 51′ 16.6 ″N, 147° 51′ 36.4″ W, 150 m above sea level) during summer 2013 to observe interactions between the soil and the atmosphere. The soil within the lysimeter plots were used for this study because large amounts of data were available. The soil was a sandy loam with 66% sand, 29% silt, and 5 % clay, with the available water holding capacity of about 0.18-0.36 m^3 m^{-3} that was obtained from a soil moisture characteristic curve (Chapter 2). Table 5-1 shows the hydraulic properties used for the numerical solution.

Volumetric soil moisture content was measured using three soil moisture sensor (10HS; Decagon Devices Inc.) at 5, 10 and 20 cm. The sensor has 14.5 cm long prongs and 3.3 cm wide, so the 5 cm sensor spanned the depth 3.3-6.7 cm, the 10 cm sensor spanned the depth 8.3-11.3 cm,

and the 20 cm sensor spanned the depth 18.3-21.3 cm. Gravimetric samples were also taken to calibrate the 10HS sensor (Chapter 2). Soil moisture was continuously measured with a record interval of 30 minutes. The bulk density was measured to be about 0.70 g cm^{-3}. The soil temperature (S-TMB-M006, Onset Computer Corporation, Bourne, MA) was measured at depths of 5, 10, and 20 cm below the soil surface, and. also used to obtain the ground heat flux in this study.

The observation-based meteorological parameters included air temperature (T_{air}), relative humidity (RH), air pressure, wind speed (u) and direction, and precipitation at 2 m height above the ground were obtained at 1 minute intervals at the experiment station. One minute recordings of these data were averaged to hourly for initial input to the simulation.

An independent measure of evapotranspiration was determined using Penman-Monteith methods and the more continuous series of data available on this period.Sensible heat flux was measured by using eddy covariance (EC) and large aperture scintillometer (LAS). The theory and techniques can be found in Chapter 4.

5.2.2 Model Implementation

5.2.2.1 Model modules in Python

The numerical model was coded in Python and is set in a time evolving one-dimensional simulation of coupled flow of liquid water, heat and water vapor. The model description can be found in APPENDIX-B. Figure 5-1 shows the scheme indicating the coupling of the driving terms (temperature, liquid water and conductive terms) and the resistive and conductive terms. This model also includes the computation of soil energy budget. Each component of the energy balance is calculated and saved into an output file, to allow for the analysis of the rest of the magnitudes and diurnal oscillations of the different terms. The model is called **PSP_coupled** and it is made of

ten modules with two input data files. One data file contains the soil data and the other one contains the weather data.

1. main.py
2. PSP_boundary.py
3. PSP_public.py
4. PSP_soil.py
5. PSP_couple1D.py
6. PSP_readDataFile.py
7. PSP_longWaveRadiation.py
8. PSP_grid.py
9. PSP_plot.py
10. PSP_plotEnergy.py
11. PSP_ThomasAlgorithm.py
12. soil.txt
13. weather.dat

The main file is main.py which contains the calls to other embedded subroutines listed. The module PSP_boundary defines the initial and boundary conditions. The PSP_public contains all variables that are read by all modules such as latitude, longitude, altitude, albedo, atmospheric pressure and clay content, initial soil temperature, soil matric potential. The PSP_soil is written to define the soil properties. The PSP_couple1D is the module that implements the solver for the different flux equations. The PSP_longWaveRadiation is for computing the long wave radiation component of the radiation balance at the soil surface. The PSP_grid module is for building the computational grid and PSP_ThomasAlgorithm for solving the system of equations. The PSP_plot and PSP_plotEnergy are modules for visualizing the data input and output from the model.

5.2.2.2 The initial setting for model simulation

The initial conditions for dry and wet period were selected to test the model. To implement the scenarios two data files needed to be created “soil.txt” and “weather.dat”. The soil.txt file is required for data input of soil properties such as soil depth (the model set up from 0 to 1.5 m), the saturated soil moisture, residual water content, hydraulic properties of soil, and soil metric

potential (Table 5-1). The soil file can be used for two periods according to the same soil properties in this study but additional setting for initial value need to be modified in the PSP_public module. The weather file is required at hourly weather parameters such as solar radiation, air temperature, precipitation, relative humidity (RH), and wind speed as an input to calculate other parameter. Time step is set to 300 sec and input data of one hour resolution. The PSP_public is the file that need to be adapted in all parameters that are read by all modules for the given area in which the simulation is carried out. In this case the site information for the FEF was input into this file which includes the latitude, longitude, altitude. Moreover, the initial condition of soil such as soil water potential, soil temperature, albedo for dry and wet need to be applied into this module (Table 5-2).

In this study the value of albedo for simulation was set as 0.2 for the dry period (Davin et al., 2014), while a value of 0.15 was applied for the wet period in agriculture land in subarctic region Sharratt (1993).

5.3 Simulations scenarios

The model was applied to two selected periods (dry and wet) in an agricultural land during the summer 2013. Model performance was tested under two conditions: a dry and a wet period. The dry period (no precipitation event) spun from 26 -30 July (Julian day 207-211) and wet period from 25-30 August (Julian day 230-234).

5.3.1 Dry period

The experimental data is taken from the lysimeter plots that monitored soil moisture and temperature. The meteorological parameters measured about 10 m away from the plot for the dry period are given in Table 3 (Figure 5-2a). The hourly average of vapor pressure deficit (VPD) was 1.18 kPa. Mean hourly air temperature was 21°C with maximum of 30.7 °C and minimum of 9.8

°C also reported in this period. The average RH was approximately 58% and wind speed of 2.36 m s^{-1}.

5.3.2 Wet period

The meteorological conditions in the wet period (Figure 5-2b) was cooler than the dry period in terms of an average hourly air temperature and soil temperature, while the solar radiation difference from the dry was small (Table 5-3). The RH was approximately 77% with low level of VPD (0.36 kPa) on average during the wet period (Table 5-3). A total precipitation of 37.60 mm was also reported in this period.

5.4 Results and discussion

5.4.1 Net radiation

Net radiation (R_{net}) is the main energy balance component driving evapotranspiration process. In this regard, a comparison between the net radiation observed ($R_{net\ obs}$) and modeled ($R_{net\ mod}$) was performed. Figure 5-3a show simulated and measured hourly data of net radiation as a function of time for the dry period (26 July to 3 August 2013). Results show a good agreement between modeled and observed R_{net} with the correlation coefficient (R^2) of 0.92 and Root Mean Square Error (RMSE) of 45 Wm^{-2} (Figure 5-4a) during the dry period. There are about six days out of nine total days that the model performed remarkably well to simulate the R_{net} in which the maximum difference did not exceed 157 Wm^{-2} which was found on 27 July (Julian day 208). Overall, the $R_{net\ mod}$ overestimated $R_{net\ obs}$ by about 16%. Similar results have been reported by Carrasco and Ortega-Farías (2007) in commercial vineyard where the R_{net} simulation showed a good agreement with the measured R_{net} (R^2=0.92) with the RMSE less than 48 Wm^{-2}. On the other hand, a lower correlation between $R_{net\ obs}$ and $R_{net\ mod}$ was found during the wet period with the R^2 of 0.72 and RMSE of 67 Wm^{-2} (Figure 5-4b). However, there were two days from 25-26 August

that the model simulated very well compared with the measured $R_{net,}$ while it underestimated the following two days (27-28 August) and overestimated the last two days for the wet period (Figure 5-3b). The maximum underestimation for the entire time series was about 85 Wm^{-2} and the maximum overestimate was 199 Wm^{-2}.

The high and low correlation between measured and modeled R_{net} in different periods can be related to the condition of cloud cover. This may be explained based on the variability of incoming solar radiation between those periods as we can see in Figure 5-5. An average of solar radiation of 215 Wm^{-2} with the maximum and minimum of 680 Wm^{-2}, 150 Wm^{-2} respectively were reported in dry period, while a lower mean and maximum R_{net} were found in wet period (Table 5-3). Ortega-Farías et al. (2000) indicated that errors in the calculation of R_{net} over a well-irrigated festuca grass were associated with the estimation of atmospheric radiation under cloudy sky conditions. Therefore, to summarize this point $R_{net\ mod}$ was able to estimate net radiation with a good degree of precision during the dry period than the wet period.

5.4.2 Latent heat

Figure 5-6 shows simulated and observed latent heat flux (LE) as a function of time during dry and wet periods. High rates of solar radiation heating the soil surface caused the soil to lose water vapor to evapotranspiration from the surface. During the nighttime there was negative conduction to cool the soil surface, and LE became negative due to condensation. The LE was better predicted by the numerical model during the dry period, with an R^2 of 0.70 and RMSE of 53 Wm^{-2} than the wet period (R^2=63 and RMSE=58 Wm^{-2}). There were two days that the model overestimated but the times series followed each other, one day about the same, and three days of modeled LE not correlated with the observed LE. The maximum difference between observed and simulated LE was about 200 Wm^{-2}. Cumulative ET from the observed quantities reached 22 mm

with an average of 2.44 mm d^{-1}, while cumulative ET from the simulation was 15 mm with the mean of 1.67 mm d^{-1} for the dry period (Figure 5-7a). In contrast, during the wet period the cumulative ET from the observed was about 6 mm over six days, whereas only about 2 mm was found from the simulation ET (Figure 5-7b). An average precipitation for observed was 1.0 mm d^{-1} while only 0.3 mm d^{-1} was found for the simulation during the wet period.

5.4.3 Ground heat fluxes

The average daytime of ground heat flux (G) contribution to vapor flux was in the order of 26 Wm^{-2} (ranging from 1 to 79 Wm^{-2}) while the value from the simulation was 25 Wm^{-2} (ranging from 0.8 to 49 Wm^{-2}) (Figure 5-8). In Figure 5-8a, the G from the model was an overestimate in the first two days, and then closely approached the G observed at day three, and underestimated G observed in the last two days of the dry period. The maximum difference of 44 Wm^{-2} was reported in the overestimating period, whereas the value of 32 Wm^{-2} was found in underestimating period. On the contrary, the simulation of G during the wet period was an over estimate all the days (Figure 5-8b) with the maximum difference of more than 100 Wm^{-2} during the daytime.

5.4.4 Sensible heat

The sensible heat (H) fluxes obtained from measurements and from the simulation for agricultural field in the northern high latitude were compared during the dry period. The time-series composite of hourly diurnal variation during dry and wet was illustrated in Figure 5-9. In the dry period, results showed a good correlation between H measured by EC and simulated from models with R^2=0.63 and RMSE = 32 Wm^{-2}, whereas a lower correlation was found between H observed by LAS (R^2 of 0.52 and RMSE of 40 Wm^{-2}) (Figure 5-9a). The H simulated was compared with the H measured by LAS during the daytime period. However, overall simulated H overestimated H from EC except in the morning where they were closer in value. The ratio of H

by EC and simulated was about 0.47, while ratio of H modeled versus H by LAS was 0.82. The maximum of H from model, EC, and LAS were 139, 110 and 169 Wm^{-2} respectively during midday.

Concerning the wet period, very poor correlation was found between H measured by LAS and simulated H (R^2 =0.15, RMSE =13 Wm^{-2}). It should be noted that H by EC was not illustrated during this period because of insufficient data for the analysis. The time-series composite of hourly diurnal variation of H from both methods are illustrated in Figure 5-9b. Mean hourly of H observed was 30 Wm^{-2} while only 15 Wm^{-2} was reported from modeled H. In general, H observed showed higher values than H simulated by about 51% with the maximum difference of 36 Wm^{-2} during the wet period.

We can conclude here that the model simulation for H may be applicable for use as a minimum level of H flux for this ecosystem for the dry period than the wet period.

5.4.5 Soil moisture and soil temperature

The soil moisture was measured in the lysimeter plot at three depths. From the measurement we found that the high moisture content was found in the lower depth than in the surface layer. The initial soil moisture during the dry period above the soil surface was about 0.28 m^3m^{-3} (5 cm depth). The numerical model gave a good prediction of soil moisture around the same depth with a difference of 0.02 $m^3\ m^{-3}$. (Figure 5-10). The low agreement was found during the wet period where the measurement of soil moisture from the plot was about 0.30 $m^3\ m^{-3}$ for the first day of wet period, however the simulation gave a higher value of soil moisture with a difference larger than 0.02 $m^3\ m^{-3}$. The large difference of soil moisture in the wet period could be due to the hydraulic properties. Because hydraulic conductivity versus the soil moisture potential curve is highly non-linear and, therefore, the flow of soil moisture from the upper layer to the

lower layer in the wet period leads to a large decrease in hydraulic conductivity and liquid water distribution (Bittleli et al., 2008), while during the dry period the soil moisture was more constant along the depths (Figure 5-10) with less dependence on the liquid fraction. The soil moisture content fluctuated during the day according to the vapor flux as was reported by several other authors (Jackson, 1973; Cahill and Parlange, 1998; Parlange, 1998). From the simulation, the water potential in the wet period has the same pattern like soil moisture content and has more variation over the soil layer than the dry period.

Soil temperature was measured at the same depth as soil moisture. Figure 5-10 shows the soil temperature as a function of depths predicted by the numerical model. The value of soil temperature from experiment (18 °C) was lower than the simulated (23 °C) at 20 cm depth. This large difference can cause differences in the temperature gradient which affect the ground heat flux as described in the previous section. Therefore, the model still predicted soil temperature for this environment.

5.5 Conclusions

This model solves the coupled vapor and liquid water phase exchange between soil and atmosphere. The model uses meteorological data, radiation and precipitation, and introduces a variable boundary condition which includes the soil temperature, soil moisture, and hydraulic properties of soil. Overall, dry period parameters seemed to be reproduced fairly well than those in wet periods by using this model in a high latitude farmland. In general R_{net} has a good agreement between modeled and observed data for both periods with RMSE of 45 Wm^{-2} in dry period and 48 Wm^{-2} during wet period. The LE also was well predicted by the model with RMSE not exceed 53 Wm^{-2}. On the other hand, G was overestimated with the maximum difference of more than 100 Wm^{-2} in wet period and 44 Wm^{-2} in dry period. In addition, the measured H by EC and LAS

correlated well with the model with the RMSE being in the range of 32-40 Wm^{-2}, and the modeled EC seemed to agree well with the measured H by EC. The soil moisture also correlated better during the dry period than the wet period, while the soil temperature was overestimated compared to the observed values. The low correlation in the wet period might be due to significant influences of the synoptic variability introducing large changes in cloud coverage and precipitation which are difficult to reproduce by a single point one-dimensional model formulation. Nevertheless, dry conditions which by far the most stringent conditions for agriculture sustainability reproduces well.

There are still several parameters that need to be investigated more in depth and the most important factor is the hydraulic properties of soil. This variable is more complicated and there are many steps to reach the correct value. In the current study existing values were applied from previous work done around the same study site while some other values were obtained from field and laboratory experiments. The soil in agroecosystems tend to experience large changes in some of these properties, are difficult to capture. This factor needs to be taken into account when implementing this model over unnatural setting systems. Based on field intensive experiments the model can be calibrated so that with simple meteorological parameters can drive the models to initialize different agroecosystems across spatial scales.

5.6 Acknowledgements

The authors thank the Agricultural and Forestry Experiment Station (AFES) School of Natural Resources and Extension at the University of Alaska Fairbanks and the Department of Agricultural Sciences, at the University of Bologna, Italy. Also, the authors are indebted to Marco Bittelli for help in facilitating the model implementation. Ms. Watcharee Ruairuen was funded by Suratthani Rajabhat University, Thailand. G. J. Fochesatto was supported by the Geophysical Institute, University of Alaska Fairbanks. Elena B. Sparrow was supported by the International Arctic Research Center and Alaska EPSCOR, also at the University of Alaska Fairbanks.

Figures

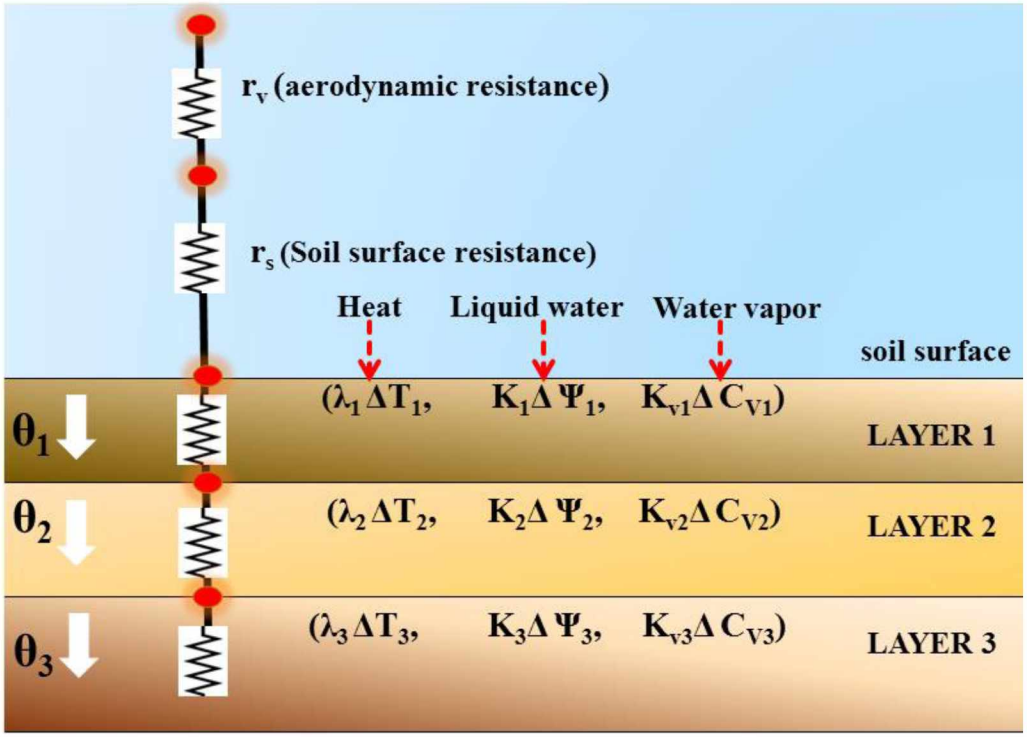

Figure 5-1 Scheme of the computational grid with the driving force terms (temperature, soil water potential and soil vapor concentration), the soil conductivities and the resistances involved at the soil–atmosphere interface (Adapted from Bitelli et al., 2008). The red dot is the mass balance for heat flow and water flux at a node.

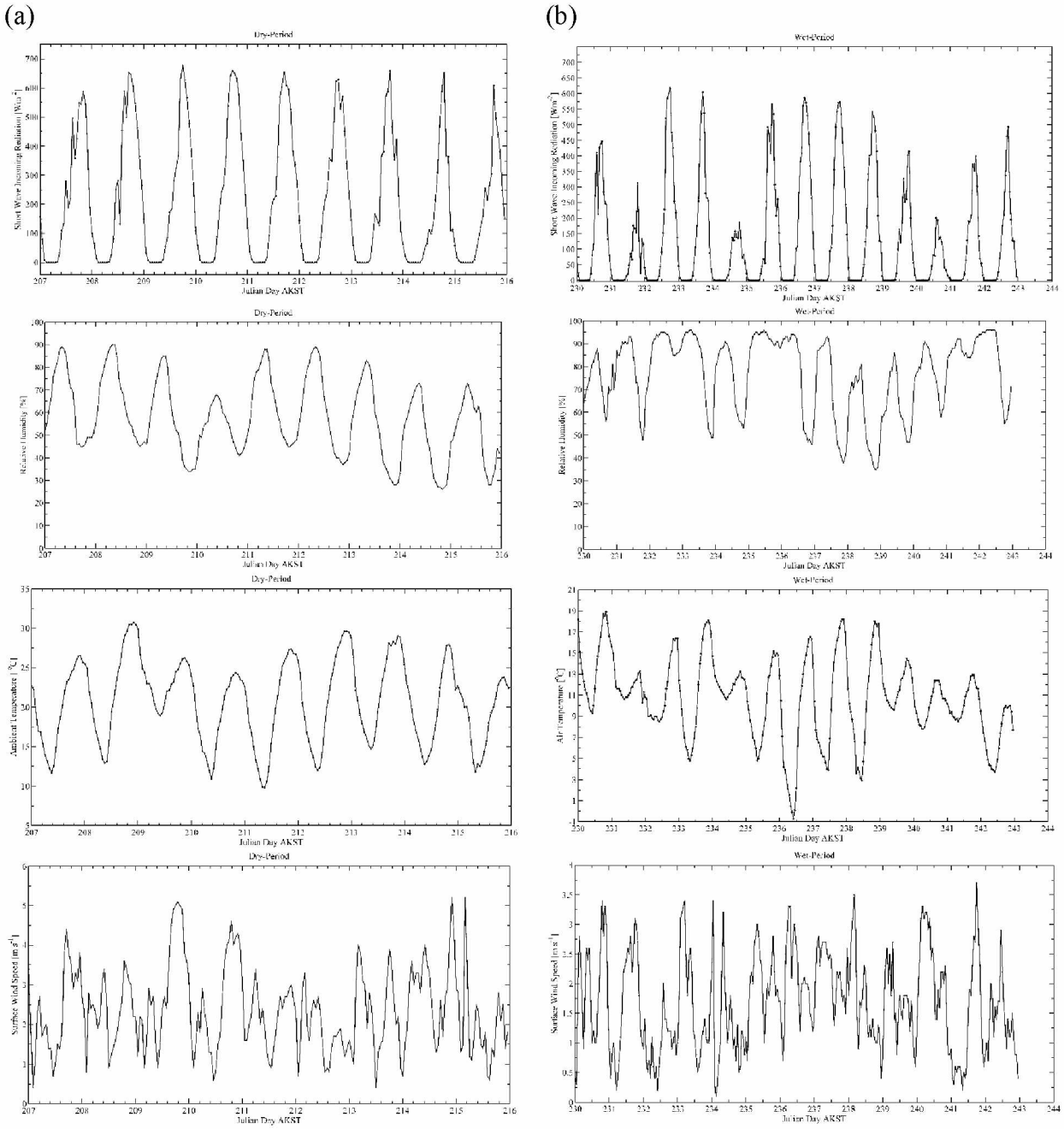

Figure 5-2 Global radiation, relative humidity, air temperature, and wind speed measured in the Atmospheric Surface Layer from top to bottom at the experimental plot during the dry period (left panel; 26 July-4 August 2013[Julian day 207-215]) and wet period (right panel; 18-31 August 2013 [Julian 230-242]).

(a)

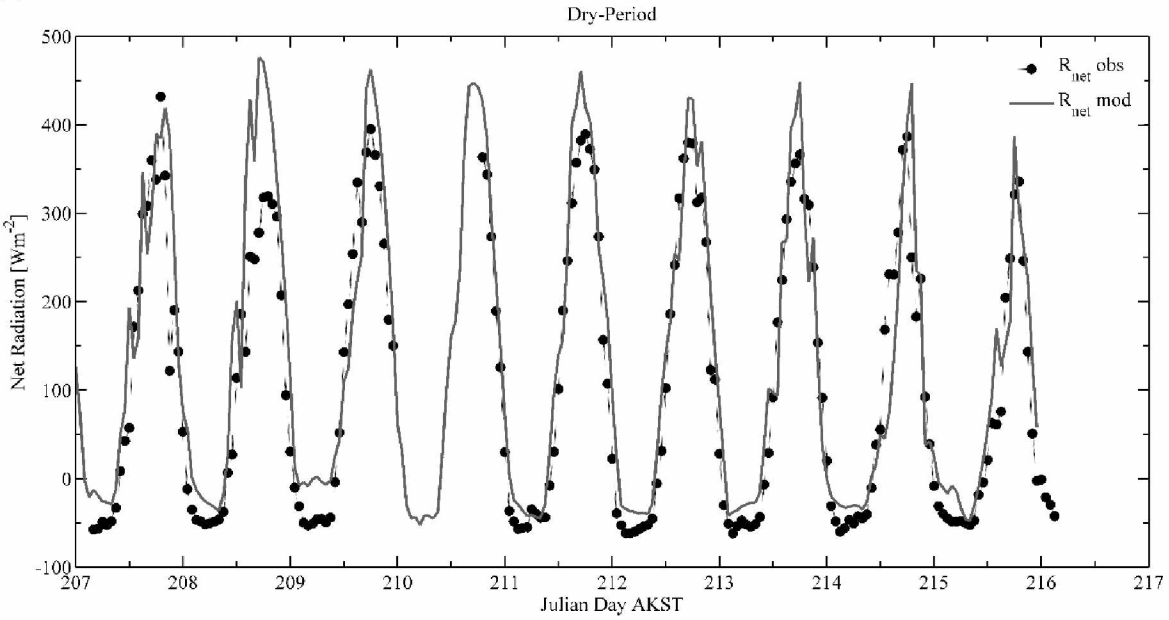

(b)

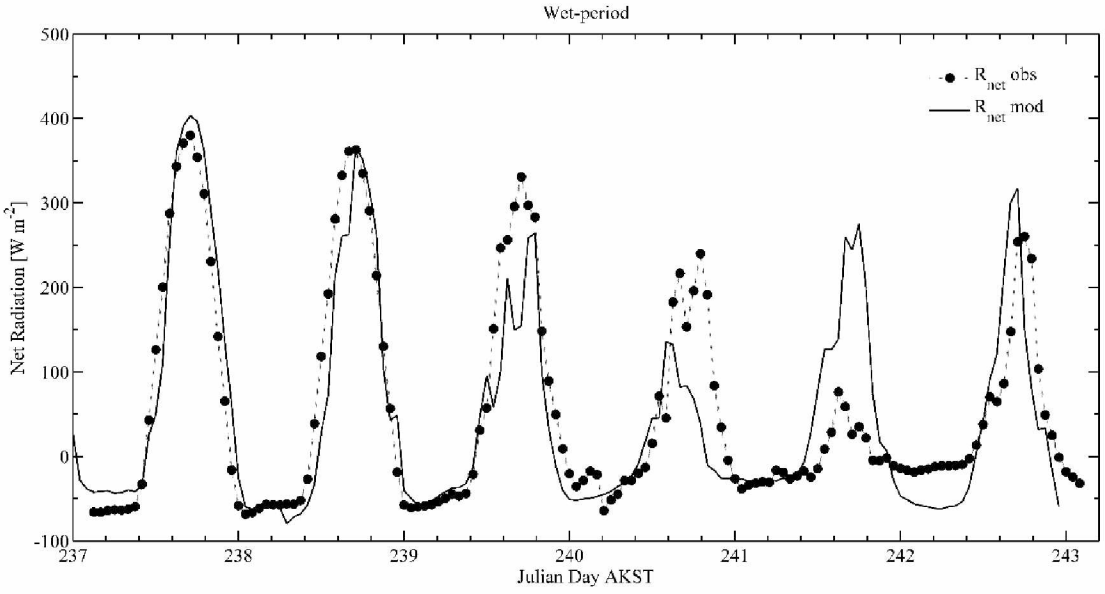

Figure 5-3 Simulated and measured hourly data of net radiation during the dry and wet period as a function of time. (a) Dry period from 26 July to 3 August 2013 (Julian day 207-216), (b) wet period from 25-30 August 2013 (Julian day 237-242)

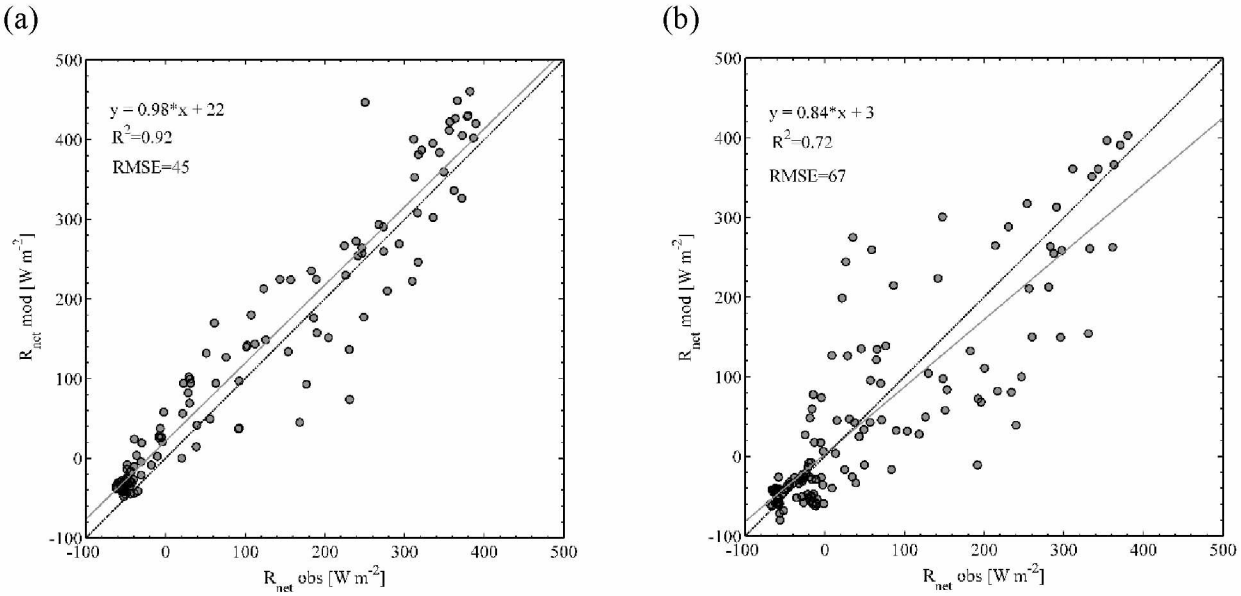

Figure 5-4 Comparison between the hourly observation of net radiation (Rnet obs) and the simulation of net radiation (Rnet mod) during the dry and wet period. (a) Dry period from 31 July to 3 August 2013 (Julian day 210-215) and during the wet period (b) from 25-30 August 2013 (Julian day 237-242).

(a)

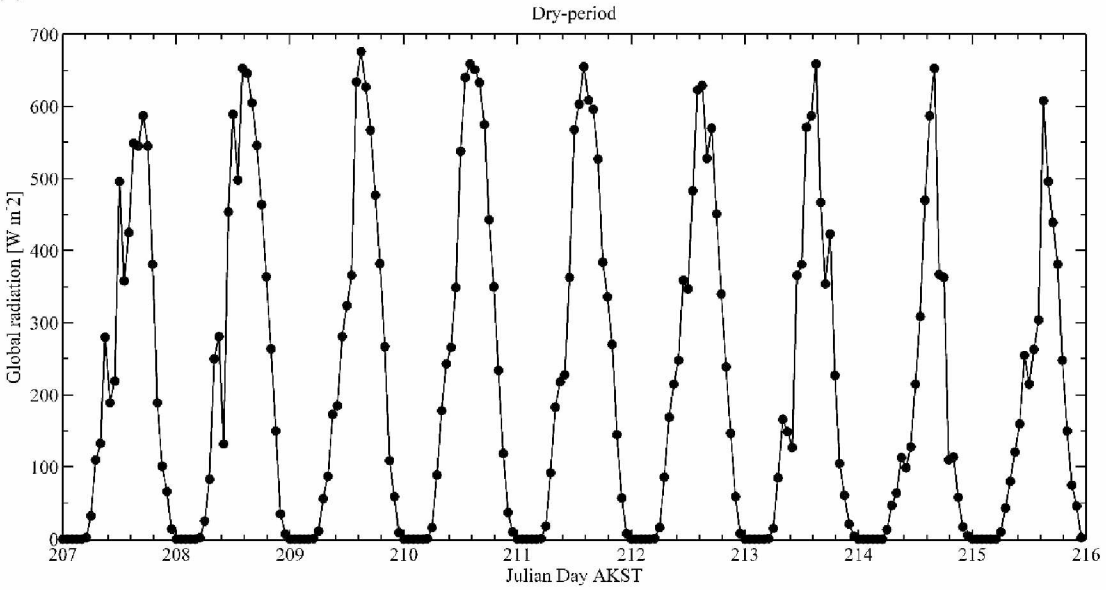

(b)

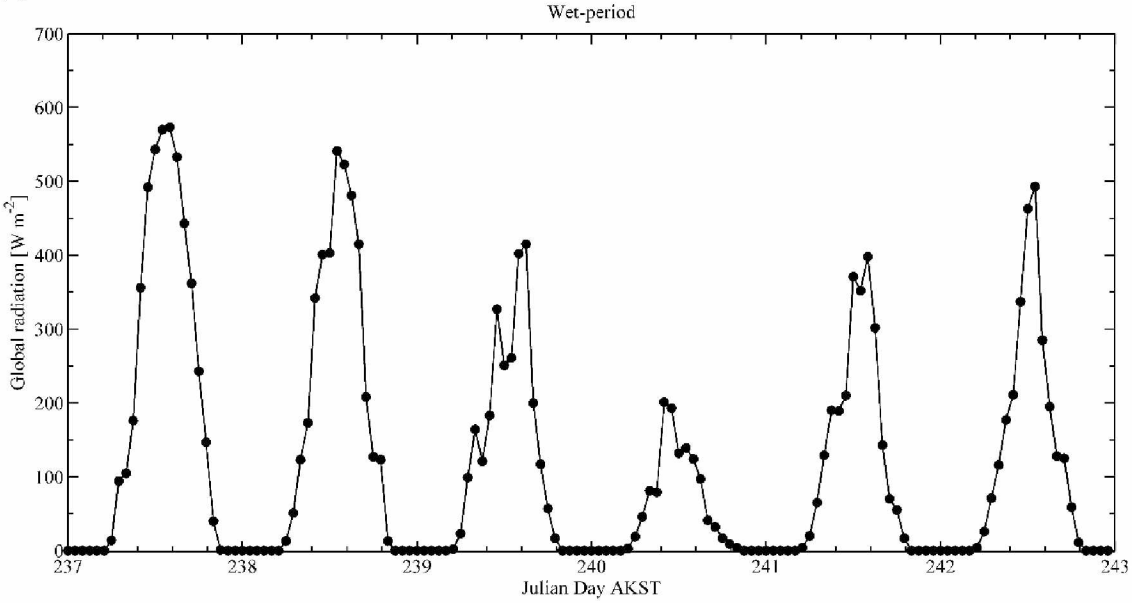

Figure 5-5 Solar radiation as a function of time during dry and wet periods. (a) Dry period from 26 July to 3 August 2013 (Julian day 207-215) and (b) Wet period from 25-30 August 2013 (Julian day 237-242)

(a)

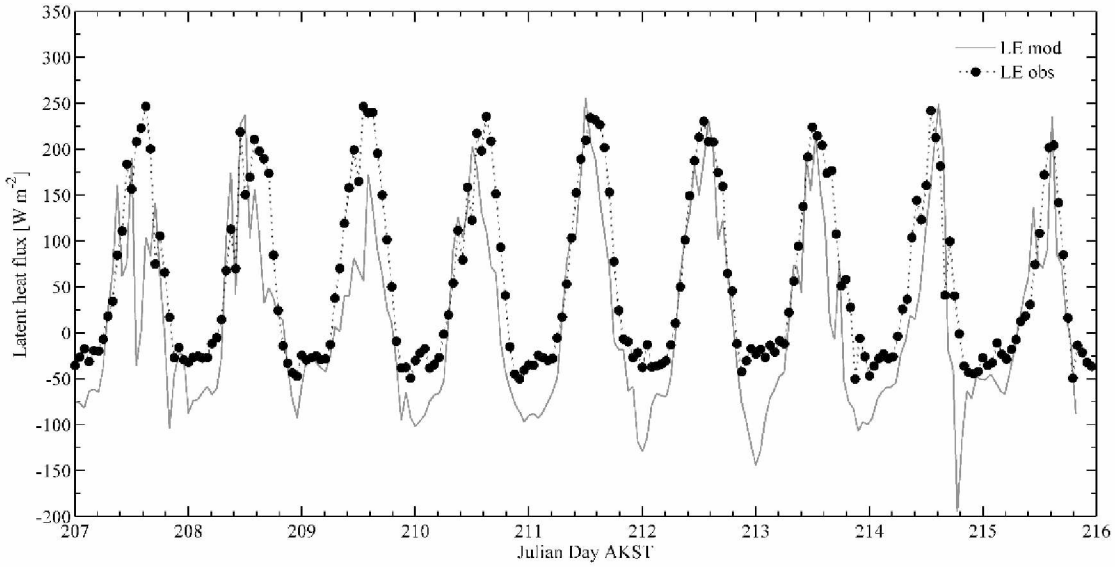

(b)

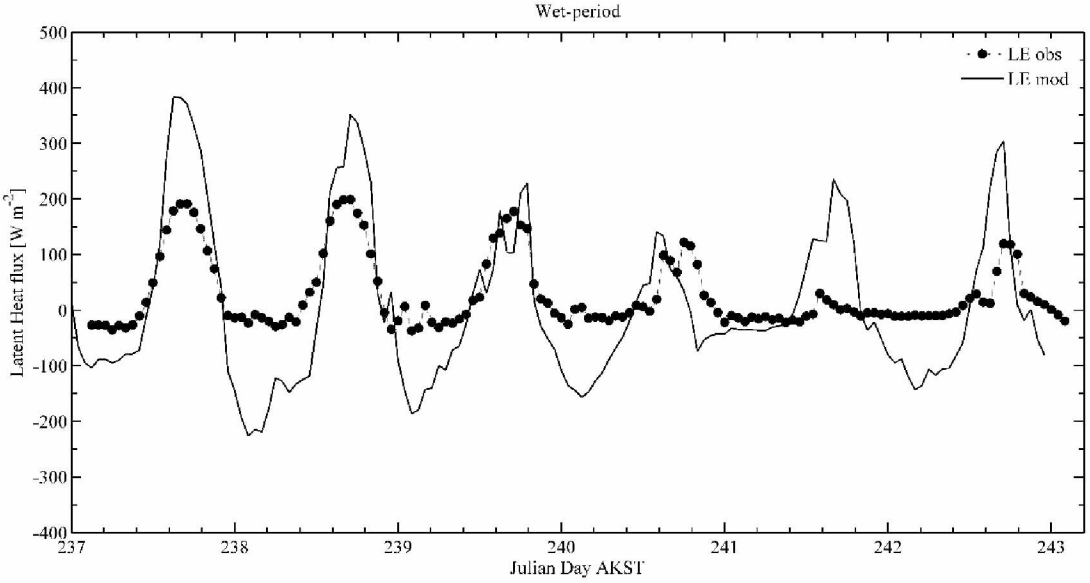

Figure 5-6 Evapotranspiration time series observed and modeled. (a) Dry period from 26 July to 3 August 2013 (Julian day 207-216), (b) wet period from 25-30 August 2013 (Julian day 237-242).

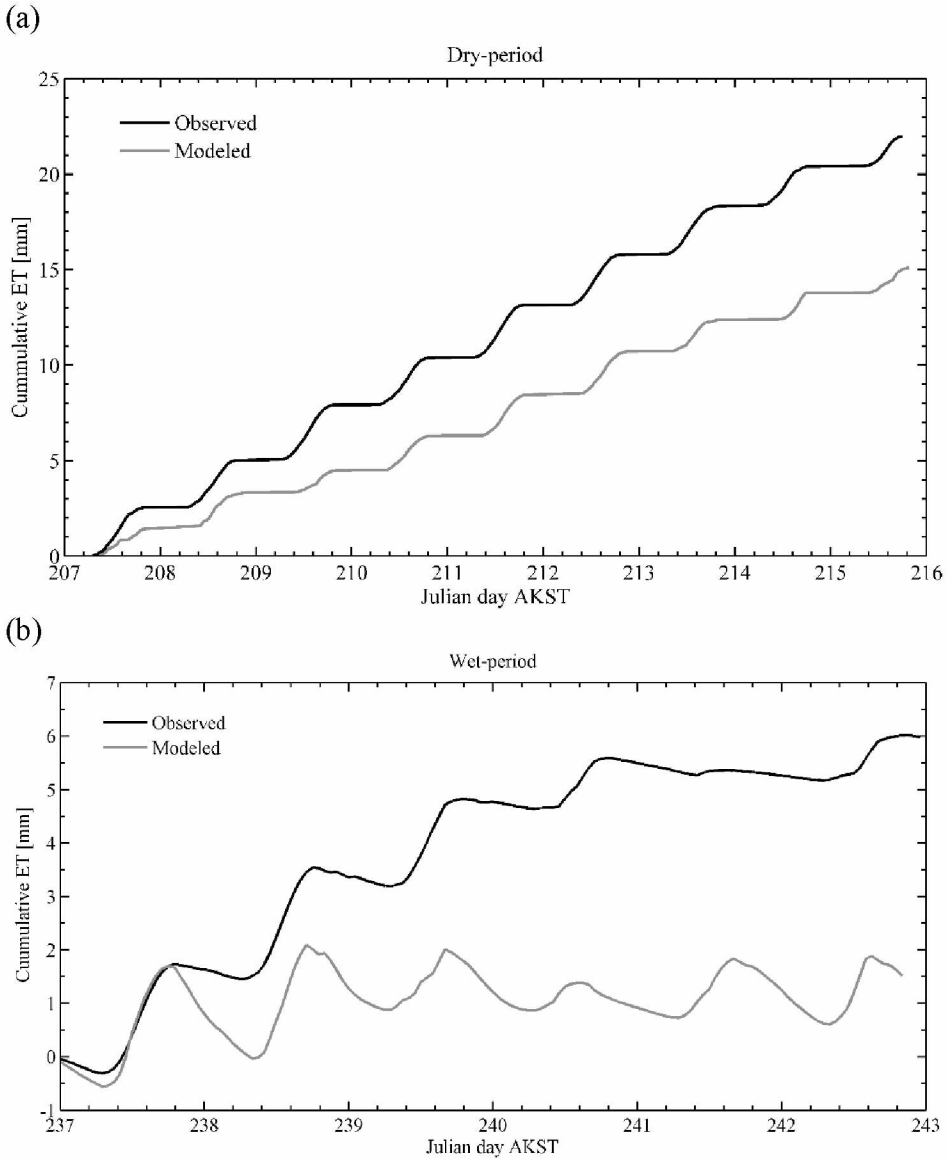

Figure 5-7 Simulated and observed cumulative evapotranspiration for the dry (a) and wet period (b).

(a)

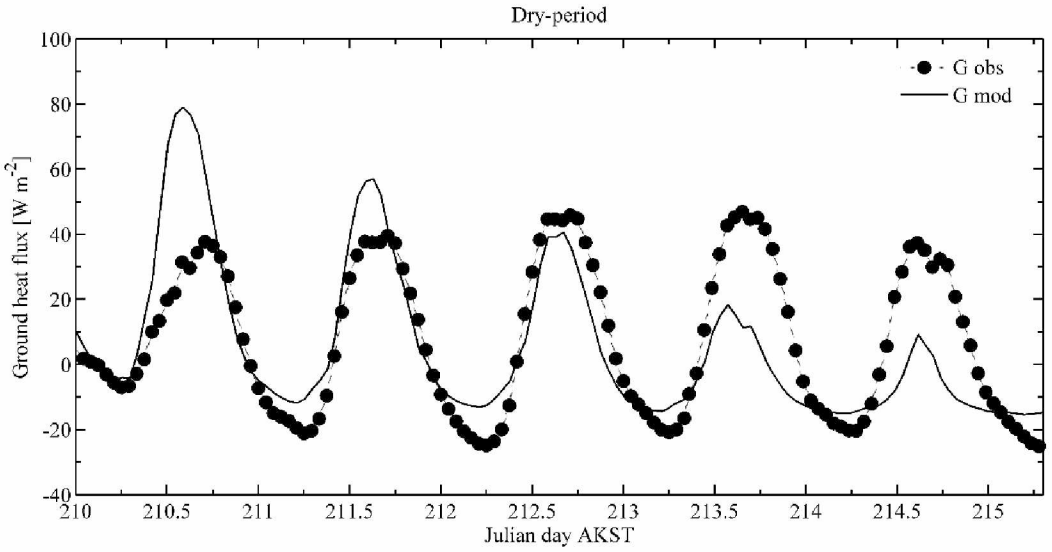

(b)

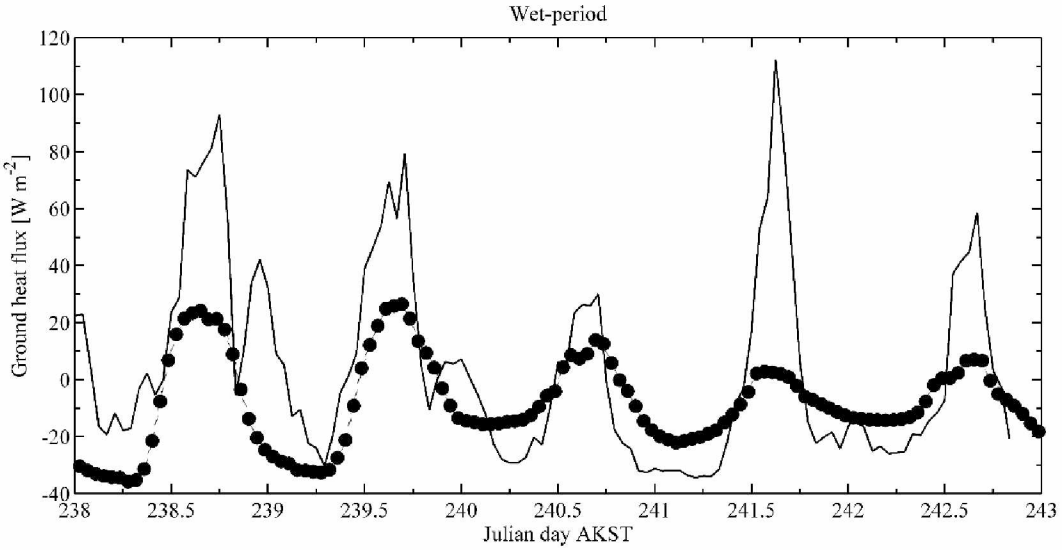

Figure 5-8 Time series of simulated and estimated ground heat flux. (a) Dry period from 29 July to 2 August 2013 (Julian day 210-214), (b) wet period from 26 -30 August 2013 (Julian day 238-242)

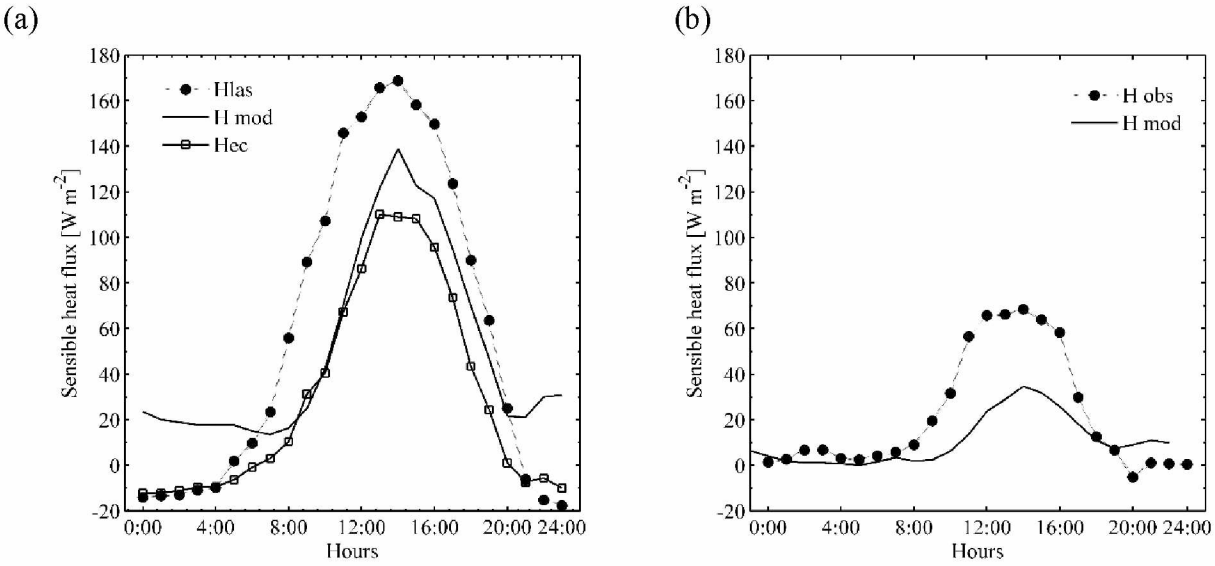

Figure 5-9 Time-series composite of hourly diurnal variation of sensible heat flux during (a) dry and (b) wet period.

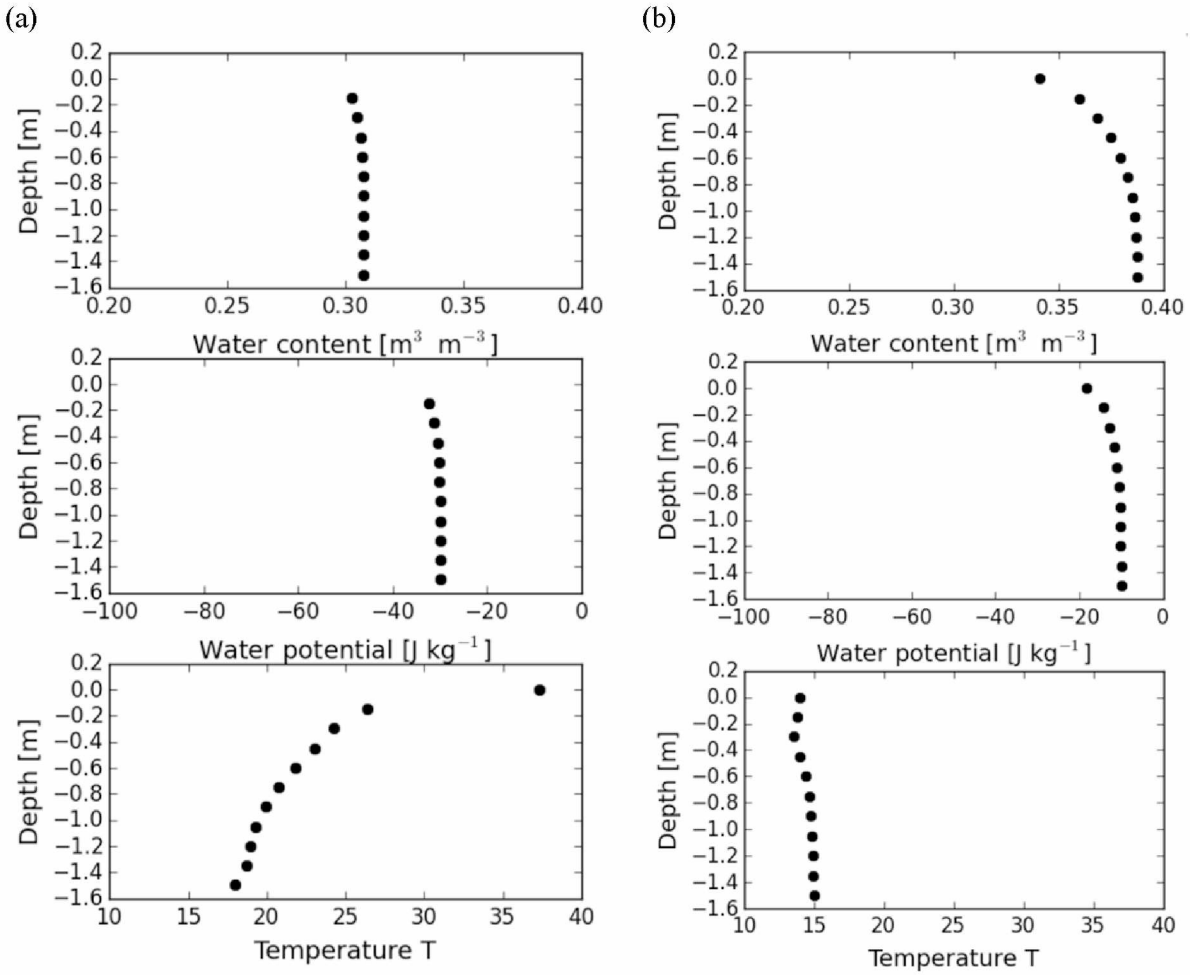

Figure 5-10 Coupled model simulation output for soil water content, soil water potential, and soil temperature as function of depth (from top to bottom) during dry (left panel) and wet (right panel) periods.

Tables

Table 5-1 Soil properties within lysimeter

Soil property	Value
Bulk density (g cm^{-3})	0.7
Air entry potential (J kg^{-1})	-1.5
Mass sand (kg kg^{-1})	0.66
Mass silt (kg kg^{-1})	0.29
Mass clay (kg kg^{-1})	0.05
Saturated moisture content; θ_s (m^3 m^{-3})	0.56
b value (-)	-3.1
K_s (kg s m^{-3})	$7.2x10^{-4}$

The mass of sand, silt, clay, and bulk density were obtained from in-situ measurements. The parameter for the hydraulic properties was obtained from Cambell and Shiozawa (1998), K_s is saturated hydraulic conductivity, θ_s is the saturated soil moisture content, and b is constant value.

Table 5-2 Initial setting for model simulation

Parameters	Dry period	Wet period
Number of days	9	6
Soil temperature (°C)	18.3	15.0
Soil water potential (J kg^{-1})	-30	-6
Albedo	0.20	0.15
Initial soil moisture (m^3 m^{-3})	0.28	0.30

Table 5-3 Main meteorological conditions, soil properties and surface characteristics during periods under study.

Parameters	**Dry**	**Wet**
Mean T_{air} (°C)	20.66±5.32	11.78±3.41
Mean T_s (°C)	18.96±3.2	16.64±1.51
T_s at the beginning period (°C)	18.3	15.2
Mean RH (%)	57.74±17.26	76.72±16.76
Mean VPD (kPa)	1.18±0.76	0.36±0.32
Mean u (m s^{-1})	2.36±1.07	1.68±0.82
Mean solar radiation (W m^{-2})	215.23±221.69	131.31±172.42
Mean soil moisture (m^3 m^{-3})	0.2098±0.0015[a]	0.2097±0.0035[a]
Precipitation (mm)	-	37.60

Soil temperate at 5 cm was considered in the study

[a] soil moisture from 5 cm depth

5.7 References

Balshi, M.S., McGuire, A.D., Zhuang, Q., Mellio, J., Kicklighter, D.W., Kasichke, E., Wirth, C., Flannigan, M., Harden, J., Clein, J.S., Burnside, T.J., McAllister, J., Kurz, W.A., Apps, M., and Shvidenko, A., 2007. The role of historical fire disturbance in the carbon dynamics of the pan-boreal region: a process-based analysis. Journal of Geophysical Research, 112:G02029.

Banimahd, S.A., and Zand-Parsa, S., 2013. Simulation of evaporation, coupled liquid water, water vapor and heat transport through the soil medium. Agricultural Water Management, 130: 168–177.

Bittelli, M., Ventura, F., Campbell, G.S., Snyder, R.L., Gallegati, F., and Pisa, P.R., 2008. Coupling of heat, water vapor, and liquid water fluxes to compute evaporation in bare soils, Journal of Hydrology, 362(3):191-205.

Cahill, A.T., and Parlange, M.B., 1998. On water vapor transport in field soils. Water Resources Research, 43: 731–739.

Chapin, F.S., III., McGuire, A.D., Randerson, J., Pielke, R., Baldocchi, D., Hobbie, S.E., Roulet, N., Eugster, W., Kasischke, E., Rastetter, E.B., Zimov, S.A., and Running, S.W., 2000. Arctic and boreal ecosystems of western North America as components of the climate system. Global Change Biology, 6 (Suppl. 1): 211–223.

Chapin, F.S., III, Sturm, M., Serreze, M.C., McFadden, J. P., Key, J.R., Lloyd, A.H., McGuire, A.D., Rupp, T. S., Lynch, A. H., Schimel, J. P., Beringer, J., Chapman, W. L., Epstein, H.E., Euskirchen, E.S., Hinzman, L.D., Jia, G., Ping, C.L., Tape, K.D., Thompson,

C.D.C., Walker, D.A., and Welker, J.M., 2005. Role of land surface changes in Arctic summer warming. Science, 310: 657–660.

Clein, J.S., Kwiatkowski, B.L., McGuire, A.D., Hobbie, J.E., Rastetter, E.B., Melillo, J.M., and Kicklighter, D.W., 2000. Modelling carbon responses of tundra ecosystems to historical and projected climate: A comparison of a plot- and global-scale ecosystem model to identify process-based uncertainties. Global Change Biology, 6: 141–159.

Davin, E.L., Seneviratne, S.I., Ciais, P., Olioso, A., and Wang, T., 2014. Preferential cooling of hot extremes from cropland albedo management. Proceedings of the National Academy of Sciences, 111(27): 9757–9761.

Euskirchen, E.S., McGuire, A.D., Kicklighter, D.W., Zhuang, Q., Clein, J.S., Dargaville, R., Dye, D.G., Kimball, J.S., McDonald, K.C., Mellilo, J.M., Romanovsky, V.E., and Smith, N.V., 2006. Importance of recent shifts in soil thermal dynamics on growing season length, productivity, and carbon sequestration in terrestrial high-latitude ecosystems. Glob Change Biology, 12: 731–750.

Hinzman, L.D., and Kane, D.L., 1992. Potential response of an Arctic watershed during a period of global warming. Journal of Geophysical Research, 97(D3): 2811–2820.

Hinzman, L.D., Bettez, N.D., Bolton, W.R., Chapin, F.S., Dyurgerov, M.B., Fastie, C.L., Griffith, B., Hollister, R.D., Hope, A., Huntington, H.P., Jensen, A.M., Jia, G.J., Jorgenson, T., Kane, D.L., Klein, D.R., Kofinas, G., Lynch, A.H., Lloyd, A.H., McGuire, A.D., Nelson, F.E., Oechel, W.C., Osterkamp, T.E., Racine, C.H., Romanovsky, V.E., Stone, R.S., Stow, D.A., Sturm, M., Tweedie, C.E ., Vourlitis, G.L., Walker, M.D., Walker, D.A., Webber, P.J., Welker, J.M., Winker, K.S., and Yoshikawa, K., 2005. Evidence and implications of recent climate change in northern Alaska and other arctic regions. Climatic Change, 72(3): 251–298.

Intergovernmental Panel on Climate Change, 2007. Climate Change 2007: The Physical Science Basis. Contribution of Working Group I to the Fourth Assessment Report of the Intergovernmental Panel on Climate Change. Solomon, S., Qin, D., Manning, M., Chen, Z., Marquis, M., Averyt, K.B., Tignor, M., and Miller, H.L. (Editors.). Cambridge University. Press, New York, pp. 996.

Jackson, R.D., 1973. Diurnal changes in soil water content during drying, in field soil water regime. In: Bruce, R.R. (Ed.), Field Soil Water Regime. 5. SSSA Special Publication, pp. 37–55.

Jorgenson, M. T., Romanovsky, V., Harden, J., Shur, Y., O'Donnell, J., Schuur, E. A. G., Kanevskiy, M., and Marchenko, S., 2010. Resilience and vulnerability of permafrost to climate change. Canadian Journal of Forest Research, 40: 1219–1236.

Lawrence, D.M., Slater, A.G., Romanovsky, V.E., and Nicolsky, D.J., 2008. Sensitivity of a model projection of near-surface permafrost degradation to soil column depth and representation of soil organic matter. Journal of Geophysical Research, 113: F02011.

McFadden, F.S., Chapin, F.S. III., and Hollinger, D.Y., 1998. Subgrid-scale variability in the surface energy balance of arctic tundra. Journal of Geophysical Research, 103(D22): 28947–28961.

McFadden, J. P., Eugster, W., and Chapin, F. S., III., 2003. A regional study of the controls on water vapor and CO_2 exchange in Arctic tundra. Ecology, 84: 2762–2776.

McGuire, A.D., Clein, J.S., Melillo, J.M., Kicklighter, D.W., Meier, R.A., Vorosmarty, C.J. and Serreze, M.C., 2000. Modelling carbon responses of tundra ecosystems to historical and projected climate: sensitivity of pan-Arctic carbon storage to temporal and spatial variation in climate. Global Change Biology, 6(Suppl. 1): 141–159.

Mack, M.C., Shuur, E.A.G., Bret-Harte, M.S., Shaver, G.R., and Chapin, F.S., III., 2004. Ecosystem carbon storage in Arctic tundra reduced by long-term nutrient fertilization. Nature, 431: 440–443.

Mölders, N., and Romanovsky, V.E., 2006. Long-term evaluation of the Hydro-Thermodynamic Soil-Vegetation Scheme's frozen ground/permafrost component using observations at Barrow. Alaska. Journal of Geophysical Research, 11: D04105.

Ortega-Farías, S., Antonioletti, R., and Olioso. A., 2000. Net radiation model evaluation at an hourly time step for Mediterranean conditions. Agronomie, 20: 157-164.

Ortega-Farías, S., Carrasco, M., Olioso, A., and Poblete, C., 2007. Latent heat flux over Cabernet Sauvignon vineyard using the Shuttleworth and Wallace model. Irrigation Science, 25:161-170.

Osterkamp, T. E., 2007. Characteristics of the recent warming of permafrost in Alaska. Journal of Geophysical Research, 112: F02S02.

Parlange, M.B., Cahill, A.T., Nielsen, D.R., Hopmans, J.W., and Wendroth, O., 1998. Review of heat and water movement in field soils. Soil & Tillage Research, 47: 5–10.

Romanovsky, V., Burgess, M., Smith, S., Yoshikawa, K., and Brown, J., 2002. Permafrost temperature records: indicators of climate change. EOS Transactions, 80: 589–594.

Serreze, M.C., Walsh, J.E., Chapin, F.S., Osterkamp, T., Dyurgerov, M., Romanovsky, V., Oechel,W.C., Morison, J., Zhang, T., and Barry, R.G., 2000. Observational evidence of recent change in the northern high-laltitude environment. Climatic Change, 46: 159–207.

Serreze, M.C., and Francis, J.A., 2006. The Arctic amplification debate. Climatic Change, 76: 241–264.

Sharratt, B.S., 1993. Water use, intercepted radiation and soil temperature of skip-row and equidistant-row barley. Agronomy Journal, 85: 686-691.

Sharratt, B.S., 1994. Observations and modeling of interactions between barley yield and evapotranspiration in the Subarctic. Agricultural Water Management, 25: 109–119.

Sharratt, B.S., 1998. Barley yield and evapotranspiration governed by tillage practices in interior Alaska. Soil Tillage Research, 46: 225–229.

Sitch, S., McGuire, A.D., Kimball, J.S., Gedney, N., Gamon, J., Engstrom, R.N., Wolf, A., Zhuang, Q., Clein, J.S., and McDonald, K.C., 2007. Assessing the carbon balance of circumpolar Arctic tundra with remote sensing and process based modeling approaches. Ecological Applications, 17: 213–234.

Smith, L.C., Sheng, Y., MacDonal, G.M., and Hinzman, L.D., 2005. Disappearing Arctic lakes, Science, 308: 1427.

Yoshikawa, K. and Hinzman, L.D., 2003. Shrinking thermokarst ponds and groundwater dynamics in discontinuous permafrost near Council, Alaska, Permafrost and Periglacial Processes, 14: 151–160.

Zhuang, Q., McGuire, A.D., Mellilo, J.M., Clein, J.S., Dargaville, R.J., Kicklighter, D.W., Myneni, R.B., Dong, J., Romanovsky, V.E., Harden, J., and Hobbie, J.E., 2003. Carbon cycling in extratropical terrestrial ecosystems of the northern hemisphere during the 20th century: a modeling analysis of the influences of soil thermal dynamics. Tellus, 55B: 751–776.

CHAPTER 6

Summary and conclusion

Climate impacts on agriculture or how agriculture responds to climate in northern latitudes are not yet fully understood, but certainly it will introduce new challenges for Alaskan agriculturists. Since agroecosystems are intensively managed, as farming practices increase with increase in agricultural lands, the role of agriculture as a climate driver at regional scale will undoubtedly change from what we currently know. On the other hand, the major land-surface modification introduced by agricultural practices to the climate of a region is among others the change in the surface energy budget which also is reflected in overturning of some of the turbulent fluxes and soil medium regimes. Additionally, besides changes in surface energetics, it may also extend to changes in the water cycle. The water cycle is inexorably linked with the cycles of carbon, nitrogen and other nutrients, with agriculture and the sustainability of ecosystems and human society. Understanding of surface energetics especially turbulent sensible and latent (evapotranspiration) heat fluxes is of utmost importance since any assessment of climate impacts and economic development and sustainability in the near future need to be based on accurate estimates of these basic quantities that are the response of the surface interface to the atmospheric and radiative forcing. Therefore in this study we have concentrated our efforts in delineating a series of experiments in high latitude agroecosystems to bring a better understanding for this land-surface modification in terms of energetic changes and to provide a springboard to new strategies to overcome the differences in flux measurements at landscape scale and local scale that is pertinent to the long term monitoring, evaluation and assessment for agriculture development in the State of Alaska. More precisely this study included the descriptions of the methodologies for evaluation of evapotranspiration (ET), the strategic

development of a field experiment to account for the facets needed to delineate future steps and the preparation of numerical simulations based on full account of physical processes involved in the transfer of moisture from the soil medium to the atmosphere. The research was conducted at the Fairbanks Experiment Farm in the UAF AFES which is representative of a large portion of the subarctic region and also considered to be representative of floodplain Interior Alaska growing conditions.

Specifically, results of this research showed that the ET cycles represent a large portion of surface energy balance accounting for approximately 64% of the net radiation. The ET ratio obtained by water mass balance related to the measured potential ET ranged from 0.59 to 0.66 for ET rates based on unvegetated and vegetated lysimeters respectively. Additionally, it was found that ET was responsible for removing 97% and 88% of the moisture added to the vegetated and non-vegetated lysimeters, respectively. In order to put the land-surface modification due to agricultural developments in perspective regarding challenges due to climate change, a systematic comparison was carried out across the Pan-Arctic region among the existing ecosystems at high latitudes. Surface energy fractioning was compared in agricultural lands, boreal forests, Arctic wetlands and tundra. Results indicated that the energy fraction in terms of ET/R_{net} of an agroecosystem exhibits similar characteristics to the tundra ecosystem in the Arctic and significantly contrasting to boreal forest ecosystems. In addition, the high ratio of ET/P in agroecosystem may indicate a major sensitivity to changes in soil moisture than other ecosystems across Pan-Arctic. When these results are placed in terms of land surface at the scales beyond the dimension of farms and including the interaction of the atmospheric flow with land patches defining specific ecosystem properties we found that agroecosystems can potentially drive small-scale circulation creating horizontal advective transport by landscape

differential heating which in turn can introduce a new imbalance term in the energy budget. Therefore, as the acreages of agricultural lands increase, unexpected changes in surface energetics and particularly overturning of ET rates and changes in soil moisture regime, especially soil moisture depletion, will be the more likely scenario for the future.

When focusing on fluxes on heterogeneous surfaces an important difference in the conductive ground heat flux was found between different surface patches (local scales) in the farmland. These differences can reach approximately 30 Wm^{-2}. This difference which is strictly at the soil level is manifested at the ground surface interface with the atmosphere forcing turbulent heat flux differences at local and large scales that has been verified to reach levels of 45 Wm^{-2} on average in the central part of the diurnal cycle. Based on the strategic deployment of multiple scale flux retrievals it was found that during observations of diurnal cycles of sensible heat fluxes based on eddy-covariance, only about 58% of sensible heat fluxes were captured when compared to measurements of the same variable at the farm scale by means of large aperture scintillometer. Evaluation of upscaling factors necessary to understand large scale observations from mesoscale models and satellite remote sensing information able to produce large scale regional and global assessment of the impacts of this land-use change have given ratios of 0.80 ± 0.68 under conditions of sensible heat flux $>50Wm^{-2}$ at both local and large scales. This means that despite considering only high fluxing level periods, still the local scale fluxes only sample on average about 80% of the large scale fluxes. On the other hand, based on traditional approaches using energy balance to derive ET from local scale measurements resulted in an overestimation of 37 W m^{-2} more than 27% of the diurnal cycle when compared to determinations of energy balance established at the farm scale. After scrutinizing the time series of radiative fluxes and extracting only periods where the atmospheric surface layer flow are

stationary it is concluded that the difference between closure at local compared to large scale is due to differences in the thermodynamic regimes in the soil sources of latent heat across the landscape. This physical process indicates the extent to which surface and sub-surface heterogeneities can introduce changes in the surface layer fluxing regime. A further evaluation of traditional methodologies for determining evapotranspiration was performed at different scales (local and farm/large scales) with the constraint to optimize the energy balance closure fraction. This study concludes that the Penman-Monteith methodology for evapotranspiration perform best under low turbulent flux regime and low mechanical turbulent intensity development reflected in low friction velocity, while; the Priestley-Taylor methodology was verified to increase the energy balance closure fraction under high fluxing regime and high friction velocity larger than 0.2 ms^{-1} and basically under all unstable conditions in the atmospheric surface layer. Finally this study also found that spatial variations of turbulent heat fluxes and ground heat fluxes impose an ultimate limitation in the accuracy by which modeling and satellite remote sensing retrievals of large scale area-average surface fluxes can be obtained under pure simple energy balance considerations whenever the pixel size or model scale represent larger areas than the surface patches characterizing the landscape heterogeneities. This knowledge will contribute to more sustainable crop and water management, and land use.

As a step forward in this thesis work, a fully coupled model to simulate the transport of liquid and vapor fluxes from the sub-medium to the land-surface interface was adapted to agricultural fields in high latitudes. The model was initialized with meteorological and radiation inputs and boundary conditions calculated based on introducing estimated soil properties and observed thermodynamic parameters. The evaluation of the model adaptation was strategized based on considering two specific well-differentiated scenarios: dry period where no

precipitation occurred and in which the meteorology was dominated by an anticyclone situation and a wet-period where precipitation did occur and cyclonic meteorological processes was the dominating case. The model reported fairly good agreement on radiation levels between observed and simulated time series while divergence in ET was found to be 0.7 mm d^{-1}. On the other hand the model poorly performed during the wet period since the model did not account for the scale of the meteorological forcing and also because some radiative properties of the surface might not be fully reproduced by the model as a function of precipitation (emissivity and albedo). Nevertheless, the period without precipitation is the more interesting because it is the period that the soil tends to lose water that directly affects plant development. There is a need for agriculturists or farm managers to know and address this problem of maintaining agroecosytem resilience or coping with these conditions for the goal of agriculture production.

The adaptation of this model to agroecosystems in high latitudes is considered a natural step as an application of the data-synthesis of the field experiments and also to prepare for future development in which data-fusion combining meteorological mesoscale models and satellite remote sensing information that would allow application of this model to larger areas and evaluate more in depth the impact of climate change and the possible feedbacks that can be expected by the changes in land-use.

Because only a few studies particularly onsite experimentation for the determination of ET in agroecosystems, have been done in Alaska, this study utilized multi-approaches to determine ET not only small scale measurement but also in the large scale of farmlands. Numerous techniques including manually-controlled instruments as well as automatic and complicated instruments were used to measure all parameters related to ET with a high quantity of data collection. This is a complete set of experimentation that has never happened in this

region before. Therefore, these results are significantly important to improve our knowledge about what we have known from the past as well as to gain better understanding of the ET's role in agroecosystems. Based on results from this study an hypothetical scenario can be formulated in terms of the changes in land use from natural state and its consequences in future climate scenarios. If boreal forests were to be transformed to agricultural lands in high latitudes significant changes in the energetics of the surface-atmosphere interface may instigate the overturning of ET against the rest of the fluxes. This change will increase the severity of droughts and the need for more water to sustain agricultural fields. Due to the significant rates and changes on the surface energy regime that have been demonstrated in this research it is suggested that this new scenario be considered and incorporated in future assessments of climate change and impacts as one of the potential drivers at the surface-atmospheric interface in terms of anthropogenic climate interactions. These findings also raise potentially serious consequences for agriculture sustainability if potential consequences of land-surface changes are not adequately considered by policy makers for planning and strategizing the future.

A limitation in the present study is represented by the lack of inclusion of specific crop-water requirement which is an important piece of information to optimize water resources management and planning and therefore improve water-use efficiency in agroecosystems. This is a further step that would help improving water supply and demand for productivity and sustainability in any further irrigation scheme, ecosystem management for mitigation as well as adaption to global hydrological change.

Warming of climate will likely be positive for agriculture yields in high latitudes but may also bring an increase in risk and unpredictability for farmers – from shifts in rainfall patterns, and from the growing incidence of extreme weather events since Alaska is highly susceptible and

sensitive to these changes. The positive effect of climate warming in terms of lengthening growing season for crops will mean better food security, however, at the same time will require more water and need for more nutrients to sustain agriculture activities. Water stress may become an important factor in many areas, and irrigation may be necessary to produce good yields. Then, building resilience by reducing exposure and sensitivity of the system and increasing adaptive capacity are necessary steps for farmers to address and cope with these changes. For example, selecting crops that require less water (drought-resistance crops), cover cropping, proper tillage methods, and use of appropriate irrigation techniques that save more water, need to be considered. Clear cutting boreal forests for agricultural development in Alaska might be another issue as we can see from the results of energy partitioning in agroecosystems in this study compared to that in boreal forests. There are huge uncertainties in the way climate change will directly and indirectly impact agricultural and food systems, and related vulnerabilities including the sustainability of agriculture.

This research has initiated an international collaboration to adapt the coupled model to estimate soil dynamics and surface atmospheric fluxes based on meteorological, radiation and soil properties. This will help understand more about how this modeling work can be applied to different environmental conditions and what main parameters need to be included for landscape extension. This will improve our capabilities to predict ET at regional scales and therefore account for future climate regimes.

As a final perspective, this study supported by several institutions at the University of Alaska Fairbanks (International Arctic Research Center, Geophysical Institute, Institute of Northern Engineering and the School of Natural Resources and Extension) as well as Suratthani Rajabhat University in Thailand, has provided training and expertise in agriculture,

micrometeorology and hydrology research in an international university with a long standing tradition to form and prepare researchers for future faculty positions on agroecosystems, agricultural meteorology and/or other fields of research in their home countries.

APPENDIX-A

Appendix A-1. Gravimetric soil moisture content in the lysimeter before growing and after harvesting the lettuce during summer 2012

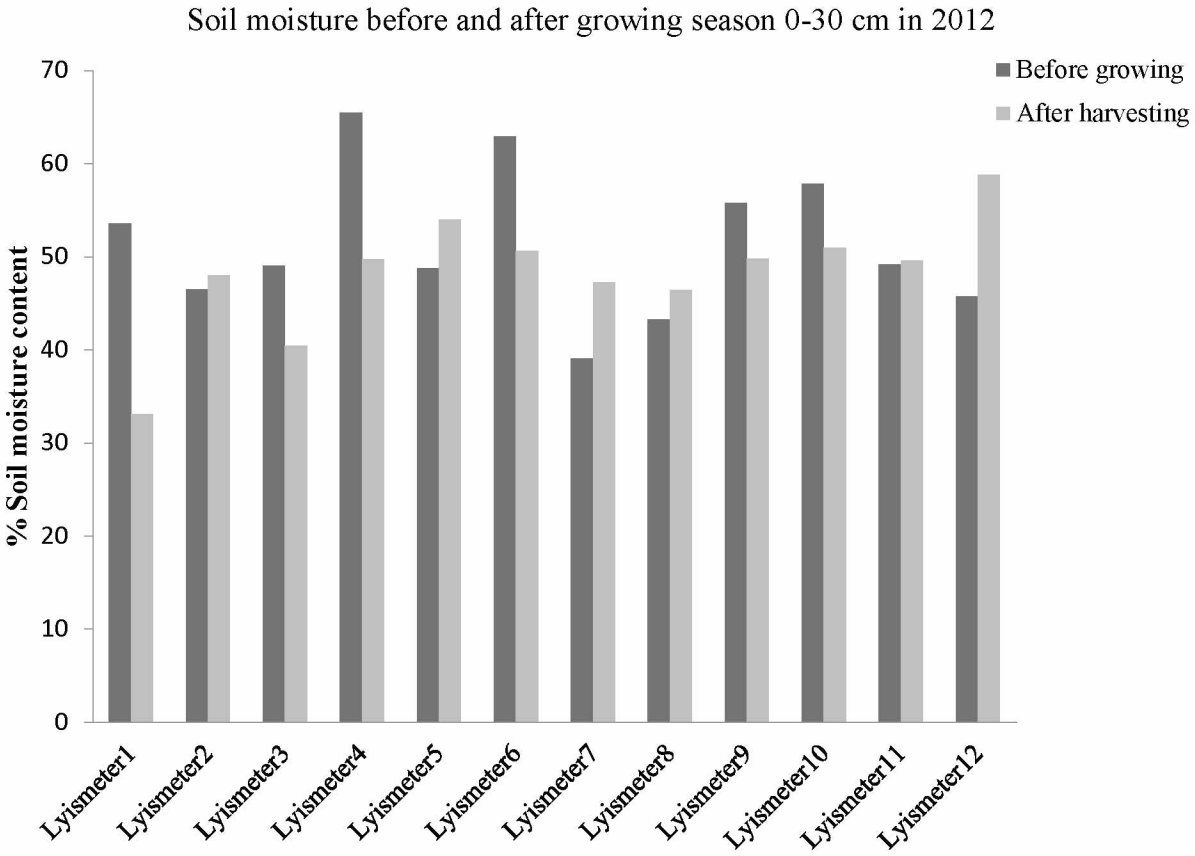

Appendix A-2. Gravimetric soil moisture content at different location in the farmland summer 2011

Study site	Date	Mean of (%) Soil moisture	Standard Error
Barley	06/26/11	24.06	1.31
	07/13/11	18.91	1.75
	07/28/11	17.75	1.99
	08/08/11	19.71	1.97
	08/18/11	21.01	1.41
Bromegrass	06/26/11	28.90	1.29
	07/13/11	20.27	1.96
	07/28/11	21.12	2.63
	08/08/11	23.04	2.45
	08/18/11	21.99	2.28
Fallow (Bare)	06/26/11	22.44	0.59
	07/13/11	19.27	1.02
	07/28/11	20.94	0.55
	08/08/11	22.75	0.59
	08/18/11	19.99	0.66
Slope area	06/26/11	28.85	2.63
	07/13/11	19.38	2.61
	07/28/11	18.16	3.05
	08/08/11	20.40	2.77
	08/18/11	18.12	4.09
Wet land[a]	06/26/11	40.95	10.73
	07/13/11	37.13	8.46
	07/28/11	41.62	12.73
	08/08/11	43.01	12.37
	08/18/11	35.91	7.81

[a] Soil wet almost throughout the summer season

Appendix A-3. Leaf area index (LAI) over bromegrass and barley field during the summer 2011 and 2012

Date	Brome	Barley
LAI summer 2011		
6/7/2011	0.6	0.9
6/14/2011	0.8	1.65
6/21/2011	0.8	1.9
6/28/2011	0.5	2.55
7/5/2011	0.55	3.25
7/12/2011	0.8	3.55
19-Jul	NA	NA
7/26/2011	1.8	1.9
8/2/2011	1.6	1.6
8/9/2011	1.7	1.7
8/16/2011	0.25	0.35
LAI 2012		
6/15/2012	1.45	1.4
6/22/2012	0.1	2.6
6/29/2012	0.5	3.1
7/6/2012	0.4	4.25
7/13/2012	0.75	2.9
7/20/2012	NA	NA
7/27/2012	0.75	2.25
8/3/2012	1.6	2.75
8/10/2012	1.2	2
8/17/2012	NA	NA
8/24/2012	0.35	0.2

APPENDIX-B

Coupled numerical model overview

The model description follows mainly Bittelli et al. (2008) where a one dimensional model of coupled heat, water and vapor flow has been introduced and validated with an evaporation experiment from bare soil under real weather conditions in California.

Transport equations

Heat transport

Thermal energy in the soil can be partitioned into sensible heat, latent heat and the convective part by flowing liquid water (Kroener et al. 2014). Sensible heat flow is driven by a vertical gradient (considered here) in temperature and is proportional to the soil thermal conductivity. Latent heat flow is the thermal energy carried by water vapor which is proportional to the sum of latent heat of vaporization and thermal energy of liquid water. Thermal energy carried by liquid water is proportional to water flow and thermal energy of water. Therefore the total soil heat flux density q_h is described as

$$q_h = -\lambda \nabla T + (L + TC_w)q_v + TC_w q_w \qquad \text{Eq. (1)}$$

where q_h is the heat flux density (W m^{-2}), λ is the thermal conductivity (W m^{-1} K^{-1}), T is soil temperature (K), L is the latent heat of vaporization ($\approx 2.45 \times 10^6$ J kg^{-1}), C_w is volumetric heat capacity of water (J m^{-3} K^{-1}), q_v is vapor flow (kg m^{-2} s^{-1}) and q_w is water flow.

Water transport

Water transport in the soil surface zone can be described using Richards' equation (Philip and de Vries 1957; de Vries 1963), where water flow q_w is driven by a gradient in water

potential (sum of matric potential ψ and gravitational potential gz) and is proportional to the hydraulic conductivity K:

$$\frac{\partial \theta}{\partial t} = q_w = -K\nabla(\psi + \mathrm{gz}) \qquad \text{Eq. (2)}$$

where θ ($m^3\ m^{-3}$) is the volumetric moisture content, ψ (J kg^{-1}) is the matric potential, K (kg s m^{-3}) is hydraulic conductivity, t is the time (s), g is the acceleration due to gravity, z is vertical distances (positive upwards). K depends highly non-linear way on ψ.

Vapor transport

According to Fick's law, the isothermal vertical water vapor flow ($q_{v,i}$) is driven by a gradient in water vapor concentration as follows:

$$q_{v,i} = -D_v \frac{dc_v}{dz} \qquad \text{Eq. (3)}$$

where $q_{v,i}$ is the vapor flux density (kg m^{-2} s^{-1}), D_v is vapor diffusivity in soil ($m^2\ m^{-1}$), c_v is the soil vapor concentration (g m^{-3}). Vapor concentration is obtained by:

$$c_v = hc_v' \qquad \text{Eq. (4)}$$

where h is fractional relative humidity and c_v' saturated vapor concentration. If the soil is in isothermal condition, the variation of vapor concentration with depth can be defined as:

$$\frac{dc_v}{dz} = c_v' \frac{dh}{dz} \qquad \text{Eq. (5)}$$

The h was calculated from the pressure head using thermodynamics relationship between liquid water and water vapor in soil pores as:

$$h = exp\left(\frac{M_w \psi}{RT}\right) \qquad \text{Eq. (6)}$$

where M_w is the molecular weight of water (0.018 kg mol^{-1}), ψ is soil water potential (J kg^{-1}), R is the gas constant (8.31 J mol^{-1} K^{-1}) and T is temperature (Kelvin). Substituting these expression into Eq. (3), vapor flow can be written as:

$$q_{v,i} = -k_v \frac{d\psi}{dz} \quad \text{Eq. (7)}$$

and

$$k_v = \frac{D_v c_v' h_r M_w}{RT} \quad \text{Eq. (8)}$$

where k_v is the water vapor conductivity. This description only accounts for matric potential gradients. The vapor concentration gradient is the driving force and it can be separated into thermal and water potential driven flow. A more general analysis of soil evaporation must include the effect of temperature gradients on water transport. Therefore, the total water vapor flow (q_v) is described as sum of an isothermal flux component ($q_{v,i}$), and a temperature driven flux component($q_{v,T}$) as described by Bittelli et al. (2008).

$$q_v = q_{v,i} + q_{v,T} = -D_v c_v' \nabla h - D_v hs \nabla T \quad \text{Eq. (9)}$$

where q_v is non-isothermal vapor flow, $q_{v,i}$ is isothermal vapor flow (equivalent to Eq.(3)) and $q_{v,T}$ is the temperature driven vapor flow, which can be given as:

$$q_{v,T} = -D_v hs \frac{dT}{dz} \quad \text{Eq. (10)}$$

where s is the slope of saturation vapor concentration function is given by:

$$s = \Delta M_w V_m / P \quad \text{Eq. (11)}$$

where Δ is the slope of the saturation vapor pressure curve at temperature T , V_m is the molar volume of air (41.4 mol m^3, at sea level and 20 °C), and P (kPa) is the barometric pressure.

Multiplication by $M_w V_m$ is necessary to convert (mol/mol) to (kg m^{-3}). For the vapor pressure curve, the equation of Buck (1981) has been applied at temperature T ,

$$e_s(T) = 0.611 exp\left(\frac{17.27T}{T + 237.3}\right) \quad \text{Eq. (12)}$$

where T is temperature in (°C). The slope of the saturation vapor pressure (kPa K^{-1}) over liquid water at temperature T is given by:

$$\Delta = \frac{4098 e_s}{(T + 237.3)^2} \quad \text{Eq. (13)}$$

Saturation vapor concentration is: $c_v' = e_s M_w/(RT)$.

Soil parameters

Thermal properties

Soil thermal conductivity λ in Eq. (1) is a function of the geometrical arrangement of the phases (air, water and mineral) of the soil material which strongly depends on both mineral as well as water content and on the soil temperature. Therefore an estimation of the thermal conductivity of soils with varying moisture content and temperature is necessary to account for soil moisture changes. Model incorporates the parameterization proposed by Campbell et al. (1988) which is based on the theory of de Vries (1963). They fitted the model to thermal conductivity measurements of soil samples differing in texture, bulk density, water content and temperature. In their model, the soil is considered as a mixture of water, gas and solid material and each element has a thermal conductivity, λ_w (water), λ_a (air), λ_m (mineral), and k_w, k_a, k_m are the weighted factors. Computation of the weighting factors is described in Campbell et al. (1988).

This relationship is:

$$\lambda = \frac{k_w \theta \lambda_w + k_a x_a \lambda_a + k_m x_m \lambda_m}{k_w \theta + k_a x_a + k_m x_m} \quad \text{Eq. (14)}$$

where θ, x_a and x_m are volumetric fraction of water, air, and solid material, respectively. More information about how to calculate weighting factors is described by de Vries (1963).

Soil hydraulic properties

Campbell's model (Campbell and Shiozawa, 1992) was used to predict the soil hydraulic properties and water potential:

$$\theta = \begin{cases} \theta_s \left(\frac{\psi_e}{\psi}\right)^{-1/b} & if\ (\psi < \psi_e) \\ \theta_s & if\ (\psi \geq \psi_e) \end{cases} \quad \text{Eq. (15)}$$

where ψ (J kg^{-1}) is the matric potential, ψ_e (J kg^{-1}) is the air entry potential, θ (m^3 m^{-3}) is the volumetric moisture content, θ_s is the saturated volumetric moisture content, b is shape parameter related to pore size distribution of the porous medium. The hydraulic conductivity function is written as:

$$K = \begin{cases} K_s \left(\frac{\psi_e}{\psi}\right)^{2+3/b} & if\ (\psi < \psi_e) \\ K_s & if\ (\psi \geq \psi_e) \end{cases} \quad \text{Eq. (16)}$$

where K (kg s m^{-3}) unsaturated hydraulic conductivity and K_s (kg s m^{-3}) is saturated hydraulic conductivity. Saturated water content θ_s is equal to the porosity (Φ) and is related to bulk density (ρ_b) and average density of soil minerals(ρ_m):

$$\Phi = \frac{\rho_b}{\rho_m} \quad \text{Eq. (17)}$$

Direct measurement of the soil moisture characteristics can be obtained from the laboratory and field measurement but the hydraulic conductivity was derived using pedotransfer functions (Cambell and Shiozawa, 1992) and measurement soil texture (% of sand, silt and clay) and bulk density.

Vapor parameters

The vapor diffusivity D_v in soil depends on the air filled volume fraction and is expressed as:

$$D_v = D_0(T,P)\varepsilon(x_a) \quad \text{Eq. (18)}$$

where ε is a soil parameter that depends on the air filled volume fraction x_a on soil geometrical properties. Under saturated soil condition, $\varepsilon(x_a)$ goes to zero and no vapor flows. The air filled porosity is computed by the difference between moisture content at saturation (θ_s) and actual moisture content. The parameter $\varepsilon(x_a)$ is given by,

$$\varepsilon(x_a) = \beta(x_a)^m \quad \text{Eq. (19)}$$

where β and m are empirical parameters that depends on the shape of the soil particles. With β = 0.9 and m =2.3 were used in this simulation (Penman 1940).

The binary diffusion coefficient for water vapor in the air which depend on pressure and temperature, is given as:

$$D_0(T,P) = D_0(273.15K, 101.3\ kPa)\left(\frac{T}{273.15}\right)^{1.75}\left(\frac{101.3}{P}\right) \quad \text{Eq. (20)}$$

where standard conditions $D_0(T273.15K, 101.3\ kPa) = 2.12 \times 10^{-5}$ ($m^2\ m^{-1}$) for water vapor in the air phase. The diffusivity of air in liquid water is much smaller (about 2×10^{-9} $m^2\ m^{-1}$) and the air exchange in the soils without a continuous gas phase is negligible (Campbell 1985).

Boundary conditions for water vapor transport

The flow of energy and water across the interface between ground surface and atmosphere in the model were determined by using the meteorological (air temperature, relative humidity, precipitation, wind speed, wind direction, and global radiation) and soil data (e.g. saturated moisture content, thermal conductivity, saturated conductivity).

Water

Water flow in the upper surface is given by precipitation but if the system has the irrigation it has to be added to the precipitation.

Vapor

Vapor flow is given by evaporation (E) with the rate of E is based on the vapor transport formula, driven by the vapor concentration gradient between the air and the soil surface:

$$E = \frac{1}{r_v + r_s}\left(\frac{c_{va} - c_{vs}}{z_{ref} - z_0}\right) \quad \text{Eq. (21)}$$

where E is the evaporation rate, r_v is aerodynamic resistance for water vapor transfer (s m^{-1}), r_s is the soil surface resisitance for water vapor transfer (s m^{-1}), c_{va} is the atmosphere vapor concentration at height z_{ref} (mol mol^{-1}), c_{vs} is the vapor concentration of the soil surface (z_0) (mol mol^{-1}). The surface is at height z_0= 0 m.

The soil surface resistance can be calculated as follow (Griend and Owe, 1994):

$$r_s = 10sm^{-1}exp\big(0.3563(\theta_{min} - \theta_{top})\big) \quad \text{Eq. (22)}$$

where $\theta_{min} = 15\%$ is an empirical parameter and θ_{top} [%] is the water content in the top 1 cm layer.

Aerodynamic resistance r_v depends on wind speed, level of turbulence, soil surface roughness and thermal stratification of the boundary layer. For the calculation of r_v we will follow the description of Campbell (1985).

$$r_v = \frac{1}{u^* k}\left[ln\left(\frac{z_{ref} - d_0 + z_H}{z_H}\right) + \Phi_H\right] \quad \text{Eq. (23)}$$

where u^* is friction velocity, k von Karman's constant, z_{ref} the height where air temperature is measured, d_0 is the zero plane displacement for the surface, z_H is called surface roughness parameter for heat and Φ_H is a stability correction factor for heat.

Friction velocity can be given by:

$$u^* = uk\left[ln\left(\frac{z_{ref} - d_0 + z_M}{z_M}\right) + \Phi_M\right]^{-1} \quad \text{Eq. (24)}$$

where z_M is called surface roughness parameter for momentum and Φ_M is a stability correction factor for momentum. A typical value of soil surface roughness is 0.01 m, which was used here to calculating r_v (Campbell and Norman, 1998). In addition, the parameters for typical crop surfaces are:

$$d_0 = 0.77h_c \quad \text{Eq. (25)}$$

$$z_M = 0.13h_c \quad \text{Eq. (26)}$$

$$z_H = 0.2z_M \quad \text{Eq. (27)}$$

where h_c is the height of the surface elements, in the simulations of bare soil this is around: $h_c =$ 0.01 m.

The atmospheric stability correction factor depends on the difference between air and soil temperature: When soil temperature is colder than air, the atmosphere is stable. But when soil is

warmer, warmed-up air moves upwards and leads to turbulence. Therefore the stability correction factor depends on a stability parameter in this case the Obukhov number ζ was consider to parameterize the non-neutral condition:

$$\zeta = \frac{-kz_{ref}gH}{c_h T_k u^{*3}} \qquad \text{Eq. (28)}$$

where H is the sensible heat flux in the boundary layer. $H < 0$ means that sensible heat flux is negative, hence soil temperature is lower than air temperature and the atmosphere is in stable conditions. The stability correction factor can now be calculated:

$$\Phi_H = \begin{cases} 4.7\zeta & if\ H < 0 \\ -2ln\left[\frac{1}{2}\left(1 + [1 - 16\zeta]^{\frac{1}{2}}\right)\right] & if H \geq 0 \end{cases} \qquad \text{Eq. (29)}$$

And

$$\Phi_M = \begin{cases} \Phi_H & if\ H < 0 \\ -0.6\Phi_H & if H \geq 0 \end{cases} \qquad \text{Eq. (30)}$$

The stability parameter ζ depends on the sensible heat flow H at the upper boundary, H, however, depends in turn on ζ. Therefore there is no way to know a priori in what stability condition the atmosphere is if fluxes cannot be calculated. Therefore ζ and the corresponding heat flow H have been calculated in three numerical loops: 1) we consider $\Phi_H = 0$ and $\Phi_M = 0$ ad from there fluxes an momentum can be calculated; 2) using those values of heat and momentum a value of ζ can be calculated which then enters in the set of non-neutral corrections Eq.(29, 30) which then allow for actualization of heat and momentum; 3) last loop is just to confirm that a new value of ζ is calculated and therefore new values Φ_H, Φ_M, ζ and H are therefore updated.

Energy

Thermal energy flow at the surface boundary consists of sensible heat, latent heat, a convective part transported by liquid water during precipitation and radiative energy flow:

$$q_h = H + LE + TC_w Pr + R_{net} \quad \text{Eq. (31)}$$

where positive q_h means that net thermal energy is moving from the soil surface upwards. H is sensible heat flow, E evaporation rate, L latent heat of vaporization, T air temperature, Pr precipitation rate and R_{net} is net radiation from the soil surface upwards, that means radiation from sun and atmosphere contribute negatively and radiation from the soil is positive.

Sensible heat flow can be given as:

$$H = \frac{C_h(T_s - T_a)}{r_h} \quad \text{Eq. (32)}$$

where $r_h = r_v$ is aerodynamic resistance for heat which is equal to aerodynamic resistance for vapor. T_a is temperature of the air at reference height z_{ref} and T_s the soil surface temperature.

The radiative energy exchange at the soil surface is composed of the absorbed short wave radiation from the sun (R_{sun}), the long wave radiation from the atmosphere (R_{atm}) and the long wave radiation emitted by the soil surface (R_{soil}).

The energy emitted from the soil is given by Stephan Boltzmann's law:

$$R_{soil} = \varepsilon_s \sigma T_{K,soil}^4 \quad \text{Eq. (33)}$$

where ε_s is the soil emissivity, σ Stephan Boltzmann's constant, and $T_{K,soil}^4$the soil surface temperature in [K].

The absorbed short wave radiation is measured incoming short wave radiation R_{meas} weighted by the absorptivity (1-albedo):

$$R_{sun} = (1 - albedo)R_{meas} \quad \text{Eq. (34)}$$

An average albedo value for agriculture field was about 0.15 during growing season (Sharrat 1993).

Long-wave radiation from the atmosphere is:

$$R_{atm} = \varepsilon_{ac}\sigma T_{K,air}^4 \quad \text{Eq. (35)}$$

where $T_{K,air}^4$ is the temperature of the air and ε_{ac} is the atmospheric emissivity, that depends on vapor concentration of the air c_{va}, and fractional cloud cover c_1:

$$\varepsilon_{ac} = (1 - 0.84c_1)0.58c_{va}^{\frac{1}{7}} + 0.84c_1 \quad \text{Eq. (36)}$$

The fractional cloud cover is related to the transmissivity Tt of the atmosphere: $c_1 = 2.33 - 3.33Tt$ (valid for $0 < c_1 < 1$). The transmissivity of the air is a daily value calculated by comparing the measured daily incoming short-wave radiation $R_{meas,day}$ to the potential incoming short wave radiation$R_{pot,day}$:

$$T_t = \frac{R_{meas,day}}{R_{pot,day}} \quad \text{Eq. (37)}$$

The potential incoming short wave radiation during one day depends on latitude f, solar declination d and half daylength h_s (in rad):

$$R_{pot,day} = 117.5\ MJ\ m^{-2}[h_s\ sin\emptyset\ sin\delta + cos\emptyset\ cos\delta\ sin\ h_s]/\pi \quad \text{Eq. (38)}$$

where half day length is given by $cos\delta h_s = -tan\emptyset/tan\delta$ and the solar declination δ depends on the day of the year, d:

$$sin\delta = 0.399 \sin[4.87 + 0.0172d + 0.0335\sin(6.22 + 0.0172d)] \quad \text{Eq. (39)}$$

The total radiative energy flux is written as:

$$R_{sun} = R_{soil} - R_{sun} - R_{atm} \quad \text{Eq. (40)}$$

Soil surface temperature

A reliable value of soil surface temperature (Ts) is needed to compute the soil surface relative humidity (h) from soil surface water potential (Eq. (6)) when using Eq. (21). In the Eq. (6) shows that for the same value of soil water potential, at a higher soil surface temperature there will be a higher soil surface relative humidity (the water potential has a negative value in the Eq. (6)), while at the same atmospheric vapor pressure, there will be a smaller vapor pressure gradient between the atmosphere and the soil surface, affecting evaporation rates. For instance, under the same soil water potential conditions, if soil surface temperature is underestimated, evaporation rates are overestimated. Soil surface temperature has also been used as a proxy to compute soil evaporation by using the temperature differential between the soil surface temperature under a dry and a wet soil conditions, instead of the sensible heat flux (Guo Yu et al., 1999). Using this method the author proposed an evaporation transfer coefficient that replaced the aerodynamic resistance term. However, in their work the soil surface resistance term is not considered and evaporation is overestimated. Using a numerical solution of heat flow allow to obtain reliable values of soil surface temperature, by using thin (1 mm) computational layers at the top. In this work hourly values of air temperature were available, which were used as upper boundary condition for soil temperature, when daily maximum and minimum temperature only are available, it is possible to use trigonometric functions with a period of 24 h (Campbell, 1985).

Numerical implementation

The scheme indicating the coupling of driving terms (temperature, liquid water and vapor concentration) and the resistive and conductive terms was depicted in Figure 1. In the model, surface boundary conditions were set using the measured atmospheric boundary conditions (i.e., air temperature, vapor pressure and radiant energy). For the computation of liquid water flow, specified soil water potential boundary conditions were set during an irrigation period, by setting the upper computational layer at a water potential $\psi_m = \psi_e$, as specified in Eq. (15). After the end of the irrigation the upper boundary condition was variable water potential. The computed water potentials and temperatures of the soil surface layers were used to calculate the relative humidity (therefore the vapor pressure) used for vapor flow calculations (Eq. (6)). Free drainage (unit gradient) boundary conditions were set at the lower boundary, since the water table was far below the 1 m depth, set at lower boundary for the numerical experiment. The simulation was performed for 216 h (9 days) corresponding to the experiment duration. A time step of 1 h was used both for the simulation and the experimental data collection. After implementation of the initial and boundary conditions, the program simultaneously solved for the liquid water, water vapor, and heat fluxes.

The flow region is one-dimensional with total length z = 100 cm divided into 100 elements. To improve the precision of the numerical solution in the surface layers (relevant for computation of evaporation) the first two centimeters of soil were discretized into 10 layers of 0.2 cm depth, therefore using a finer grid near the surface. A Crank–Nicholson scheme was used (Ames, 1992). The mass balance equation for heat flow at a node is (Campbell, 1985).

$$\frac{(\lambda_i T_i - \lambda_{i-1} T_{i-1})}{Z_i - Z_{i-1}} - \frac{(\lambda_{i+1} T_{i+1} - \lambda_i T_i)}{Z_{i+1} - Z_i} = \frac{C_h (T_i^{j+1} - T_i^j)(Z_i - Z_{i+1})}{2\Delta t} \quad \text{Eq. (41)}$$

where λ is the element thermal conductivity, T is the node temperature and C_h is the node heat capacity. The subscript i identifies the node, and the superscript j indicates time. Similarly, the mass balance equation for water flux at a node is

$$\frac{(K_i \psi_i - K_{i-1} \psi_{i-1})}{Z_i - Z_{i-1}} - \frac{(K_{i+1} \psi_{i+1} - K_i \psi_i)}{Z_{i+1} - Z_i} - g(K_{i-1} - K_i) = \frac{\rho(\theta_i^{j+1} - \theta_i^j)(Z_{i+1} - Z_{i-1})}{2\Delta t} \quad \text{Eq.(42)}$$

where $K(\psi)$ is the element hydraulic conductivity, ψ is the node water potential, θ is the node water content, g is the gravitational constant and ρ is water density (1000 kg m^{-3} at 4 °C). Eq. (41) and (42) are mass balance equations where the right side is the change in heat or water content at position x_i xi over the time period Δt, and the left side is the difference between influx and outflux to and from the computational element, which depends on the temperature and water potential gradient. Mass balance equations similar to Eq. (41) and (42) were written to solve for vapor flux (Campbell, 1985).

Numerical solutions of Eq. (41) and (42) were obtained by using a Newton–Raphson (NR) algorithm for the nonlinear difference equations for heat, liquid water and vapor flow. The NR algorithm is a robust numerical solution (Paniconi and Putti, 1994), where the jacobian matrix is tri-diagonal, and consequently the Thomas algorithm can be used (Press et al., 1992). The advantage from using the NR algorithm are the numerical robustness and the non-dependence of the algorithm to the time-step choice that can be much larger without any stability restriction on Δt (Morton and Mayers, 1994). The NR algorithm requires that iterations find new values for $\Delta\psi$ and Δt, thereby reducing the mass balance error for that node. This feature allows a full coupling of the different flow phenomena at each time step because the solver simultaneously computes

new values of node temperature, water content, and vapor concentrations. Iteration continues until the mass and heat balance are within a specified limit. In this work, the maximum allowable limit was 10^{-6} kg m^{-2} s^{-1} for liquid and vapor water fluxes, and 10^{-8}W m^{-2} for heat fluxes.

References

Ames, W.F., 1992. Numerical Methods for Partial Differential Equations, third edition. Academic Press, San Diego.

Bittelli, M., Ventura, F., Campbell, G.S., Snyder, R.L., Gallegati, F., and Pisa, P.R., 2008. Coupling of heat, water vapor, and liquid water fluxes to compute evaporation in bare soils, Journal of Hydrology, 362(3): 191-205.

Buck, A.L., 1981. New equations for computing vapor pressure and enhancement factor. Journal of Applied Meteorology and Climatology, 20: 1527–1532.

Campbell, G.S., 1985. Soil Physics with Basic, Transport Models for Soil–Plant Systems. Elsevier, Amsterdam, Netherlands.

Campbell, G.S., Jungbauer, J.D., Bidlake, W.R., and Hungerford, R.D., 1988. Predicting the effect of temperature on soil thermal conductivity. Soil Science, 158: 307–313.

Campbell, G.S., and Shiozawa, S., 1992. Prediction of hydraulic properties of soils using particle-size distribution and bulk density data. In: van Genuchten, M.T., Leij, F.J., Lund, L.J. (Editors.), Indirect Methods for Estimating the Hydraulic Properties of Unsaturated Soils. University of California, Riverside, pp. 317–328.

Campbell, G.S., Norman, and John M., 1998. An Introduction to Environmental Biophysics, second edition. Springer-Verlag, New York.

Carrasco, M., and Ortega-Farías, S., 2008. Evaluation of a model to simulate net radiation over a vineyard cv. cabernet sauvignon. Chilean Journal of Agricultural Research, 68:156-165.

Cary, J.W., 1963. Onsanger's relation and the non-isothermal diffusion of water vapor. The Journal of Physical Chemistry, 67: 126–129.

de Vries, D.A., 1963. Thermal properties in soil. In: van Wijk, W.R. (Ed.), Physics of Plant Environment. North Holland Pub. Co., Amsterdam, pp. 210–235.

Guo Yu, Q., Ben-Asher, J., Yano, T., and Momii, K., 1999. Estimation of soil evaporation using the differential temperature method. Soil Science Society of America Journal, 63: 1608–1614.

Idso, S.B., Reginato, R.J., Jackson, R.D., Kimball, K.B., and Nakayama, F.S., 1974. The three stages of drying in a field soil. Soil Science Society of America, Proceedings, 38: 831–837.

Jassal, R.S., Novak, M.D., and Black, M.D., 2003. Effect of surface layer thickness on simultaneous transport of heat and water in a bare soil and its implications for land surface schemes. Atmosphere-Ocean, 41: 259–272.

Jensen, A.E., Lohse, K.A., Crosby, B.T., and Mora, C.I., 2014. Variations in soil carbon dioxide efflux across a thaw slump chronosequence in northwestern Alaska, Environmental Research Letters, 9: 025001.

Kroener, E., Vallati, A., and Bittelli, M., 2014. Numerical simulation of coupled heat, liquid water and water vapor in soils for heat dissipation of underground electrical power cables. Applied Thermal Engineering, 70: 510-523.

Morton, K.W., and Mayers, D.F., 1994. Numerical Solution of Partial Differential Equations. Cambridge University Press, Cambridge, UK.

Paniconi, C., and Putti, M., 1994. Comparison of Picard and Newton iteration in the numerical solution of multidimensional variably saturated flow problems. Water Resource Research, 30: 3357–3374.

Philip, J.R., and de Vries, D.A., 1957. Moisture movement in porous materials under temperature gradients. Transactions - American Geophysical Union, 38: 222–231.

Press, W.H., Teukolsky, S.A., Vetterling, W.T., and Flannery, B.P., 1992, 2nd ed. Numerical Recipes the Art of Scientific Computing, vol. 5 Cambridge University Press, Cambridge.

Rose, C.W., 1968a. Water transport in soil with a daily temperature wave. I Theory and experiment. Australian Journal of Soil Research, 6: 31–44.

Taylor, S.A., and Cavazza, L., 1954. The movement of soil moisture in response to temperature gradients. Soil Science Society of America, Proceedings, 18: 351–358.